CHRONIC HYPOXIA AND THE CAROTID BODY: THE ROLE OF CD73 IN CAROTID BODY HYPERACTIVITY AND CARDIO-RESPIRATORY FUNCTION

by

DEMITRIS NATHANAEL

A thesis submitted to

The University of Birmingham

for the degree of

DOCTOR OF PHILOSOPHY

Department of Biomedical Sciences

School of Infection, Inflammation and Immunology

College of Medical and Dental Sciences

University of Birmingham

March 2025

Abstract

Carotid body hyperactivity is increasingly recognised as a major contributor to neurogenic hypertension, particularly in cardiovascular-respiratory related diseases including chronic obstructive pulmonary disease (COPD). In COPD, chronic hypoxia persistently excites the carotid body, driving excessive sympathetic outflow contributing to hypertension. However, the mechanisms underlying carotid body hyperactivity remain unclear. CD73, an ecto-nucleotidase, plays a crucial role in setting basal carotid body activity and hypoxic sensitivity. Whether CD73 contributes to chronic hypoxia-induced carotid body hyperactivity is unknown. This thesis initially characterised and validated a chronic hypoxia model in rats using 10 days exposure to 12% F_iO_2. Experiments subsequently investigated alterations in the cellular distribution of CD73 in the carotid body in response to chronic hypoxia and the functional importance of CD73 in promoting chemoafferent hyperexcitability. Final experiments examined whether *in vivo* pharmacological targeting of CD73 produced beneficial cardiovascular alterations in chronically hypoxic animals. Chronic hypoxia increased the number of $CD73^+TH^+$ cells within the carotid body. Pharmacological inhibition of CD73 abolished chronic hypoxia-induced basal chemoafferent hyperactivity and normalised heightened hypoxic sensitivity *ex vivo*. CD73 antagonism *in vivo* reduced blood pressure in a carotid body-dependent manner while preserving cardiovascular-respiratory reflexes during hypoxia. This research suggests that CD73 is an important modulator of carotid body hyperactivity in chronic hypoxia. The work highlights a potential new strategy for reducing carotid body hyperactivity and blood pressure without impairing hypoxia responsiveness. These findings should promote the development of carotid body/CD73-targeted treatments for chronic hypoxia-related conditions such as COPD.

Dedication

I would like to dedicate this thesis to Professor Janice Marshall, who sadly passed away in late February 2025. Janice was a cornerstone of the Biomedical Science course and played an instrumental role in my undergraduate education. Even in her later years, her enthusiasm for teaching and mentoring the next generation of scientists remained truly inspirational. Much of the work presented in this thesis builds upon the strong foundation she and her team established in the study of cardiovascular adaptations to chronic hypoxia. It is a great sadness that she did not get to see this thesis completed after many discussions about some of the data, but I hope this work meets the high standard she set throughout her remarkable 50-year career in science and that it would have made her proud. I will always cherish our conversations in the common room and the student office, where she never failed to make us students laugh. She genuinely cared about my well-being and my future, and for that, I will be forever grateful. Her kindness and passion for science will be deeply missed. Rest in peace, Professor Janice Marshall.

Acknowledgements

I would like to express my sincere appreciation to my funders, the British Heart Foundation, whose unwavering support of this studentship made it possible for me to complete this PhD. Their generosity has allowed me to conduct meaningful research and develop as a young scientist, for which I am truly grateful. I extend my gratitude to my main supervisor, Andy Holmes, for providing such a supportive environment for me to express myself, in addition to the many hours spent training me in the carotid body nerve technique, going over my data and helping me produce a thesis to be proud of. I am also immensely thankful to Andy Coney for his training and support with the in vivo experiments, without him, these vital experiments would not have been completed. A special thank you to Prem Kumar for not only being a mentor but also a great friend. Your wisdom, encouragement and kindness have meant so much to me throughout this journey. Another thank you to Clare Ray for all the lunch time talks, checking I am okay and the feedback of my work over the years. A thank you to the imaging team in the TechHub for all their support with the confocal and image analysis. To the many people I have met along the way, particularly my lab colleagues, both past and present: Aziz, Eyas, Lily, Hayyaf, Sean, James, Sophie, Emily, Hanadi, Stefana, Anna and Dhaif, as well as the French summer students: Wasim, Sheïmaa, Mathilde, Hanae and Ayna. Thank you all for the memories we have shared. Lastly, I cannot thank my family enough for their continuous support. To my grandparents, parents, siblings, cousins, uncles and aunties-though you may not fully understand what I do, your unwavering love, encouragement and belief in me have meant the world.

Table of Contents

List of Figures

Chapter 1

Chapter 2

Chapter 3

Chapter 4

Chapter 5

Chapter 6

Chapter 7

Appendix: Supplementary

List of Tables

Chapter 2

Chapter 3

Chapter 6

List of abbreviations

4-AP	4-aminopyridine
8-SPT	8-(p-sulfophenyl) theophylline (adenosine receptor antagonist)
A_2	adenosine receptor subtype 2
AC	adenylyl cyclase
AC3	adenylyl cyclase 3
ACh	acetylcholine
ADP	adenosine diphosphate
AF	autofluorescence
AMP	adenosine monophosphate
AMPK	AMP-activated protein kinase
AOPCP	a,β-methylene ADP (CD73 inhibitor)
ASIC	acid sensing ion channel
ATP	adenosine triphosphate
BK_{Ca}	large-conductance calcium activated potassium channel
BrdU	bromodeoxyuridine
BSA	bovine serum albumin
CA	carbonic anhydrase
cAMP	cyclic AMP
C_aO_2	arterial oxygen content
CCA	common carotid artery
CD31	PCAM-1 (vascular endothelial marker)
CD73/E5′Nt	ecto-5′-nucleotidase

CH	chronic hypoxia/chronically hypoxic
CNG	cyclic nucleotide-gated
CO	carbon monoxide
COPD	chronic obstructive pulmonary disease
CSE	cystathionine-γ-lyase
CSN	carotid sinus nerve
CSNX	carotid sinus nerve section
ECA	external carotid artery
ENT	equilibrative nucleoside transporter
EPAC	exchange protein activated by cAMP
EPO	erythropoietin
FIH	factor-inhibiting HIF
F_iO_2	fraction of inspired oxygen
GFAP	glial fibrillary acidic protein
GPN	glossopharyngeal nerve
H_2S	hydrogen sulphide
Hb	haemoglobin
HCN4	hyperpolarization-activated cyclic nucleotide-gated cation channel
HIF	hypoxia inducible factor
HO-2	haemoxygenase-2
HVR	hypoxic ventilatory response
ICA	internal carotid artery
ID	internal diameter
K_V	voltage-gated K^+ channel

M1 and M2	Manders' coefficients 1 and 2
mABP	mean arterial blood pressure
MSNA	muscle sympathetic nerve activity
N	normoxic
NA	numerical aperture
NF	neurofilament light chain
NICE	National Institute for Health and Care Excellence
NPP	ecto-nucleotide pyrophosphatase/phosphodiesterase
NTPDase/CD39	ecto-nucleoside triphosphate diphosphohydrolase
NTS	nucleus tractus solitarius
OA	occipital artery
OD	outer diameter
Olfr78	olfactory receptor 78
P2	purinergic receptor subfamily 2
P_aCO_2	arterial partial pressure of carbon dioxide
P_aO_2	arterial partial pressure of oxygen
PBS	phosphate buffered saline
PBS-T	phosphate buffered saline in Tween 20
PCO_2	partial pressure of carbon dioxide
PFA	paraformaldehyde
PHD	prolyl hydroxylase domain
PKA	protein kinase A
PO_2	partial pressure of oxygen
RBC	red blood cell
ROS	reactive oxygen species
RVH	right ventricular hypertrophy

sAC	soluble adenylyl cyclase
S_aO_2	arterial oxygen saturation
SCG	superior cervical ganglion
SQ22536	9-(Tetrahydro-2-furanyl)-9H-purin-6-amine (transmembrane adenylyl cyclase inhibitor)
TASK	TWIK-related acid-sensitive potassium channel
TH	tyrosine hydroxylase
tmAC	transmembrane adenylyl cyclase
TREK	TWIK-related potassium channel
VAH	ventilatory acclimatisation to hypoxia
VEGF	vascular endothelial growth factor
VHL	von Hippel-Lindau
VN	vagus nerve
WHO	world health organisation

CHAPTER 1

1. Introduction

1.1 Overview of carotid body physiology

1.1.1 Anatomy of the carotid body

The carotid body is an important, ovoid organ located in the neck at the bifurcation of the left and right common carotid arteries. In most mammals, it is a single compact structure, measuring approximately 13 mg in humans and 60 µg in rats (Heath et al., 1970; McDonald, 1981). Its long axis measures 2-3 mm in humans and 0.40-0.70 mm in rats (Heath et al., 1970; Hess, 1975; McDonald & Blewett, 1981).

The carotid body has an extensive vascular network primarily supplied by branches of the internal carotid artery (ICA), external carotid artery (ECA) and occipital artery (OA). Blood distribution occurs through fenestrated capillaries (8-28 µm in diameter) and non-fenestrated capillaries (6-12 µm) (McDonald, 1983; McDonald & Larue, 1983). Some of these vessels are surrounded by pericytes, which play a role in regulating blood flow, though their precise function in the carotid body remains unclear. Despite its small size, the carotid body receives an exceptionally high blood flow, estimated at 1-2 L $min^{-1}.100g^{-1}$, which is about 10 times greater than the brain's relative blood flow (Barnett et al., 1988; Daly et al., 1954).

The carotid body is richly innervated by both afferent and efferent nerves. Efferent fibres primarily arise from the superior cervical ganglion (SCG), and sympathetic noradrenergic fibres supply the vascular bed. Afferent neurons project from the carotid sinus nerve (CSN), a branch of the glossopharyngeal nerve (IX^{th} cranial nerve), with

their cell bodies located in the petrosal ganglion. When stimulated, these afferent fibres relay signals to the nucleus tractus solitarius (NTS) in the brainstem (Finley & Katz, 1992; Panneton & Loewy, 1980).

The carotid body contains oxygen-sensitive type I cells, which cluster in groups of 2–12 cells (Kumar & Prabhakar, 2012). These cells act as the primary chemosensory transducers, containing dense-core vesicles that facilitate neurotransmitter release to excite afferent terminals. Surrounding them are glia-like type II cells, which are sparser, with a ratio of approximately 1 type II cell for every 4 type I cells. Within a cluster, there are also immature type I cells known as neuroblasts which contribute to carotid body adaptation (Platero-Luengo et al., 2014). The strategic location of the carotid body, combined with its dense vascularisation, intricate neuronal connections and specialised cell composition, enables it to efficiently monitor and respond to changes in blood chemistry, particularly in stressful conditions (Nurse, 2014).

1.1.2 Chemotransduction and reflex responses

The detection of chemosensory signals by type I cells triggers a well-defined transduction cascade, ultimately increasing action potential generation in the CSN. This signal is transmitted to the brainstem, where it elicits protective cardio-respiratory reflexes. While hypoxia has traditionally been studied as the primary carotid body stimulant, it is now recognised that the carotid body functions as a polymodal receptor, capable of responding to various stressors, including hypercapnia, acidic pH, inflammation, hypoglycaemia and temperature changes (Kumar & Bin-Jaliah, 2007). This thesis will focus primarily on carotid body responses to hypoxia and hypercapnia.

Although the molecular mechanisms underlying stimulus detection remain debated, the subsequent transduction cascade is widely accepted.

Cellular depolarisation in type I cells is primarily attributed to the inhibition of outward K^+ currents. Several K^+ channels have been implicated in this process, including TWIK-related acid-sensitive (TASK), TWIK-related (TREK), large-conductance calcium-activated (BK_{Ca}/maxi-K) and voltage-gated (K_V) channels (Buckler et al., 2000; Kim et al., 2009; Wyatt & Peers, 1995). The resulting membrane depolarisation opens voltage-sensitive L-type Ca^{2+} channels, leading to a proportional rise in intracellular calcium levels with increasing hypoxic intensity (Buckler & Vaughanjones, 1994; Urena et al., 1994).

This rise in intracellular calcium triggers the release of various neurotransmitters and neuromodulators that regulate the excitation or inhibition of post-synaptic CSN afferents, through ionotropic or metabotropic receptor activation. Some of these neurotransmitters include dopamine, serotonin, endothelin-1, acetylcholine (ACh), adenosine triphosphate (ATP) and adenosine (Nurse, 2010). The presence of corresponding receptors on type I cells suggests a potential autocrine feedback mechanism for modulating chemosensory responses. ATP is well-established as an excitatory neurotransmitter in the carotid body, and more recently, adenosine, a breakdown product of ATP, has gained attention as a key regulator of carotid body activity (Conde et al., 2017; Holmes et al., 2018b). These topics will be discussed further in Section 1.2.

CSN excitation leads to increased action potential transmission to the brainstem, triggering protective cardiovascular and respiratory reflexes. These include enhanced

phrenic nerve activity, increasing ventilation, and heightened sympathetic output, causing vasoconstriction and adrenaline release from the adrenal medulla (Kumar, 2009). While the carotid body's primary response to hypoxia induces bradycardia, the increased respiratory drive leads to overall vagal inhibition and tachycardia (Zera et al., 2019). These reflexes work collectively to elevate arterial oxygen levels and enhance blood flow to vital organs. A summary of the carotid body chemotransduction cascade and reflex responses to hypoxia is provided in Figure 1.1.

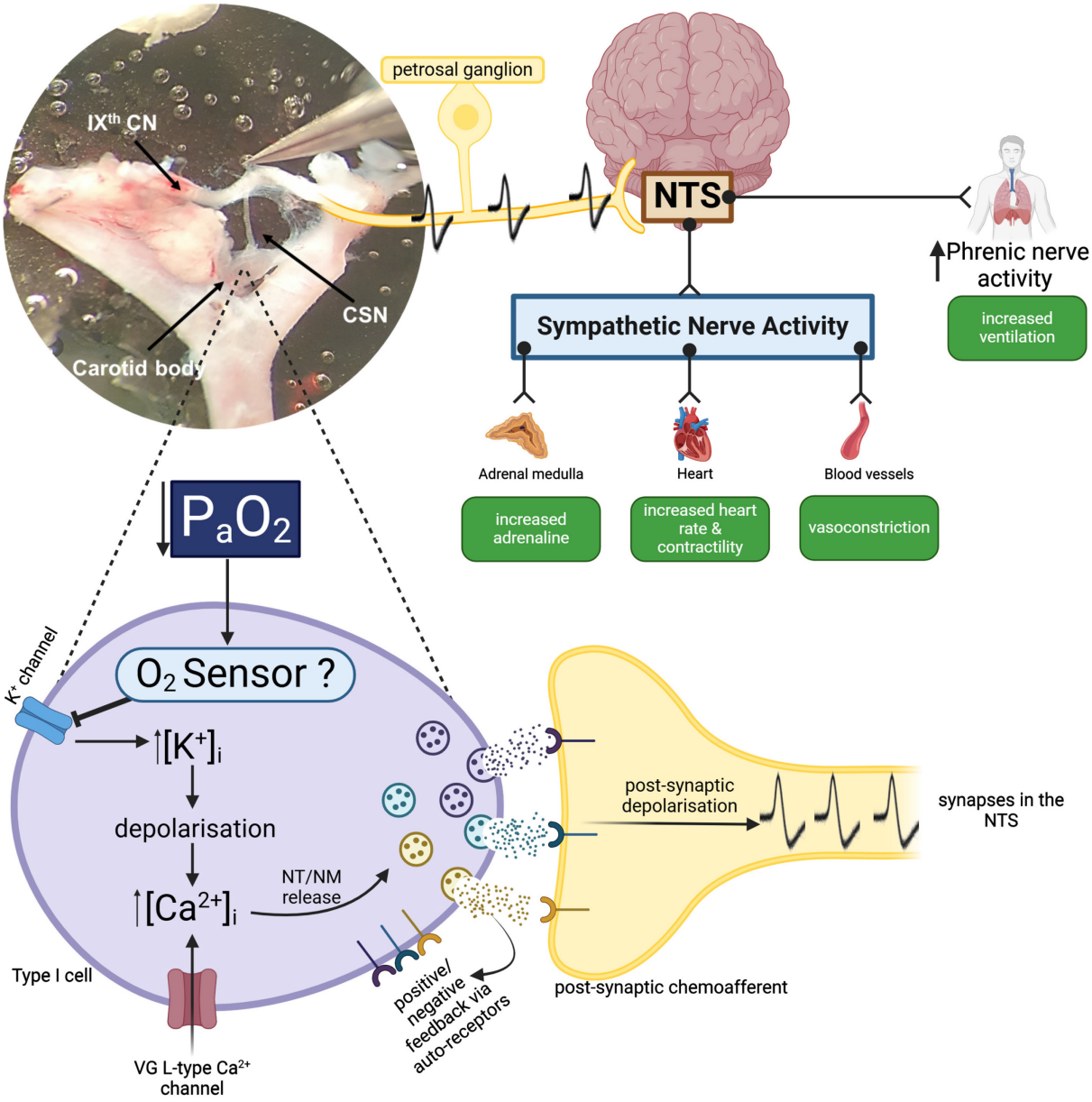

Figure 1.1 Carotid body chemotransduction and reflex responses

This illustration depicts a summary of the general carotid body chemotransduction cascade and reflex responses in response to a fall in arterial oxygen (P_aO_2). The top left inset shows an anatomical image of the carotid body, highlighting the carotid sinus nerve (CSN) and glossopharyngeal nerve (IX^{th} cranial nerve; CN). Upon sensing a decrease in P_aO_2, highly oxygen-sensitive type I cells initiate a signalling cascade, including K^+ channel closure, depolarisation and elevations in intracellular calcium $[Ca^{2+}]_i$ through voltage-gated (VG) L-type channels. This triggers neurotransmitter/neuromodulator (NT/NM) release into the synapse, inducing postsynaptic depolarisation. Action potentials travel through the carotid sinus nerve, whose afferents arise in the petrosal ganglion and ultimately reach the nucleus tractus solitarius (NTS) in the brainstem. Activation of NTS neurons stimulates phrenic nerve activity thus increasing ventilation. NTS neurones also elevate sympathetic nerve activity, leading to increased adrenaline release from the adrenal gland, increased heart rate and contractility and vasoconstriction. Figure created using BioRender.com

1.1.3 Carotid body oxygen sensing

Extensive evidence suggests that hypoxia attenuates K^+ currents, but whether this results from a direct effect of oxygen on K^+ channels or an intracellular O_2 signalling cascade remains debateable. The mitochondrial hypothesis of carotid body O_2-sensing is one of the most well established theories. In mammalian mitochondria, O_2 serves as the terminal electron acceptor in the CuB/haem a3 binuclear centre of cytochrome c oxidase (Complex IV), driving electron transport and ATP production (Holmes et al., 2018a). Many mitochondrial inhibitors mimic hypoxic responses, such as reduced TASK-like currents (Turner & Buckler, 2013; Wyatt & Buckler, 2004), intracellular calcium increases (Buckler, 2012), neurotransmitter release (Obeso et al., 1989) and chemoafferent excitation in whole carotid body preparations (Donnelly et al., 2014; Holmes et al., 2016).

Despite this, the precise mechanism linking mitochondrial inhibition to type I cell depolarisation remains under investigation. Reduced oxidative phosphorylation likely decreases intracellular ATP, increasing the AMP-to-ATP ratio. This may activate AMP-activated protein kinase (AMPK), which phosphorylates and inhibits K^+ channels, modulating depolarisation and chemotransduction (Evans et al., 2009; Wyatt et al., 2007). However, some studies challenge AMPK's role in TASK-like current attenuation and calcium elevation during hypoxia (Kim et al., 2014). Furthermore, it has been reported that carotid bodies isolated from mice with double α1/ α2 subunit deletion of AMPK retain hypoxic sensitivity, further questioning the importance of AMPK as a signal transducer in this context (Mahmoud et al., 2016). Most ATP is complexed with Mg^{2+} as MgATP (Gout et al., 2014). While direct intracellular ATP or MgATP measurements have been inconsistent, using a Mg^{2+}-sensitive fluorescent probe, data

showed increased free Mg^{2+} in hypoxic rat type I cells, suggesting ATP depletion (Varas et al., 2007). MgATP may indirectly activate TASK/TREK-1 K^+ channels, though the mechanism remains unclear, especially given that these channels do not possess the ability to bind MgATP (Enyeart et al., 2002; Varas et al., 2007; Williams & Buckler, 2004). However, keeping ATP constant in type I cells did not prevent K^+ current inhibition during hypoxia. Furthermore, recent experiments quantifying ATP levels indicate that they remain unchanged during hypoxia, suggesting that K^+ current inhibition occurs through a mechanism independent of MgATP (Lopez-Barneo et al., 2016; Lopez-Barneo et al., 1988; Torres-López et al., 2025).

Mitochondrial metabolism also generates reactive oxygen species (ROS), primarily at Complexes I and III (Murphy, 2009). Acute hypoxia elevates ROS in the mitochondrial intermembrane space. Deleting *Ndufs2*, a gene encoding a Complex I protein, prevents hypoxia-induced ROS increase and abolishes the hypoxic ventilatory response in mice (Fernández-Agüera et al., 2015). Hypoxia is proposed to enhance succinate metabolism at Complex II, leading to electron leakage into Complex I via reverse electron transport (RET). However, Complex II inhibition with dimethyl malonate only partially suppresses the catecholamine and chemoafferent response to hypoxia (Arias-Mayenco et al., 2018; Swiderska et al., 2021). ROS can also be generated through Complex III. In mice with a genetic deletion of Complex III, intermembrane ROS levels are reduced during hypoxia. Type I cells isolated from these mice exhibit a complete loss of calcium influx and neurosecretory responses to hypoxia, along with a severely diminished *in vivo* response (Cabello-Rivera et al., 2022). While ROS likely modulates K^+ channels, their precise molecular effects remain unclear (Wyatt & Buckler, 2004). The accumulation of reduced metabolites shifts the redox balance toward a more reduced state, which has been proposed to activate the

redox-sensitive protein PIN1. This in turn may activate NADPH oxidase, a membrane-bound protein that also generates ROS. Inhibiting PIN1 partially blocks hypoxia-induced depolarisation (Bernardini et al., 2020). While these findings implicate Complex I-III and NADPH oxidase in hypoxic sensing, feeding electrons into cytochrome c can bypass Complex I inhibition, suggesting Complex IV plays a more pivotal role in hypoxic chemotransduction (Wyatt & Buckler, 2004).

Other molecules may compete with oxygen binding at Complex IV. Carbon monoxide (CO), generated by the O_2-dependent enzyme haem-oxygenase-2 (HO-2), inhibits carotid body activity in normoxia by activating BK_{Ca} channels (Peng et al., 2010; Riesco-Fagundo et al., 2001; Williams et al., 2004). In hypoxia, reduced HO-2 activity decreases CO-dependent K^+ channel activation. However, HO-2 knockout mice retain hypoxic sensitivity, questioning CO's role in oxygen sensing. CO may instead regulate another gasotransmitter, hydrogen sulphide (H_2S), which increases in HO-2-null mice. Type I cells express cystathionine-γ-lyase (CSE), an H_2S-producing enzyme negatively regulated by CO via Protein Kinase G-dependent phosphorylation. Hypoxia lifts CSE inhibition, increasing H_2S and promoting chemoexcitation by modulating ion channels and mitochondria (Prabhakar & Semenza, 2015).

Recent research suggests H_2S excitation may be independent of mitochondria and background K^+ channels, involving the G protein-coupled olfactory receptor 78 (Olfr78). Transcriptome analysis identified Olfr78 as highly expressed in type I cells, though its role in oxygen sensing is debated (Chang et al., 2015; Zhou et al., 2016). Lactate, an Olfr78 agonist, can stimulate carotid body activity, but physiological lactate levels in hypoxia may not be sufficient for this effect (Chang et al., 2015; Peng et al.,

2020; Torres-Torrelo et al., 2021). Contradictory Olfr78-knockout mouse studies leave lactate's role unresolved (Chang et al., 2015; Torres-Torrelo et al., 2018). However, Olfr78 mutants exhibit impaired ventilatory responses to mild but not severe hypoxia (Peng et al., 2020). Recent findings show that H_2S post-translationally modifies Olfr78 via persulphidation, activating adenylyl cyclase 3 (AC3), increasing cAMP, and triggering cyclic nucleotide-gated (CNG) channels to induce calcium influx and chemoreflex activation (Peng et al., 2025; Prabhakar et al., 2023). The role of cAMP in mediating chemoafferent activity in normoxia and hypoxia will be explored in this thesis.

More research is needed to reconcile these mechanisms, which may all interact and play a part in oxygen sensing. However, it is evident that carotid body mitochondria are highly oxygen-sensitive, with electron transport impairment occurring at higher oxygen tensions than in other tissues (Buckler & Turner, 2013; Duchen & Biscoe, 1992a, 1992b). This low oxygen affinity is partly due to high mRNA levels of *Cox4i2* and *Cox8b*, which encode cytochrome c oxidase subunits along with other Complex IV-related proteins such as HIGD1C which is almost exclusively expressed in the carotid body (Gao et al., 2017; Timón-Gómez et al., 2022; Zhou et al., 2016). Many of these atypical mitochondrial subunits have been associated with the relatively high expression of hypoxia inducible factor (HIF)-2α (Bishop & Ratcliffe, 2020; Moreno-Domínguez et al., 2020). Additionally, the selective loss of O_2 sensitivity while preserving CO_2 sensitivity highlights distinct sensing mechanisms for these stimuli. Figure 1.2 shows a summary of the proposed signalling mechanisms caused by hypoxia.

1.1.4 Carotid body carbon dioxide sensing

The reflex response to increased arterial CO_2 (hypercapnia) triggers a significant rise in ventilation. While this response is primarily driven by chemosensitive neurons in the brainstem's medullary regions, studies indicate that 20-50% of the ventilatory response to hypercapnia is mediated by the carotid body (Heeringa et al., 1979; Rodman et al., 2001; Thomas et al., 1999). Further experiments show that tonic carotid body activity is essential for central chemoreceptor sensitivity to hypercapnia, as silencing carotid body output with hyperoxic-hypocapnic solutions greatly reduces the ventilatory response in extracorporeal perfused dogs (Blain et al., 2009). The carotid body not only enhances central chemoreceptor sensitivity to hypercapnia but also accelerates the response, with studies showing an ~11-second delay when central chemoreceptors are stimulated alone (Smith et al., 2006).

Hypercapnia initiates a chemotransduction cascade similar to hypoxia, involving type I cell depolarisation, increased intracellular calcium and neurotransmitter release (Kumar & Prabhakar, 2012). The prevailing theory is that extracellular CO_2 diffuses into type I cells, where carbonic anhydrase catalyses its conversion into carbonic acid (H_2CO_3), which then dissociates into bicarbonate (HCO_3^-) and hydrogen ions (H^+) (Iturriaga et al., 1991). Carbonic anhydrase isoforms I, II and III have been localised in the rat carotid body (Yamamoto et al., 2003). The resulting intracellular acidification inhibits outward currents from TASK-like, BK_{Ca} and acid-sensing ion channels (ASIC), leading to depolarisation (Buckler et al., 2000; Peers, 1990; Tan et al., 2007). While TASK-1 knockout mice exhibit a blunted hypercapnic chemoafferent and ventilatory response *ex vivo* and *in vivo* respectively, a later study on TASK-1-null mice found no significant changes in background K^+ currents or catecholamine secretion. However,

dual TASK-1/3 knockout mice exhibited reduced resting K^+ current and decreased sensitivity to hypercapnia, despite unaltered catecholamine secretion (Ortega-Sáenz et al., 2010). Further research is needed to clarify the role of TASK-1, TASK-3 and TASK-1/3 heterodimers in hypercapnic sensing.

Other ion channels, such as ASICs, may also contribute to hypercapnic sensing (Caraftino & Montalbetti, 2020). ASIC1 and ASIC3 are expressed in type I cells and ASIC3-knockout mice show a reduced Ca^{2+} response to hypercapnia while maintaining normal responses to hypoxia, suggesting distinct acid and O_2 sensing pathways (Lu et al., 2013; Tan et al., 2007). However, mice with homozygous deletions of ASIC1, ASIC2, or ASIC3 show no significant differences in ventilatory responses to hypercapnia compared to wild-type controls (Detweiler et al., 2018). Figure 1.2 shows a summary of the proposed signalling mechanisms caused by hypercapnia.

Hypercapnic chemotransduction may also occur independently of acidification. Studies indicate that isohydric hypercapnia (high CO_2 at constant pH) induces Ca^{2+} influx, neurotransmitter release and increased chemoafferent activity (Rigual et al., 1991; Summers et al., 2002; Zhang & Nurse, 2004). This Ca^{2+} rise is cAMP and Protein Kinase A (PKA)-dependent (Summers et al., 2002). Soluble adenylyl cyclase (sAC), a key enzyme activated by bicarbonate (HCO_3^-), has been proposed to contribute to hypercapnic sensitivity (Nunes et al., 2009). However, functional studies found no changes in cAMP, PKA activity or chemoafferent discharge in isohydric hypercapnia, challenging previous findings (Nunes et al., 2013). In contrast, acid hypercapnia does increase cAMP, suggesting it may modulate ion channel function in response to CO_2, though the underlying mechanism remains unclear (Perezgarcia et al., 1990).

Additionally, type I cell depolarisation and Ca^{2+} influx lead to neurotransmitter release including ATP and adenosine. ATP-derived adenosine enhances chemoafferent activity and can stimulate transmembrane adenylyl cyclase (tmAC) in an autocrine manner, increasing cAMP (Monteiro et al., 1996). The interplay between adenosine, cAMP and sensitivity to hypoxia and hypercapnia will be explored in this thesis.

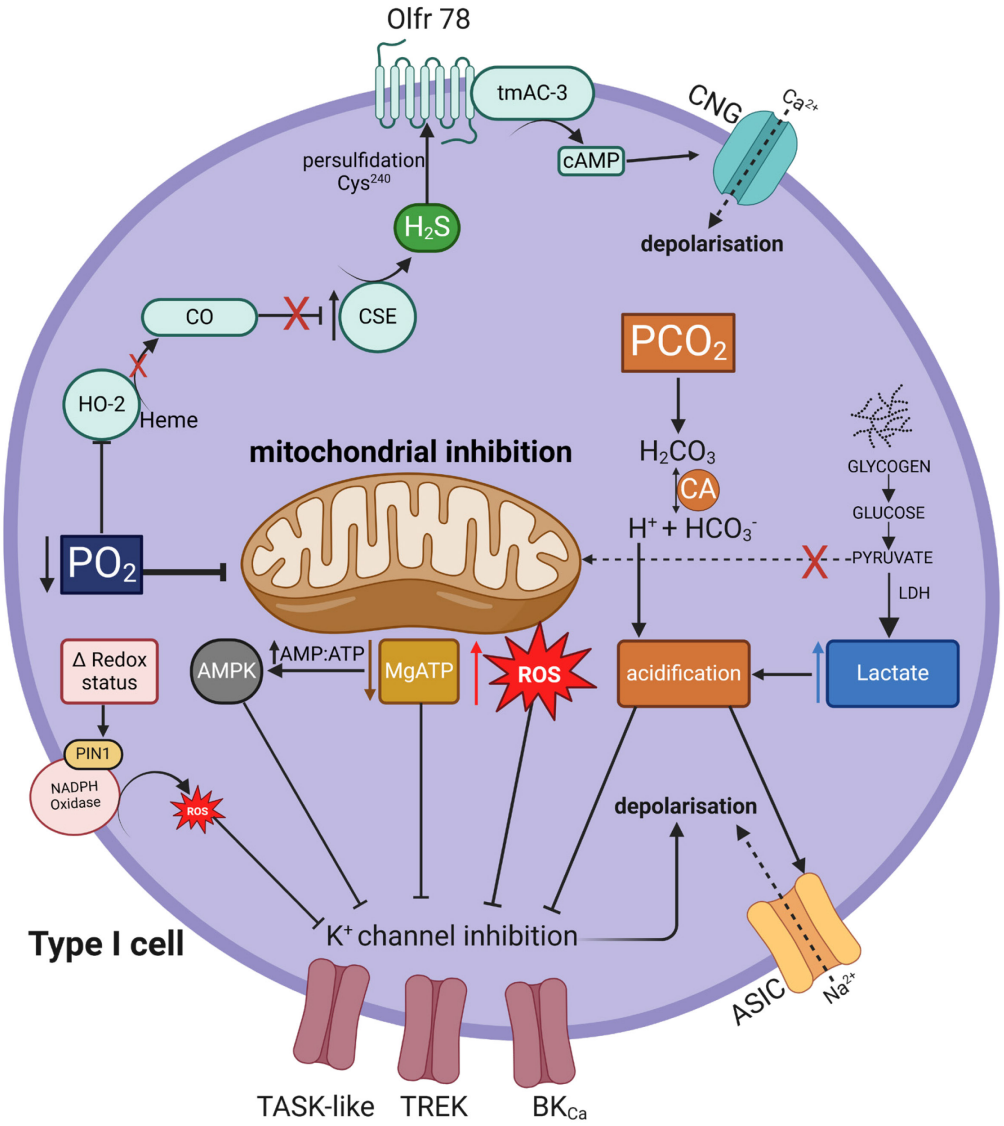

Figure 1.2 Proposed signalling pathways in carotid body type I cells during hypoxia and hypercapnia

Schematic illustration depicting the intracellular signalling mechanisms of O_2 and CO_2 sensing in carotid body type I cells. Reduced PO_2 leads to mitochondrial inhibition, influencing multiple signalling molecules and processes including decreased MgATP, elevated reactive oxygen species (ROS), increased AMP:ATP ratio which activates AMPK and altered cellular redox status. These changes inhibit various K^+ channels, including TASK-like, TREK and BK_{Ca}, causing cellular depolarisation. In parallel, decreased oxygen availability downregulates heme oxygenase-2 (HO-2), reducing carbon monoxide (CO) production and subsequently lifting inhibition on cystathionine γ-lyase (CSE), which produces hydrogen sulphide (H_2S). H_2S can activate the olfactory receptor (Olfr78) via persulfidation at Cys^{240}, stimulating transmembrane adenylyl cyclase-3 (tmAC-3), increasing cyclic AMP (cAMP) and causing depolarisation via cyclic nucleotide-gated (CNG) channels. Elevated PCO_2 contributes to cellular acidification through carbonic anhydrase (CA)-mediated production of protons (H^+), and through increased lactate production from glycogen metabolism thought to occur during severe hypoxia. Acidification inhibits K^+ channels and activates acid-sensitive ion channels (ASICs), leading to additional depolarisation. Collectively, these pathways drive neurotransmitter release and chemoafferent excitation. Figure created using BioRender.com.

1.2 Purinergic signalling in the carotid body

1.2.1 The role of ATP

ATP is primarily known as a cellular energy source, but over the past 60 years, it has also been recognised as a key neurotransmitter involved in cell-cell signalling (Burnstock, 1972). In the carotid body, ATP functions as an excitatory neurotransmitter, playing a crucial role in chemosensory signalling (Zhang et al., 2000). Histochemical studies have shown that ATP is abundantly stored in secretory granules within type I cells and released during hypoxia following depolarisation and calcium influx (Böck, 1980; Conde & Monteiro, 2004; Prasad et al., 2001). Infusion of ATP leads to a dose-dependent increase in ventilation, an effect that is partly blocked by antagonising P2 ATP receptors with suramin (Reyes et al., 2007). This is consistent with *in vivo* findings where ATP increases chemoafferent activity (McQueen & Ribeiro, 1983). Similarly, in *ex vivo* carotid body preparations, stable ATP analogues enhance chemoafferent activity, indicating a strong post-synaptic role for ATP (Rong et al., 2003).

Pharmacological data suggesting the presence of P2 receptors were confirmed by immunohistochemical studies, which identified $P2X_2$ and $P2X_3$ receptors on synaptic terminals closely associated with type I cells (Zhang et al., 2000). These receptors form functional $P2X_{2/3}$ heterodimers (Prasad et al., 2001). In an *in vitro* co-culture model of type I cells and petrosal neurons, blocking P2 receptors partially reduced the hypoxia-induced firing frequency of petrosal neurons (Zhang et al., 2000). Further supporting this role, $P2X_2$ and $P2X_{2/3}$ knockout mice exhibit a diminished hypoxic ventilatory response, and show significantly blunted chemoafferent discharge during hypoxia *ex vivo* (Rong et al., 2003). Additionally, ATP release from rat carotid bodies increases proportionally with hypoxic intensity, with ATP blockade effects being more pronounced

under severe hypoxia (Conde et al., 2012b). ATP may also be released by the glia-like type II cells which are intimately associated with the type I cells. Immunofluorescence staining has confirmed the expression of $P2Y_2$ receptors on rat carotid body type II cells. Its activation by ATP generates Ca^{2+} from intracellular stores and subsequent ATP release through pannexin-1 channels (Piskuric & Nurse, 2013; Xu et al., 2003; Zhang et al., 2012).

Collectively, these findings highlight ATP as a critical mediator of carotid body responses to hypoxia, becoming more important as the stimulus intensity increases. However, its role in maintaining basal chemoafferent activity remains debated. Some studies show that blocking P2 receptors with suramin reduces basal chemoafferent discharge, while others find no such effect (Conde et al., 2012b; Zhang et al., 2000). Indeed, it appears that $P2X_2$ and $P2X_{2/3}$ knockout mice retain a normal basal chemoafferent discharge frequency despite responses to hypoxia being severely diminished (Rong et al., 2003). Moreover, ATP's influence appears stronger at severe hypoxic levels, raising questions about which neuromodulator governs basal and mild hypoxic responses. Notably, ATP is continually released from carotid bodies under normoxia, with an estimated 4 pmol per carotid body. However, extracellular adenosine concentrations are approximately five times higher than ATP, suggesting rapid ATP breakdown in the synaptic cleft, meaning adenosine may mediate many of ATP's excitatory effects (Conde et al., 2009; Conde et al., 2012b).

1.2.2 The role of CD73 and adenosine in normoxia

Unlike typical neurotransmitters, adenosine is not stored in secretory vesicles but is instead generated through the breakdown of nucleotides, primarily ATP. ATP is

metabolised by a series of ecto-nucleotidases, which belong to four major families: ecto-nucleoside triphosphate diphosphohydrolase (NTPDase/CD39), ecto-nucleotide pyrophosphatase/phosphodiesterase (NPP), alkaline phosphatases, and ecto-5′-nucleotidase (E5′Nt/CD73). NTPDases play a key role by hydrolysing ATP to ADP and ADP to AMP (Knowles, 2011). In the rat carotid body, NTPDase1-3 mRNA is expressed, and NTPDase2/3 proteins are localised to nerve processes, type I cells, and some glia-like type II cells (Salman et al., 2017).

CD73 is the rate-limiting enzyme in ATP degradation, converting AMP into adenosine, and is found on type I and type II cell membranes (Bianchi & Spychala, 2003; Salman et al., 2017; Zimmermann et al., 2007). Adenosine can also be formed through the hydrolysis of S-adenosylhomocysteine (Broch & Ueland, 1980). Once produced, adenosine is either released via equilibrative nucleoside transporters (ENTs) or formed extracellularly from ATP breakdown. It is subsequently degraded by adenosine kinase and adenosine deaminase (Conde et al., 2009).

Early studies demonstrated that intra-carotid adenosine administration in anaesthetised cats increased chemoafferent discharge frequency and intensity in a dose-dependent manner (McQueen & Ribeiro, 1981), a finding later supported by *in vitro* experiments (Runold et al., 1990; Vandier et al., 1999). In rats, both exogenous adenosine administration and endogenous accumulation acutely increased minute ventilation, tidal volume and respiratory frequency. This effect was reduced following CSN resection or A_2 receptor blockade (Monteiro & Ribeiro, 1987; Ribeiro & Monteiro, 1991). These findings suggest that adenosine is endogenously produced in the carotid body and plays a regulatory role in chemoafferent activity under normoxic conditions.

Adenosine's excitatory effect on respiration has also been demonstrated in humans. Intra-aortic adenosine administration increased ventilation, with a stronger response observed when adenosine was infused closer to the carotid circulation, suggesting a carotid body-mediated mechanism (Watt et al., 1987). Further supporting evidence comes from studies using dipyridamole (an adenosine re-uptake inhibitor), which increased ventilation, heart rate, systolic blood pressure and muscle sympathetic nerve activity in healthy individuals. In a more recent study, intra-carotid adenosine injections in human patients led to a dose-dependent increase in ventilation and blood pressure, effects that were significantly blunted by carotid body ablation (Tubek et al., 2016). These results confirm the key role of adenosine in modulating ventilatory and cardiovascular responses via the carotid body.

Understanding the mechanisms that lead to adenosine-induced carotid body excitation may help further our understanding of how carotid body function may be altered in disease. Carotid body hyperactivity is associated with various pathological states which lead to an elevated basal carotid body output. Whether adenosine could be mediating these changes is currently unknown.

It is becoming increasingly evident that adenosine sets the basal carotid body discharge as opposed to ATP. Inhibition of adenosine receptors using 8-SPT or caffeine, attenuates basal chemoafferent activity *ex vivo* (Holmes et al., 2018b) and catecholamine secretion *in vitro* respectively (Conde et al., 2006). By selectively inhibiting membrane bound CD73 using a,β-methylene ADP (AOPCP), the amount of adenosine recovered from normoxic carotid bodies was reduced. This reduction did not occur in the presence of an ENT blocker, strongly suggesting that adenosine

formation in normoxia is driven by extracellular catabolism of ATP (Conde & Monteiro, 2004). Indeed, inhibition of CD73 in the intact whole carotid body-nerve preparation, severely abolishes chemoafferent discharge, an effect not seen with ENT inhibition, thus indicating CD73 as a vital enzyme in generating adenosine and establishing normoxic carotid body activity (Holmes et al., 2018b). Figure 1.3 summarises adenosine formation and actions in the carotid body.

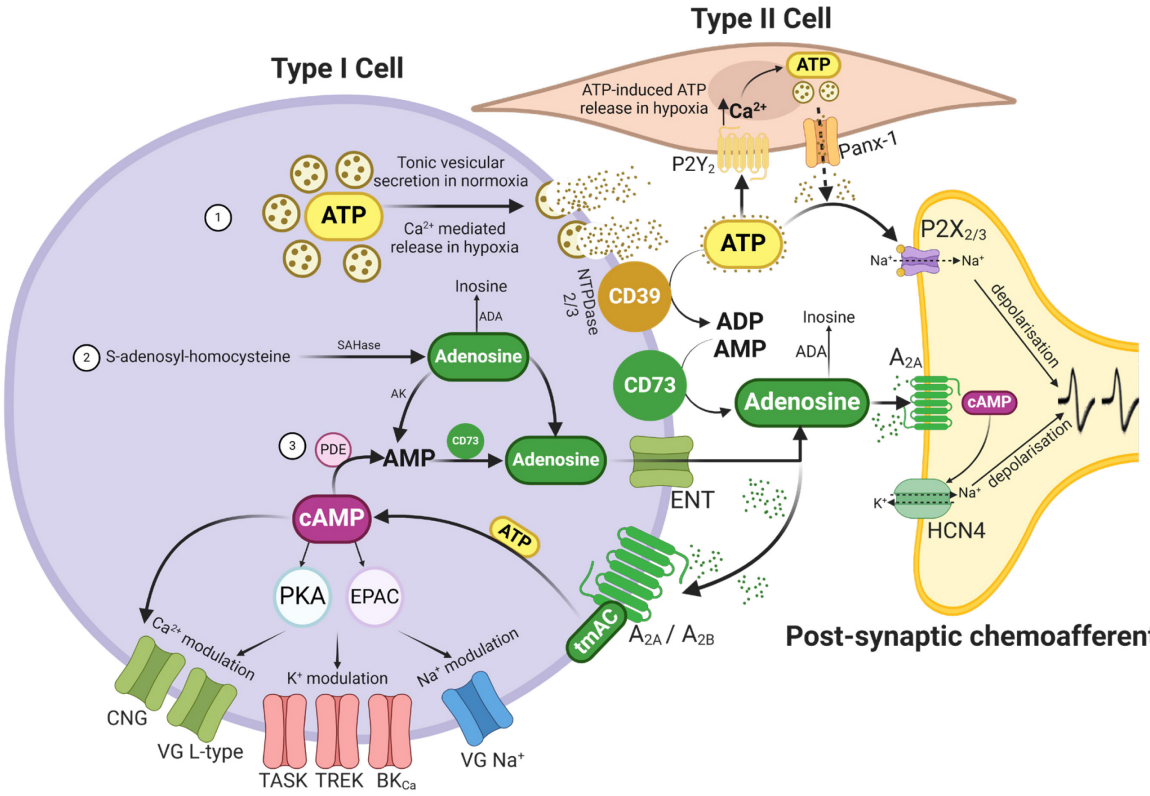

Figure 1.3 The central importance of CD73 in ATP breakdown and adenosine signalling

Diagram illustrating the mechanisms of purinergic signalling and neurotransmission in the carotid body. **(1)** In normoxia, type I cells continuously release ATP, which is metabolised extracellularly by ecto-nucleotidases such as CD39 (NTPDase) into ADP and AMP, with AMP further converted into adenosine by CD73 (ecto-5'-nucleotidase). Adenosine is degraded by adenosine deaminase (ADA) into inosine or by adenosine kinase (AK) into AMP. **(2)** Alternatively, adenosine can be generated intracellularly via hydrolysis of S-adenosyl-homocysteine by S-adenosyl-homocysteine hydrolase (SAHase) and transported into the synapse via equilibrative nucleoside transporters (ENT), increasing synaptic adenosine levels. Under hypoxia, elevated intracellular Ca^{2+} enhances ATP release, which activates $P2Y_2$ receptors on type II cells, triggering further ATP release through Pannexin-1 (Panx-1) channels. ATP excites chemoafferents via ionotropic $P2X_{2/3}$ receptors or is further degraded by CD39 and CD73, contributing to the adenosine pool. Adenosine binds post-synaptically to A_{2A} metabotropic receptors, activating transmembrane adenylyl cyclase (tmAC) to generate cAMP, which increases excitability. Pre-synaptically, adenosine also binds to A_{2A} and A_{2B} receptors on type I cells, where increased cAMP activates Protein Kinase A (PKA) and exchange proteins activated by cAMP (EPAC), modulating ion channel activity to reduce hyperpolarization and increase excitability, thereby promoting ATP release and adenosine formation in a positive feedback loop. **(3)** cAMP is broken down by phosphodiesterases (PDE) into AMP, which can be further metabolised into adenosine. Ion channel abbreviations: cyclic nucleotide-gated (CNG), TWIK-related acid-sensitive K^+ (TASK), TWIK-related K^+ (TREK), large conductance calcium-activated K^+ (BK_{Ca}), voltage-gated (VG), and hyperpolarization-activated cyclic nucleotide-gated (HCN4). Figure created using Biorender.com.

1.2.3 The role of CD73 and adenosine in hypoxia/hypercapnia

Adenosine plays a well-documented role in the carotid body's response to hypoxia. Early studies showed that *in vivo* administration of 8-SPT, an A_2 receptor antagonist, attenuated the increase in chemoafferent discharge during hypoxia (McQueen & Ribeiro, 1986). This antagonist also reduced the acute phase of the hypoxic ventilatory response in rats. In humans, adenosine infusion enhanced the hyperventilatory response to hypoxia, further supporting its role in peripheral chemoreceptor activation (Maxwell et al., 1986).

Under mild hypoxia (10% O_2), extracellular adenosine levels rise significantly by 174% above normoxic levels. However, at more severe hypoxia (5% and 2% O_2), ATP levels continue to increase, while adenosine levels remain unchanged. This suggests that CD73 may have reached its maximal activity and saturation point (Conde et al., 2012b). The origin of adenosine in hypoxia remains debated. Measurements in whole carotid body tissue showed that blocking ENTs along with CD73 inhibition (using AOPCP) reduced adenosine levels by an additional 45% compared to CD73 inhibition alone, suggesting that some adenosine is produced intracellularly and exported (Conde et al., 2012b). However, another study found that while ENT blockade had no effect on the chemoafferent response to hypoxia, CD73 inhibition alone significantly blunted the response, implying that extracellular ATP breakdown is the primary source of adenosine (Holmes et al., 2018b).

Further analysis showed that while AOPCP did not alter the peak hypoxic discharge at a single severe hypoxia level, it modified the response to graded hypoxia. In whole carotid body preparations, reducing the superfusate PO_2 typically results in an

exponential increase in chemoafferent discharge. AOPCP caused a leftward shift in the oxygen-response curve, meaning a lower PO_2 (more severe hypoxia) was required to trigger exponential discharge (Holmes et al., 2018b). This suggests that CD73 influences the sensitivity of the hypoxic response, though the precise mechanism remains unclear.

CD73 and adenosine also play a role in carotid body hypercapnic chemotransduction. During hypercapnia, extracellular adenosine levels increase by approximately 50% above normocapnic levels (Sacramento et al., 2018). In isolated rat type I cells, hypercapnia induces calcium influx, which can be blocked by the A_{2B} receptor antagonist MRS-1754, indicating a role for A_{2B} receptor activation (Livermore & Nurse, 2013). In whole carotid body preparations, hypercapnia-induced chemoafferent discharge is reduced by 34% with A_{2A} receptor inhibition and by up to 59% with combined A_{2A} and A_{2B} blockade (Sacramento et al., 2018). This aligns with findings showing that blocking CD73, adenosine receptors and tmAC, but not sAC, reduces the chemoafferent response to hypercapnia by 50% or more (Holmes et al., 2015). These results suggest that the excitatory action of CD73 and adenosine in both hypercapnia and hypoxia are mediated by the second messenger cAMP through activation of tmAC.

1.2.4 The importance of cAMP as a key second messenger in the carotid body

Adenosine activates four G protein-coupled receptors: A_1, A_{2A}, A_{2B}, and A_3. These receptors regulate adenylyl cyclase (AC) activity, influencing intracellular cAMP levels. A_1 and A_3 receptors are G_i-coupled and inhibit cAMP production, while A_{2A} and A_{2B} receptors are G_s-coupled and increase cAMP (Sheth et al., 2014). However, growing evidence suggests that adenosine receptors can also activate other G proteins, such

as G_q, indicating a more complex signalling network (Conde et al., 2017; Nunes et al., 2014). In the carotid body, A_{2A} and A_{2B} receptors are expressed on type I cells, with A_{2A} also present on post-synaptic afferent terminals (Figure 1.3). In contrast, A_1 and A_3 receptor mRNA is not found in the carotid body but A_1 mRNA is abundantly expressed in the petrosal ganglion (Conde et al., 2006; Gauda et al., 2000; Kobayashi et al., 2000a; Livermore & Nurse, 2013).

Adenosine can excite carotid body activity both pre- and post-synaptically by activating tmAC, which converts intracellular ATP into cAMP. Multiple tmAC isoforms are expressed in the rat carotid body, with tmAC-1 and tmAC-4 showing the highest levels, tmAC- 2, tmAC-3, tmAC-6 and tmAC-9 showing moderate expression, while tmAC-5, tmAC-7 and tmAC-8 are absent (Nunes et al., 2013). Assuming mRNA levels correlate with protein expression, this suggests a high rate of cAMP production in the carotid body. Adenosine and A_2 receptor agonists have been shown to increase cAMP levels in the rat carotid body, similar to increases observed in hypoxia (Conde et al., 2008; Monteiro et al., 1996; Perezgarcia et al., 1990). However, the precise mechanism linking adenosine, cAMP and carotid body excitability remains under investigation.

Early studies showed that stable cAMP analogues reduce the amplitude of 4-aminopyridine (4-AP)-sensitive K^+ currents in dissociated rabbit type I cells (Lopez-Lopez et al., 1993). Later, adenosine was also found to decrease 4-AP-sensitive K^+ currents in isolated rat type I cells, although whether this effect is cAMP-dependent remains unclear (Vandier et al., 1999). Adenosine also inhibits TASK-1 channels, leading to depolarisation and calcium influx via a mechanism dependent on PKA, which is activated by cAMP (Xu et al., 2006). In contrast, some studies have found that

inhibiting PKA has no effect on catecholamine release induced by hypoxia, suggesting that cAMP may act independently of PKA. One alternative target of cAMP is exchange protein activated by cAMP (EPAC) which when activated can counteract AC inhibition and potentiate Ca^{2+} signalling. Notably, blocking EPAC reduced hypoxia-neurosecretion by up to 50% (Rocher et al., 2009; Thompson & Wyatt, 2011). Additionally, cAMP may activate CNG channels, further promoting calcium entry (Peng et al., 2023; Peng et al., 2025). Adenosine therefore can modulate all aspects of the hypoxic chemotransduction cascade including type I cell depolarisation, calcium influx, neurosecretion and chemoafferent discharge. A summary of proposed downstream targets of adenosine signalling is shown in Figure 1.3.

Given the important role of CD73 in establishing basal chemoafferent activity and in regulating sensitivity to hypoxic and hypercapnic stimuli, increased CD73 expression and/or function may play a significant, yet unrecognised role in contributing to carotid body hyperactivity in pathology. Carotid body hyperactivity is increasingly recognised as a driver of cardiovascular dysfunction, promoting increased sympathetic tone to the vasculature and heart in conditions such as obstructive sleep apnoea, chronic heart failure and chronic obstructive pulmonary disease (COPD) (Iturriaga et al., 2021). Chronic hypoxia (CH) is a hallmark of COPD and is associated with increased sympathetic reflex activation secondary to carotid body plasticity (Kent et al., 2011; Stickland et al., 2016). This thesis will develop and validate an animal model of CH and carotid body hyperactivity, implemented by exposing Wistar rats to 12% inspired oxygen (F_iO_2) for 10 days. Experiments will then use this CH model to determine the importance of CD73 in promoting carotid body hyperactivity and evaluate if targeting CD73 can acutely modify cardiovascular and respiratory function.

1.3 The importance of CH in health and disease

1.3.1 COPD, CH and cardiovascular disease

COPD is a collective term for a group of respiratory diseases characterised by airflow obstruction, persistent cough, mucus hypersecretion, dyspnoea (breathlessness) and exercise intolerance. Airflow obstruction is progressive and is not fully reversible with bronchodilators, separating it from other obstructive respiratory diseases like asthma (Mannino & Buist, 2007). The two primary subtypes of COPD are emphysema and chronic bronchitis, which often coexist. Emphysema is defined by the destruction of lung tissue, leading to permanent enlargement of alveolar spaces and reduced gas exchange efficiency. Chronic bronchitis is characterised by inflammation of the airways, resulting in persistent cough and mucus hypersecretion. Over time, chronic bronchitis can progress to emphysema (Decramer et al., 2008).

COPD is a major global health burden and is currently the fourth leading cause of death worldwide, following ischemic heart disease, COVID-19 and stroke. According to the World Health Organisation (WHO), in 2021 alone, COPD caused 3.5 million deaths, accounting for approximately 5% of global deaths (WHO, 2025). Although COPD primarily affects the lungs, it has significant systemic consequences. The condition is heavily linked to cardiovascular complications including hypertension, arrhythmias and heart disease, with emerging evidence suggesting that cardiovascular disease is a major cause of death in COPD patients, second only to respiratory failure (Agusti & Soriano, 2008; Morgan et al., 2018; Rabe et al., 2018). Given the growing recognition of these complications, further research is needed to understand the mechanisms linking COPD and cardiovascular dysfunction, with the goal of developing treatments to improve patient outcomes.

The WHO places tobacco smoking as the greatest risk factor for COPD, accounting for approximately 70% of cases in high-income countries (WHO, 2025). Long-term exposure to harmful chemicals in cigarette smoke triggers a persistent inflammatory response in the lungs, leading to the recruitment of immune cells that release proteases and toxins, causing irreversible tissue damage (Barnes et al., 2003). In developing countries, air pollution and occupational harmful inhalants are significant risk factors due to the continued use of fossil fuels (Antuni & Barnes, 2016).

Genetics also play a critical role, with alpha-1 antitrypsin deficiency (caused by mutations in the *SERPINA1* gene) being the most well-documented genetic predisposition. This deficiency disrupts the balance of proteases in the lungs, leading to excessive tissue breakdown and increased susceptibility to emphysema (Ingebrigtsen et al., 2010). While single nucleotide polymorphisms in various other genes have been linked to COPD, none have been specifically associated with CD73 (Wain et al., 2017). In recent years, women have shown a higher susceptibility to COPD, although the reasons remain unclear. Possible explanations include similar smoking habits to men, the loss of oestrogen's protective effects post-menopause and sex differences in immune responses to tobacco smoke (Antuni & Barnes, 2016; Han et al., 2007). SNPs in CD73 do occur, however, they have primarily been associated with epilepsy and schizophrenia (Peng et al., 2024; Shi et al., 2023). Additionally, respiratory infections, both bacterial and viral, can not only contribute to COPD development but also trigger acute exacerbations, worsening symptoms and disease progression (Antuni & Barnes, 2016).

Despite its significant impact, one of the most overlooked aspects of COPD is the effect of CH on carotid body function. In moderate to severe COPD, prolonged exposure to low arterial oxygen levels induces a state of CH, forcing the body to adapt in an attempt to maintain oxygen homeostasis (Kent et al., 2011). While systemic adaptations, such as increased oxygen-carrying capacity help to compensate for hypoxia (Marshall, 2015), adaptations in the carotid body play an important role in respiratory and cardiovascular regulation. In response to CH, the carotid body undergoes profound changes, including sustained hyperactivity and heightened sensitivity to hypoxia. This increased excitability leads to excessive ventilatory drive, but more importantly, it also stimulates the sympathetic nervous system, which can significantly elevate blood pressure and contribute to cardiovascular morbidity (Iturriaga et al., 2021; Lopez-Barneo et al., 2016).

The role of the carotid body in COPD-related cardiovascular dysfunction remains a severely under-researched area, despite mounting evidence that its persistent activation may be a key driver of vascular dysfunction and heart disease in COPD patients (Phillips et al., 2018; Stickland et al., 2016). The link between CH, carotid body overactivity and excessive sympathetic output presents a critical yet underexplored mechanism contributing to the systemic complications of COPD. Given that cardiovascular disease is one of the leading causes of death in COPD, investigating how carotid body dysfunction influences autonomic and vascular regulation could offer novel therapeutic targets to mitigate the long-term consequences of the disease and improve survival.

1.3.2 Haematological and cardiovascular adaptations to CH

Our understanding of physiological adaptations to CH has largely been shaped by studies on high-altitude exposure, where reduced barometric pressure leads to a lower PO_2 and decreased blood oxygen levels (Peacock, 1998). The initial response to high altitude involves immediate activation of the carotid body, which increases ventilation and triggers other reflex mechanisms, helping to compensate for reduced oxygen availability (Figure 1.1).

Over time, cardiovascular adaptations also take place. In the early days of CH, local vasodilation in skeletal muscle and other tissues is enhanced, augmenting blood flow and oxygen delivery, primarily through the actions of adenosine, nitric oxide and prostaglandins (Marshall & Davies, 1999; Ray et al., 2002; Thomas & Marshall, 1997). However, after approximately seven days, the sensitivity to these vasodilators begins to decline (Walsh & Marshall, 2006). This is thought to be due to an increase in red blood cell (RBC) production and haemoglobin levels, which raise blood oxygen content and restore oxygen delivery to tissues (Marshall & Davies, 1999; Walsh & Marshall, 2006). Angiogenesis also contributes to improving oxygen supply and reducing vascular resistance, counteracting the waning vasodilation (Krock et al., 2011; Smith & Marshall, 1999; Thomas & Marshall, 1997; Walsh & Marshall, 2006).

In contrast to the systemic circulation, hypoxia induces vasoconstriction in the pulmonary circulation, which helps redirect blood flow to better oxygenated regions of the lung, maintaining ventilation-perfusion matching (Sommer et al., 2016). However, prolonged pulmonary vasoconstriction can lead to pulmonary hypertension and pulmonary oedema, often followed by right ventricular hypertrophy (RVH) and cardiac

remodelling (Nathan et al., 2019). Pulmonary hypertension is a major complication in COPD patients and significantly worsens disease progression (Kent et al., 2011; Loring et al., 2009). CH also triggers metabolic adaptations at the cellular level, including a shift toward glycolysis, reduced fatty acid oxidation and increased lactate production (O'Brien et al., 2020; Semenza et al., 1994).

At the molecular level, these adaptations are primarily regulated by the HIF transcriptional pathway, which controls the expression of hundreds of genes involved in oxygen homeostasis (Bishop & Ratcliffe, 2014; Bishop & Ratcliffe, 2025; Ortiz-Barahona et al., 2010). HIF is a heterotrimeric transcription factor composed of a constitutively expressed HIF-β subunit and an oxygen-regulated HIF-α subunit. Under normal oxygen conditions, oxygen-sensitive prolyl hydroxylase domain (PHD) enzymes hydroxylate two proline residues on HIF-α, allowing the von Hippel-Lindau (VHL) ubiquitin ligase complex to target it for proteasomal degradation (Semenza, 2012). Additionally, factor-inhibiting HIF (FIH) hydroxylates an asparagine residue in the transactivation domain of HIF-α, preventing the recruitment of transcriptional co-factors required for gene activation (Lando et al., 2002). Under hypoxic conditions, PHD and FIH enzymes become inactive, allowing HIF-α to escape degradation, dimerise with HIF-β and initiate transcription of hypoxia-responsive genes. HIF-1α is expressed in all multicellular organisms, while the HIF-2α isoform is vertebrate-specific and exhibits more cell-type selectivity (Bishop & Ratcliffe, 2014; Bishop & Ratcliffe, 2025; Semenza, 2012).

Some well-known examples of HIF-dependent transcription include the upregulation of erythropoietin (EPO), which stimulates RBC, haemoglobin synthesis and elevation of

vascular endothelial growth factor (VEGF) promotes angiogenesis (Bishop & Ratcliffe, 2015; Kaissling & Le Hir, 2008; Krock et al., 2011; Semenza & Wang, 1992). Evidence suggests that many of these adaptations are species dependent, in addition to the intensity and duration of the hypoxic stimulus (Arias-Reyes et al., 2021; Pamenter & Powell, 2016). Therefore, initial experiments in this thesis characterised the haematological and cardiac adaptations in a model of CH in Wistar rats exposed to an F_iO_2 of 12% for 10 days. Once validated, this CH model was then used to evaluate the importance of CD73 in promoting carotid body hyperactivity and cardio-respiratory pathology. In the kidney, CD73 has been used to identify EPO-producing renal interstitial fibroblasts (Bachmann et al., 1993; Maxwell et al., 1993). Studies have shown that anaemia (mimics systemic hypoxia) increases the number of CD73-positive interstitial cells, alongside elevated EPO production (Pan et al., 2011). This supports the rationale for investigating whether the distribution of CD73-expressing cells is also altered in CH carotid bodies, as explored in Chapter 4.

1.3.3 Carotid body adaptations to CH: a potential role of CD73

During prolonged exposure to hypoxia, ventilatory acclimatisation to hypoxia (VAH) occurs, characterised by a progressive increase in baseline ventilation and, in some cases, an enhanced hypoxic ventilatory response (HVR). The carotid body plays a key role in this adaptation, as evidenced by carotid body denervation studies across various species where VAH fails to occur (Barnard et al., 1987; Bouverot et al., 1973; Forster et al., 1981). Similarly, humans who have undergone carotid surgery exhibit poor adaptation to high altitudes (Roeggla et al., 1995). While CH generally augments HVR, prolonged exposure can blunt this response, as seen in native high-altitude populations (Lahiri et al., 1976; Pamenter & Powell, 2016). Consequently, CH

enhances carotid body sensitivity, leading to a higher chemoafferent output at any given oxygen level. However, the specific mechanisms underlying carotid body plasticity and VAH remain under investigation.

Carotid body type I cells express low levels of HIF-1α under normoxic conditions, whereas HIF-2α mRNA is present at significantly higher levels and has been shown to be the driver of carotid body development during embryogenesis (Fielding et al., 2018; Macias et al., 2018; Zhou et al., 2016). Mice with partial HIF-1α deficiency show a diminished chemoafferent response to acute hypoxia but retain a normal HVR *in vivo*. Interestingly however, these mutant mice fail to develop VAH following CH exposure. (Kline et al., 2002). However, other studies utilising both inducible and constitutive HIF-1α inactivation in mice found no effect on HVR after seven days of CH (Hodson et al., 2016). This led researchers to question the role of HIF-1α in carotid body adaptation to CH and instead propose that HIF-2α may be responsible. Indeed, both inducible and constitutive inactivation of HIF-2α significantly blunted the augmented HVR in CH (Hodson et al., 2016). Interestingly, despite this, HIF-2α-deficient mice still exhibit a robust response to acute hypoxia prior to CH exposure. While pharmacological inhibition of HIF-2α with PT2385 does mildly blunt the HVR in air-reared wild type mice, suggesting a possible role, future studies are warranted (Cheng et al., 2020). At the cellular level, genetic inactivation HIF-2α in carotid body type I cells show a severe attenuation in catecholamine release, calcium influx and ROS production. Similar effects are observed in *Cox4i2* knockout models, indicating that HIF-2α regulates this unique mitochondrial subunit, which is key to the oxygen sensitivity and hypoxic responses of the carotid body (Moreno-Domínguez et al., 2020). Furthermore, the functional significance of HIF-2α on carotid body adaptation to CH was confirmed through experiments specifically inactivating HIF-2α in tyrosine hydroxylase-positive

(TH^+) cell populations, which include carotid body type I cells (Fielding et al., 2018). Inducible inactivation of HIF-2α in these TH^+ cells markedly blunted the enhanced HVR following CH which was later supported by similar findings with pharmacological targeting of HIF-2α using PT2385 (Cheng et al., 2020; Fielding et al., 2018). While these findings establish a functional role for HIF-2α *in vivo*, the precise mechanisms underlying carotid body plasticity and its contribution to adaptation remain unknown.

Carotid body hypertrophy has been proposed as a major factor contributing to increased carotid body hyperactivity and sensitivity to hypoxia, likely due to an expansion of oxygen-sensitive type I cells and increased vascular and extravascular volume (Clarke et al., 2000; Fielding et al., 2018; Lopez-Barneo et al., 2016). However, the origin of new type I cells in response to CH remains a subject of debate. One hypothesis suggests that a population of quiescent, glia-like type II cells functions as adult stem cells under normoxic conditions. In hypoxic environments, these cells differentiate into $Nestin^+$ progenitors, which then mature into type I cells (Pardal et al., 2007). However, *in vitro* experiments culturing these progenitors, also referred to as neuroblasts or neurospheres, showed no proliferative response to hypoxia even at oxygen levels as low as 1% O_2. This raises the question of what specific stimulus drives type II cell differentiation into new type I cells. Structural evidence from electron microscopy studies reveals that type I and type II cells form close synaptic interactions, with a gap of less than 50nm (Leonard & Nurse, 2022; Platero-Luengo et al., 2014). Notably, a high proportion of secretory vesicles in type I cells are oriented toward these synapses, suggesting a paracrine signalling mechanism. Type I cells are believed to release mediators such as endothelin-1, which stimulate type II stem cells to differentiate. This differentiation process occurs gradually over days to weeks of

sustained hypoxia (Chen et al., 2002; Chen et al., 2007; Paciga et al., 1999; Platero-Luengo et al., 2014).

An alternative hypothesis proposes that type I cell expansion results from self-renewal of pre-existing type I cells. Lineage-tracing studies indicate that newly dividing TH^+ cells originate from an existing TH^+ population, with their proliferation highly dependent on HIF-2α (Fielding et al., 2018). Sobrino and colleagues identified a subpopulation of mitotic TH^+ cells, termed immature neuroblasts which express low levels of TH alongside the HNK-1 marker. These cells may contribute to fast neurogenesis rapidly expanding the type I cell population within 24-48 hours of hypoxia without altering overall carotid body size. This mechanism allows for a swift adaptive response to low oxygen levels (Sobrino et al., 2018). The potential changes in carotid body morphology, including alterations in volume, type I cell density and vascularity, will be investigated in the CH model used in this thesis.

While type I cell hyperplasia and carotid body hypertrophy may explain enhanced carotid body hyperactivity, they are unlikely to be the sole contributors. Evidence suggests that even when carotid body hypertrophy is prevented using an endothelin-1 antagonist in CH, basal chemoafferent activity and hypoxia sensitivity *ex vivo* remain significantly elevated compared to controls (Chen et al., 2007). This indicates that other cellular mechanisms contribute to carotid body hyperexcitability, independent of growth-related changes.

One potential mechanism involves altered ion channel expression and activity, which could reduce hyperpolarization and make type I cells more excitable (Pulgar-Sepúlveda et al., 2018). Indeed, studies show a reduction in K^+ current density and an increase in Na^+ current proportion in CH type I cells (Hempleman, 1995). Functional carotid body hyperactivity has been linked to upregulation of the Nav1.1 subunit of voltage-gated Na^+ channels (Caceres et al., 2007). Additionally, TASK-like currents show enhanced inhibition after CH (Ortiz et al., 2009). Isolated CH rat type I cells display a 1.5-fold increase in intracellular calcium levels when measured in response to a single level of acute hypoxia compared to normoxic controls, potentially due to increased voltage-gated calcium current density (Hempleman, 1996; Livermore & Nurse, 2013). However, as yet, it is unclear if chemoafferent hypoxic sensitivity is augmented in CH carotid bodies when measured over a physiological PO_2 range. cAMP has been directly implicated in modulating Na^+ density and calcium signalling, as normoxic incubation with stable cAMP analogues mimics the adaptions seen in response to CH, strongly suggesting its role in mediating carotid body hyperactivity (Stea et al., 1995).

Given the importance of purinergic signalling in carotid body physiology and the key role of adenosine in cAMP generation, it is plausible that tonic enhancement of adenosine production via CD73 contributes to carotid body hyperactivity. Indeed, increased calcium influx in response to hypoxia can be inhibited by A_{2B} receptor antagonists (Livermore & Nurse, 2013). Chronic administration of caffeine, a non-selective A_2 receptor antagonist, significantly blunts the heightened chemoafferent discharge in CH rats *ex vivo*. Enhanced adenosine production may result from HIF-dependent upregulation of CD73. In intestinal epithelial cells, HIF-1α inhibition completely prevents the hypoxia-induced increase in CD73 expression (Synnestvedt

et al., 2002). Furthermore, chronic anaemia Similarly, in PC12 cells (a model for carotid body type I cells) CD73 protein expression increases after CH (Kobayashi et al., 2000b). HIF also regulates A_2 receptor expression, with HIF-1α playing a dominant role in A_{2B} transcription (Kong et al., 2006), while HIF-2α strongly regulates A_{2A} (Brown et al., 2011).

In the carotid body, CH has been shown to upregulate NTPDase-3 and CD73 mRNA expression while downregulating NTPDase-1 and NTPDase-2 (Salman et al., 2017). Additional analysis revealed a reduction in ENT-1 and ENT-2 expression, strongly suggesting that increased adenosine production is driven by extracellular CD73 and other ecto-enzymes (Salman & Nurse, 2018). However, these findings do not clarify whether CD73 plays a functional role in CH or whether its enzymatic activity is enhanced. To address this, carotid body activity will be measured directly using an intact superfused whole-carotid body preparation, allowing for real-time recording of chemoafferent discharge in the presence of a CD73 or tmAC inhibitor. This thesis will be the first to explore whether CD73 is the primary driver of carotid body hyperactivity and whether targeting this enzyme could serve as a potential therapeutic strategy for carotid body-related diseases.

1.3.4 The carotid body as a therapeutic target for CH-related diseases

Carotid body hyperactivity is increasingly recognised as a major contributor to cardiovascular disease and increased mortality (Iturriaga, 2018). Overexcitation of the carotid body has been linked to conditions such as obstructive sleep apnoea, heart failure, type 2 diabetes and COPD (Narkiewicz et al., 1998; Phillips et al., 2018; Schultz et al., 2015). The excessive sensory output from the carotid body heightens

sympathetic neuronal discharge to the vasculature, heart and other tissues, contributing to the development of hypertension, pro-arrhythmic events and insulin resistance (Linz et al., 2016; Paton et al., 2013; Thakkar et al., 2023). Therefore, understanding the mechanisms responsible for carotid body hyperactivity is crucial in identifying potential therapeutic targets.

In animal models of these diseases, carotid body removal via carotid sinus nerve section (CSNX) has been shown to reduce excessive sympathetic outflow, lower blood pressure, and in hypercaloric type 2 diabetic rats, restore insulin sensitivity (Abdala et al., 2012; McBryde et al., 2013; Ribeiro et al., 2013; Sacramento et al., 2017). However, no studies have yet quantified the cardio-respiratory changes in ventilation, blood pressure and heart rate in response to CSNX in the context of CH.

Preliminary human studies suggest similar benefits in patients with heart failure and neurogenic hypertension. CSNX has been shown to reduce sympathetic outflow, improve exercise tolerance and lower blood pressure, but these benefits were observed in only half of the patients studied (Narkiewicz et al., 2016; Niewinski et al., 2017). While these findings confirm that excessive carotid body activity contributes to disease progression, surgical intervention remains controversial. Unilateral CSNX appears to provide benefits for only up to 12 months, suggesting that the remaining intact carotid body can compensate over time (Narkiewicz et al., 2016). Bilateral CSNX, on the other hand, eliminates carotid body sensory activity entirely, which raises concerns, particularly during sleep when oxygen desaturation episodes occur. Moreover, in a small population of patients, it has been shown that even 5 years after bilateral carotid body ablation, the HVR remains almost completely absent, again

raising major safety concerns about the widespread therapeutic use of this surgical procedure (Niewinski et al., 2021). The carotid body plays a critical role in promoting arousal and increasing ventilation in response to hypoxia (Niewinski et al., 2017). Therefore, preserving some level of carotid body function is essential in the development of new treatments, which may be best achieved through pharmacological approaches.

In spontaneously hypertensive rats, $P2X_3$ mRNA is upregulated in chemoafferent neurons, consistent with expression data from human carotid bodies. $P2X_3$ receptor antagonists have been shown to reduce both sympathetic activity and blood pressure in hypertensive rats, but they have no effect in normotensive controls (Pijacka et al., 2016). This suggests that the carotid body is a viable pharmacological target (Paton et al., 2013). However, in diseases associated with CH, $P2X_{2/3}$ receptor expression appears to be unaltered, indicating that different pathophysiological mechanisms may underlie carotid body dysfunction in these conditions (He et al., 2006).

Notably, CD73 mRNA is suggested to be upregulated in CH, pointing towards enhanced adenosine production and signalling in playing a more significant role in diseases such as COPD. The final chapter of this thesis will explore the potential of targeting CD73 in CH animal models to determine whether CD73 inhibition can reverse carotid body hyperexcitation and, importantly, lower blood pressure. In hypercaloric models of prediabetes, adenosine receptor antagonism has been shown to normalise elevated blood pressure and restore insulin sensitivity, highlighting the therapeutic potential of targeting adenosine signalling (Conde et al., 2012a).

Identifying a treatment that can reduce resting carotid body hyperactivity while preserving its hypoxic sensitivity, particularly during sleep, would be highly advantageous. This thesis will investigate whether inhibiting CD73 achieves this balance. The findings will provide a foundation for determining whether CD73 or related adenosine signalling pathways could serve as viable therapeutic targets for carotid body-driven diseases.

1.4 General project aims and objectives

1. Develop and validate a model of CH by assessing key haematological, carotid body, cardiovascular and ventilatory adaptations (Chapter 3)

2. Examine changes in the cellular distribution of CD73 within the carotid body in response to CH using immunohistochemistry (Chapter 4)

3. Determine the functional importance of CD73 and cAMP in promoting carotid body hyperactivity in response to CH, using *ex vivo* measurements of carotid body chemoafferent activity (Chapter 5)

4. Examine if *in vivo* pharmacological targeting of CD73 in the carotid body is effective in modifying cardiovascular and respiratory parameters in CH animals without eliminating its ability to respond to acute hypoxia (Chapter 6)

CHAPTER 2

2. Methods

2.1 Animals and ethical approval

Male Wistar rats aged 6-9 weeks weighing 150-300g (Charles River Laboratories & Envigo, UK) were housed in a 12h-light/12h-dark cycle with unrestricted access to food and water (LabDiet®). All experiments and procedures were performed in accordance with the UK Animals (Scientific Procedures) Act 1986 and were approved by the University of Birmingham Animal Welfare and Ethical Review Body. Project licence PP9019875 was granted by the Home Office (UK) to carry out this research. A total of 84 rats were used.

2.2 Generation of a CH rat model

To investigate the role of CD73 in mediating carotid body hyperactivity and subsequent cardiovascular dysfunction under CH, a CH model was established. Rats were housed in pairs within an environmental chamber (BioSpherix, USA). On the first day, the F_iO_2 was gradually reduced from 21% to 12% over a 2-hour period. This gradual adjustment was designed to minimise stress compared to a sudden change in oxygen levels. The F_iO_2 was then maintained at 12% for 9-10 days.

Temperature and humidity were continuously monitored (Electronic Temperature Instruments Ltd, UK), with silica gel used to absorb excess water vapour and soda lime to remove CO_2 and ammonia. Built-in circulating fans ensured constant airflow. Rats were monitored daily for welfare, including brief removal (10-15 minutes) from the chamber for routine husbandry tasks such as replacing silica gel and soda lime,

changing the home cage, bedding and providing physical enrichment through handling. Control rats (normoxic group) were kept in ambient air for the same duration and received the same enrichments.

2.3 Surgical removal of carotid body tissue

Carotid body tissue was surgically excised, bilaterally, from rats under inhalation anaesthesia with 2-5% isoflurane in oxygen at a flow rate of 1.5 L min^{-1}. The correct depth of anaesthesia was confirmed by the absence of a pedal withdrawal reflex upon firm pinching of the hind paws. The dissected tissue included the common carotid artery (CCA), ECA, ICA, glossopharyngeal nerve (GPN) and a branch of the vagus nerve (VN). The CCAs were occluded using suture and cut above this tie, along the lateral margin and the final cut was made above the GPN. To preserve carotid body function and minimise severe hypoxia due to ischemia, the excised tissue was immediately transferred to an ice-cold bicarbonate-buffered extracellular physiological salt solution equilibrated with 95% O_2 and 5% CO_2. The solution contained (in mM): 25 $NaHCO_3$, 119 NaCl, 4.5 KCl, 1.2 $MgSO_4.7H_2O$, 1.2 NaH_2PO_4, 11 D-glucose, and 2.4 $CaCl_2$, equilibrated with 95% O_2 and 5% CO_2. Rats were culled via cervical dislocation, with death confirmed by exsanguination. Figure 2.1 illustrates a fully dissected carotid bifurcation ready for extraction.

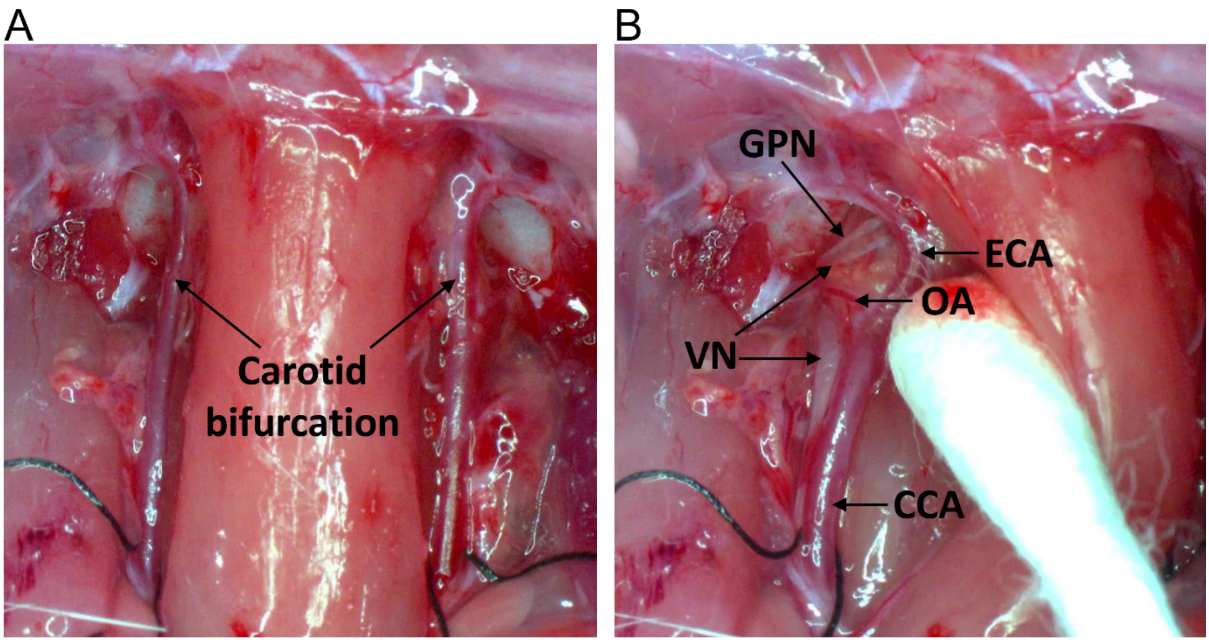

Figure 2.1 *in vivo* dissection and identification of rat carotid bifurcation

In vivo images of a dissected rat carotid bifurcation ready to be excised. **(A)** image shows identification of the carotid bifurcation after dissection. **(B)** image shows key structures to help guide the correct excision. Common carotid artery (CCA), external carotid artery (ECA), occipital artery (OA), vagus nerve (VN) and glossopharyngeal nerve (GPN). Surgery was performed under general anaesthesia in accordance with Home Office License approval (project licence PP9019875).

2.4 Extracellular chemoafferent electrophysiological recordings

2.4.1 Fine dissection of the carotid body and carotid sinus nerve

Direct measurements of carotid body activity can be achieved by recording chemoafferent discharge in an intact whole carotid body-carotid sinus nerve preparation *ex vivo* as previously described (Pepper et al., 1995). This technique was utilised in this thesis to explore the role of CD73 and adenosine mediated signalling on carotid body hyperactivity in CH. To achieve a good neuronal recording, the carotid bifurcation must be finely dissected *ex vivo* to isolate the carotid body and carotid sinus nerve which is encompassed by an abundance of connective tissue. The subsequent steps of this procedure can be categorised into 4 main stages as illustrated in Figures 2.2-2.5.

After surgical excision of the carotid bifurcation, the tissue was transferred to a small dissecting chamber (approx. 0.2mL) and pinned out at the CCA, ECA and the ICA. The carotid body tissue was continuously superfused with a bicarbonate-buffered extracellular physiological salt solution (see section 2.3) equilibrated with 95% O_2 and 5% CO_2. Initially, the lateral margins of the ECA and the ICA were trimmed to remove surrounding glandular, muscular and fatty tissue (Figure 2.2).

The carotid body tissue was turned over to expose the SCG as shown in Figure 2.3 A. Using fine forceps, the SCG was gently separated from surrounding connective tissue until a branch extending into the carotid body was visible (Figure 2.3 B). This branch was carefully cut, allowing the SCG to be removed (Figure 2.3 C). Any remaining superficial connective tissue and fat was also removed (Figure 2.3 D).

The tissue was turned back over, and the OA was located and removed (Figure 2.4 A & B). By dissecting the connective tissue around the GPN, an opening was created, revealing the CSN and a branch of the VN (Figure 2.4 C). The CSN, which crosses over the VN before joining the GPN, was carefully teased apart and detached from the VN. Once free, the VN can be removed. At this point, only the carotid body and CSN, attached to the GPN remain. For structural stability during further dissection, leaving some fat and connective tissue lateral to the GPN can be beneficial. This remaining tissue acts as an anchor, facilitating easier handling and dissection of the CSN.

Connective tissue lateral to the CSN was meticulously teased apart to optimise the extracellular neuronal recording signal (Figure 2.5 A-C). Further examples of the CSN dissection are shown in Figure 2.5 D-F. The CSN was sectioned to expose nerve fibres and axons (Figure 2.5 H-I). The tissue was partially digested by incubation in a bicarbonate-buffered physiological salt solution containing 0.075mg mL^{-1} Collagenase Type II (Sigma-Merk, C6885, UK) and 0.0025mg mL^{-1} Dispase Type I (Sigma-Merk, D4818, UK), equilibrated with 95% O_2 and 5% CO_2 at 37°C for approximately 30 minutes.

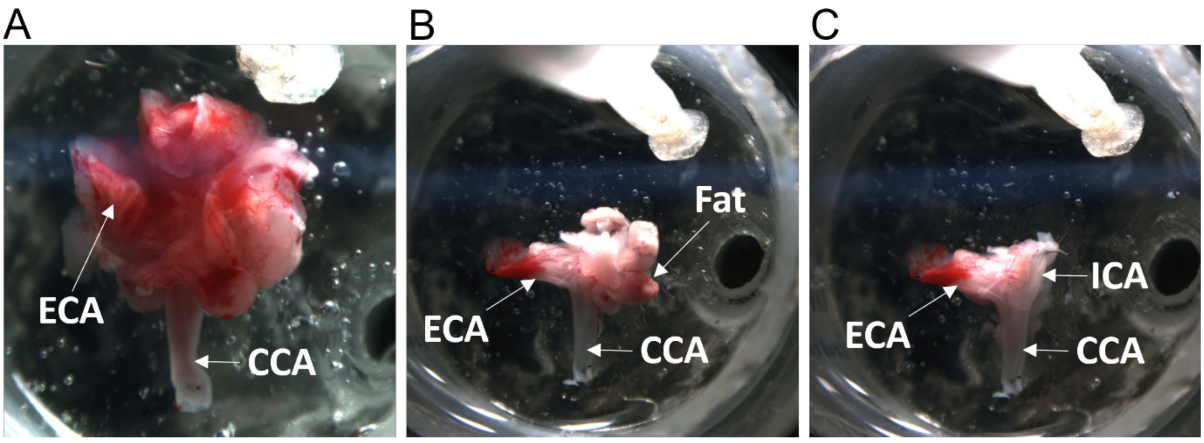

Figure 2.2 Pinning of rat carotid bifurcation

(A) an example of a surgically excised rat carotid bifurcation with surrounding glandular, muscular and fatty tissue still present. Tissue was initially pinned out by the common carotid artery (CCA). **(B)** trimmed lateral margin of the external carotid artery (ECA). **(C)** trimmed lateral margin of the internal carotid artery (ICA).

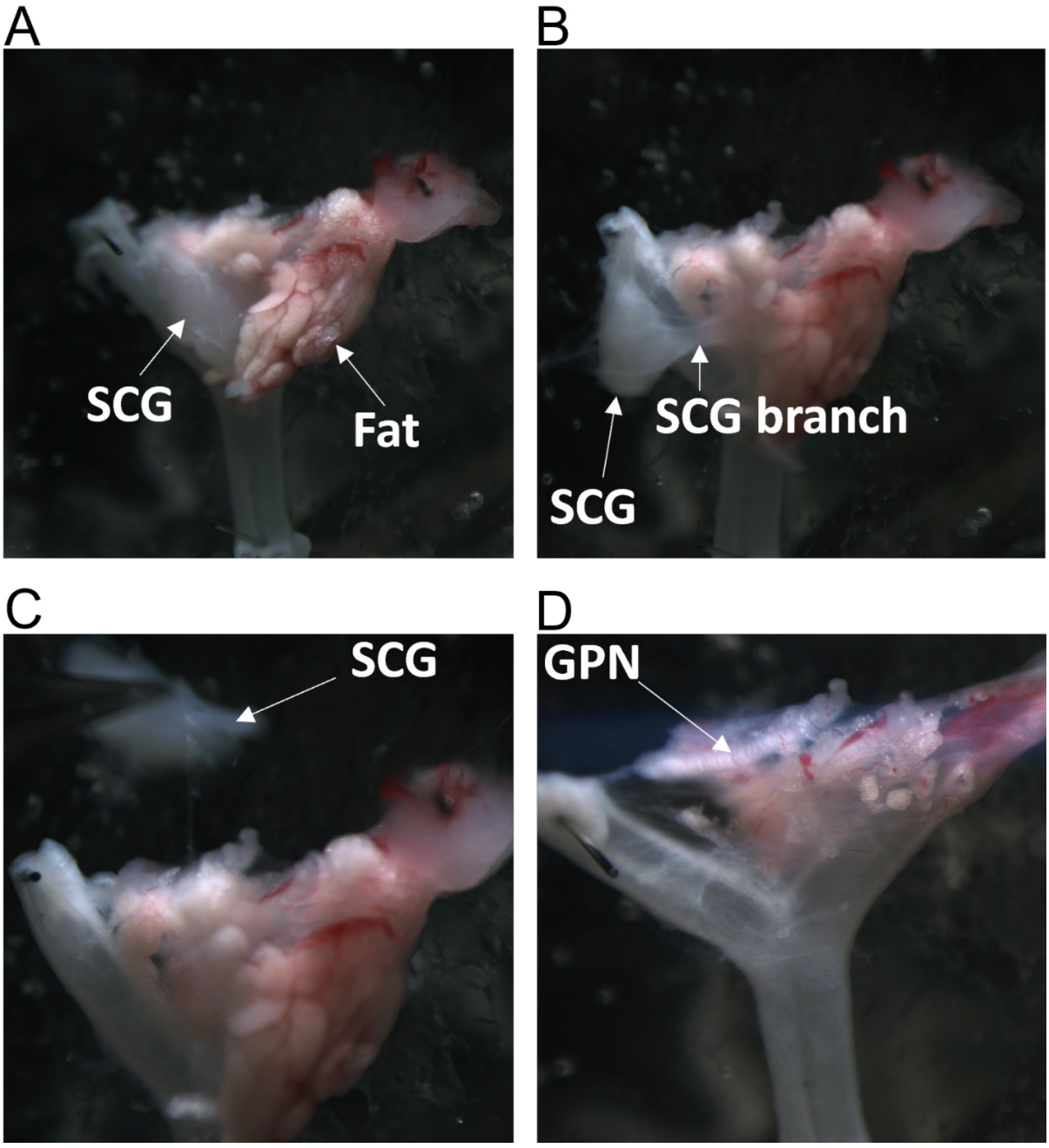

Figure 2.3 Removal of the super cervical ganglion

(A) identification of superior cervical ganglion (SCG) and superficial fat. **(B)** SCG was teased free using fine forceps until a branch can be seen going deep into the tissue. **(C)** removal of SCG after the branch was cut. **(D)** remaining fat was removed, and glossopharyngeal nerve (GPN) becomes visible.

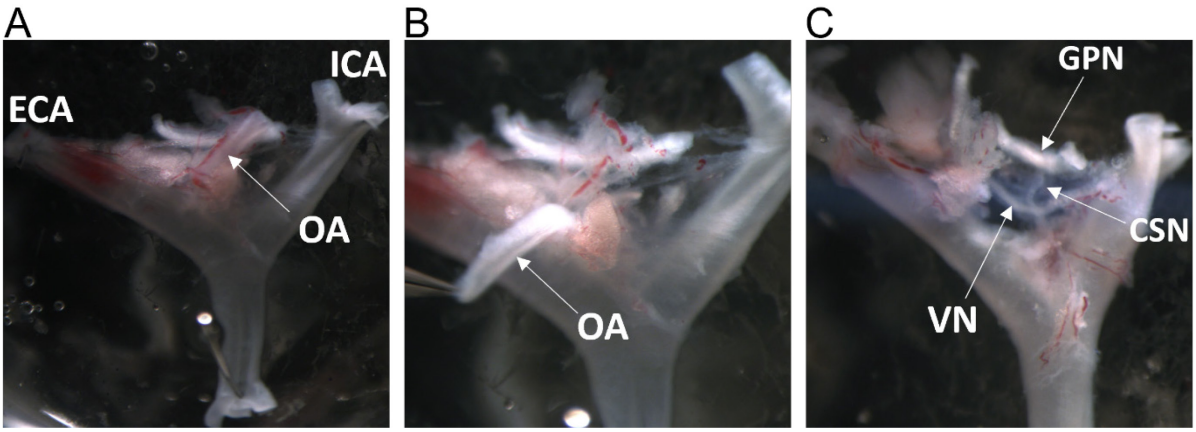

Figure 2.4 Removal of occipital artery and vagus nerve branch

(A) The occipital artery (OA) is identified as it branches from the external carotid artery (ECA) and extends toward the internal carotid artery (ICA). **(B)** The OA was teased free, retracted and cut at its base. **(C)** Removal of additional connective tissue and fat exposes the glossopharyngeal nerve (GPN), branch of the vagus nerve (VN) and carotid sinus nerve (CSN). The CSN, which is slightly attached to the VN, is carefully teased apart and separated.

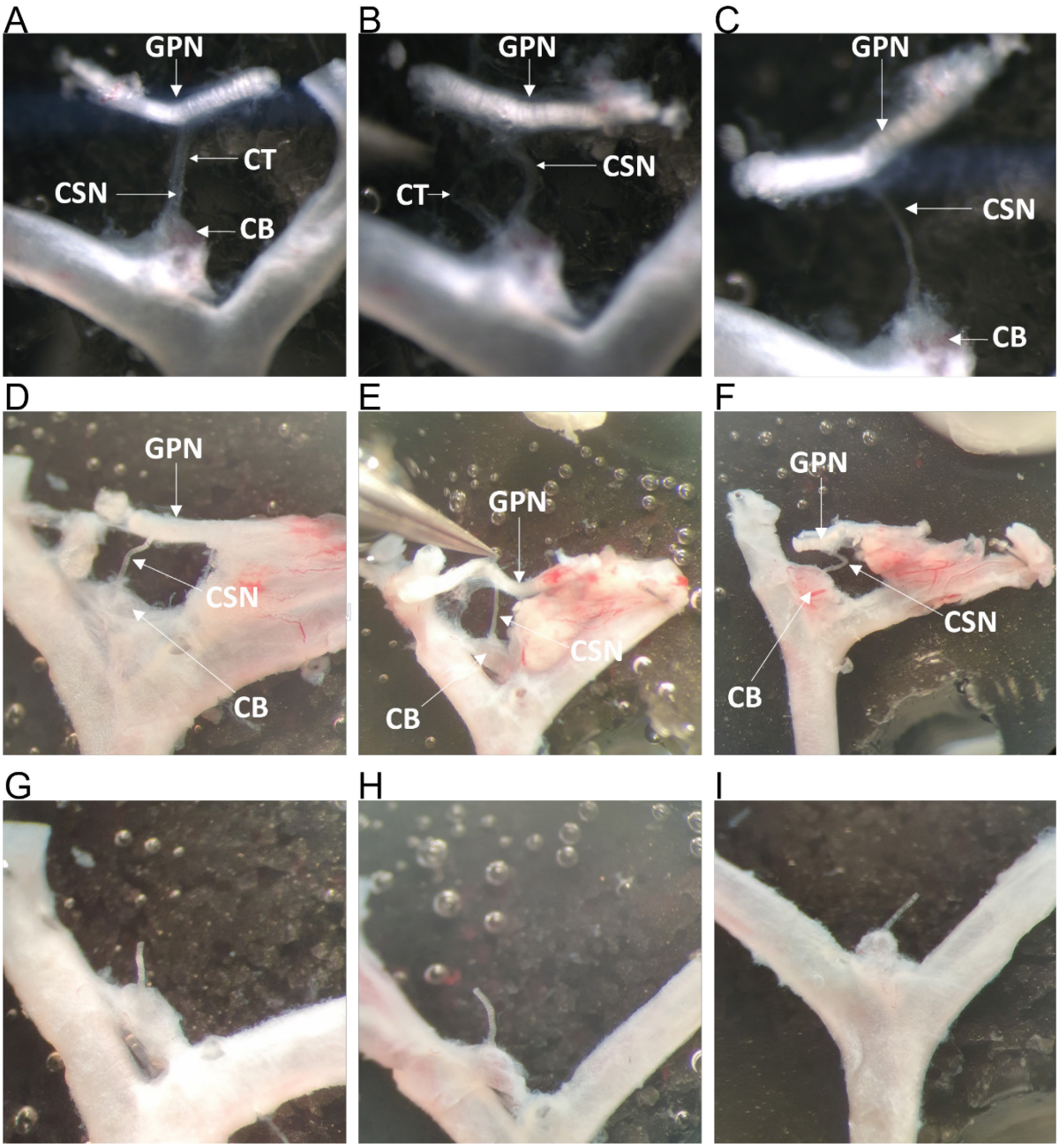

Figure 2.5 Removal of connective tissue on the carotid sinus nerve

(A) Lateral to the carotid sinus nerve (CSN) is connective tissue (CT) which can be seen as two brighter bands running along the nerve. **(B)** example dissection showing CT being teased from the CSN. **(C)** example image showing CSN free of CT ready to be sectioned. **(D-F)** Example dissections from three rat carotid bodies showing the CSN attached to the glossopharyngeal nerve (GPN) with the CSN free from CT. **(G-I)** example dissections at a higher magnification showing the CSN sectioned, ready for enzymatic digestion.

2.4.2 Superfusion system and extracellular recordings

After enzymatic incubation, the carotid body was pinned out in a small recording chamber of approximately 0.1mL and continuously superfused with a bicarbonate-buffered extracellular physiological salt solution equilibrated with 95% O_2 and 5% CO_2 to maintain pH at 7.4. The superfusate was heated to 37°C using a water bath and transferred to the recording chamber using a peristaltic pump through oxygen impermeable Tygon tubing (ID: 1.59mm, OD: 3.18mm, VWR, UK) at an approximate flow rate of 10mL min^{-1}. To compensate for heat loss during transfer, the superfusate was re-heated to 37°C before entering the chamber and constantly monitored using an in-line thermistor (RS Pro, K type probe, RS components Ltd, UK). The superfusate was removed from the chamber via another peristaltic pump through Tygon tubing (ID: 2.38mm, OD: 3.97mm, VWR, UK), either for disposal or recirculation into the original solution. Flow meters were used to accurately deliver the correct mixture of gases to the superfusate to achieve the required level of PO_2 and PCO_2. A schematic illustration of the superfusion set up is shown in Figure 2.6.

Extracellular recordings were made using glass suction electrodes pulled from GC150-10 capillary glass (Harvard Apparatus, USA). A silver-sliver chloride wire was placed inside the glass electrode which is connected to a NL100 NeuroLog head stage (Digitimer, UK). The voltage signal was initially pre-amplified (NeuroLog NL104 AC, X100, Digitimer, UK), band-pass filtered between 50Hz and 20kHz (NeuroLog NL125, Digitimer, UK) and amplified again (NeuroLog 105, X50, Digitimer, UK). Overall, the total amplification was X5000. The output signal was digitised using a CED micro3 1401 analogue-digital converter and displayed on a PC running Spike2 (Cambridge Electronic Design, Version 7.2). A separate silver chloride wire served as the reference

electrode and was placed in the recording chamber. Figure 2.7 illustrates the glass suction electrode connected to the CSN.

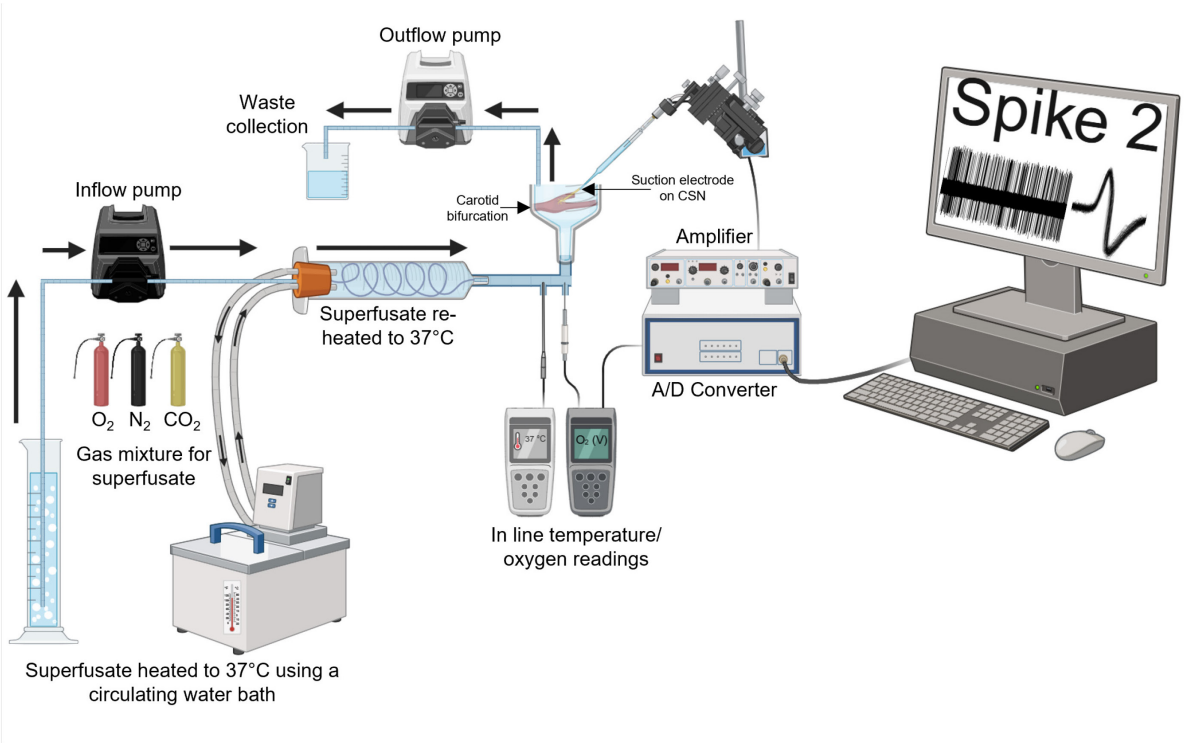

Figure 2.6 Schematic illustration of the carotid body superfusion system

This superfusion experimental setup is designed for recording electrophysiological activity from an isolated carotid bifurcation. A 50 mL glass cylinder holds the superfusate, which is bubbled with a gas mixture to achieve the desired levels of O_2 and CO_2, balanced with N_2. Simultaneously, the superfusate is heated to 37°C using a circulating water bath. The inflow is driven by a peristaltic pump and passes through a re-heating system, where the tubing is looped multiple times to ensure effective heat transfer. Once reheated, the superfusate enters the recording chamber, where the carotid bifurcation is pinned out and the carotid sinus nerve (CSN) is exposed. A second peristaltic pump continuously removes the used superfusate, directing the outflow to waste, ensuring a constant supply of fresh solution in the recording chamber. A temperature probe and oxygen sensor continuously monitor the superfusate conditions. A glass suction electrode, positioned by a micromanipulator, records voltage signals from the CSN, which are amplified, digitised via an analogue-to-digital (A/D) converter and displayed on a PC running Spike2 software.

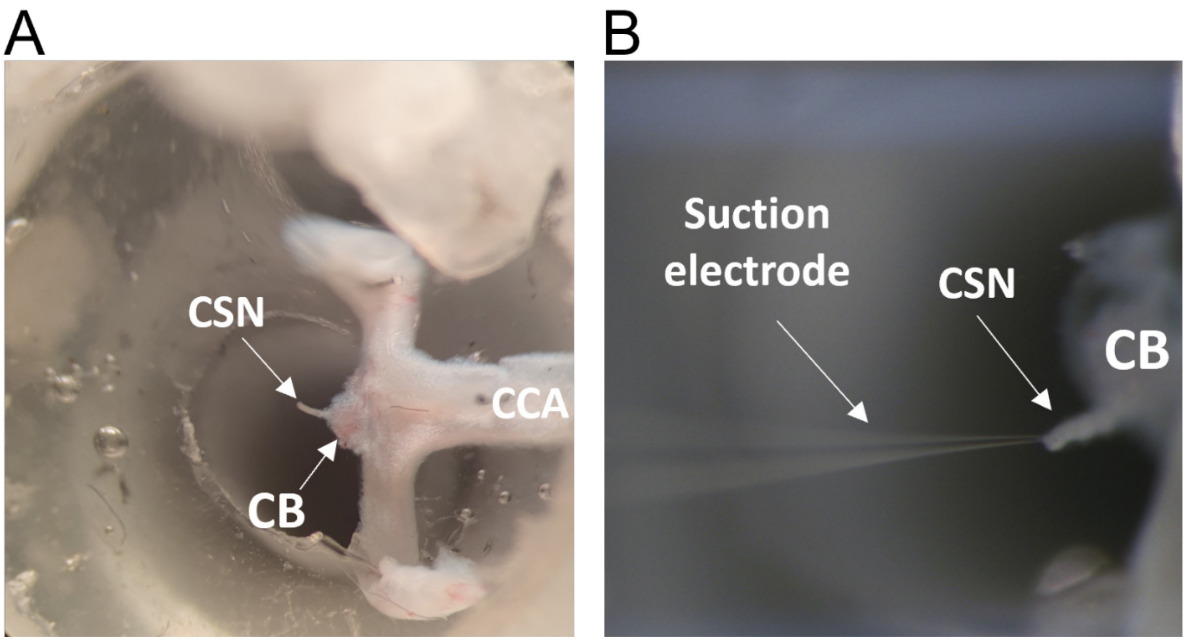

Figure 2.7 Measuring carotid sinus nerve activity *ex vivo* using a glass suction electrode enclosing a silver-silver chloride wire

(A) an example image showing a dissected and partially digested carotid bifurcation containing the carotid body (CB) and the carotid sinus nerve (CSN). Tissue was held in the recording chamber by pinning the common carotid artery (CCA) and both external and internal carotid arteries so that the CB and CSN hover directly over the inflow. **(B)** glass suction electrode placement onto the sectioned end of the CSN. The glass electrode encloses a silver-silver chloride wire which detects the changes in voltages.

2.4.3 Oxygen electrode calibration

The superfusate PO_2 was continuously measured throughout experiments using a O_2 electrode placed close to the entry of the recording chamber. An O_2 meter (OXELP, World Precision Instruments, UK) was used to measure the O_2 electrode signal which was digitised at 200Hz by the same CED 1401 mentioned in section 2.4.2. The O_2 electrode was calibrated using solutions with a known concentration of oxygen (or as close as possible). Calibration solutions were heated to 37°C and bubbled in tightly sealed bottles with 0mmHg, 400mmHg and 722mmHg PO_2. The voltage signal from the electrode was recorded and plotted against its known PO_2 value generating a linear calibration curve with the equation below, where *y* is equal to the PO_2 (mmHg), *x* is the O_2 electrode voltage (volts), *m* is the gradient of the line and *c* is equal to the PO_2 when the O_2 electrode voltage is zero.

$$\boldsymbol{y = mx + c}$$

Using this calibration curve, the PO_2 can be calculated for any given voltage. A superfusate PO_2 value within the recording chamber of approximately 300mmHg was considered to be normoxic as this has been shown to generate basal carotid discharge of 0.25-1.5 Hz (Holmes et al., 2014), which is consistent with that reported *in vivo* in the rat in arterial normoxia (Vidruk et al., 2001).

2.4.4 Measuring hypoxic response curves to determine carotid body O_2 sensitivity

To investigate changes in carotid body hypoxic sensitivity in response to CH and pharmacological agents, O_2 response curves were generated whereby the single fibre chemoafferent discharge was plotted against the gradually decreasing superfusate PO_2 at a fixed PCO_2 of 40mmHg. The data were fitted to an exponential decay curve with offset, described below where *y* is equal to the chemoafferent discharge in Hz, *a*

is the discharge at which the PO_2 tends to infinity, *b* is the theoretical discharge when the PO_2 is 0mmHg, *c* is the exponential rate constant and *x* is equal to the superfusate PO_2 in mmHg.

$$y = a + be^{-cx}$$

Gradually reducing the superfusate PO_2 was controlled using flow meters with high precision valves (Cole Palmer Instruments, UK) connected to oxygen, nitrogen and carbon dioxide cylinders. The mixture of gases could be altered to achieve a desired PO_2 by balancing with nitrogen at a fixed PCO_2 of 40mmHg (total output pressure was constant at 760 mmHg). Flow meter calibration data was provided by the manufacturers. As the PO_2 decreases, chemoafferent discharge begins to increase exponentially after a certain PO_2 threshold (usually around 90-130mmHg). To produce multiple consistent hypoxic response curves and minimise preparation run-down, the hypoxic superfusate was rapidly switched to a hyperoxic solution when the chemoafferent discharge reached approximately 10Hz, which is well before a maximum response is achieved. Ensuring reproducible hypoxic responses is critical to be able to reliably compare carotid body hypoxic sensitivity between the N and CH groups in addition to pharmacological agents.

Additionally, the corresponding PO_2 for any given discharge frequency was calculated using the inverse of the exponential decay function where *x* represents the PO_2 (mmHg), *y* is the single fibre discharge frequency (Hz) and *a, b* and *c* are constants determined as above.

$$x = -\frac{ln(y - a)/b}{c}$$

To quantify a right-left shift in the hypoxic response curve, the PO_2 at a discharge frequency of 5Hz was used. This frequency was chosen because it falls within the exponential region of the hypoxic response curve, ensuring it is sufficiently sensitive to PO_2 changes without reaching a level where discharge might begin to diminish.

2.4.5 Spike sorting and waveform analysis

To discriminate action potentials arising from a single chemoafferent fibre, offline analysis using Spike2 (Version 9) was needed. Initially, a threshold was set to detect any electrical activity above this level whilst at the same time removing background noise and low firing action potentials. Upon threshold triggering, voltage signals are extracted into discrete 0.8-1.0ms duration wavemarks. The Spike2 software allows for the creation of templates, into which these wavemarks can be categorised depending on their shape, amplitude and frequency to further discriminate electrical activity from a single fibre. The wavemarks from a single template were counted and binned into 10 second time intervals, allowing for the calculation of frequency. Figure 2.8 shows an example of two distinguishable spikes from the same fibre.

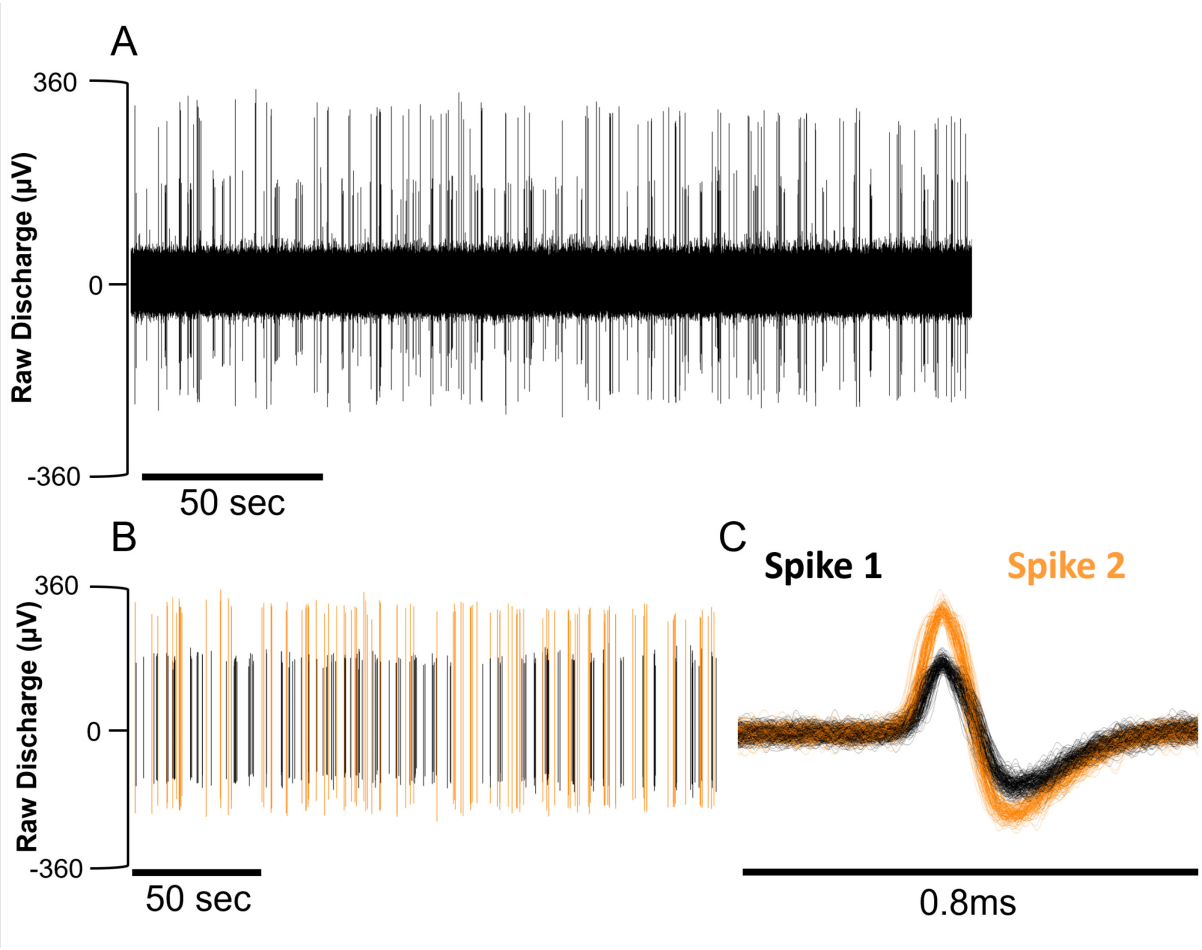

Figure 2.8 Spike sorting in a multi-fibre preparation

(A) raw multi-fibre recording of carotid body chemoafferent activity. **(B)** A voltage threshold was applied to reduce noise and detect both large and small amplitude spikes. Automated spike templating was used to classify spikes based on amplitude, frequency and duration, resulting in two distinct spike templates. **(C)** Overlaid spike waveforms from B, illustrating the two identified spike types. Spike detection, sorting and analysis were performed using Spike2 Version 9.

2.4.6 Data analysis

Frequency data was grouped into 10-second intervals. For basal discharge measurements, the average frequency over a 120-second period was used. Pharmacological agents and hypercapnia were administered for 5 minutes, with the mean of the final 60 seconds used for analysis, once a steady-state discharge had been achieved. For hypoxia experiments, initial raw O_2 response curves were fitted to derive equation constants, as described in Section 2.4.4. These constants were used to calculate the discharge at defined PO_2 values, allowing for direct comparisons between N and CH or control and pharmacological agent.

All data are presented as the mean, with error bars indicating the standard error of the mean (SEM). Individual data points represent the discharge from a single fibre. Statistical differences were assessed using Student's t-test or two-way ANOVA with Bonferroni post-hoc analysis where appropriate. Analyses were performed using GraphPad Prism (Version 10), with significance set at $p<0.05$.

2.5 Measuring heart weight and haematocrit

Rat hearts were surgically extracted following confirmation of death after carotid bifurcation removal. This was performed by the author of this thesis. Hearts were further dissected to isolate the left and right ventricles and the septum with excess fluid dabbed on paper towel before being weighed. This was performed by Mr James Saleeb-Mousa and Dr Andrew Holmes. To identify whether CH had induced typical right ventricular hypertrophy, Fulton's index was used which is the mass of the right ventricle divided by the left ventricle plus septum.

To determine haematocrit and haemoglobin levels, an arterial blood sample was taken at the end of *in vivo* experiments described in Chapter 6. Blood was drawn into heparinised capillary tubes and placed immediately on ice. Blood samples were analysed using a haematology analyser (Pentra ES 60, Japan) and parameters automatically calculated.

2.6 Immunohistochemistry

2.6.1 Tissue preparation and cryosectioning

To evaluate the density and location of CD73 and how this is altered in CH, immunohistochemistry was performed on frozen whole carotid body sections. The carotid bifurcation was surgically removed as described in 2.3 and was immediately immersed in freshly made 4% paraformaldehyde (PFA) in PBS (pH 7.2) for 4hr at room temperature. The tissue was rinsed 3 times in PBS and then placed into the dissecting chamber used previously and superfused with ice-cold PBS. The tissue was cleaned by removing any muscle, fat and nerves but leaving the SCG intact. The SCG can be used as a positive control for the TH stain and enables better integrity of the tissue when sectioning. The OA was dissected free and cut near the level of the carotid body. This will serve as a guide to know when the carotid body has been reached. After dissecting, the carotid body tissue was placed into a 30% sucrose-PBS solution overnight at 4°C. The tissue was dabbed on paper towel to wipe away any excess sucrose which will aid in the embedding in OCT. The tissue was placed into a cryomold containing OCT and frozen using crushed dry ice and then stored at -80°C until further use.

Frozen carotid body tissue was sectioned at 10μm using a cryostat (Bright Instruments, UK) set to -18°C and adhered onto charged microscope slides (Epredia Superfrost™ Plus, Fisher Scientific, UK). The sample was checked using a light microscope to ensure the carotid body was present and its structural integrity intact demonstrated by Figure 2.9. This shows a non-dissected carotid bifurcation but as described above, this process was optimised by dissecting the tissue before freezing which enabled more consistent cryosectioning and easier identification of the carotid body. Slides were placed on a hot plate at 37°C for 2 hours to ensure slides were fully dry before storing them in tightly sealed boxes at -80°C.

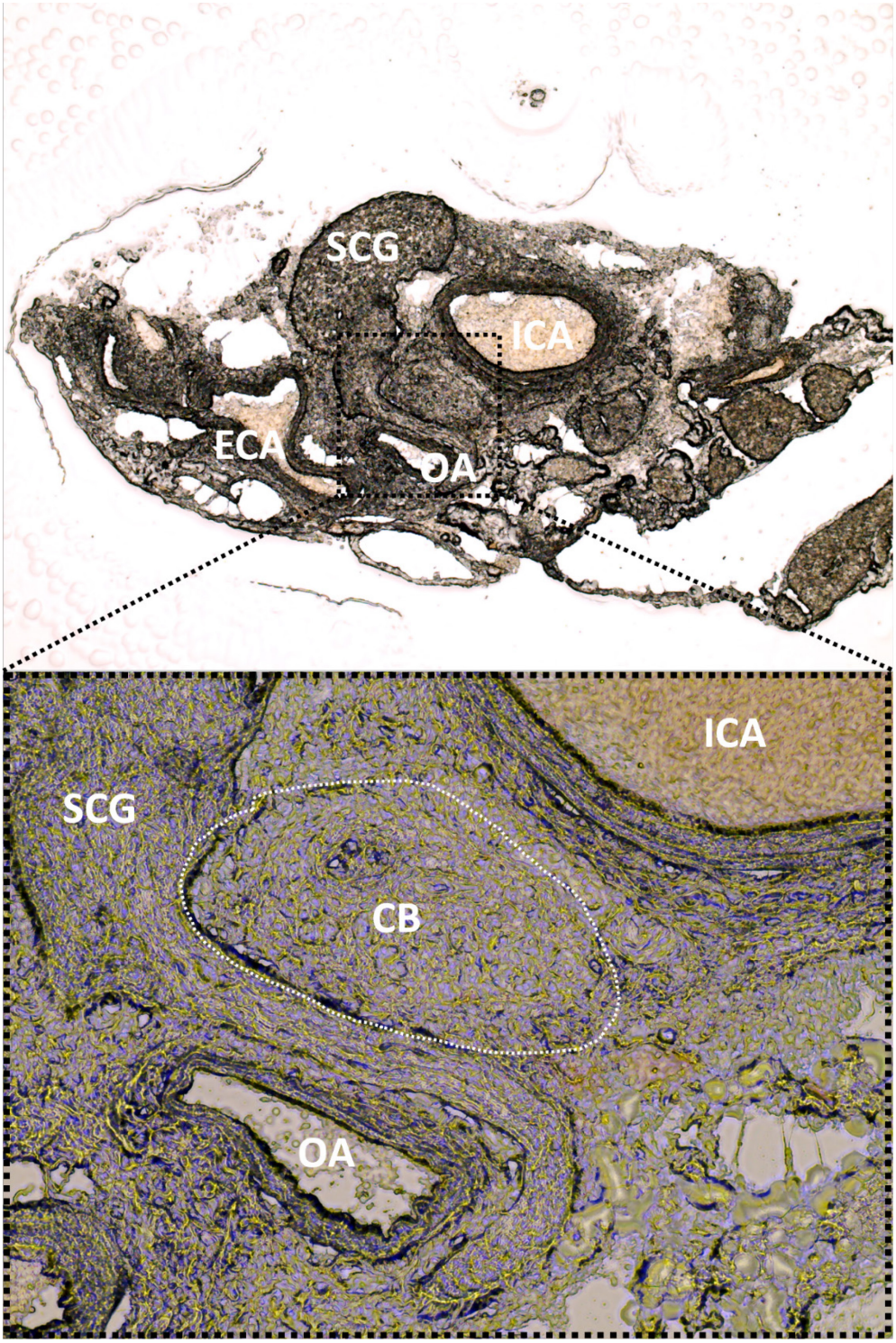

Figure 2.9 Visualisation of the carotid body in cryosections

Light microscope image of cryosectioned whole carotid body (CB) tissue. The CB can be identified as an oval shape in close proximity to the occipital artery (OA) and the internal carotid artery (ICA). Other key structures include the external carotid artery (ECA) and the superior cervical ganglion (SCG). The SCG normally surrounds the ICA and protrudes into the CB. The lower image shows an enlarged view of the dotted boxed region above.

2.6.2 Indirect immunofluorescence staining

Frozen tissue slides were thawed at room temperature for 20 minutes and rehydrated in PBS. To unmask epitopes potentially cross-linked during PFA fixation, heat-mediated antigen retrieval was performed. Slides were immersed in citrate buffer (10mM citric acid in diH_2O adjusted to pH 6.0 using NaOH solution and 0.05% Tween20) and incubated overnight in a 60°C water bath. The following day, slides were removed from the water bath and allowed to cool to room temperature while still in the citrate buffer.

After cooling, slides were washed twice with PBS. Tissue sections were permeabilised with 0.3% Triton-X for 15 minutes and blocked with 1% BSA in 0.1% PBS-Tween20 (PBS-T) for 30 minutes at room temperature. A hydrophobic barrier was drawn around the sections using a PAP pen (ImmEdge®, VectorLabs, UK) to minimise the volume of antibody needed. Primary antibodies targeting CD73, TH, PCAM-1 (CD31), and neurofilament-light chain (NF) were diluted in 0.1% BSA in 0.1% PBS-T and applied to the sections within the hydrophobic barrier. Slides were placed in a humidified chamber and incubated overnight at 4°C. The next day, slides were washed three times with 0.1% PBS-T and incubated with fluorescently conjugated secondary antibodies for 1 hour at room temperature in the dark. Following incubation, slides were washed three times with 0.1% PBS-T and given a final rinse in PBS. Pre-immune serum, obtained from the host animal prior to immunisation with the CD73 antigen, was used as a negative control. Additional negative controls included sections processed without the primary antibody, using only secondary antibodies. A summary of antibodies used is shown in Table 1.

One drop (~15µL) of Vibrance® anti-fade hard-set mounting medium containing DAPI (Vector Laboratories, H-1800, UK) was applied to the sections. A 13mm round coverslip (#1.5 thickness, hydrolytic class 1 glass, VWR, UK) was placed carefully to avoid air bubbles. Slides were allowed to cure in the dark for 2 hours at room temperature (exposed to air) and imaged using a confocal microscope within 48 hours. The combinations of antibodies and their concentration used for each specific protocol are summarised in Figure 2.10.

Antibody	Manufacturer	Catalogue number
Rabbit polyclonal anti-CD73	Ectonucleotidases.com, Canada	rNu-9L
Mouse monoclonal anti-TH	Cell Signalling Technology, UK	45648S
Goat polyclonal anti-CD31	Bio-techne, UK	AF3628
Chicken polyclonal anti-NF-L	Bio-techne, UK	NBP1-05219
Donkey anti-rabbit Alexa Fluor 488	ThermoFisher, UK	A21206
Donkey anti-mouse Alexa Fluor 594	ThermoFisher, UK	A21203
Donkey anti-goat Alexa Fluor 647 plus	ThermoFisher, UK	A32849
Donkey anti-chicken Alexa Fluor 647	ThermoFisher, UK	A78952

Table 2.1 List of antibodies

Primary and secondary antibodies used in this thesis with the manufacturer and catalogue numbers.

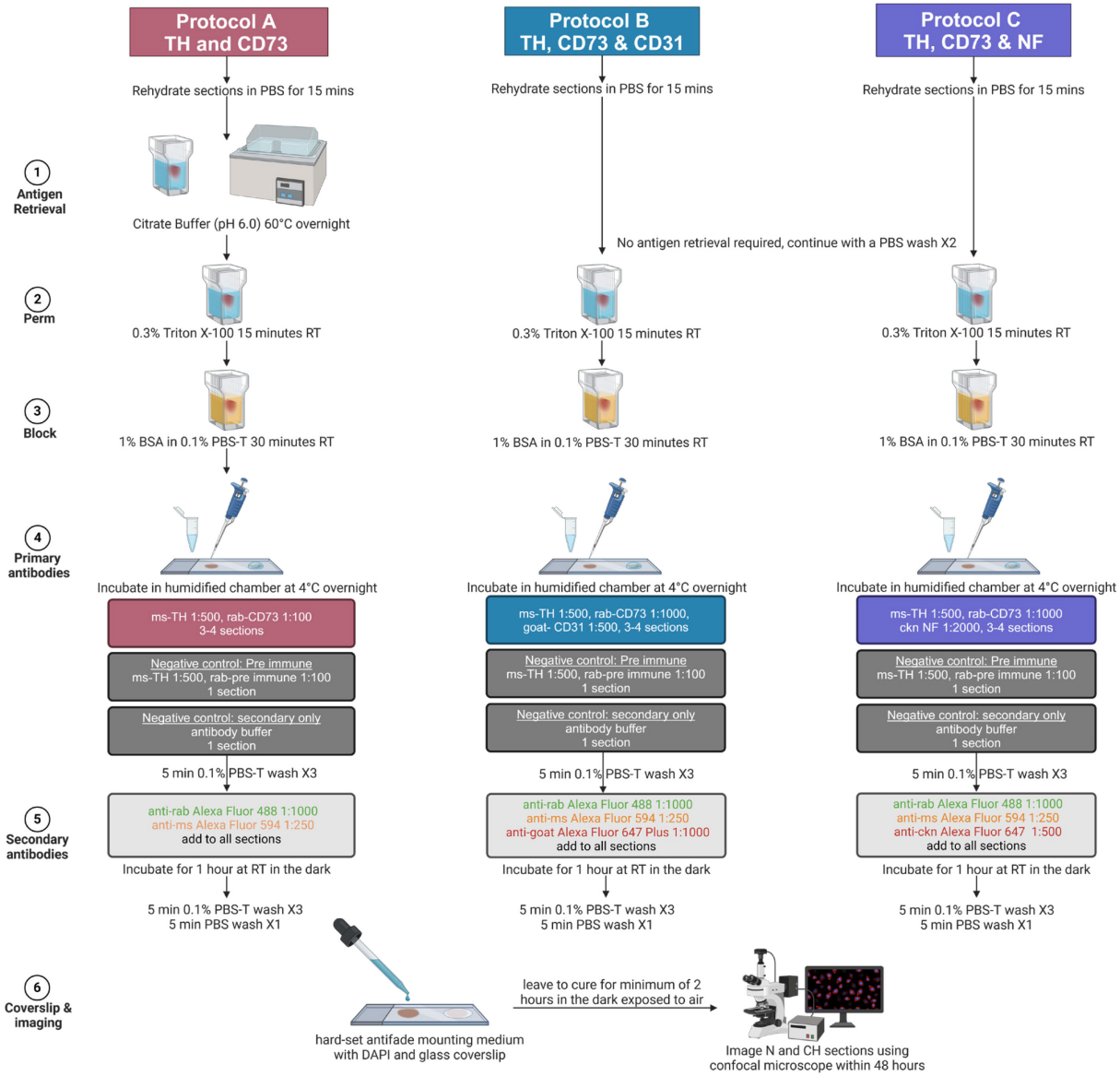

Figure 2.10 Immunohistochemistry protocols

This flow diagram illustrates the immunostaining protocol for carotid body cryosections. Each carotid body provided enough sections for all three protocols, which were performed on three carotid bodies from separate normoxic (N) and chronically hypoxic (CH) rats. Protocol A included an antigen retrieval step, with sections incubated in citrate buffer at 60°C overnight to enhance the $CD73^+$ signal in tyrosine hydroxylase (TH)-expressing type I cells. Protocol B was optimised for detecting a more sensitive $CD73^+$ signal that did not require antigen retrieval. To investigate the origin of this signal, the vascular endothelial marker PECAM-1 (CD31) was used alongside TH and CD73. Protocol C incorporated neurofilament-light chain (NF) to determine whether the $CD73^+$ signal also had a neuronal origin. Sections were permeabilised with 0.3% Triton X-100, blocked with 1% BSA in 0.1% PBS-Tween 20 (PBS-T), and incubated overnight at 4°C with primary antibodies at the dilutions indicated in the flow diagram. Negative controls included pre-immune serum and secondary antibody-only conditions. Following multiple washes in 0.1% PBS-T, fluorophore-conjugated secondary antibodies were applied at dilutions indicated in the flow diagram for 1 hour at room temperature in the dark. Sections were mounted using a DAPI-containing antifade medium and cured for at least 2 hours before imaging. Confocal microscopy was performed within 48 hours, capturing images of N and CH sections for all three protocols. Antibody species abbreviations: ms=mouse, rab=rabbit, ckn=chicken.

2.6.3 Confocal microscopy

Stained sections were imaged using different confocal microscopes. Optimisation images, including those for antibody dilutions and antigen retrieval, were captured using an Olympus Fluoview FV1000 microscope (40X magnification, 0.80 NA, water objective). For comparing N and CH carotid bodies, images from rat 1 were acquired using a Zeiss LSM 880 microscope (40X magnification, 1.2 NA, water objective). However, due to technical issues with this microscope, images from the carotid bodies of rats 2 and 3 were taken using a Leica Stellaris 8 microscope (40X magnification, 1.4 NA, oil objective). Both the Zeiss and Leica microscopes utilised a tile scanning function, which allowed for capturing large areas of the section at high resolution. This involved imaging multiple adjacent regions and stitching them together to create a comprehensive view. This approach was particularly useful for imaging larger carotid bodies that could not fit within a single frame during regular acquisition. All microscopes employed sequential scanning, where each fluorescent channel was acquired separately using its respective excitation laser, preventing fluorophore spill-over between channels.

2.5.4 Machine learning for post-acquisition removal of RBC autofluorescence

Carotid body tissue was immersion-fixed rather than perfusion-fixed, which resulted in residual RBCs within the tissue. RBCs exhibit strong autofluorescence (AF) due to porphyrins in haemoglobin (Whittington & Wray, 2017). This AF signal was confirmed to originate from RBCs based on their localisation within vascular structures marked by the endothelial marker CD31 and their bi-concave shape (Chapter 4). The high pixel intensity of RBC AF made regular thresholding unsuitable for removal.

To address this, a machine learning approach was employed using the Python-based software, *ilastik* (Berg et al., 2019). The software uses user-provided annotations and selected pixel features, such as smoothed pixel intensity, colour gradients, shape and texture to classify pixels. Gaussian smoothing with varying sigma values can be applied to control the level of detail captured, with larger sigma values gathering more contextual data but losing finer details. For training, immunofluorescence images were manually annotated to label RBC pixels. This process was repeated across approximately four images to train the model. Once trained, the software predicted pixel classifications and batch-processed subsequent images.

The output was a segmented image with RBC pixels clearly distinguished. This segmented image was imported into Fiji (Fiji Is Just Image J, Version 2.14) where RBC-specific pixels were isolated and converted into a binary mask. The binary mask was subtracted from the original raw image, effectively removing RBC AF. The mask could also be subtracted from other channels in the same image, ensuring accurate quantitative analysis of all proteins of interest. A step-by-step workflow for using *ilastik* to remove RBC AF is provided in Chapter 4.

2.6.5 Estimating carotid body volume and calculating area

All images were analysed using Fiji. The rat carotid body has an ellipsoid three-dimensional structure and its volume was estimated using the ellipsoid formula:

$$\boldsymbol{V = \frac{4}{3}\pi abc}$$

Here, *a*, *b* and *c* are the semi-axes of the ellipsoid along the x,y and z directions respectively, representing the distances from the ellipsoid's centre to its surface. To determine the semi-axes, an elliptical shape was fitted around the carotid body in

cross-sectional images to measure the area. This region of interest (ROI) was used for all further quantitative analyses. Semi-axes *a* and *b* were derived from the major and minor axes of the ellipse (illustrated in Figure 2.11), while *c* was calculated as half the total thickness of the carotid body, corresponding to half the total number of sections multiplied by the section thickness (10μm). The semi-axes from the largest section were used in the calculation which most accurately represents the full extent of the ellipsoid shape.

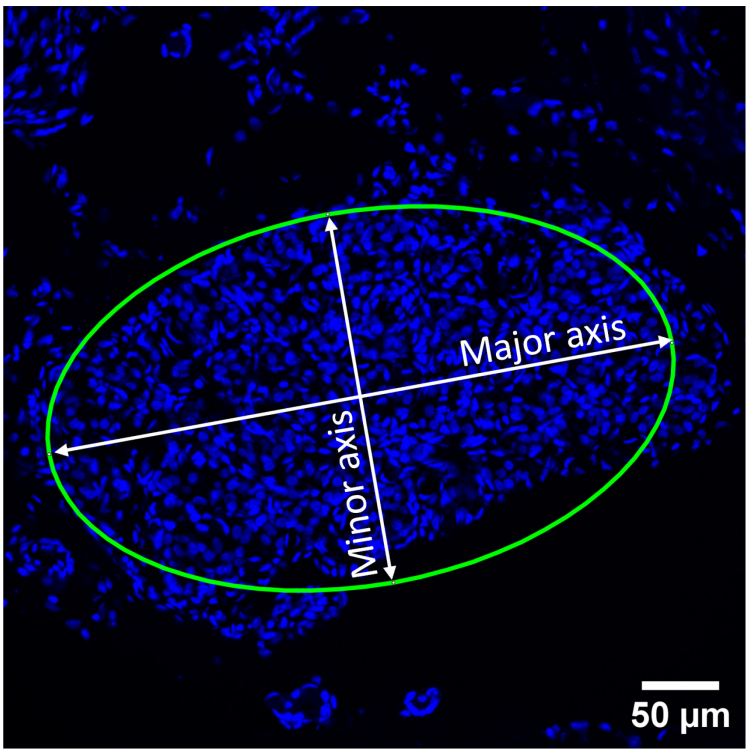

$$\boldsymbol{a} = \frac{major\ axis\ (\mu m)}{2}$$

$$\boldsymbol{b} = \frac{minor\ axis\ (\mu m)}{2}$$

Figure 2.11 Determination of the major and minor axis for carotid body volume estimation

A region of interest (ROI) was drawn around the carotid body and fitted to an ellipse to determine its boarder. From this fitted ellipse, the major and minor axes can be measured in micrometres (µm) using Fiji. The semi-axes are half of these values and can be used in the standard formula for calculating the volume of an ellipsoid. This image serves as an example of how to determine the semi axis *a* and *b* for volume estimation of the carotid body. DAPI stain was used to label nuclei.

2.6.6 Cell counts and positive signal area

The number of TH^+ cells per carotid body was estimated by multiplying the TH^+ cell density (per section volume) by the estimated carotid body volume calculated above. TH^+ and $CD73^+$ cells were identified by overlaying DAPI staining and manually counting nucleated cells surrounded by positive TH or CD73 signals. Fiji's cell counting tool was used to label and number each counted cell, minimising double counting. Total cell counts were determined by thresholding the DAPI channel, applying a watershed filter and using the 'Analyse Particles' function. The proportion of TH^+ or $CD73^+$ cells was calculated as the ratio of these counts to the total cell count in the carotid body. The total area of positively stained signal was measured by applying a threshold, removing noise (excluding outliers smaller than 2 pixels) and using the 'Analyse Particles' function. Threshold values were automatically determined by the software. However, in cases of high background where automatic thresholding was unreliable, threshold values were manually set based on the approximate pixel intensity observed in the pre-immune serum condition (negative control).

2.5.7 Co-localisation analysis

To quantify co-localisation between two proteins, Manders' coefficients (M1 and M2) were calculated using the JaCoP plugin in Fiji. M1 represents the fraction of channel 1 overlapping with channel 2, while M2 represents the fraction of channel 2 overlapping with channel 1. These coefficients provide a measure of the proportion of one protein overlapping or co-localising with another in the same image (Dunn et al., 2011).

2.6.8 Data and statistical analysis

Each individual point represents single animal data, calculated as the mean of multiple sections (3-8) per rat. Error bars indicate SEM. Statistical analysis was established ($p<0.05$) using an unpaired Student's t-test performed in GraphPad Prism (Version 10).

2.7 Whole-body plethysmography

2.7.1 Experimental set up and principle

The plethysmography data was acquired by a trained member of the research group, Mr Dhaifallah Alotaibi, and analysed by the author of this thesis. Whole-body plethysmography was used to measure respiratory variables at rest and in response to varying severities of hypoxia and hypercapnia in awake and unrestrained rats.

This technique is based on the principle that, during inspiration, the animal inhales air at chamber temperature, which is then warmed and humidified to alveolar temperature in the lungs. This warming increases the volume of the air in the lungs, increasing the overall volume of gas within the chamber thereby causing a rise in chamber pressure. During expiration, the exhaled air cools back to chamber temperature, reducing its volume and decreasing the chamber pressure (Stephenson & Gucciardi, 2002).

The barometric pressure and humidity of the chamber are monitored using a reference chamber. A differential pressure transducer connects the subject chamber and the reference chamber, detecting pressure differences and outputting these as analogue voltage signals. These voltage signals are amplified (usbAMP, EMKA Technologies),

digitised at 1000Hz by an A/D converter and viewed on a PC running iox2 (Version 2.10.8).

2.7.2 Chamber calibration and gas adjustments

To calculate rat tidal volumes, the equipment must be calibrated before each experiment. A known volume of air (20 mL) was injected into the subject chamber through a side port, creating a pressure difference and an associated voltage change. The pressure gradient, and voltage generated by this known volume are recorded as the high calibration value. The voltage from a completely sealed chamber provides the low calibration value. Airflow was calculated as a function of the calibrated volume (derived from pressure change) over time. These calibration points enable the conversion of chamber pressure changes induced by rat ventilation into tidal volumes. All other respiratory parameters such as respiratory frequency and minute ventilation can then subsequently be calculated.

The iox2 software allows adjustment of gas flow into the chamber to create different environments, such as normoxia/normocapnia, hypoxia or hypercapnia. Gas flow is set using mass flow controllers and measured using a gas analyser (ADInstruments, UK). Gas mixtures were delivered using BOC cylinders of O_2, N_2 and CO_2 with a constant flow rate of approximately 2 L min^{-1} regulated by the Vent 4-C1 pump (EMKA Technologies). This pump also removes excess air, preventing the buildup of CO_2 and humidity, which are absorbed by silica gel. Bedding from the animals' home cage was also placed in the chamber to keep stress levels to a minimum.

2.7.3 Experimental protocols

Protocol A aimed to investigate ventilatory differences between N (n=6) and CH (n=6) rats breathing air (chamber set to F_iO_2 21%) and in response to moderate hypoxia (F_iO_2 10%) and hypercapnia (F_iCO_2 6%). After reaching a steady baseline in air, the inflow gas mixture was then switched to mild hypoxia for 10 minutes and retuned back to 21%. The F_iO_2 within the chamber took approximately 5 minutes to decrease down from 21% to 10%, therefore the animal was only exposed to an F_iO_2 of 10% for the final 5 minutes. After a 10 minute recovery and a steady baseline again, the inflow gas was switched to hypercapnia for 10 minutes. Similarly, it took approximately 5 minutes for the F_iCO_2 to reach 6% and so the animal was only exposed to an F_iCO_2 of 6% for the final 5 minutes, before once again returning to normocapnia. A summary of Protocol A is shown in Figure 2.12.

Initial results showed that with Protocol A, CH rats breathing air had a severely depressed response to moderate hypoxia (F_iO_2 10%). It has been questioned as to whether normal room air is relatively hyperoxic for these animals and so should be kept on 12% F_iO_2 as their 'normoxic' baseline. Considering this, Protocol B was utilised to investigate changes in baseline ventilation in N rats (n=4) breathing air and CH rats (n=12) breathing F_iO_2 of 12%. Furthermore, the poor response to moderate hypoxia led to a stronger hypoxic stimulus being given (F_iO_2 8%). A summary of Protocol B is shown in Figure 2.12.

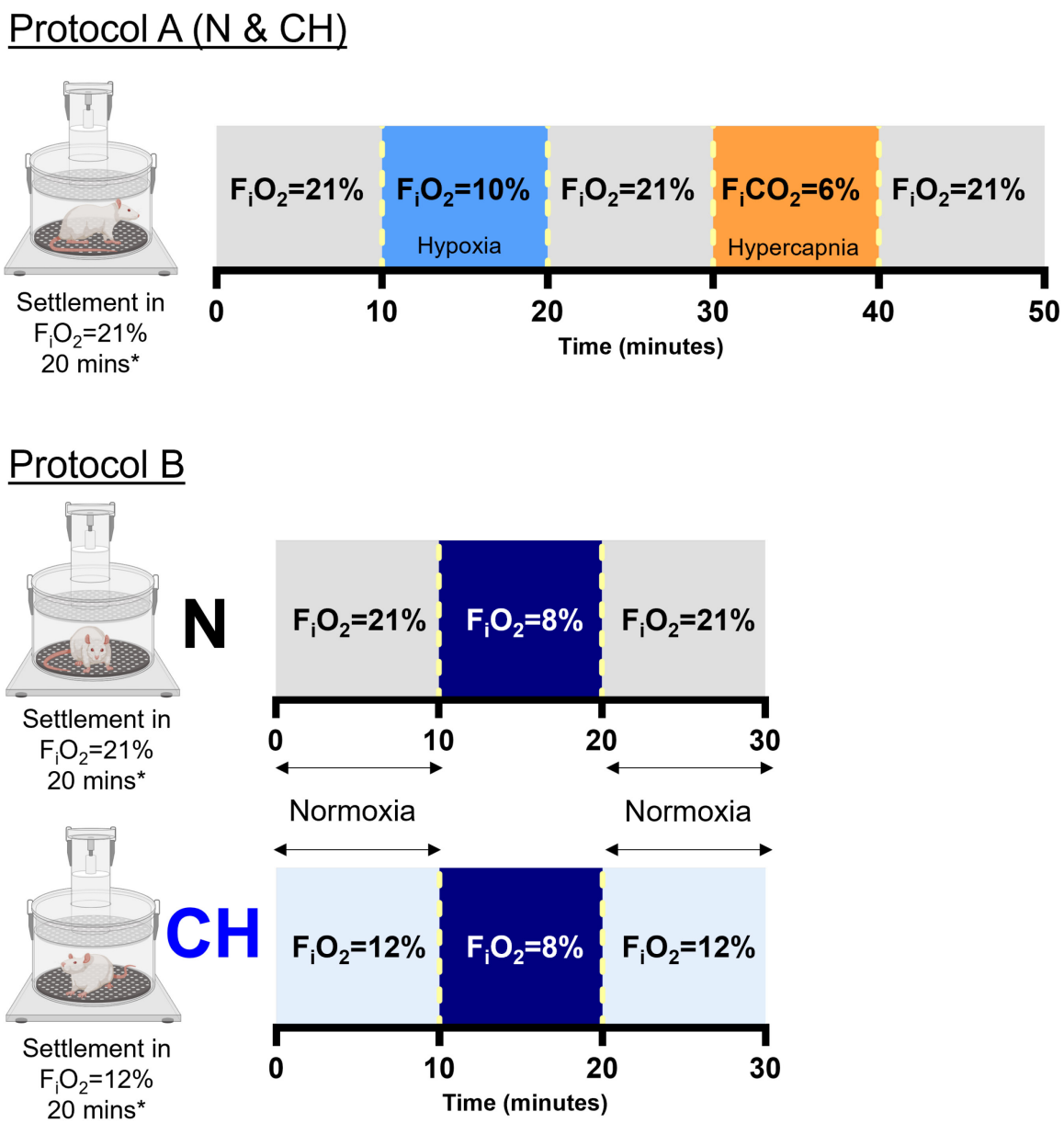

Figure 2.12 Whole body plethysmography protocols

Experimental protocol used for measuring ventilation in awake and unrestrained normoxic (N) and chronically hypoxic (CH) rats. Initially, Protocol A was applied to both N (n=6) and CH (n=6) rats, where a settlement period (21% F_iO_2) was followed by baseline ventilation also at 21% F_iO_2 (shaded grey). A moderate hypoxic stimulus (10% F_iO_2; shaded blue) was administered for 10 minutes before returning to 21% F_iO_2, followed by a 10 minute exposure to hypercapnia (6% F_iCO_2; shaded orange) and subsequent recovery to 21% F_iO_2. In Protocol B, N (n=4) and CH (n=12) rats were maintained at different normoxic gas levels, with CH rats settling at 12% F_iO_2 (shaded pale blue) and N rats at 21% F_iO_2; these oxygen levels served as each group's normoxic baseline. A more severe hypoxic stimulus (8% F_iO_2; shaded dark blue) was then given to both groups before recovery into their respective normoxia. In both protocols, bedding from the animals' home cage was placed in the plethysmography chamber to induce familiarity and reduce stress. * denotes a minimum of 20 minutes of settlement. It took approximately 5 minutes for the plethysmography chamber to equilibrate at the desired gas concentration. All animals were weighed prior to the experiments to normalise tidal volumes per weight, and all animals returned to their home cage after the final recovery in normoxia.

2.7.4 Data extraction and analysis

Raw data was acquired using iox2 (Version 2.10.8). Post-acquisition, raw data was converted to a European Data Format and was subsequently analysed using LabChart (ADInstruments, Version 8). An average of the last 10-seconds of every minute was used to plot the respiratory time courses. As ventilation reached a steady state during the last three minutes of the hypoxic and hypercapnic exposure, the last three minutes of breathing was taken as an average and used for analysis. Tidal volumes were normalised to rat weight, thus minute ventilation was expressed as mL min^{-1} g^{-1}. Data is shown as the mean ± SEM with individual data points representing a single rat. Statistical significance was established using unpaired Student's t-test. Analysis was performed using GraphPad Prism (version 10) and significance was set at $p<0.05$.

2.8 *In vivo* cardiorespiratory measurements

To investigate the cardio-respiratory effects of CD73 inhibition and/or CSNX animals were anaesthetised for non-recovery experiments. This involved cannulating the femoral blood vessels, dissecting the carotid bifurcation (as described in section 2.3) and cannulating the trachea. Femoral cannulations were performed by Dr Andrew Coney and carotid body and tracheal cannulations were conducted by the author of this thesis.

2.8.1 Anaesthetic induction and maintenance

Firstly, rats were induced with 5% isoflurane in O_2 at a flow rate of 1.5L min^{-1} and after loss of their righting reflex were placed on the surgical table heated to 37°C and subsequent anaesthetic was delivered using a nose mask. The level of anaesthesia

was maintained between 2-4% and monitored by an absent pedal withdrawal reflex in addition to the depth and frequency of breathing. Due to the physiological and practical limitations of using isoflurane to measure cardiorespiratory reflexes to hypoxia (Karanovic et al., 2010), Alfaxalone (Alfaxan®, Vetoquinol Ltd, UK) was used as an intravenous anaesthetic throughout the rest of the experiment. This anaesthetic has commonly been used within the research group and others and better preserves cardio-respiratory reflex responses under prolonged experiments (Guo et al., 2024; Marshall & Davies, 1999; Muir et al., 2008; Ray et al., 2002; Skinner & Marshall, 1996; Thompson et al., 2016; Walsh & Marshall, 2006; Warne et al., 2015). The right femoral vein was cannulated (ID 0.5mm, OD 1.5mm, silicone tubing) and connected to an infusion pump. Once the cannula was secured using 4-0 non-absorbable suture, the gaseous isoflurane was turned off and the animal was able to blow off some residual isoflurane before switching to Alfaxalone. This ensures minimal mixing between anaesthetics which could be detrimental to the animal. Initially, small boluses of approximately 0.05mL were applied until the correct dept of anaesthesia was achieved. Afterwards, the intravenous infusion of anaesthesia was maintained at 17-20 mg kg^{-1} h^{-1} and 0.1mL boluses were given as necessary. A schematic illustration of the experimental set up is shown in Figure 2.13.

2.8.2 Measuring arterial blood pressure

To measure arterial blood pressure (ABP), the right femoral artery was cannulated (0.58mm ID, 0.96mm OD, polythene tubing) and connected to a pressure transducer (ADInstruments, UK). This transducer was connected to a PowerLab (ADIntruments, UK) which converts the voltage signal generated from the pressure transducer to a digital signal at 1000Hz. To determine ABP in mmHg, a 2-point calibration was

performed using a mercury sphygmomanometer. The voltage at 0mmHg (open to atmosphere) was used as the zero and the voltage at 200mmHg was used as the top calibration point. Therefore, for any given voltage, ABP in mmHg can be determined. Heart rate was derived from the ABP trace.

2.8.3 Pharmacological preparation

To investigate the effects of CD73 inhibition, a well-established pharmacological agent, AOPCP was used. This drug is known to reduce adenosine concentrations in *ex vivo* carotid body preparations and has been shown to prevent vasodilation caused by ATP infusion, indicating a lack of adenosine formation (Conde & Monteiro, 2004; Conde et al., 2012b; Skinner & Marshall, 1996) . First, the left femoral vein was cannulated and filled with heparinised saline in a 1mL syringe. At the time of AOPCP injection, the saline syringe was swapped for a syringe containing the required dose of AOPCP. Three doses of AOPCP were given throughout the experiment including 160µg kg^{-1}, 320µg kg^{-1} and 1120µg kg^{-1}. AOPCP was injected as a bolus at a volume dose of 1mL kg^{-1}. This ensured the volume remained constant at each dose, reducing any effect of volume loading. Once all cannulas were in place, the carotid bifurcation was dissected (but not excised) as previously described in section 2.3. This surgery was preparation for CSNX as part of the experimental protocol.

2.8.4 Measuring ventilation

The trachea was cannulated with a custom-made T piece. The side part was connected to a spirometer which allows pressure differences related to volume changes to be measured, and airflow calculated. Connected to the top part of the tracheal cannula was additional tubing connected to a gas analyser for sampling of end-tidal O_2 and

CO_2. Coming off the spirometer was another inlet port which allowed for tubing connected to gas cylinders to be attached. This allowed for the alteration of respiratory gases as required throughout the experiment. A schematic diagram of the experimental set up is shown in Figure 2.13.

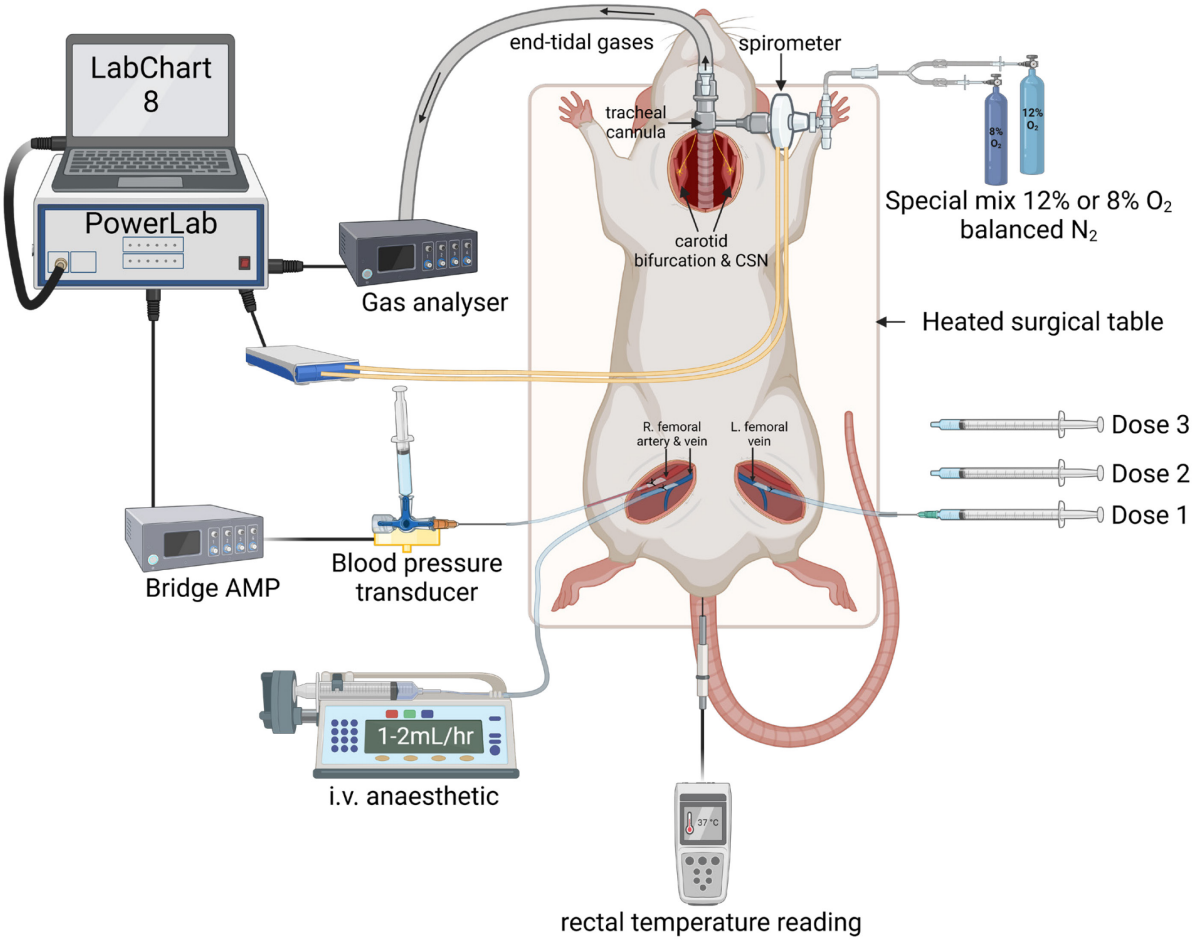

Figure 2.13 *In vivo* experimental setup for measuring cardiovascular and respiratory parameters in an anesthetised rat

This schematic illustrates the experimental setup for *in vivo* recordings of arterial blood pressure and ventilation in an anesthetised rat. Animals were induced with isoflurane (inhalation) and maintained on Alfaxan via intravenous infusion in the right femoral vein. The right femoral artery was cannulated and connected to a blood pressure transducer, which was linked to a bridge amplifier and PowerLab system for data acquisition. The carotid bifurcation and carotid sinus nerve (CSN) were exposed for subsequent experiments. The trachea was intubated with a tracheal cannula, with a side port connected to a spirometer to measure ventilation. A secondary port extracted end-tidal gases (O_2 and CO_2) for quantification using a gas analyser. Pre-mixed O_2 cylinders were used to induce hypoxia (8% O_2), while 12% O_2 was used as the baseline for chronically hypoxic rats. Normoxic rats breathed ambient air as their baseline. The left femoral vein was cannulated for the administration of pharmacological agents. Rectal temperature was continuously monitored, and a heated surgical table maintained body temperature at approximately 37°C. All data were recorded using PowerLab hardware and visualized with LabChart software (version 8).

4.8.5 Experimental protocols

For N animals, baseline measurements were made in air and hypoxic responses were made in 8% F_iO_2 for 2 minutes (special mix BOC cylinder balanced nitrogen). For CH animals, baseline measurements were conducted in 12% F_iO_2 and hypoxic responses measured in 8% F_iO_2. During the CH experiments, air was also given for 2 minutes. The first set of experiments (n=6 rats in each group) aimed to look at the effect of CSNX on cardio-respiratory responses to baseline ventilation and in response to hypoxia. A summary of this experimental protocol is shown in Figure 2.14 A.

The second group of experiments aimed to investigate the pharmacological inhibition of CD73 on cardio-respiratory responses to baseline ventilation and in response to hypoxia (N: n=8, CH: n=7). After injecting the required bolus dose, the syringe was swapped back to the heparinised saline and the dead space volume was flushed ensuring the total volume of AOPCP desired had entered the circulation. Hypoxia was given 5 minutes after the bolus injection of AOPCP. After a brief recovery back to normoxia, this was repeated for two increasingly higher doses. In a subset of animals, to determine any carotid body specific effects of systemic CD73 inhibition, AOPCP was given in addition to CSNX at the end of the pharmacology protocol (N: n=4, CH: n=6). A summary of these experimental protocols is shown in Figure 2.14 B.

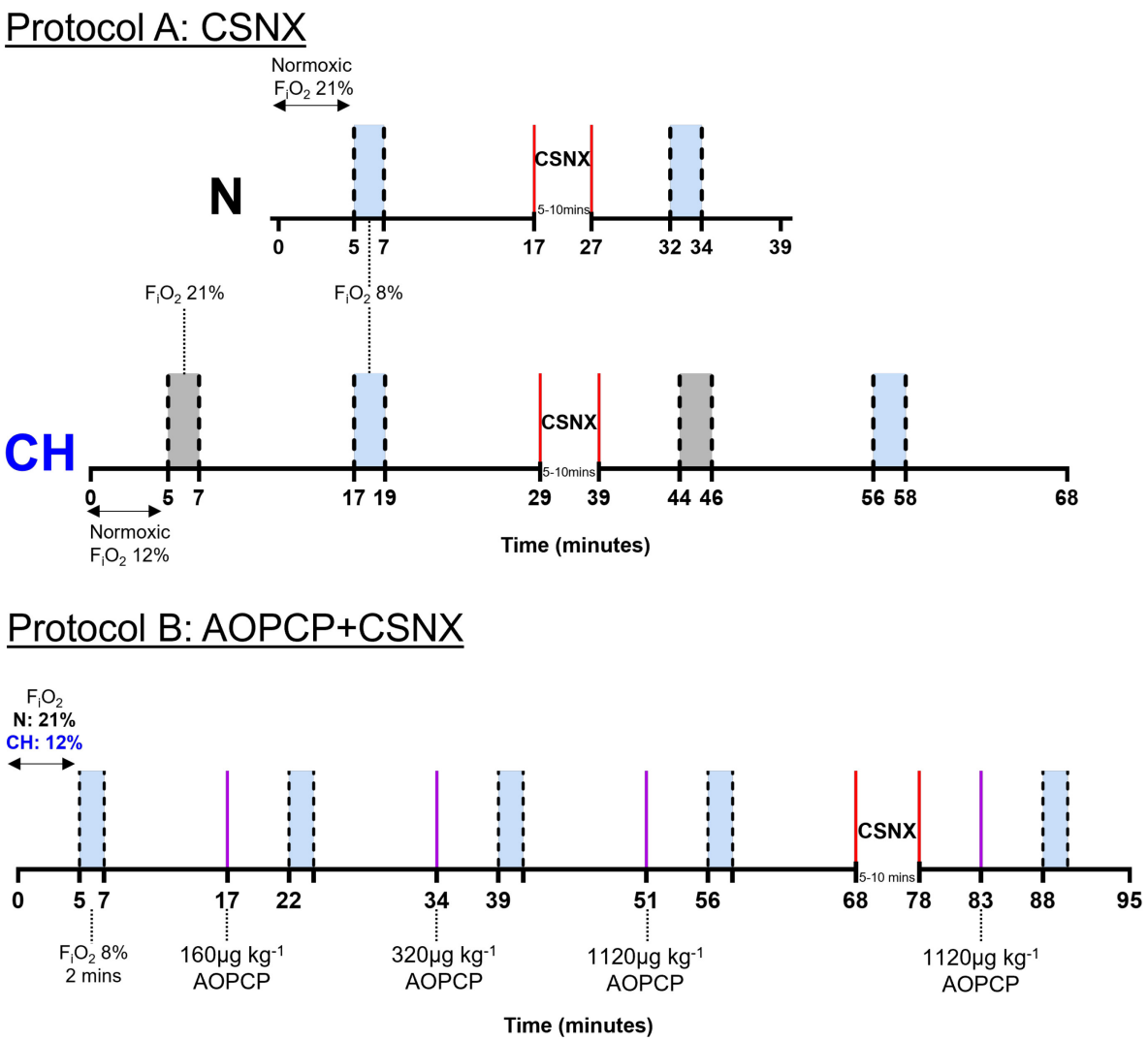

Figure 2.14 *In vivo* cardiorespiratory protocols under terminal anaesthesia

This figure illustrates the experimental protocol used to measure ventilation, heart rate and blood pressure in terminally anaesthetised normoxic (N) and chronically hypoxic (CH) rats in Chapter 6. Protocol A assessed the effect of carotid sinus nerve section (CSNX) on cardiorespiratory parameters in response to air (21% F_iO_2; shaded grey) or hypoxia (8% F_iO_2; pale blue), with normoxic baselines recorded in air for N rats and in 12% F_iO_2 for CH rats. Each stimulus was administered for 2 minutes, and the carotid bifurcation was dissected before the experiment, with CSNX performed after the final recovery from hypoxia. After allowing baseline parameters to stabilise, acute stimuli were re-administered (N: n=6, CH: n=6 rats). Protocol B investigated the effects of pharmacological inhibition of CD73 using AOPCP, with baselines recorded under the same normoxic conditions in Protocol A followed by a 2 minute hypoxic stimulus (8% F_iO_2). After recovery and baseline re-established, an AOPCP bolus (160µg kg^{-1}; 1 mL kg^{-1}) was administered via the left femoral vein, followed by a 5 minute period before re-introducing hypoxia. This process was repeated with two increasing doses of AOPCP, as indicated in the figure (N: n=8, CH: n=7 rats). After the final dose and recovery, CSNX was performed on a subset of these rats, and the highest dose (1120µg kg^{-1}) was administered again, followed by repeated stimuli to determine the carotid-specific effects of AOPCP (N: n=4, CH: n=6 rats). At the end of the experiment, blood was collected from the right femoral artery into heparinised capillary tubes for blood analysis, and animals were euthanised via cervical dislocation, with death confirmed by exsanguination.

2.8.6 Data extraction and analysis

Data was acquired and analysed using LabChart (ADInstruments, UK). A 10 second average was plotted every 10 seconds for time courses. Due to the biphasic hypoxic response which peaks and then either plateaus or begins to decline, comparisons between N and CH were analysed at different time periods during hypoxia. These included a 20 second average from the rising phase (time point 30 & 40 seconds) and the end of hypoxia (time point 110 & 120 seconds). Data is expressed as the mean with error bars representing SEM and individual data points show each rat. Statistical differences were established using Student's t-test and two-way ANOVA with Bonferroni post-hoc analysis. Analyses were performed in GraphPad Prism (Version 10) and significance taken at $p<0.05$.

CHAPTER 3

3. Developing and validating a rat model of chronic hypoxia and carotid body hyperactivity

3.1 Introduction and aims

CH is a feature of both physiological and pathophysiological conditions such as sojourns at high altitude and COPD respectively (Kent et al., 2011; Peacock, 1998). There are well defined physiological carotid body, cardiovascular and respiratory adaptations which occur to primarily normalise oxygen delivery despite the lowering of arterial oxygen partial pressure (P_aO_2)(Aaron & Powell, 1993; Hansen & Sander, 2003; Smith & Marshall, 1999; Walsh & Marshall, 2006). Numerous different animal models of CH have been reported, achieved by a sustained reduction in the F_iO_2 and/or barometric pressure, and applied at varying stimulus intensities and durations (Aaron & Powell, 1993; Clarke et al., 2000; Conde et al., 2012c; Fielding et al., 2018; Hodson et al., 2016; Pardal et al., 2007; Salman et al., 2017; Sobrino et al., 2018; Thomas & Marshall, 1997; Walsh & Marshall, 2006). The main aim of this current chapter was to establish and validate an animal model of CH with characteristic carotid body, cardiovascular and respiratory adaptations that could then be used throughout the rest of the thesis to probe the importance of CD73.

One key adaptation is an increase in red blood cell production and haemoglobin which is mediated by EPO released by the kidney (Haase, 2010). It is well established that the control of EPO and many other transcription factors are controlled by HIF (Bishop & Ratcliffe, 2015; Semenza & Wang, 1992). Significant increases in haematocrit and haemoglobin concentration occur in a time-dependent manner, though this timing varies between species and even within strains of the same species (Arias-Reyes et

al., 2021; Walsh & Marshall, 2006). Increases in haematocrit and, consequently haemoglobin concentration, raise the blood's O_2 content. In the initial days of CH, local vasodilatory responses enhance blood flow to tissues to improve oxygen delivery. This effect is primarily mediated by adenosine-driven nitric oxide production. After approximately seven days of CH, this vasodilatory response subsides as the increased haemoglobin concentration sufficiently boosts O_2 content, normalising oxygen delivery (Marshall & Davies, 1999; Thomas & Marshall, 1997; Walsh & Marshall, 2006). This chapter aimed to validate that Wistar rats exposed to 12% F_iO_2 for 10 days was sufficient to significantly increase the haematocrit, haemoglobin and O_2 content.

A further adaptation to CH is pulmonary vasoconstriction which is thought to help redistribute blood to better oxygenated regions of the lung and improve ventilation-perfusion matching (Sommer et al., 2016). However, CH leads to persistent vasoconstriction and subsequent pulmonary hypertension in conjunction with RVH (Nathan et al., 2019; Smith et al., 2020). Although the specific mechanisms that mediate pulmonary remodelling were not investigated in this chapter, RVH was measured to further validate the CH model.

The ability to rapidly increase ventilation during the ascent to high altitude is mediated by the carotid bodies and is essential for overcoming deleterious physiological effects. During prolonged periods of hypoxia, VAH occurs and is a key respiratory adaptation defined by an increase in baseline ventilation and in some cases an augmented HVR which is found in both humans and animals (Powell et al., 2000a). This adaptation is associated with morphological changes in the carotid body, including type I cell hypertrophy and hyperplasia, along with vascular expansion and an increase in overall

carotid body size (Clarke et al., 2000; Fielding et al., 2018; Platero-Luengo et al., 2014). The origin of these newly formed type I cells is still debated. Some studies suggest they arise from an adult stem cell niche originating from glial-like type II cells (Pardal et al., 2007; Platero-Luengo et al., 2014) while others propose that they derive from the type I cells themselves (Fielding et al., 2018). Type I cells also undergo neurochemical adaptations that increase carotid body oxygen sensitivity, a change thought to contribute to VAH (Kumar & Prabhakar, 2012; Pulgar-Sepúlveda et al., 2018). The mechanisms underlying these adaptations are still being investigated, with likely involvement of changes in neurotransmission, including ATP and adenosine, as explored in later chapters. This chapter aimed to validate that Wistar rats exposed to 12% F_iO_2 for 10 days effectively produced carotid body type I cell expansion and exaggerated chemoafferent activity.

It has been suggested that both the intensity and duration of the hypoxic stimulus, along with the species and even the strain of the animal, play crucial roles in the development of VAH (Arias-Reyes et al., 2021; Pamenter & Powell, 2016; Powell et al., 1998). This chapter characterised the carotid body, respiratory and cardiac adaptations in male Wistar rats exposed to normobaric 12% F_iO_2 for 10 days. There has been ongoing debate over what should be considered 'normoxic' for a rat adapted to CH, and this was further evaluated in light of the data presented in this chapter. These findings were used to establish a foundation and provide a rationale for the protocols in later chapters, aiding in the interpretation of subsequent data investigating the importance of carotid body CD73 signalling in response to CH exposure.

Aims of this chapter were as follows:

1. Develop and validate an animal model of CH induced by exposure of male Wistar rats to an F_iO_2 of 12% for 10 days

2. Characterise the effects of CH on rat cardiovascular parameters including haematocrit, haemoglobin concentration and right ventricular hypertrophy

3. Investigate whether this model of CH caused carotid body hypertrophy and type I cell expansion

4. Determine whether this model of CH altered carotid body chemosensory output

5. Characterise the effects of CH on baseline ventilation and the HVR

3.2 Results

3.2.1 The rat model of CH caused a significant reduction in growth rate, an increase in haematocrit, a rise in haemoglobin concentration and right ventricular hypertrophy

To characterise the rat CH animal model (12% F_iO_2 for 10 days), typical physiological adaptations to CH were measured in Wistar rats. CH rats had reduced body mass and exhibited a reduction in growth rate over the 10 days compared to N (Table 1). CH rats demonstrated a robust increase in haematocrit concomitant with an approximate 20% increase in haemoglobin concentration. Consistent with the hypoxia-induced pulmonary vasoconstriction and subsequent right ventricular remodelling, CH rats developed significant RVH, with a 1.4 fold increase in right ventricular mass. Although, left ventricle mass was slightly lower in CH rats, it was similar to that of N rats when normalised to body mass (Table 1).

	N	CH	*p value*
Animal mass at terminal exp (g)	246 ± 4 (42)	223 ± 5 (40)	<0.001
Growth rate (g day^{-1})	4.6 ± 0.4 (11)	2.3 ± 0.2 (39)	<0.0001
Haematocrit (%)	46 ± 1 (4)	55 ± 0.6 (13)	<0.0001
Haemoglobin (g/dL)	15.8 ± 0.3 (4)	19.0 ± 0.2 (13)	<0.0001
Ventricular septum (mg)	152 ±6 (21)	141 ± 6 (16)	0.227
Left ventricle (mg)	367 ± 11 (21)	325 ± 14 (16)	<0.05
Left ventricle/body mass	1.50 ± 0.04 (21)	1.42 ± 0.07 (16)	0.315
Right ventricle (mg)	116 ± 5 (21)	164 ± 11 (16)	<0.0001
Right ventricle/body weight	0.47 ± 0.01 (21)	0.71 ± 0.04 (16)	<0.0001
Right ventricle/left ventricle+septum	0.22 ± 0.01 (21)	0.36 ± 0.03 (16)	<0.0001

Table 3.1 Haematological and cardiac characteristics of normoxic and chronically hypoxic rats

Haematological and cardiac adaptations of chronically hypoxic rats (CH, 12% F_iO_2 for 10 days) compared to normoxic (N) rats reared in air. Haematocrit and haemoglobin levels were measured using an automated blood analyser. The absolute masses of the cardiac ventricles were determined and further normalised relative to body weight and the left ventricle plus septum (Fulton's index). Data are presented as mean ± SEM, with the animal numbers shown in brackets. Statistical significance between N and CH groups was assessed using an unpaired Student's t-test, with p-values included in the rightmost column.

3.2.2 The model of CH tended to increase TH^+ cell density without changing carotid body size and vascularity

To determine whether 10 days exposure to an F_iO_2 of 12% induced morphological changes in the carotid body, carotid bifurcations were excised and frozen as outlined in the methods in Chapter 2. The carotid bodies were cryosectioned, and 8-10 sections per sample were analysed to quantify the density of TH^+ cells for a single animal. Final observations were presented as per animal data. Example TH-stained sections from N and CH carotid bodies from 3 rats are shown in Figure 3.1 A. Estimations of carotid body volume suggested that 2 out of 3 CH animals had larger carotid bodies compared to N controls, and this was accompanied by an estimated increase in the total number of TH^+ cells (Figure 3.1 B & C). However, although one CH rat had a carotid body similar in size to that of an N rat, all CH rats showed a consistent trend toward a denser TH^+ cell population (Figure 3.1 D, $p = 0.08$). This trend was further supported by an increase in the area of TH^+ signal normalised to carotid body section area ($p = 0.06$) (Figure 3.1 E-G).

Carotid body growth has been reported to involve vascular expansion (Clarke et al., 2000; Fielding et al., 2018). To evaluate whether vascular growth occurred in this CH model, the endothelial marker CD31 was used. Figure 3.2 shows that there were no significant differences between N and CH rats in either the absolute area of CD31 signal or CD31 density within the carotid body. Thus, it appears that this model of CH did not induce significant angiogenesis, despite the rise in TH-cell density.

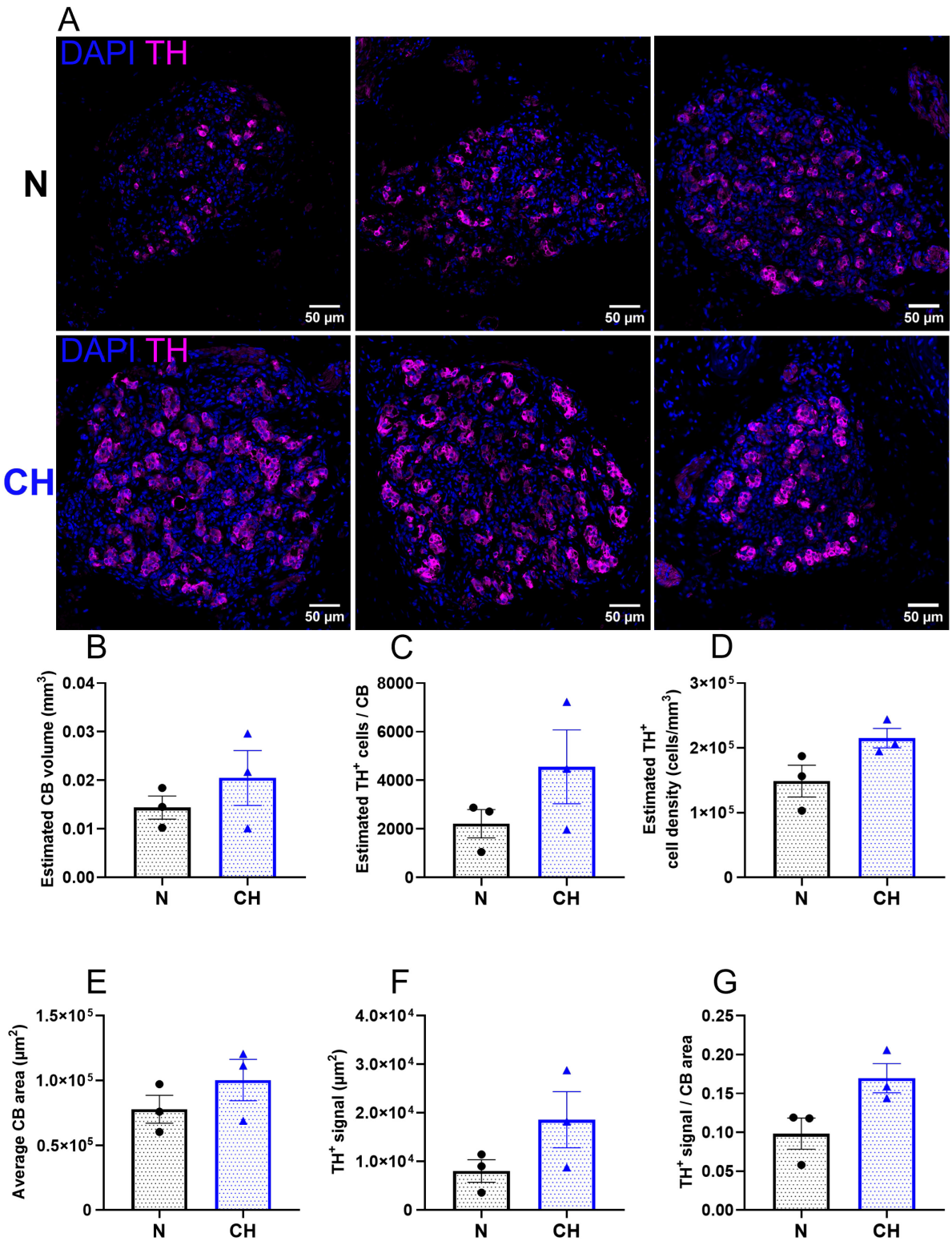

Figure 3.1 Tyrosine hydroxylase expression in the carotid body of normoxic and chronically hypoxic rats

(A) Immunofluorescence images of carotid body (CB) sections from 3 normoxic (N) and 3 chronically hypoxic (CH) rats, stained with DAPI (blue) to label nuclei and tyrosine hydroxylase (TH, magenta) to indicate type I cells. **(B-G)** Quantification of various morphological and cellular characteristics, comparing N and CH CBs. Measurements were averaged from 8-10 sections throughout each carotid body in a single rat. Data are shown as mean ± SEM, with individual data point representing an individual rat (n=3). Statistical significance was assessed using an unpaired Student's t-test.

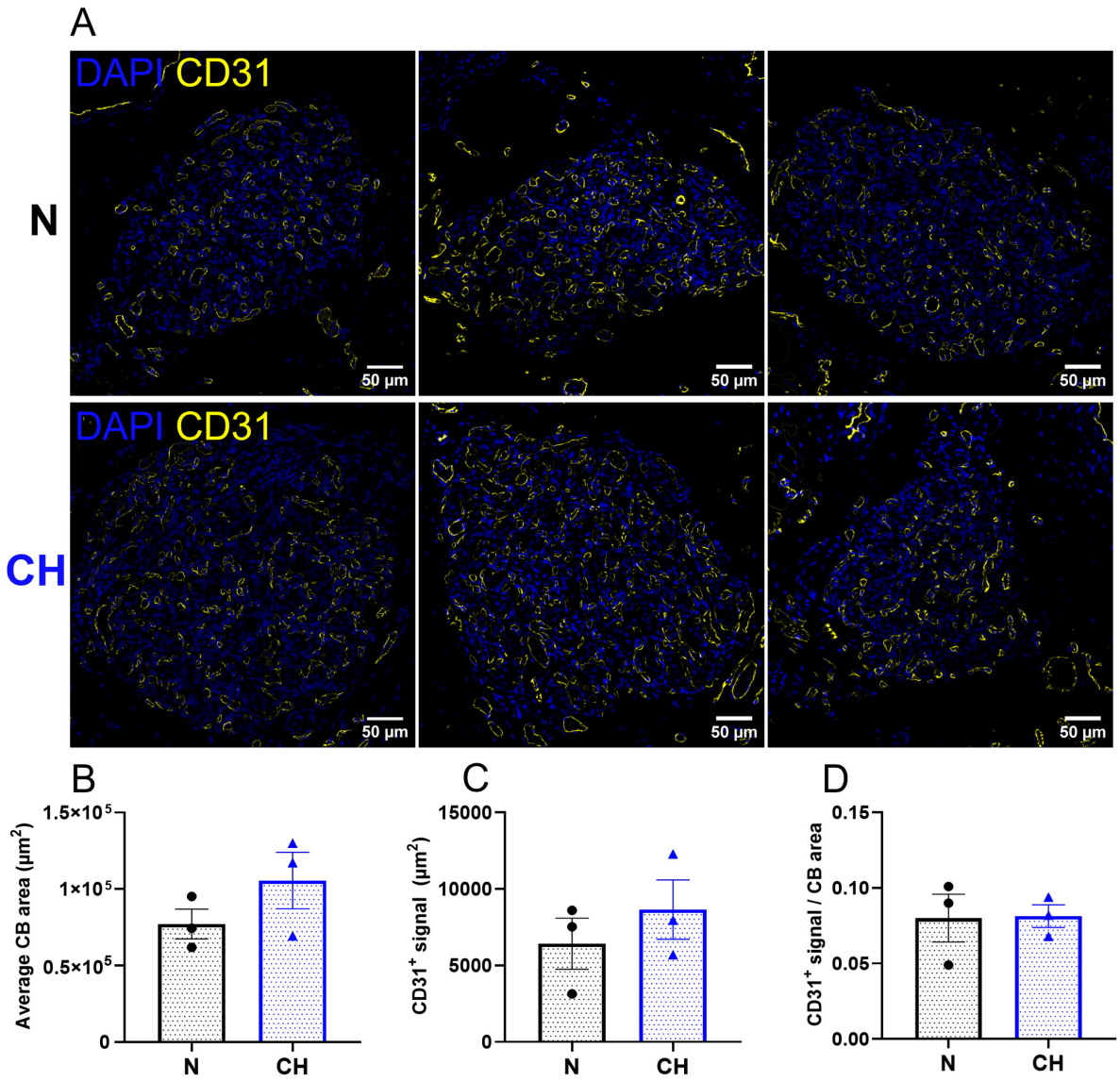

Figure 3.2 Effect of chronic hypoxia on carotid body vascularisation

(A) Immunofluorescence images of carotid body (CB) sections from 3 normoxic (N) and 3 chronically hypoxic (CH) rats, stained with DAPI (blue) to label nuclei and CD31 (yellow) to identify vascular endothelial cells. **(B-D)** Quantification of CB area, total $CD31^+$ signal and the relative $CD31^+$ signal per CB area in N and CH CBs. Measurements were averaged from 3-4 sections throughout each carotid body in a single animal. Data are presented as mean ± SEM, with individual data points representing a single rat (n=3). Statistical significance was assessed using an unpaired Student's t-test.

3.2.3 CH induced carotid body basal hyperactivity and an augmented hypoxic and hypercapnic sensitivity

To characterise whether CH has modified carotid body sensory output, CSN activity was measured *ex vivo*. Figure 3.3 A shows representative raw traces of baseline CSN activity in an N and CH carotid body. 10 days of CH caused a 2-3 fold increase in basal activity and an augmented response to graded hypoxia (Figure 3.3 B-C). The hypoxic response curve in CH caused a rightward PO_2 shift of approximately 44mmHg at a discharge of 5Hz. In addition to investigating hypoxic sensitivity, hypercapnic sensitivity was also measured. Increasing the superfusate PCO_2 from 40mmHg to 80mmHg significantly elevated discharge in both N and CH by a magnitude that overall demonstrated an increased carotid body CO_2 sensitivity (Figure 3.3 D & E).

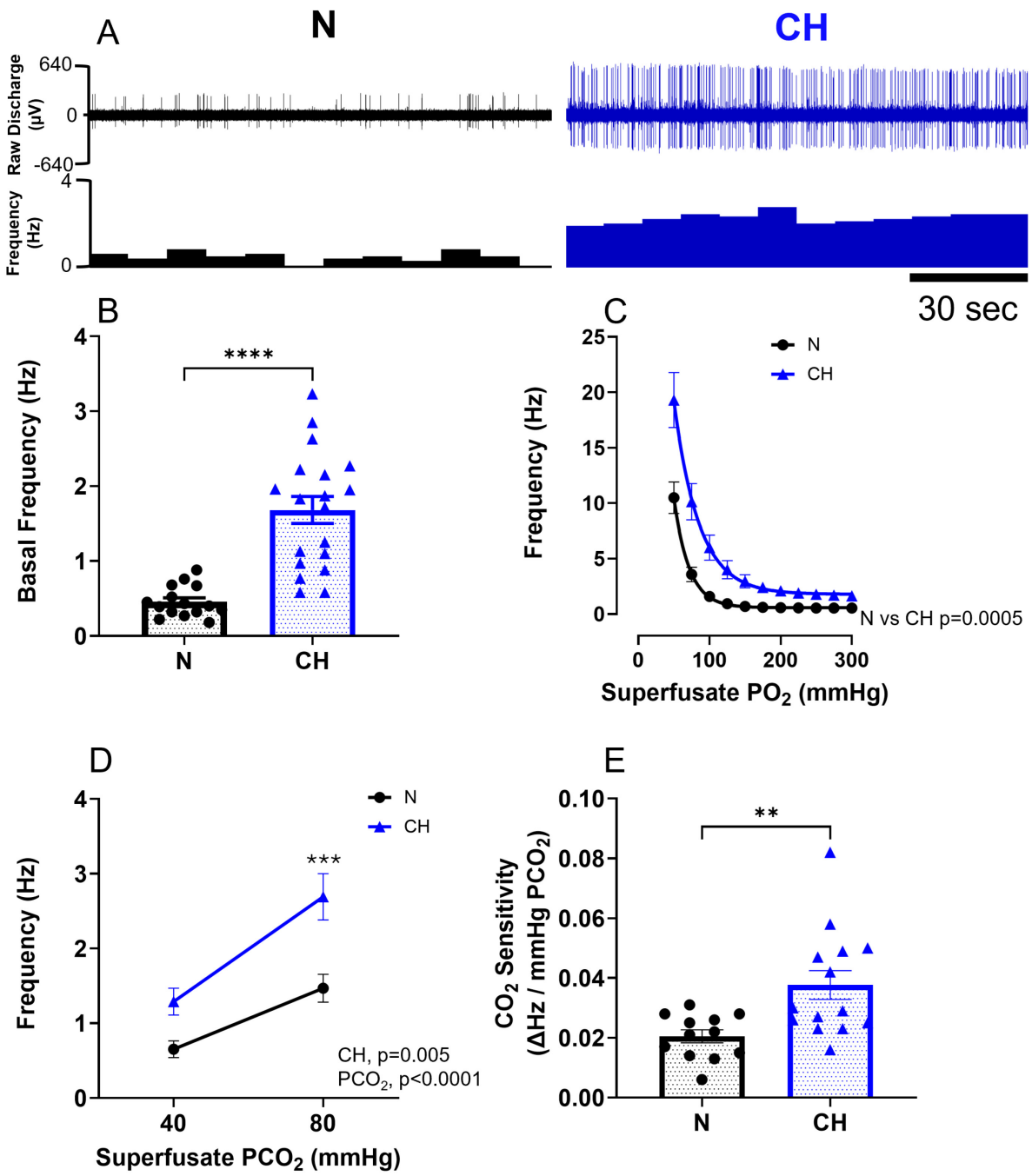

Figure 3.3 The effect of chronic hypoxia on carotid body chemoafferent activity

(A) Representative raw recordings of basal chemoafferent activity from a normoxic (N-left) and chronically hypoxic (CH-right) rat carotid body. Raw discharge (upper) and frequency (lower) shows number of action potentials binned into 10 second intervals. **(B)** comparison of baseline frequency in normoxia. **(C)** comparison of response to graded hypoxia. **(D)** comparison of hypercapnic response. **(E)** comparison of CO_2 sensitivity. Data expressed as mean ± SEM with individual data points representing a single fibre. For N, n=12-15 from 8 rats and for CH, n=14-19 fibres 8 rats. Statistical significance was assessed using an unpaired Student's t-test in A & E, **p<0.01, ****p<0.0001. A two-way repeated measures ANOVA was performed in B & D with overall p values displayed. Bonferroni post-hoc analysis used to compare within groups, ***p<0.001 compared to N.

3.2.4 CH animals exhibited an increase in normoxic minute ventilation but did not have an exaggerated ventilatory response to hypoxia

To determine whether respiratory reflexes differ between N and CH rats, whole-body plethysmography was used to measure ventilation at rest and in response to an F_iO_2 of 10% (moderate hypoxia) and an F_iCO_2 of 6% CO_2 (hypercapnia). For both N and CH rats, baseline ventilation was initially measured in air. Figure 3.4 A presents the time course of minute ventilation during air breathing, in response to moderate hypoxia and following recovery in air before a hypercapnic stimulus was administered. CH rats showed a trend toward an elevated baseline ventilation in air ($p = 0.07$) but exhibited a reduced ventilatory response to moderate hypoxia compared to N controls (Figure 3.4 B-D). In contrast, CH rats displayed a significantly enhanced response to hypercapnia, peaking at 144% above baseline compared to N rats (Figure 3.4 E-G).

Given the observed decrease in the HVR in CH rats, questions arose about whether it was appropriate to use air as a measure of baseline 'normoxic' breathing before administering a hypoxic stimulus, especially since CH animals had spent the previous 10 days adapting to a lower F_iO_2. Therefore, the next set of experiments aimed to measure baseline 'normoxic' ventilation in air for N animals but in 12% F_iO_2 for CH animals. Additionally, as indicated by the haematological data in Table 1, CH rats have an increased oxygen-carrying capacity. This raised the possibility that an F_iO_2 of 10% represented a mild hypoxic stimulus for these animals and might not induce substantial cardiovascular-respiratory reflex activation. Consequently, a stronger hypoxic stimulus of 8% F_iO_2 was used in this subsequent set of experiments.

Figure 3.5 A shows the ventilatory response over time with this revised protocol. CH rats displayed a significantly elevated ‘normoxic’ baseline ventilation. Furthermore, CH rats exhibited a more sustained and greater hypoxic response when challenged with an F_iO_2 of 8%, without signs of hypoxic ventilatory depression (Figure 3.5 A). In contrast, N rats showed an initial peak in the hypoxic response at minute 5, which diminished by half after 10 minutes but remained above baseline. Although the absolute minute ventilation was significantly increased in CH animals in both normoxia and hypoxia, the HVR was not significantly different between groups (Figure 3.5 B-D).

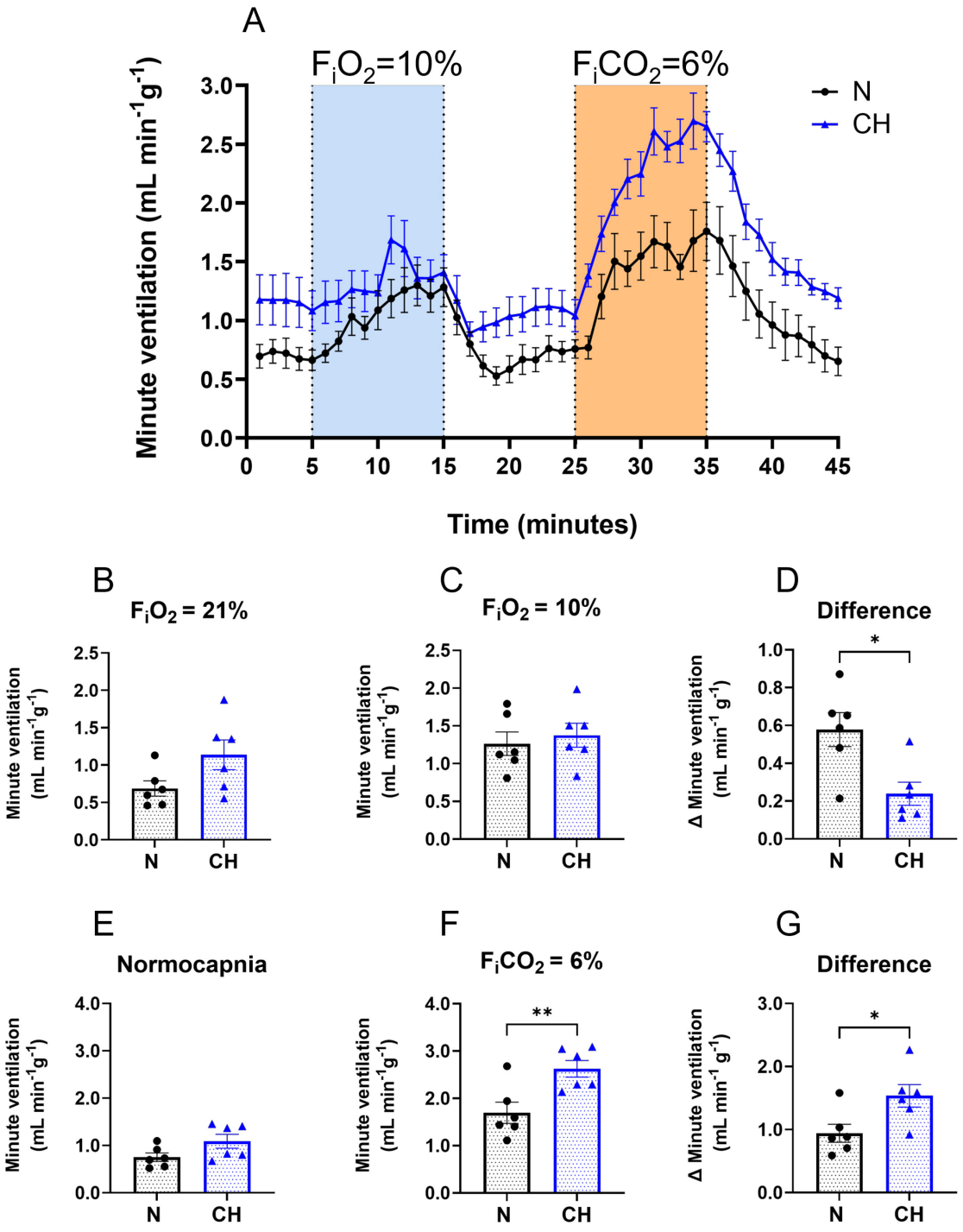

Figure 3.4 Ventilatory responses to moderate hypoxia and hypercapnia in normoxic and chronically hypoxic rats

(A) Time course of minute ventilation in normoxic (N-black) and chronically hypoxic (CH-blue) rats exposed to a moderate hypoxic stimulus (F_iO_2=10%; shaded pale blue) followed by hypercapnic stimulus (F_iCO_2=6%; shaded orange). Bar graphs summarising minute ventilation in air **(B)**, moderate hypoxia **(C)** and change in minute ventilation **(D)**. Bar graphs summarising the minute ventilation in normocapnia **(E)**, hypercapnia **(F)** and the change in minute ventilation **(G)**. Data in A is plotted as the last 10 seconds of every minute. Summary data in B-G is plotted as a mean of the last 3 minutes from A. Error bars show SEM with data points representing an individual rat. n= 6 rats for both N and CH. Unpaired Student's t-test performed in B-D, *p<0.05 and **p<0.01.

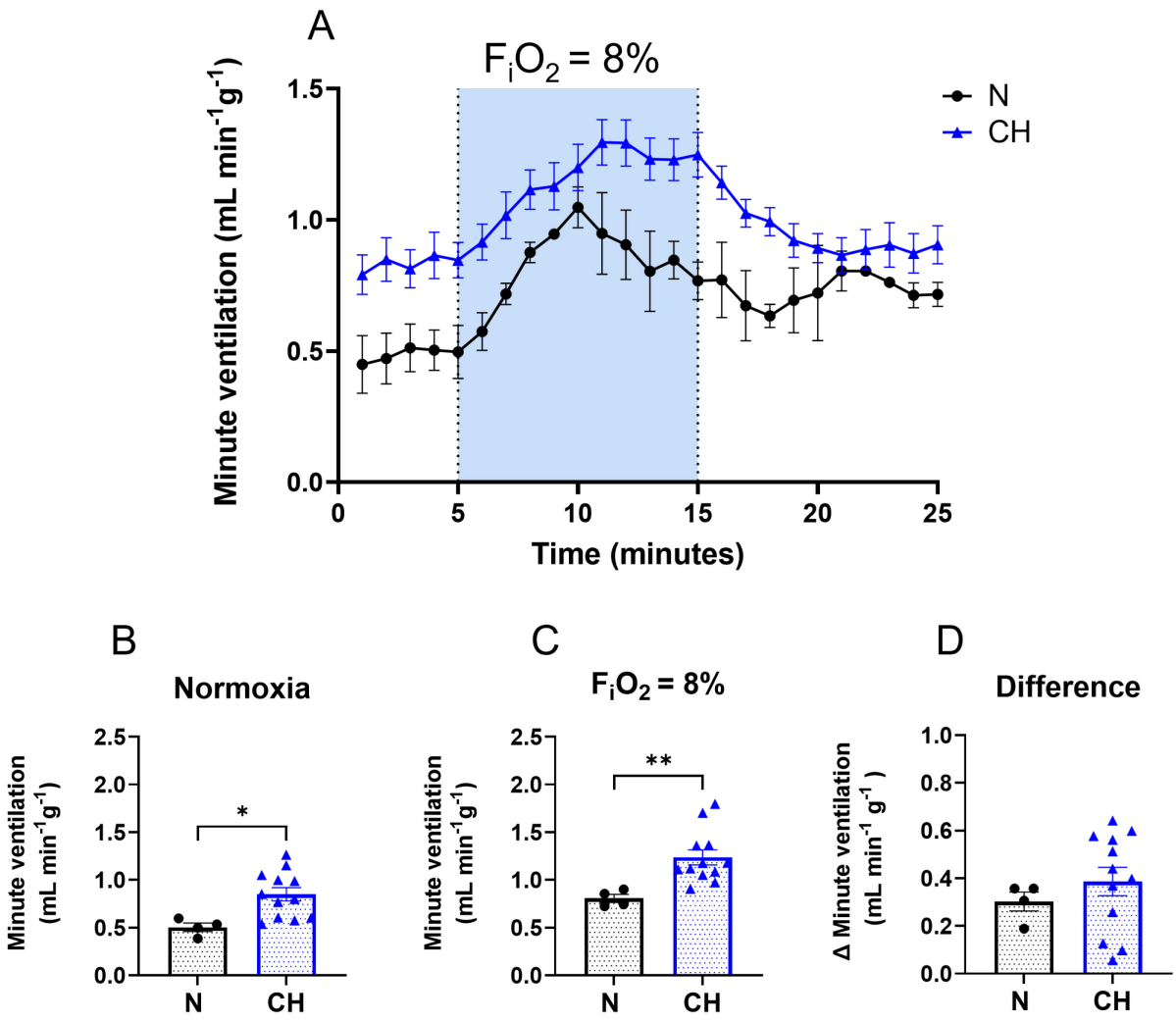

Figure 3.5 Ventilatory responses to a stronger hypoxic stimulus in normoxic and chronically hypoxic rats

(A) Time course of minute ventilation in normoxic (N-black) and chronically hypoxic (CH-blue) rats in response to a stronger hypoxic stimulus (F_iO_2=8%; shaded pale blue). Normoxia was defined as breathing F_iO_2= 21% for N and 12% for CH. Bar graphs summarising the normoxic minute ventilation **(B)**, response to hypoxia **(C)** and change in ventilation **(D)**. Data in A is plotted as the mean of the last 10 seconds of every minute. Summary data in B-D is plotted as a mean of the last 3 minutes from A. Error bars show SEM with data points representing an individual rat. For N, n=4 rats and for CH, n=12 rats. Unpaired Student's t-test performed in B-D, *p<0.05 and **p<0.01.

3.3 Discussion

3.3.1 Summary of key chapter findings:

- CH rats breathing an F_iO_2 of 12% for 10 days had an increased haematocrit, haemoglobin concentration and right ventricular hypertrophy
- CH tended to increase TH^+ cell density in the carotid body
- CH caused carotid body chemoafferent hyperactivity in normoxia
- CH increased carotid body chemoafferent hypoxic sensitivity
- CH rats had a significantly higher minute ventilation in normoxia which was sustained during hypoxia, without modifying the overall HVR
- CH rats have an augmented hypercapnic ventilatory response
- The magnitude of the carotid body, cardiovascular and respiratory adaptations caused by CH were viewed as being sufficient to proceed with this model throughout the rest of the thesis

3.3.2 Haematological and cardiac adaptations to CH

This chapter aimed to characterise the haematological and cardiac adaptations in Wistar rats exposed to an F_iO_2 of 12% for 10 days. The rats exhibited a typical response to CH, marked by significant increases in haematocrit and haemoglobin levels, consistent with findings from other rodent models (Arias-Reyes et al., 2021; Hodson et al., 2016; Marshall & Davies, 1999; Walsh & Marshall, 2006).

The regulation of red blood cell production during CH is well established to be mediated by EPO, a hormone primarily produced by peritubular fibroblasts in the kidney. Under hypoxic conditions, the inhibition of PHD enzymes stabilises HIF-2α, which then promotes EPO transcription. EPO enters the bloodstream and stimulates erythropoiesis in the bone marrow, leading to increased haemoglobin synthesis (Gruber et al., 2007; Haase, 2010). To determine whether the increase in haematocrit observed in this CH model was driven by EPO-induced erythropoiesis rather than by a reduction in plasma volume, direct measurement of EPO levels would be informative. Additionally, assessing reticulocyte counts (immature red blood cells) would provide further evidence of active erythropoiesis in this model.

RVH is also a common consequence of CH. In this study, rats exposed to 12% F_iO_2 for 10 days had approximately 1.4 times greater right ventricular mass than normoxic controls, along with a significantly higher Fulton's Index (right ventricular mass relative to the left ventricle and septum). These findings align with previous rodent studies demonstrating CH-induced RVH (Ball et al., 2014; Horscroft et al., 2015; Horscroft et al., 2019; Smith et al., 2020).

RVH is primarily attributed to increased right ventricular afterload due to pulmonary hypertension. Acute pulmonary vasoconstriction in response to hypoxia helps maintain ventilation-perfusion matching by redirecting blood to better-oxygenated lung regions. However, prolonged hypoxia leads to persistent pulmonary vasoconstriction (Nathan et al., 2019). Interestingly, RVH may also develop independently of pulmonary hypertension. For instance, the selective deletion of HIF-1α in pulmonary artery smooth muscle reduces pulmonary hypertension in CH but does not prevent RVH, suggesting

a direct effect of hypoxia on the heart (Ball et al., 2014). In a later study, cardiac-targeted deletion of HIF-1α paradoxically exacerbates RVH in CH, implying a protective role in moderating ventricular remodelling (Smith et al., 2020). The additional inactivation of cardiac HIF-2α mitigates this effect, indicating a potential role for HIF-2α in regulating RVH, though further research is needed.

3.3.3 CH causes carotid body sensory hyperactivity in line with patterns of increased type I cell density

This chapter aimed to investigate whether 10 days of CH leads to changes in carotid body morphology and altered chemoafferent activity. As shown in Figure 3.1, there were no statistically significant differences in overall carotid body size, both in volume and sectional area, compared to N carotid bodies. However, there was a trend suggesting a higher density of TH^+ cells. This finding contrasts with existing literature from several studies which indicate that while the absolute number of TH^+ cells increases, it does so in proportion to carotid body size, resulting in no observed changes in type I cell density (Bishop et al., 2013; Fielding et al., 2018; Hodson et al., 2016; Pardal et al., 2007; Platero-Luengo et al., 2014).

Several factors may account for these discrepancies, including differences in the animal species used. Results presented in this thesis, utilised rats, whereas studies previously mentioned used mice. The exact reason for these species differences is unknown. Another factor could be the intensity and the duration of the hypoxic stimulus, which is known to affect the ventilatory adaptations, and so whether changes in carotid body morphology also occur is plausible (Pamenter & Powell, 2016; Powell et al., 1998). Rats in this thesis were subjected to an F_iO_2 of 12% for 10 days whereas

previous studies in mice went as low as 10% for 7-21 days (Fielding et al., 2018; Platero-Luengo et al., 2014). It is possible that a stronger hypoxic stimulus is needed to drive a greater expansion of the vasculature, which contributes significantly to carotid body growth and could, in turn, normalise TH^+ cell density. A study using a model of CH based on 12% F_iO_2 in rats reported a 64% increase in overall carotid body volume concomitant with an expansion of blood vessels larger than 12-microns in diameter (Clarke et al., 2000). However, the rats in this study were exposed to CH for 32 days, significantly longer than the 10-day exposure used in this thesis. This suggests that while 12% F_iO_2 is sufficient to trigger angiogenic changes, a prolonged stimulus is required.

The absolute number of TH^+ cells estimated in this thesis is slightly lower than other estimates for the rat carotid body (Kumar & Prabhakar, 2012). One possible explanation for this discrepancy could be differences in section thickness and imaging parameters. In this study, sections were cut at a thickness of 10-microns and imaged in a single focal plane, which may have caused some cells to be missed or out of focus within the full 10-micron depth. A potential solution to capture the full cell count more accurately would be to acquire images using a z-stack, taking images at 1-micron intervals. This approach would provide a more complete representation of cells throughout the 10-micron section. However, because these images were obtained using a tile-scanning function to capture the entire carotid body at high magnification, adding a z-stack would have been more time-consuming and increased the risk of photobleaching due to prolonged exposure to excitation lasers.

Regardless of this discrepancy in the TH^+ density, what remained consistent with all studies including the data presented in this chapter, is that the overall number of TH^+ cells in the carotid body expanded. The origin of new type I cells remains a subject of debate. Initially, it was hypothesised that glia-like type II cells serve as an adult stem cell niche, differentiating into $Nestin^+$ progenitors and eventually maturing into type I cells under hypoxic conditions (Pardal et al., 2007). However, these progenitors do not exhibit a proliferative response to hypoxia *in vitro*, leading researchers to question whether an alternative stimulus that is absent in an *in vitro* setting might be required for proliferation. Later, endothelin-1 was proposed as a key paracrine mediator released by type I cells to promote progenitor differentiation (Platero-Luengo et al., 2014). However, studies using advanced lineage tracing techniques revealed that newly formed type I cells actually originate from a pre-existing population of TH^+ cells. Specifically, the inactivation of HIF-2α in type I cells, but not in type II cells, significantly impairs this proliferative process (Fielding et al., 2018). Supporting this idea, Sobrino and colleagues identified a subpopulation of mitotic TH^+ cells (neuroblasts) which express low levels of TH and the marker HNK-1. These cells may drive rapid increases in the type I cell population within 24-48 hours of hypoxia without altering carotid body size (Sobrino et al., 2018). The findings presented in this chapter align with Sobrino and colleagues, as they also demonstrate an increase in type I cell numbers without changes in overall carotid body size.

While an increase in the TH^+ cell population may contribute to carotid body hyperactivity in CH, as suggested by data in Figure 3.1 and 3.3, other mechanisms are also likely involved. Preventing carotid body hypertrophy in CH with an endothelin-1 receptor antagonist reduces the elevated basal and hypoxic discharge but does not fully restore activity to control levels (Chen et al., 2007). This suggests that specific

cellular adaptations may enhance type I cell excitability. Proposed mechanisms include enhanced inhibition of TASK-like currents, reductions in K^+ current density and increases in background Na^+ current density and expression, which could make the resting membrane potential of type I cells more positive, increasing excitability (Caceres et al., 2007; Hempleman, 1995; Ortiz et al., 2009) . Additionally, calcium influx and subsequent neurotransmitter release are known to be augmented in CH (Hempleman, 1996; Livermore & Nurse, 2013; Stea et al., 1995). Whether increased CD73 activity also contributes to CH-induced elevation in basal and hypoxic sensitivity will be explored in the following chapters.

3.3.4 Carotid body vs central adaptations to CH

Although CH rats exhibited heightened carotid body hypoxic sensitivity *ex vivo*, they did not show an enhanced HVR *in vivo*. This is somewhat unexpected, as previous studies in both animals and humans have reported increased ventilatory sensitivity to acute hypoxia following CH (Aaron & Powell, 1993; Bishop et al., 2013; Fielding et al., 2018; Hodson et al., 2016; Powell et al., 2000a). One possible explanation is hyperventilation-induced alkalosis which is common during hypoxia. While arterial CO_2 (P_aCO_2) was not directly measured in these experiments, end-tidal CO_2 was assessed in anesthetised animals in Chapter 6. As shown in Figure 3.5, CH rats hyperventilate even in normoxia and exhibit hypocapnic end-tidal CO_2 readings (Chapter 6). Furthermore, end-tidal CO_2 levels were even lower at the end of acute hypoxia, with this effect being more pronounced in CH animals (Chapter 6). This hypocapnia may reduce the activity of central chemosensory neurons, thereby dampening the central respiratory drive and blunting the HVR (Aaron & Powell, 1993).

Studies have shown that when P_aCO_2 is held constant during hypoxia (isocapnic hypoxia), the HVR in CH animals is significantly augmented compared to normoxic controls (Aaron & Powell, 1993; Powell et al., 2000b). However, the precise level at which P_aCO_2 should be maintained during acute hypoxia remains debated, making direct comparisons between studies difficult. Nonetheless, the most accurate way to assess whether CH increases hypoxic sensitivity is by directly measuring carotid body activity at well-defined PO_2 levels. Indeed, this chapter utilised an intact whole-carotid body preparation, allowing for direct recordings of chemoafferent discharge, which showed that at any given PO_2, CH rats exhibit greater activity than normoxic controls (Figure 3.3). Thus, this model of CH does effectively induce carotid body hyperactivity.

Beyond peripheral changes, central adaptations in the brain may also contribute to enhanced ventilatory responses to hypoxia in CH. Studies in anesthetised rats exposed to 7 days of CH found significantly greater phrenic nerve activity and minute ventilation for a fixed level of CSN stimulation, suggesting plasticity in brainstem-chemoafferent signal processing (Dwinell & Powell, 1999). This increased brainstem sensitivity may result from remodelling of synaptic connections between chemoafferents, the NTS and other nuclei responsible for respiratory modulation.

Some of these changes involve altered glutamatergic transmission in the NTS. Blocking glutamate receptors in CH rats caused greater reductions in the HVR compared to normoxic rats, suggesting enhanced glutamate signalling. This may be due to increased phosphorylation of glutamate receptor subunits, specifically in the NTS of CH rats (Pamenter et al., 2014). Additionally, GABAergic inhibition appears to be reduced, as CH decreases the sensitivity of $GABA_A$ receptors in neurons isolated

from the caudal NTS (Tolstykh et al., 2004). These neural adaptations are likely mediated by HIF stabilisation in distinct brain regions. Supporting this, a recent study showed that inducible inactivation of HIF-1α in glutamatergic neurons of the NTS significantly reduces the HVR compared to control mice (Moya et al., 2020).

Interestingly, CH rats also exhibited a stronger response to hypercapnia. This may be partially explained by increased carotid body CO_2 sensitivity, as observed in this chapter (Figure 3.3 D). However, it is important to note that hypercapnic responses *in vivo* were measured while CH rats were breathing air, which may not represent their true "normoxic/normocapnic" baseline. If CH rats were hyperoxic during these measurements, this could have silenced carotid body activity (see next section). The fact that hypercapnic responses remained elevated despite this potential suppression suggests that central CO_2 sensitivity may have been enhanced. These findings indicate a complex interplay between peripheral and central mechanisms in modulating respiratory output in CH rats. To obtain more precise insights, future experiments should repeat hypercapnic response measurements with CH rats breathing 12% F_iO_2 as their baseline condition. Given the greater than additive interaction of hypoxia and hypercapnia on ventilation, one might expect this ventilatory response to be even greater under these conditions (Kumar & Prabhakar, 2012).

3.3.5 Should 12% F_iO_2 be considered normoxic for a CH rat?

This chapter demonstrates that rats exposed to 12% F_iO_2 for 10 days exhibit significant increases in haematocrit and haemoglobin concentration compared to N controls. These adaptations likely help restore oxygen delivery to tissues through enhanced carotid body chemoreflex activation, local vasodilation and increased oxygen-carrying capacity. Previous studies have shown that rats exposed to 12% F_iO_2 for 1-4 weeks

achieve normalised O_2 content (C_aO_2) and oxygen delivery to skeletal muscle (Marshall & Davies, 1999). However, it remains uncertain whether the CH model used here achieves the same C_aO_2 as air-exposed N rats, as arterial oxygen (P_aO_2) and saturation (S_aO_2) were not directly measured.

To estimate C_aO_2, reference can be made to similar experiments on the same rat strain under the same anaesthetic conditions. For instance, a study using a comparable 7-day CH model reported a P_aO_2 of approximately 41 mmHg in CH rats and 89 mmHg in N rats (Walsh & Marshall, 2006). Using the human oxyhaemoglobin dissociation curve, these P_aO_2 values correspond to estimated S_aO_2 levels of 98% for N rats and 75% for CH rats. Applying the haemoglobin (Hb) concentration data from Table 1, C_aO_2 can be estimated using the equation:

$$C_aO_2 = (Hb \times S_aO_2 \times 1.34) + (P_aO_2 \times 0.003)$$

Estimates suggest O_2 content values of 20.5 mL O_2/dL in N rats and 19.2 mL O_2/dL in CH rats, indicating that this CH model maintains near-normal O_2 content and adapts effectively (Marshall & Davies, 1999; Montero & Lundby, 2019; Walsh & Marshall, 2006). As shown in Figure 3.5 B, CH rats exhibit increased resting ventilation. Additional *in vivo* data under anaesthesia, presented in Chapter 6, show lower end-tidal CO_2 levels, indicative of hyperventilation. This finding aligns with previous studies showing reduced P_aCO_2 and a slight increase in pH in CH rats (Walsh & Marshall, 2006). Due to the Bohr effect, this mild alkalosis shifts the oxyhaemoglobin dissociation curve to the left, enhancing haemoglobin's affinity for oxygen and potentially bringing O_2 content closer to that of N rats. These estimates are approximate, and future studies should directly measure P_aO_2, S_aO_2, and pH to more accurately determine O_2 content in CH rats exposed to 12% F_iO_2 for 10 days.

Maintaining CH rats at 12% F_iO_2 throughout experiments ensures physiological stability and consistency, as they are well adapted to this oxygen level. Chapter 6 reveals that CH rats have higher blood pressure when breathing air compared to N rats, confirming that air exposure is hyperoxic for them, leading to vasoconstriction. Additionally, CSNX, which removes carotid body sensory discharge, causes a drop in ventilation in N rats but does not further decrease ventilation in CH rats breathing air. This further supports the idea that these animals experience hyperoxia in room air, with carotid body activity already suppressed under these conditions. Consequently, for the *in vivo* experiments in Chapter 6, baseline cardiovascular and respiratory measurements in CH rats were taken at 12% F_iO_2 to reflect their true normoxic condition.

A 9-10 day exposure to 12% F_iO_2 was chosen because previous evidence suggests that chemoafferent discharge peaks at 9 days and does not increase further up to 16 days (Chen et al., 2002). This timeframe allows for a focused investigation of CD73's role in promoting carotid body hyperactivity, without additional systemic or central adaptations beyond 10 days when carotid body activity remains stable. A 12% F_iO_2 level was selected over more severe oxygen tensions (e.g., 10% F_iO_2 which is commonly used) due to its clinical relevance to COPD. Patients with COPD typically have P_aO_2 values between 50–75 mmHg at rest, with severe disease defined as P_aO_2<60 mmHg (Delclaux et al., 1994; Haidl et al., 2004; Sliwinski et al., 1994; Stoller et al., 2010). While P_aO_2 was not directly measured in these CH rats, previous studies using the same rat strain and anaesthetic conditions suggest values of 40–50 mmHg (Marshall & Davies, 1999; Walsh & Marshall, 2006). It is important to note that these values come from anesthetised animals, where reduced ventilation from anaesthesia tends to lower P_aO_2, meaning that 12% F_iO_2 resembles more severe hypoxemia in

COPD patients. A reduction to 10% F_iO_2 would likely cause an even greater drop in P_aO_2 making it less clinically relevant to COPD. Although this thesis does not specifically investigate COPD models, CH is a key component of the disease. Using 12% F_iO_2 allows for a closer approximation of the CH phenotype seen in COPD, enabling the study of CH-induced carotid body hyperactivity mechanisms in a relevant physiological context. The data from this chapter also show that this duration and intensity of hypoxia is sufficient to induce significant carotid body hyperactivity and can therefore be used to evaluate the importance of CD73 in driving this process in the subsequent chapters.

3.4 Conclusions

Rats exposed to an F_iO_2 of 12% exhibited appropriate haematological and cardiac adaptations. Resting minute ventilation was elevated when breathing air and when breathing 12% F_iO_2 as their normoxic baseline compared to N controls, indicating VAH and an appropriate *in vivo* adaptation in this CH model. Direct measurements of carotid body activity confirmed significant hyperactivity compared to N controls, along with a heightened hypoxic sensitivity. Morphological analysis showed a trend toward an increased TH^+ type I cell population, which may contribute to both tonic hyperactivity and oxygen hypersensitivity. However, it remains unknown whether these newly formed type I cells also express CD73, and the functional role of CD73 in mediating CH-induced hyperactivity has yet to be determined. The findings in this chapter validate this CH model as a suitable system for investigating this in the following chapters.

CHAPTER 4

4. Chronic hypoxia and its impact on CD73 localisation within the carotid body

4.1 Introduction and aims

Purinergic signalling via ATP and adenosine plays a critical role in various tissues throughout the body. The balance between these two purines determines the signalling outcome and is regulated by a set of enzymatic proteins that hydrolyse tri-, di-, and mono-phosphates. ATP catabolism occurs in a two-step reaction, first breaking down into ADP and AMP via the NTPDase family. AMP is further hydrolysed into adenosine by the rate-limiting enzyme ecto-5'-nucleotidase (CD73)(Alcedo et al., 2021). Figure 1.3 shows a summary of the breakdown cascade.

CD73 is most abundantly expressed in human smooth muscle, where rare mutations in the CD73 gene (*NT5E*) cause arterial calcification in humans (Minor et al., 2019; Uhlen et al., 2015). Interestingly, *NT5E* knockout mice do not display this phenotype, as studies suggest a lack of CD73 expression in vascular smooth muscle of arteries of mice and rats and instead show higher expression in endothelial cells (Fausther et al., 2012; Ohta et al., 2013). These CD73 knockout mice are fertile and grow normally but show vascular leakage in multiple organs even under resting conditions. When exposed to severe hypoxia, this leakage is significantly worsened, especially in the lungs as evidenced by perivascular interstitial oedema and increased infiltration of inflammatory mediators (Thompson et al., 2004). Furthermore, mice display impaired protection via ischemic pre-conditioning as demonstrated by larger myocardial infarcts (Eckle et al., 2007) and renal injury (Grenz et al., 2007). The injection of soluble CD73 could restore cardiac and renal protection by ischemic pre-conditioning.

This effect on the renal system is not surprising given that the kidney is a site of high CD73 expression and where it exhibits one of the highest-level enzymatic activities in the body, in addition to the colon and the brain (Colgan et al., 2006). CD73 has been instrumental in identifying EPO-producing interstitial kidney fibroblasts (Bachmann et al., 1993; Kaissling & Le Hir, 2008). The reproductive organs, lungs, heart and brain also express relatively high levels of CD73, but its expression in sensory peripheral organs like the carotid body remains relatively underexplored.

Under normal conditions, CD73 mRNA is detectable in the whole carotid body and peripheral ganglia, such as the SCG and petrosal ganglion, both of which innervate the carotid body (Salman et al., 2017). Notably, CD73 mRNA expression in the carotid body is 5-8 times higher than in the SCG and nearly double that of the brain, indicating its potential significance in carotid body purinergic signalling. However, these findings do not identify which cell types express CD73. In contrast, a single-cell RNA sequencing study of mouse type I cells (n = 8) detected no mRNA for CD73, NTPDases, or the A_{2B} receptor. Instead, ENT mRNA was present, along with very high levels of A_{2A} receptor transcripts (Zhou et al., 2016). It is therefore puzzling that adenosine-producing enzymes appear absent despite the presence of adenosine receptors and transporters. These discrepancies may arise from differences in species (mouse vs rat), developmental stage (5-day-old mice vs. juvenile rats) or the presence of these transcripts in other cell types.

Further supporting CD73 expression in adult rats, Sacramento and colleagues observed $CD73^+$ signals in immunofluorescently stained carotid body sections with morphology consistent with type I cells but did not co-stain with a type I cell marker

such as TH (Sacramento et al., 2019). In rat dissociated carotid body cultures, CD73 has been co-localised with TH^+ type I cells and glial-like type II cells (Salman et al., 2017). However, co-localisation studies in intact carotid body sections, preserving complete morphology, have not yet been performed.

Although CD73 mRNA in the carotid body has been shown to increase approximately two-fold under CH, it remains unclear whether this translates to higher protein levels and/or changes in the relative cellular distribution. Studies in PC12 cells (a model for type I cells) have shown an increase in CD73 protein after 48 hours of hypoxia (Kobayashi et al., 2000b). However, spatial changes in CD73 expression throughout the carotid body following CH have not been investigated. This chapter aims to use immunofluorescence to label CD73 protein in frozen carotid body sections. Due to technical limitations, intensity comparisons between N and CH samples were not feasible, leaving expression levels undetermined. Nevertheless, analysing the area of $CD73^+$ signal relative to carotid body size may provide insights into CD73 density and any spatial changes in protein distribution.

Aims of this chapter were as follows:

1. Optimise an CD73 antibody and staining protocols in PFA-fixed frozen carotid body sections
2. Utilise a machine learning approach to identify and remove red blood cell autofluorescence
3. Determine quantitative changes in type I cell $CD73^+$ signal in N and CH rat carotid bodies

4. Determine quantitative changes in a more sensitive $CD73^+$ signal in N and CH rat carotid bodies

5. Examine the identity of the more sensitive $CD73^+$ signal by co-staining with CD31 (vascular marker) and neurofilament-light chain (nerve process marker)

4.2 Results

4.2.1 Determining the optimal CD73 antibody concentration and staining conditions

To identify the location of CD73 in the carotid body, the CD73 antibody was titrated to determine the optimal concentration. This antibody has been previously validated on dissociated rat carotid body cultures (Salman et al., 2017) using titration guidelines from the manufacturer (Fausther et al., 2012). Figure 4.1 shows representative immunofluorescent images of serially sectioned carotid bodies from control rats co-stained with CD73 and TH to identify type I cells.

At high concentrations, the CD73 antibody produced strong staining localised to type I cells but also showed significant background staining (Figure 4.1 A). A two-fold serial dilution reduced background staining but also weakened the CD73 signal in type I cell clusters. By a dilution of 1:400, staining in type I cells was no longer detectable. However, at this concentration strong positive signals remained in regions outside type I cells. These titration experiments were replicated in multiple carotid body samples, showing consistent patterns. At an even lower concentration of 1:1000 (data shown in Figure 4.7) a positive CD73 signal outside the type I cells was still detectable.

A 1:100 dilution was chosen as it consistently retained CD73 staining in type I cells while minimising background. However, as shown in Figure 4.1 A, the CD73 signal in type I cell clusters appeared less distinct compared to the TH staining. Formaldehyde-based fixatives are known to create protein cross-links that can mask target epitopes, potentially reducing antibody binding (Scalia et al., 2017). To address this, an antigen retrieval step was introduced, as recommended by the manufacturer. Several protocols were tested including heat-mediated retrieval using citrate buffer (pH 6.0) or TRIS buffer (pH 9.0) at 95°C for 20 minutes and enzyme-mediated retrieval with trypsin. Of these, citrate buffer showed the greatest improvement in CD73 signal, but sections were often damaged by high temperatures.

The protocol was refined by incubating sections in citrate buffer at 60°C overnight instead of boiling. Figure 4.2 B shows enhanced CD73 staining using this revised antigen retrieval protocol, with magnified regions demonstrating overlap with TH^+ type I cells (Figure 4.2 C). This method consistently improved the type I cell CD73 signal without compromising tissue integrity and was validated in three separate carotid body samples at a concentration of 1:100 (see Appendix Figure S.1). A $CD73^+$ signal was also detected at 1:1000 following antigen retrieval, although the signal was much weaker than 1:100 (Appendix Figure S.2). Therefore, the CD73 antibody was used at a concentration of 1:100 with antigen retrieval moving forward. A pre-immune serum control, collected from the host animal prior to immunisation with the CD73 antigen, was used as a negative control at the same concentration as the CD73 antibody (1:100). While it showed some inherent background signal, the intensity was substantially lower compared to the signal observed with the CD73 antibody.

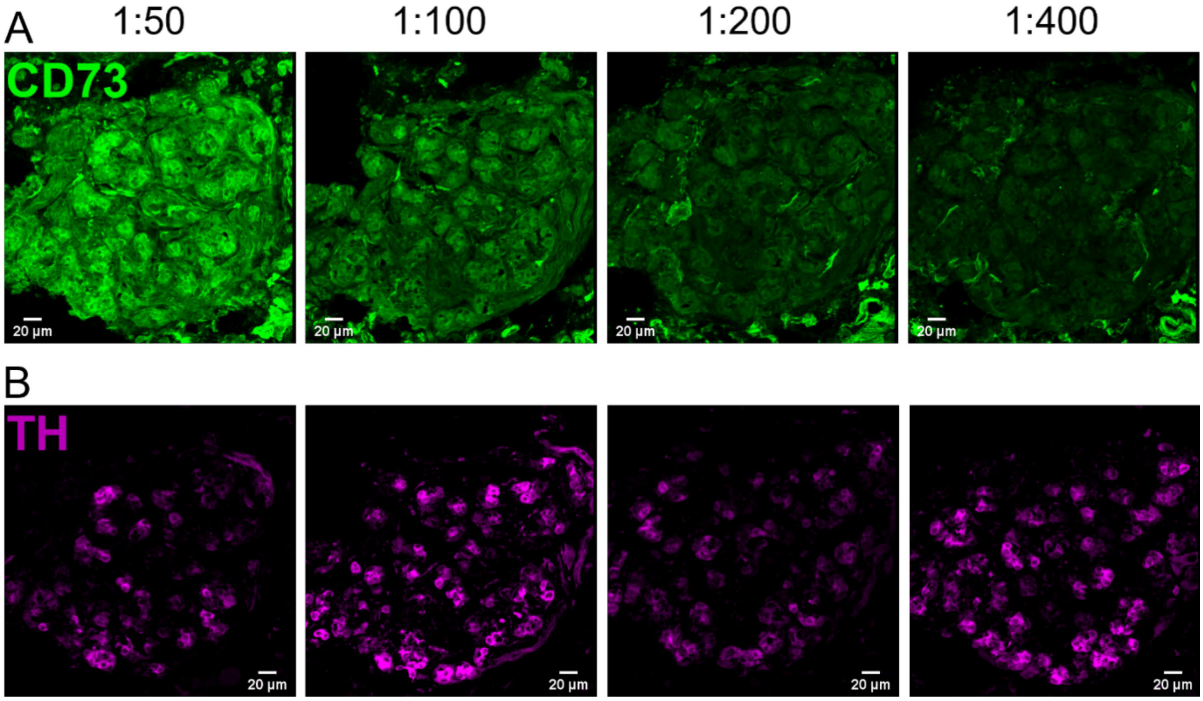

Figure 4.1 CD73 antibody optimisation: concentration

(A) Representative immunofluorescence images of serial carotid body sections from control rats showing different dilutions of the CD73 antibody to optimise signal to noise. Each panel in the top row represents a distinct antibody dilution to determine optimal signal intensity and specificity for CD73 staining (green). **(B)** Tyrosine hydroxylase (TH, magenta) serves as a marker for type I cells, providing a structural reference across sections and was kept at a constant concentration of 1:500.

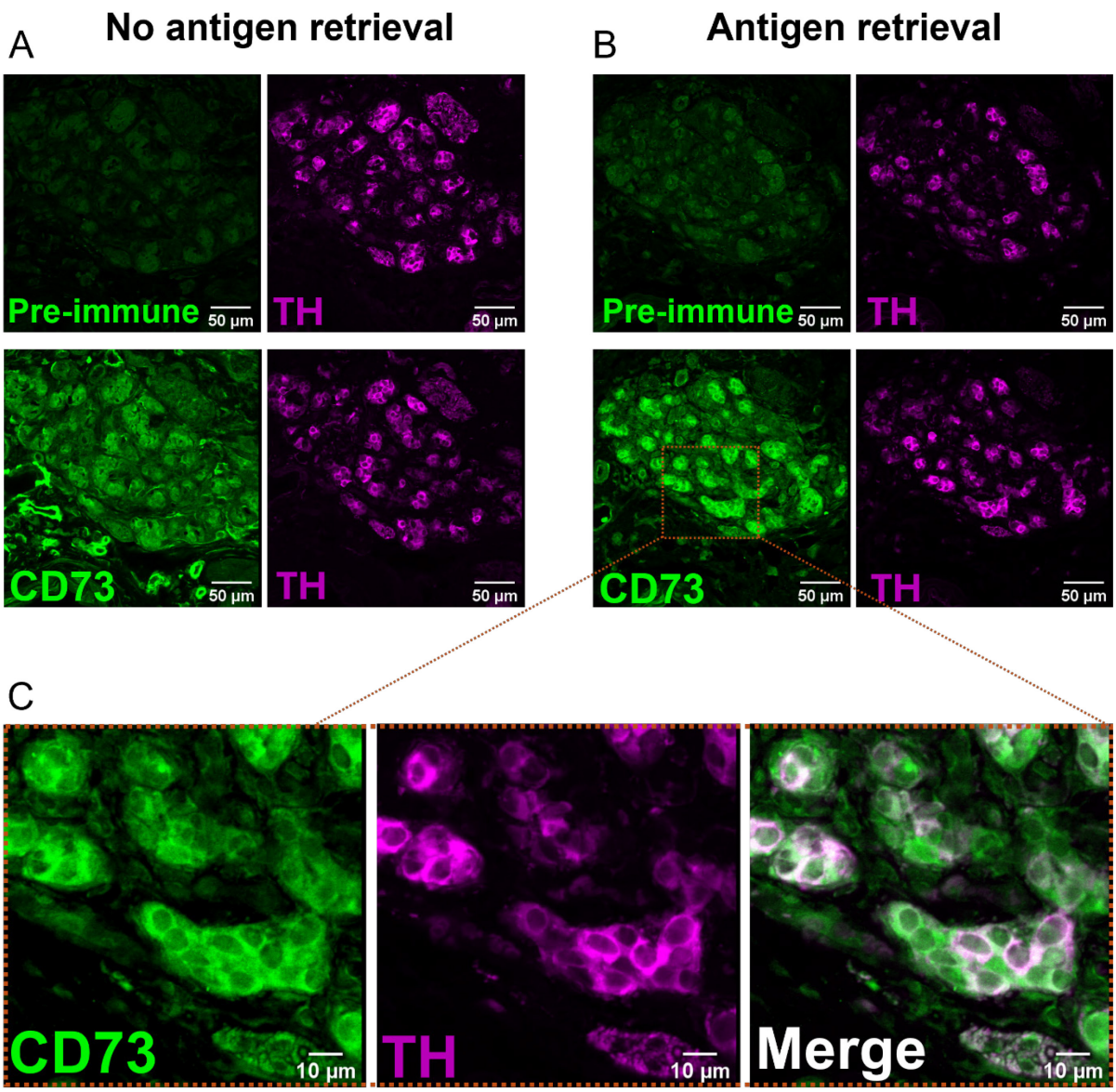

Figure 4.2 CD73 antibody optimisation: antigen retrieval

Representative immunofluorescence images of carotid body sections stained with pre-immune serum (1:100) or CD73 antibody (1:100) before **(A)**, or after **(B)** antigen retrieval. Tyrosine hydroxylase (TH, 1:500) was used to identify type I cells. **(C)** enlarged view of the area within the dotted outline in B, showing CD73, TH and merged images with antigen retrieval at higher magnification.

4.2.2 Validation of antibodies and removal of red blood cell autofluorescence

To validate the specificity of the CD73 and TH antibodies, the SCG was used as a positive control. This peripheral sympathetic ganglion is known for its abundant TH expression due to its role in catecholamine synthesis. CD73 expression in the SCG has also been previously reported (Salman et al., 2017). Figure 4.3 A demonstrates positive staining for both CD73 (1:100) and TH (1:500) in the SCG following antigen retrieval. To confirm the specificity of the secondary antibodies, carotid body sections were incubated without primary antibodies and stained with only secondary antibodies (AF488; 1:1000, AF594; 1:250 and AF647; 1:1000). These sections showed no positive staining, indicating minimal background signal from the secondary antibodies (Figure 4.3 B).

Despite optimisation, a signal remained at various wavelengths, which upon closer inspection, resembled RBCs due to their characteristic biconcave disk shape (Figure 4.3 B). RBCs are known to be highly autofluorescent due to porphyrins within haemoglobin, common in highly vascular tissues that have not been perfused fixed. This autofluorescent signal was confirmed to originate from RBCs based on their localisation within vascular structures marked by the endothelial marker CD31 (Figure 4.4).

RBC AF poses a challenge because it generates false-positive signals that cannot be easily removed by simple thresholding, particularly if the intensity of RBC AF is similar to that of the true positive signal. Therefore, it was essential to remove RBC AF before quantifying the stained images. To address this, a machine learning approach was implemented using the Python-based software, *ilastik* (Berg et al., 2019).

Figure 4.4 A shows the process of manually labelling objects as $CD31^+$, RBC^+ or background based on pixel features such as intensity, texture and shape. This labelling was performed on a small set of images (approximately 4) to train the software. Once trained, the software applied the classification model to batch process subsequent images. The output was a segmented image that differentiated background, CD31 signal and RBCs (Figure 4.4 B). In images where CD31 was not stained, another protein of interest was used to train another classification model (overall 3 classification models were trained).

This segmented image was imported into Fiji/ImageJ, where the RBC-specific pixels were isolated and converted into a binary mask. This mask was subtracted from the original raw image, effectively removing RBC AF (Figure 4.4 C & D). The final processed image displays $CD31^+$ staining with RBC AF removed (Figure 4.4 E). The RBC binary mask can also be subtracted from other channels within the same image ensuring accurate quantitative analysis across all proteins of interest.

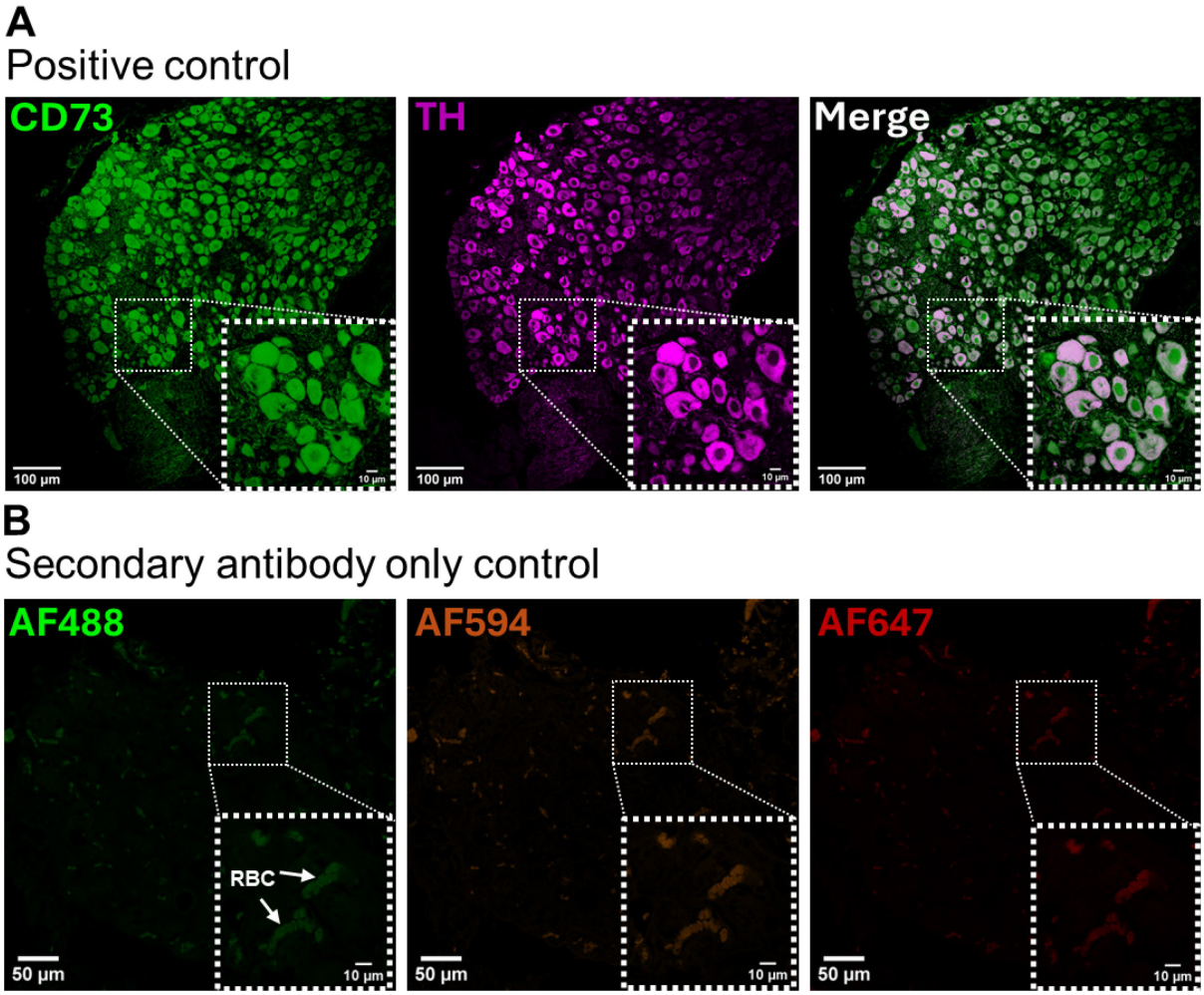

Figure 4.3 Validation of CD73 and tyrosine hydroxylase immunostaining

(A) Representative immunofluorescence images of the superior cervical ganglion (SCG) stained for CD73 (1:100), tyrosine hydroxylase (TH,1:500) and a merged image showing overlap. SCG was used as a positive control due to its previously detected expression of CD73 and TH. Insets (dotted boxes) display higher magnification of the indicated regions. **(B)** Immunofluorescence images showing carotid body sections stained with multiple secondary antibodies (anti-rabbit AF488;1:1000, anti-mouse AF594;1:250, anti-goat AF647;1:1000) in the absence of primary antibodies. AF488, AF594 and AF647 channels show minimal background staining, confirming antibody specificity but do show autofluorescent red blood cells (RBCs). Insets (dotted boxes) provide a closer view of the boxed regions, with RBCs indicated by arrows in the AF488 image as a reference.

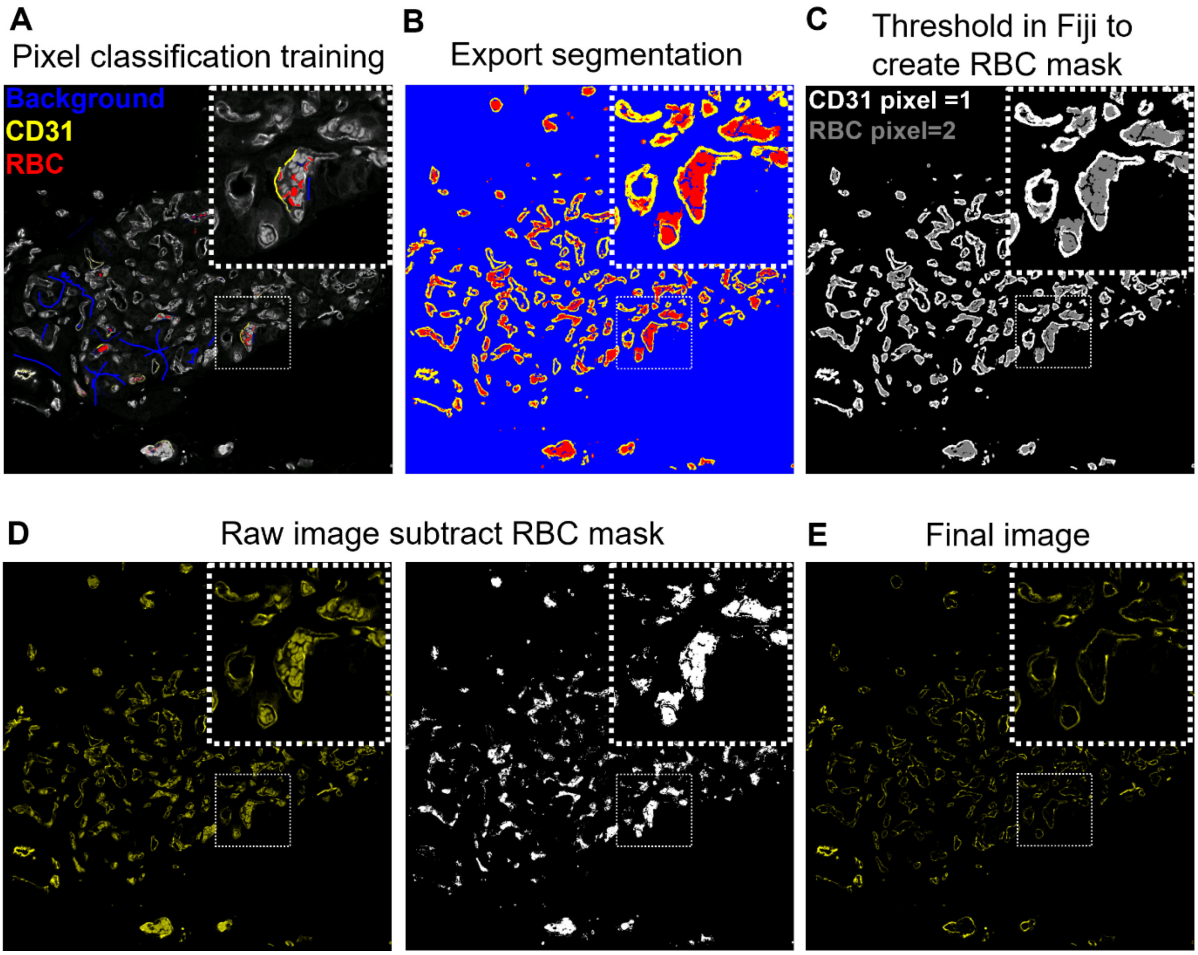

Figure 4.4 Machine learning approach for detection and removal of red blood cell autofluorescence in carotid body sections

(A) a raw immunofluorescence image of a carotid body section showing $CD31^+$ staining and RBC AF. Using the software ilastik, different signals can be classified based on their pixel properties and can be labelled accordingly, background (blue), CD31 (yellow) and RBCs (red). Training was performed on 4 different sections and the software could accurately predict what pixels belong to what label. **(B)** shows a segmented image after pixels have been classified into their labels, which is exported into Fiji. **(C)** segmented image in Fiji that shows $CD31^+$ pixels (grey scale pixel value=1) and RBC pixels (grey scale pixel value=2). A threshold can be applied with a grey scale min/max of 2 to only display RBCs. Applying this threshold creates a binary mask (bottom row, centre) which can be subtracted from the original raw image **(D)**. **(E)** final image containing $CD31^+$ signal, free from RBC AF, ready for analysis. Insets (dotted boxes) provide a closer view of the boxed regions.

4.2.3 CH tended to increase the proportion of $CD73^+TH^+$ cells in the carotid body

To determine whether the total $CD73^+$ signal is altered in CH carotid bodies, sections first underwent antigen retrieval to unmask the CD73 epitope on type I cells before immunostaining. This was performed on 3-4 carotid body sections per animal for N (n=3) and CH (n=3). Figure 4.5 A shows example immunofluorescence images of N and CH carotid bodies. Primary antibody concentrations for CD73 and TH were 1:100 and 1:500 respectively. Secondary antibodies were used at concentrations of 1:1000 (anti-rabbit AF488) for CD73 and 1:250 (anti-mouse AF594) for TH. Consistent with findings in Chapter 3, there were no differences in carotid body section area (Figure 4.5 B). Neither the absolute $CD73^+$ area nor the $CD73^+$ density were affected by CH (Figure 4.5 C & D).

To further characterise the effects of CH, the number of TH^+ type I cells and $CD73^+$ cells were counted in 3-4 sections per carotid body, and their overlap was quantified to assess co-localisation. Sections were co-stained with TH (to identify type I cells) and DAPI (to label nuclei), as shown in Figure 4.6 A. In agreement with Chapter 3, preliminary data showed that the proportion of total cells that were TH^+ tended to increase in CH ($p = 0.09$). In contrast, the proportion of $CD73^+$ cells was unaffected by CH (Figure 4.6 B).

In both N and CH, almost all TH^+ cells also expressed CD73 as evidenced by greater than 90% of the total TH signal overlapping with a $CD73^+$ signal (Figure 4.6 A, B&D). In N, the proportion of $CD73^+$ cells exceeded that of TH^+ cells by approximately 10%, suggestive of populations of both $CD73^+TH^+$ and $CD73^+TH^-$ cells (Figure 4.6 A & C). A considerable number of these $CD73^+TH^-$ cells were located adjacent to the $CD73^+TH^+$

cells within the same cluster and had a similar round morphology (Figure 4.6 A). Following CH, as the TH^+ cell number expanded but the $CD73^+$ stayed the same, the percentage of $CD73^+TH^+$ cells increased (Figure 4.6 A). This was quantified by analysis of CD73 signal overlap with TH showing that approximately 40% of CD73 colocalised with TH in N carotid bodies, which increased to approximately 70% in CH ($p = 0.06$, Figure 4.6 E).

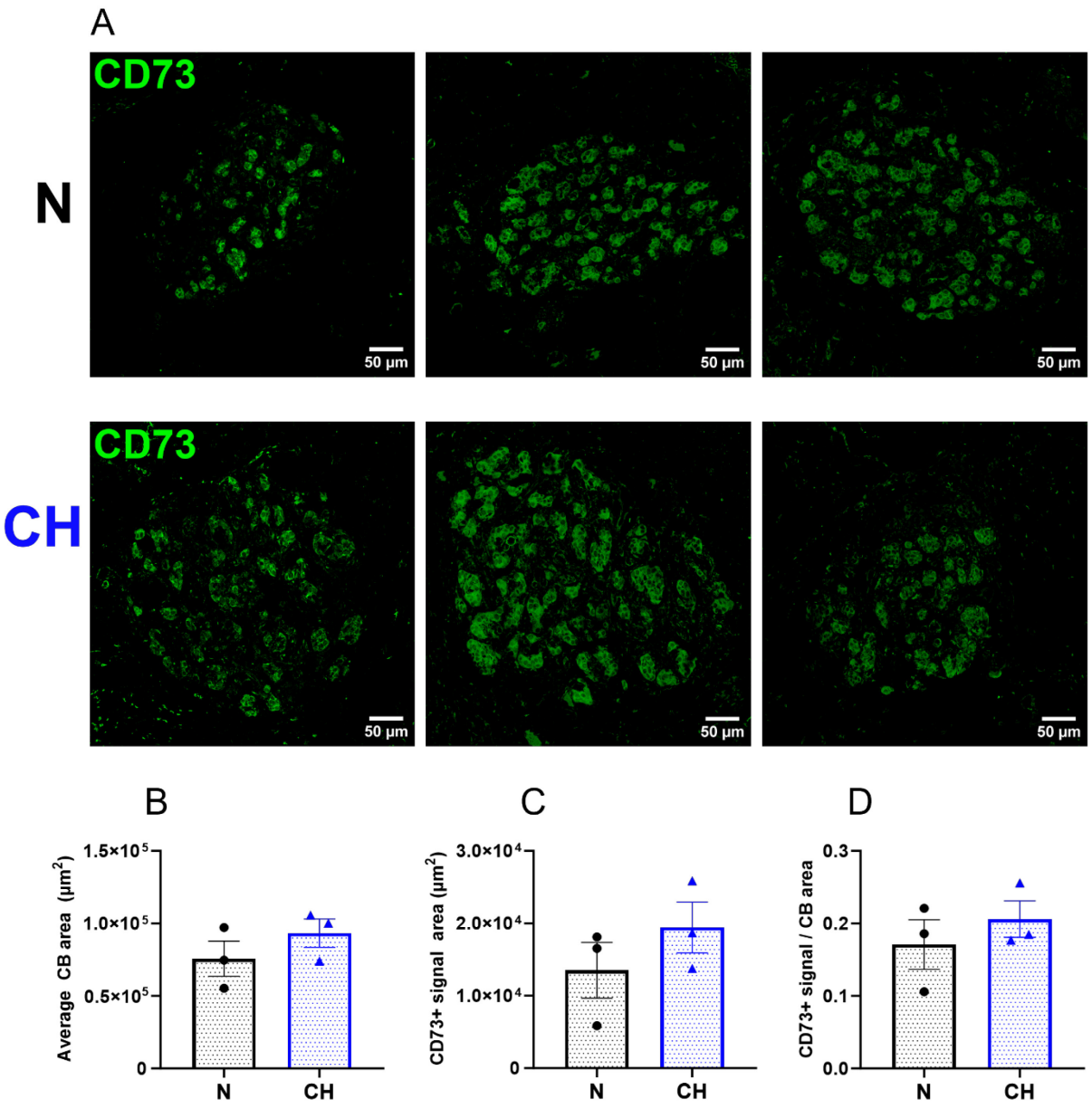

Figure 4.5 Expression of CD73 in carotid bodies from normoxic and chronically hypoxic rats

(A) Immunofluorescence images of carotid body (CB) sections from 3 normoxic (N) and 3 chronically hypoxic (CH) rats stained for CD73 (1:100 with antigen retrieval) to examine $CD73^+$ immunoreactivity. Bar graphs display **(B)** CB area, **(C)** area that is $CD73^+$ and **(D)** normalised CD73 expression to CB area. Data represents mean ± SEM with individual data points showing an average of 3-4 carotid body sections from an individual rat. n=3 rats for both N and CH. Statistical significance was assessed using an unpaired Student's t-test.

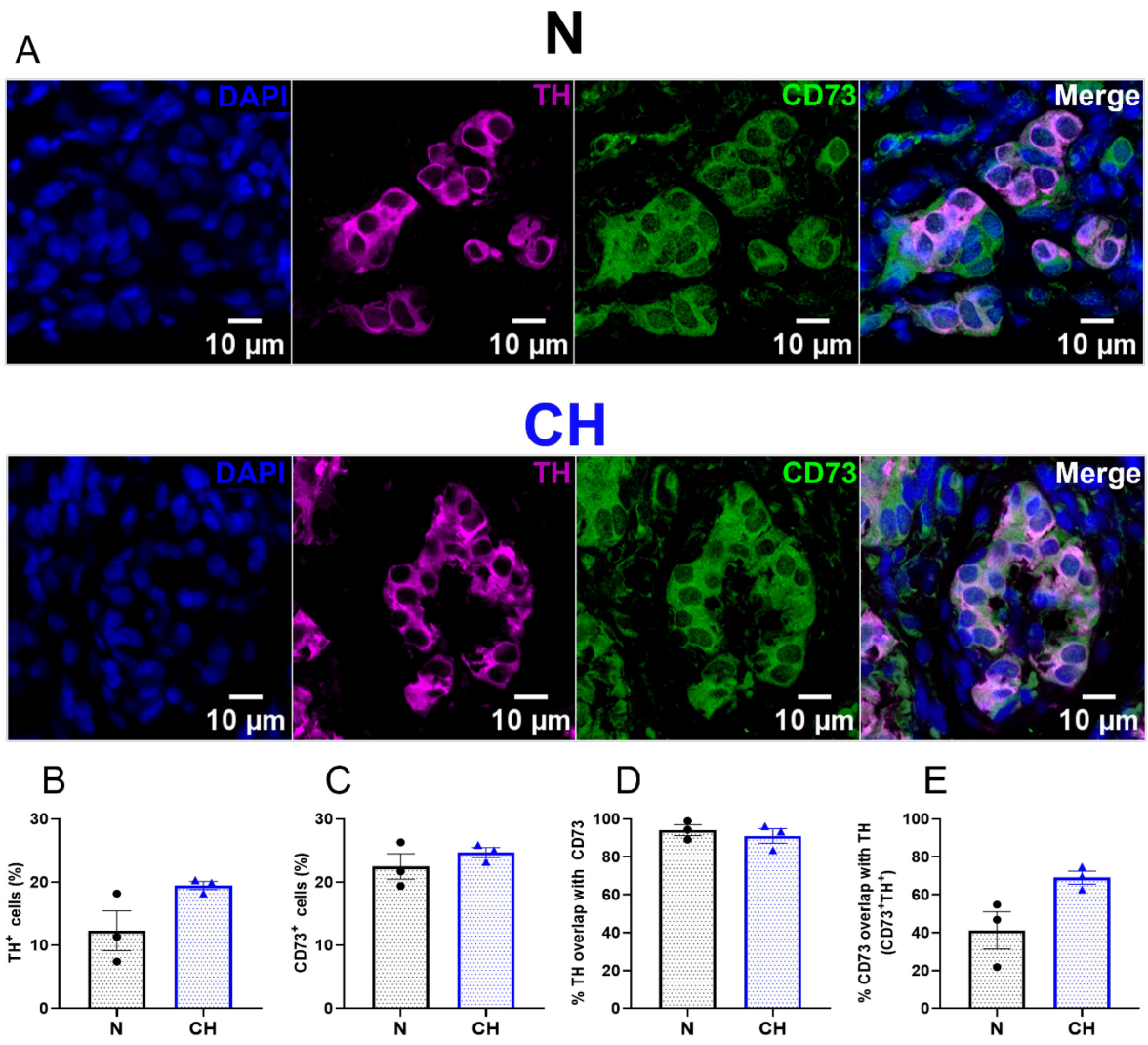

Figure 4.6 Effect of chronic hypoxia on CD73 co-localisation with TH⁺ type I cells

(A) Immunofluorescence images of carotid body sections showing a cluster of type I cells from a N (normoxic, upper) and chronically hypoxic (CH, lower) rat. Panels show DAPI to identify nuclei, tyrosine hydroxylase (TH, type I cell marker), CD73 and a merged image showing spatial overlap. **(B)** number of TH^+ cells as a proportion of the total number of cells. **(C)** number of $CD73^+$ cells as a proportion of the total number of cells. **(D)** overlap of TH^+ signal with $CD73^+$ signal (%, M1). **(E)** overlap of $CD73^+$ signal with TH^+ signal (%, M2). Overlap was quantified using Mander's co-efficient M1 and M2. Data shows mean ± SEM with individual data points showing an average of 3-4 sections from an individual rat. n= 3 rats. Statistical significance was assessed using an unpaired Student's t-test.

4.2.4 A proportion of the CD73$^+$ signal appears to be co-localised with the vasculature but not neuronal processes, and is unaffected by CH

Even after CH, there was still a significant proportion of the total CD73$^+$ signal (around 30%), the identity of which was unaccounted for. As demonstrated in the titration experiments (Figure 4.1), a proportion of the CD73$^+$ signal persisted at higher antibody dilutions (even up to 1:1000) without antigen retrieval. This more sensitive CD73$^+$ signal was found outside of TH$^+$ type I cell clusters and displayed process-like structures or circular shapes, some of which surrounded RBCs, suggesting a potential vascular origin. This led to the hypothesis that some of the CD73$^+$ expression in the carotid body might be associated with vascular endothelial cells.

Subsequent experiments therefore quantified the amount of this more sensitive CD73$^+$ signal in N and CH carotid bodies that was co-localised with CD31, a vasculature endothelial marker. Additionally, since the process-like structures resembled nerve fibres, some co-localisation of CD73 with neurofilament-light chain (NF), a marker for nerve processes, was also examined. Antibody optimisation for CD31 and NF is shown in Figure S.3 (Appendix).

To isolate this more sensitive CD73$^+$ signal, carotid body sections were stained with a more diluted CD73 antibody (1:1000) and without antigen retrieval. Figure 4.7 A shows representative images of this more sensitive CD73$^+$ signal in N and CH carotid bodies. Quantification from 6-8 sections per carotid body across 3 rats revealed no differences in the magnitude of this more sensitive CD73$^+$ signal between N and CH (Figure 4.7 B-D).

To investigate the origin of this more sensitive $CD73^+$ signal, sections were co-stained with CD73, CD31 (a vascular marker) and TH. Figure 4.8 A shows the spatial distribution of these markers. Consistent with Chapter 3, CH did not induce angiogenesis, as there were no changes in the abundance of $CD31^+$ signal (Figure 4.7 B & C; repeated data from Figure 3.1). Approximately 20% of the total $CD31^+$ signal co-localised with CD73, a proportion that was unchanged by CH (Figure 4.7 D). Furthermore, in both N and CH approximately 25-40% of this more sensitive CD73 signal co-localised with CD31 (Figure 4.7 E). Magnified regions of interest revealed that some $CD73^+$ signal directly overlapped with CD31, whilst other parts of the signal appeared to surround, or envelop, the blood vessels.

Therefore, it was estimated that at least 60% of the more sensitive $CD73^+$ signal was independent of vascular endothelial cells. Given the process-like structure of some signals, it was hypothesised that some CD73 could be located in nerve fibres. Figure 4.9 A shows the spatial distribution of the more sensitive CD73 signal along with TH and neurofilament (NF, a nerve fibre marker). Quantification of NF^+ signal from 3-4 sections per carotid body across 3 rats showed no differences in absolute or relative NF abundance between N and CH (Figure 4.9 B & C). Additionally, overlap between NF and CD73 was less than 5%, indicating almost no spatial co-localisation (Figure 4.9 D & E).

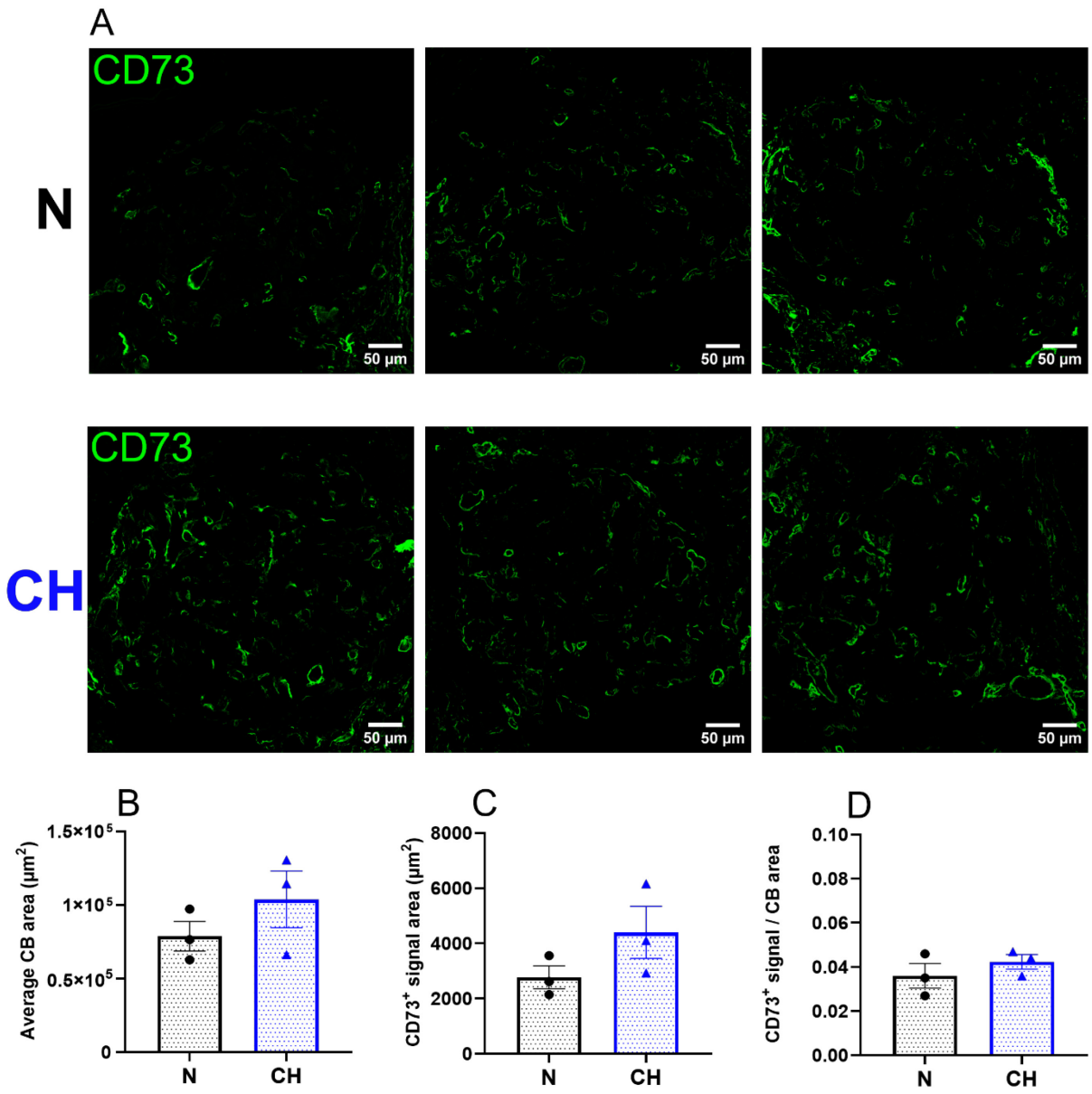

Figure 4.7 Effect of chronic hypoxia on the more sensitive CD73⁺ signal

(A) Immunofluorescence images of carotid body (CB) sections from 3 normoxic (N) and 3 chronically hypoxic (CH) rats stained for CD73 (1:1000) to examine the more sensitive CD73⁺ signal. Bar graphs display **(B)** CB area, **(C)** area that is CD73⁺ and **(D)** normalised CD73⁺ signal to CB area. Data represents mean ± SEM with individual data points showing an average of 3-4 CB sections from an individual rat. n= 3 rats. Statistical significance was assessed using an unpaired Student's t-test.

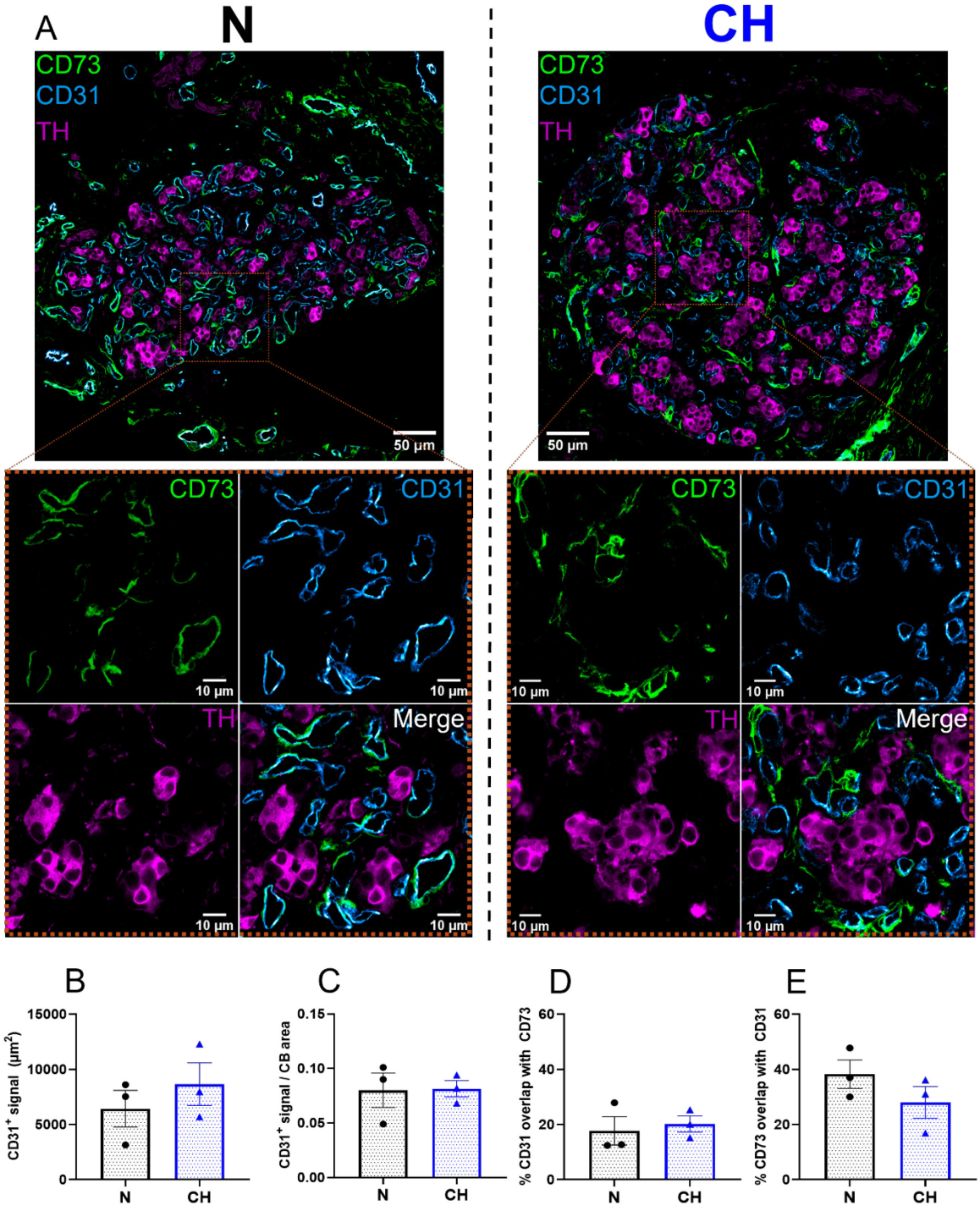

Figure 4.8 Co-localisation of the more sensitive CD73⁺ signal with vascular marker CD31 in normoxic and chronically hypoxic rat carotid bodies

(A) Example immunofluorescence images of carotid body (CB) sections showing spatial distribution of type I cells (TH; 1:500, magenta), CD73 (1:1000, green) and vascular marker (CD31; 1:500, cyan hot) in N (left) and CH (right) rats. Insets (dotted boxes) provide a closer view of the boxed regions. **(B)** area of CD31⁺ signal. **(C)** CD31⁺ signal relative to CB area. **(D)** overlap of CD31⁺ signal with the more sensitive CD73⁺ signal (%, M1). **(E)** overlap of the more sensitive CD73⁺ signal with CD31⁺ signal (%, M2). Overlap was quantified using Mander's co-efficient M1 and M2. Data shows mean ± SEM with individual data points showing an average of 3-4 CB sections from an individual rat. n= 3 rats. Statistical significance was assessed using an unpaired Student's t-test.

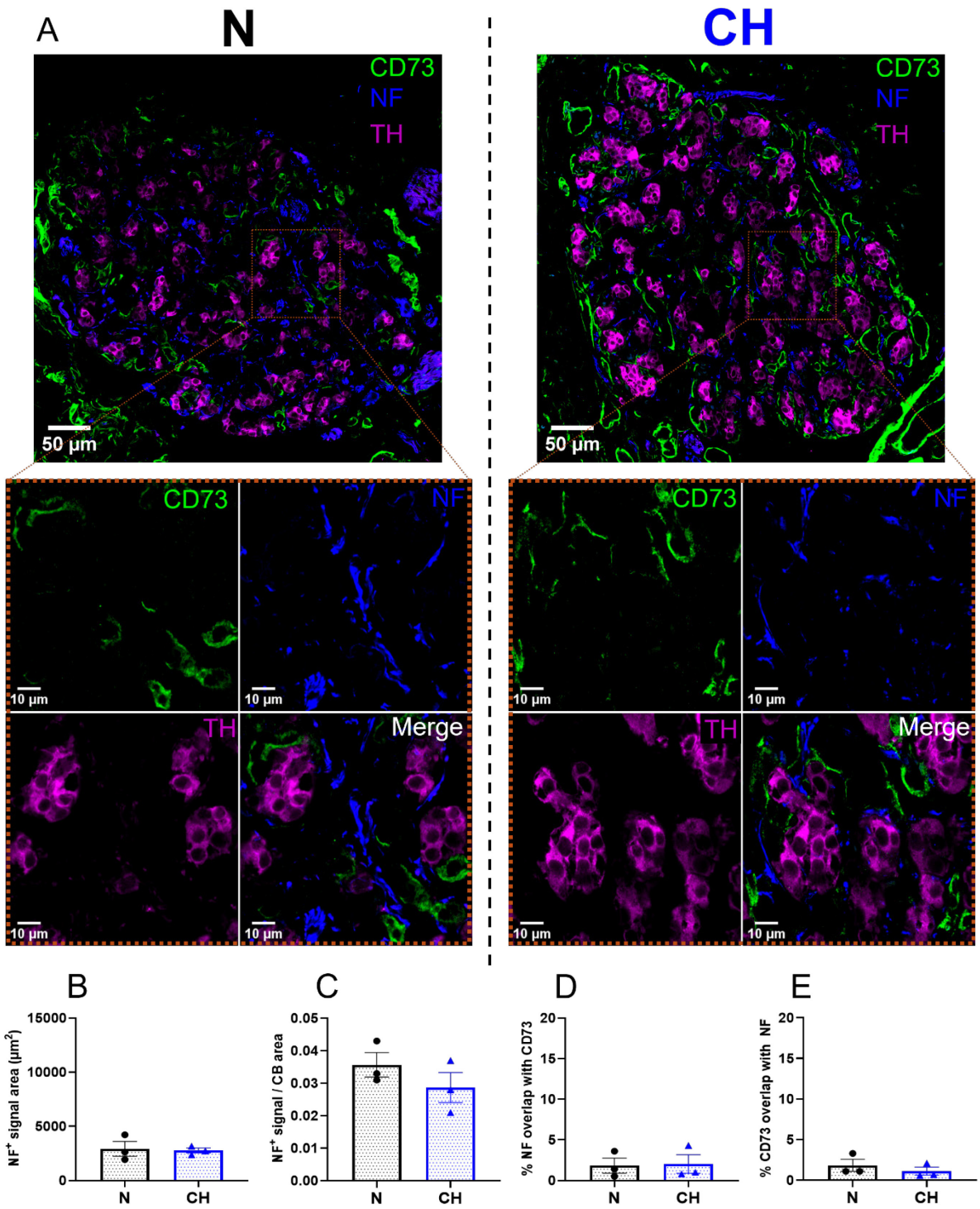

Figure 4.9 Co-localisation of the more sensitive CD73⁺ signal with nerve marker neurofilament in normoxic and chronically hypoxic rat carotid bodies

(A) Example immunofluorescence images of carotid body (CB) sections showing spatial distribution of type I cells (TH; 1:1500, magenta), CD73 (1:1000, green) and nerve marker (NF; 1:2000, blue) in normoxic (N-left) and chronically hypoxic (CH-right) rats. Insets (dotted boxes) provide a closer view of the boxed regions. **(B)** area of NF⁺ signal. **(C)** NF⁺ signal relative to CB area. **(D)** overlap of NF⁺ signal with the more sensitive CD73⁺ signal (%, M1). **(E)** overlap of the more sensitive CD73⁺ signal with NF⁺ signal (%, M2). Overlap was quantified using Mander's co-efficient M1 and M2. Data shows mean ± SEM with individual data points showing an average of 3-4 CB sections from an individual rat. n= 3 rats. Statistical significance was assessed using an unpaired Student's t-test.

4.3 Discussion

4.3.1 Summary of key chapter findings:

- The $CD73^+$ signal in the type I cell clusters was enhanced after performing antigen retrieval
- A more sensitive $CD73^+$ signal was present at a high antibody dilution without antigen retrieval which appeared outside of the type I cell clusters
- Almost all TH^+ cells in a cluster also expressed CD73 in both N and CH
- In a single cluster there were considerable numbers of both $CD73^+TH^+$ and $CD73^+TH^-$ cells
- CH did not modify the overall abundance of $CD73^+$ signal in the carotid body
- CH increased the proportion of $CD73^+TH^+$ cells and reduced the proportion of $CD73^+/TH^-$ cells in the carotid body, due to TH^+ cell expansion within clusters
- CH did not alter the abundance of the more sensitive $CD73^+$ signal in the carotid body
- The more sensitive $CD73^+$ signal in the carotid body is partly localised to the $CD31^+$ vasculature but not nerve processes
- CH did not modify the distribution of $CD73^+$ on the vasculature or nerves

4.3.2 Justification for antibodies used

This chapter aimed to optimise and validate a previously used CD73 antibody for PFA-fixed and frozen carotid body sections. While this antibody has been extensively

validated in liver sections, CD73 knockout cells (Fausther et al., 2012) and reduced carotid body preparations (Salman et al., 2017), its performance had not been characterised in whole carotid body frozen sections. Following the manufacturer's instructions, the antibody was titrated from 1:50 to 1:1000. At higher concentrations, staining showed a broad pattern on clusters but also exhibited significant background. Diluting the antibody reduced background staining but also diminished the signal potentially associated with type I cells. Notably, even at the highest dilution (1:1000), a strong $CD73^+$ signal persisted, suggesting high CD73 expression in another cell type compared to type I cells. CD31 and NF antibodies were also optimised to determine optimum signal-to-noise which is demonstrated in Figure S.3 (Appendix).

A limitation of formaldehyde-based fixatives, such as PFA, is their tendency to create protein cross-links that mask epitopes, making them unrecognisable to antibodies under standard conditions (Scalia et al., 2017). Antigen retrieval can reverse these effects by breaking cross-links and restoring epitope accessibility (D'Amico et al., 2009). Various antigen retrieval methods were tested to enhance the CD73 signal in type I cells. Incubating sections in citrate buffer (pH 6.0) at 60°C overnight produced the most consistent improvement in CD73 signal across three carotid bodies. This method also slightly enhanced TH staining, with no adverse effects on its signal. Further optimisation combining antibody titration with antigen retrieval may have revealed type I cell-specific signal at lower antibody concentrations and could be tested in future experiments to further enhance signal to noise. Supplementary Figure S.2 demonstrates a weaker $CD73^+$ at a dilution of 1:1000 (Appendix).

4.3.3 CH increases the proportion of $CD73^+TH^+$ cells in the carotid body glomeruli

This chapter shows a trend toward an increased proportion of TH^+ cells following CH, consistent with Chapter 3, which also demonstrated an increase in estimated TH+ cell number and signal density. However, the proportion of $CD73^+$ cells remained unchanged after CH. This was unexpected since CD73 is localised to type I cells, and similar patterns might have been anticipated. Preliminary data also show that while almost all TH^+ signals overlap with $CD73^+$ signals, only a subset of $CD73^+$ signals overlap with TH ($CD73^+TH^+$). Thus, in a single cluster there is a population of $CD73^+$ cells that do not express TH ($CD73^+TH^-$), as can be observed in Figure 4.6. Following CH, there was a shift toward greater overlap between CD73 and TH, indicating an increase in $CD73^+TH^+$ cells and a reduction in $CD73^+TH^-$ cells in a single cluster. Exploring the identity of these $CD73^+TH^-$ cells which subsequently express TH following CH warrants further investigation.

The expansion of TH^+ type I cells in the carotid body in response to CH remains widely contested. As discussed in Chapter 3, one hypothesis proposes an adult stem cell niche composed of quiescent type II cells during normoxia. Under hypoxia, these cells differentiate into $Nestin^+$ progenitors and eventually mature type I cells (Pardal et al., 2007). Type I cells are thought to release paracrine mediators, such as endothelin-1, that stimulate type II stem cells to differentiate (Paciga et al., 1999; Platero-Luengo et al., 2014). This process is relatively slow and occurs over prolonged hypoxia exposures lasting days to weeks. Another hypothesis suggests that type I cell expansion arises from the type I cells themselves. Lineage-tracing experiments have shown that newly dividing TH^+ cells originate from a pre-existing TH^+ population which is heavily HIF-2α dependent (Fielding et al., 2018). Similarly, Sobrino and colleagues proposed a subpopulation of mitotic TH^+ cells, termed immature neuroblasts, which express low

levels of TH and the marker HNK-1 and upon 24-48 hours exposure to hypoxia leads to a rapid increase in the mature type I cell population without carotid body hypertrophy (Sobrino et al., 2018).

A plausible explanation for the observed increase in $CD73^{+}TH^{+}$ cell density in the current project could be that some cells weakly expressing TH within a cluster in normoxia were below the detection threshold of the staining protocol. After CH, upregulation of TH may have made these cells detectable, which now overlap with the already expressed CD73. This would be more in line with a population of immature type I cells that inherently express CD73 but have very low or undetectable levels of TH, that subsequently gain maturity in response to CH. TH is a HIF target gene and so it is not surprising that TH levels would increase in CH (Millhorn et al., 1997; Schnell et al., 2003). There may be a time dependence or hypoxic stimulus dependence (or likely both) that then lead to hypertrophic changes which would then normalise the TH^{+} cell density. Alternatively, some of the increase in $CD73^{+}TH^{+}$ population could derive from type II cells. It has been previously reported that cultured type II cells do express CD73 protein (Salman et al., 2017). To quantify the extent of total $CD73^{+}$ signal attributable to type II cells before and after CH, future experiments could use a marker such as glial fibrillary acidic protein (GFAP) in immunohistochemical studies. Type II cells play an active role in carotid body physiology, in addition to their stem cell properties, they release ATP in a paracrine manner during hypoxia (Figure 1.3)(Xu et al., 2003). Given the balance between ATP and adenosine in the extracellular space, the presence of CD73 on type II cells would not be surprising. Moreover, it remains unclear whether other enzymes involved in ATP catabolism, such as the NTPDase family, are also expressed in these cells.

A slight increase in total cell number was also observed that in 2 out of 3 carotid bodies, proportional to the $CD73^+$ population, suggesting that some mitotic activity may also contribute. To further explore these findings, markers of cellular proliferation could be applied. For example, bromodeoxyuridine (BrdU) could be added to the rats' drinking water, allowing incorporation into replicating DNA (Fielding et al., 2018; Hodson et al., 2016; Sobrino et al., 2018). Subsequent detection with a fluorescently labelled anti-BrdU antibody, combined with TH and CD73 staining could identify the specific cell populations undergoing proliferation. The expansion of TH^+ type I cells is likely contributing to the elevated chemoafferent discharge. Since these 'new' cells also express CD73, it is plausible to hypothesise that carotid body activity in CH may be more sensitive to CD73 inhibition. The functional role of CD73 in CH will be investigated in the next chapter.

4.3.4 The impact of CH on a more sensitive $CD73^+$ signal

The presence of a more sensitive $CD73^+$ signal outside of the type I cell clusters could be detected at a much lower primary antibody concentration and this is estimated to account for around 30% of the total CD73 signal in the carotid body. Approximately 30-40% of this more sensitive $CD73^+$ signal was co-localised with the vasculature marker CD31 but no co-localisation was observed with neuronal marker, NF. This leaves approximately 60% of this more sensitive $CD73^+$ signal that remains unidentified.

An intriguing observation was that many of these highly sensitive non-type I $CD73^+$ signals did not perfectly overlap with the vascular endothelium but instead appeared to encapsulate it, suggesting the possible involvement of pericytes. Pericytes are mesenchymal-like cells that wrap around endothelial cells, particularly in capillaries and post-capillary venules (Attwell et al., 2016; Brown et al., 2019). A subset of

pericytes are known to express CD73, which is commonly used as a phenotypic marker to help distinguish from other cell types (Park et al., 2016; Vanlandewijck et al., 2018). These contractile cells are well-studied in the brain, where they regulate cerebral blood flow (Hall et al., 2014), maintain blood-brain barrier integrity (Armulik et al., 2010), and contribute to angiogenesis (Gerhardt & Betsholtz, 2003). Pericytes can also differentiate into neuronal, vascular or glial-like cell types suggestive of pluripotency (Brown et al., 2019). Given the carotid body's extremely high blood flow relative to its size and its rich nerve innervation, pericytes may contribute to neurovascular coupling, similar to their role in the brain (Attwell et al., 2010). However, this relationship may be more complex, as evidence suggests transcriptional differences between brain-derived pericytes and those in peripheral tissues (Vanlandewijck et al., 2018). The data presented here show that only approximately 20% of endothelial cells overlapped with CD73, suggesting that not all blood vessels are enveloped by $CD73^+$ pericytes. It is unknown whether there are subpopulations of pericytes that lack CD73 expression. Additionally, the pericyte-to-endothelial cell ratio varies across tissues, with the brain and retina having the highest ratio (1:1) and the lung having a lower ratio (1:10) (Gökçinar-Yagci et al., 2015). The exact ratio in the carotid body remains unknown, and a comprehensive characterisation and identification of pericytes in the carotid body are needed to address this question.

To confirm whether the remaining $CD73^+$ signal originates from pericytes, markers such as PDGF-β or NG2 could be co-stained with CD73. Immunostaining on liver sections using this same antibody showed some co-localisation with the intermediate filament protein, vimentin, commonly found in pericytes (Fausther et al., 2012). However, given the close association between pericytes and endothelial cells, it can be challenging to determine whether the $CD73^+$ signal originates from endothelial cells

or pericytes. Super-resolution microscopy techniques, such as structured illumination microscopy (SIM), which achieves a resolution of ~100 nm in the xy-plane, could help resolve this spatial distinction and clarify the cellular source of the $CD73^+$ signal.

How $CD73^+$ pericytes influence carotid body chemosensitivity or adaptations to CH remains unclear but presents a novel area of carotid body research. The intimate association between pericytes and endothelial cells suggests a potential role in paracrine signalling, and it is plausible that pericytes contribute to the vascular expansion typically observed during CH. However, type I cells are also known to play a critical paracrine role in vascular development. For example, TH-specific inactivation of PHD2 and HIF-2α has been shown to abolish carotid body vasculature during development and in response to CH (Fielding et al., 2018). Notably, no vascular expansion was observed in the CH model described in this thesis, leaving the mechanisms behind this unresolved.

4.4 Conclusions

In a single cluster in the carotid body, there are populations of both $CD73^+TH^+$ and $CD73^+TH^-$ cells. In this model of CH, preliminary data suggest that the TH^+ cell population tends to expand, while the $CD73^+$ population remains unchanged leading to an overall elevation in the proportion of $CD73^+TH^+$ cells. However, this does not necessarily imply that CD73 expression at the single-cell level is unaffected. Furthermore, these immunohistochemical findings, although informative, provide no insight into the functional role of CD73 in promoting carotid body hyperactivity in CH. It is possible that, even if CD73 density remains unchanged, its enzymatic activity is elevated in CH carotid bodies, leading to increased adenosine production that excites the carotid body. The next chapter investigates these functional changes by measuring

carotid body chemoafferent activity *ex vivo* in the presence of AOPCP, a well-defined CD73 inhibitor.

CHAPTER 5

5. The functional role of CD73 and adenylyl cyclase in promoting chronic hypoxia-induced carotid body hyperactivity *ex vivo*

5.1 Chapter introduction and aims

Carotid body hyperactivity is increasingly recognised as a key factor in the development of neurogenic hypertension in many cardiorespiratory-related diseases such as obstructive sleep apnoea, chronic heart failure and COPD (Iturriaga et al., 2021). CH is a common feature of the latter two conditions, which leads to carotid body overactivation and subsequent enhanced chemoafferent discharge to the brainstem, driving increased sympathetic outflow to the vasculature. The regulation of chemoafferent output involves various neurotransmitters and neuromodulators, including acetylcholine, dopamine, adrenaline, ATP and adenosine (Nurse, 2010).

Adenosine is primarily formed in the synaptic cleft following the extracellular breakdown of ATP which is tonically secreted by the type I cells in normoxia and additionally from type II cells during hypoxia through pannexin-1 channels (Conde et al., 2012b; Conde et al., 2006; Xu et al., 2003; Zhang et al., 2012). ATP catabolism is initiated via the NTPDase family into ADP and AMP. Membrane-bound CD73 hydrolyses this AMP into adenosine which is the rate limiting enzyme in this reaction.

Adenosine stimulates chemoafferent activity by directly activating metabotropic A_{2A} receptors on post-synaptic sensory fibres or indirectly via a pre-synaptic action on type I cells through A_{2A} and A_{2B} receptor stimulation (Conde et al., 2006; Livermore & Nurse, 2013; Xu et al., 2006). Both actions induce adenylyl cyclase activity thus generating

cAMP and activation of downstream effectors such and PKA and EPAC (Rocher et al., 2009; Xu et al., 2006). These effectors have the ability to modulate various ion channels that increase cell excitability (Nunes et al., 2014; Pulgar-Sepúlveda et al., 2018). See Figure 1.3 for a summary of adenosine receptor signalling.

Increasing evidence points towards adenosine in setting the basal carotid body discharge as opposed to ATP. Inhibition of adenosine receptors using 8-SPT or caffeine greatly attenuates basal chemoafferent activity *ex vivo* (Holmes et al., 2018b) and catecholamine secretion *in vitro* respectively (Conde et al., 2006). Similar decreases were observed following CD73 inhibition, indicating that it is extracellularly derived adenosine that is responsible for establishing baseline activity (Holmes et al., 2018b). As demonstrated in Chapter 3, carotid body chemoafferent discharge measured *ex vivo* is elevated 2-3 fold in CH. However, whether CD73 activity is responsible for the augmented basal chemoafferent discharge observed in CH has not been explored. Furthermore, in previous studies, concentrations of AOPCP used were relatively high (100-200μM) and although this has been shown to effectively reduce the amount of adenosine formation, it may give rise to non-specific effects (Conde et al., 2012b). Therefore, initial experiments aimed to characterise the potency of AOPCP which is a commonly used pharmacological agent to inhibit CD73, in both N and CH carotid bodies. Concentration-response experiments were performed in normoxia. This will provide the rationale for the use of specific concentrations in subsequent experiments exploring CD73 function in hypoxia.

Synaptic adenosine concentrations increase almost 2-fold under mild hypoxia and has been suggested to play a pivotal role in establishing carotid body hypoxic sensitivity

(Conde & Monteiro, 2004; Conde et al., 2012b). This is supported by findings that inhibition of adenosine receptors and CD73 decreased the PO_2 threshold required to initiate a hypoxic response as characterised by a typical leftward shift in the O_2 response curve (Holmes et al., 2018b). Furthermore, CD73 inhibition does not affect the peak hypoxic discharge which fits in with other reports demonstrating that adenosine plays a bigger role in milder hypoxic levels compared to more severe hypoxic intensities (Conde et al., 2012b). *Ex vivo* data from Chapter 3 showed that chemoafferent hypoxic responses are elevated in CH characterised by a rightward shift in the O_2 response curve, however the mechanisms behind this are still unknown. It is possible that part of this rise in discharge is due to an augmented sensitivity to adenosine, although this remains debateable. Furthermore, the importance of CD73 in determining hypoxic sensitivity of carotid bodies following adaptation to CH has not yet been studied. Whether augmented hypoxic chemoafferent responses in CH can be reversed by targeting of CD73 was therefore investigated in this chapter. SQ22536 is an inhibitor of tmAC and was used to probe the mechanistic importance of cAMP in setting the chemoafferent frequency in CH carotid bodies, in both normoxia and hypoxia.

CD73, adenosine and cAMP have all been shown as important effectors in mediating the carotid body's response to hypercapnia (Holmes et al., 2015; Sacramento et al., 2018). As shown in Chapter 3, there was a slight trend for an elevated CO_2 sensitivity in CH carotid bodies. Whether this may also be due to increased CD73 activity and downstream elevations in cAMP was investigated using AOPCP (CD73 inhibitor) and SQ22536 (tmAC inhibitor) in normocapnia (PCO_2=40mmHg) and in response to hypercapnia (PCO_2=80mmHg).

Aims of this chapter were as follows:

1. Investigate whether carotid body sensitivity to adenosine is heightened in CH

2. Determine the potency of AOPCP (CD73 inhibition) and SQ22536 (tmAC inhibition) *ex vivo* in N and CH carotid bodies, by performing concentration-response experiments in normoxia

3. Investigate whether CD73 or tmAC inhibition could reverse CH-induced carotid body hyperactivity in normoxia and hypersensitivity to hypoxia

4. Examine whether CD73 or tmAC contributes to elevated hypercapnic sensitivity in CH carotid bodies

5.2 Results

5.2.1 Carotid body sensitivity to exogenous adenosine is unaffected by CH

Initial experiments aimed to determine whether exogenously applied adenosine would amplify the carotid body chemoafferent response to a greater degree in the CH group compared to N. 100μM of adenosine was applied for 5 minutes, with firing frequencies averaged over the final 60 seconds. Figure 5.1 A shows representative raw traces of the experimental protocol for both groups. Consistent with data in Chapter 3, the baseline carotid body discharge was significantly elevated in CH (Figure 5.1 A & B). The application of 100μM adenosine increased firing frequency in both groups, with CH showing a higher absolute discharge in the presence of adenosine (Figure 5.1 B). The difference observed was attributed to the elevated basal discharge in CH, as both groups exhibited a similar absolute increase in response to adenosine. This indicates that CH did not alter the sensitivity to adenosine (Figure 5.1 C). However, the relative increase (percentage change from basal) in response to adenosine was significantly blunted in CH, suggesting a potential decrease in adenosine sensitivity (N: 215±30% vs CH: 83±21%, $p<0.01$ unpaired Student's t-test).

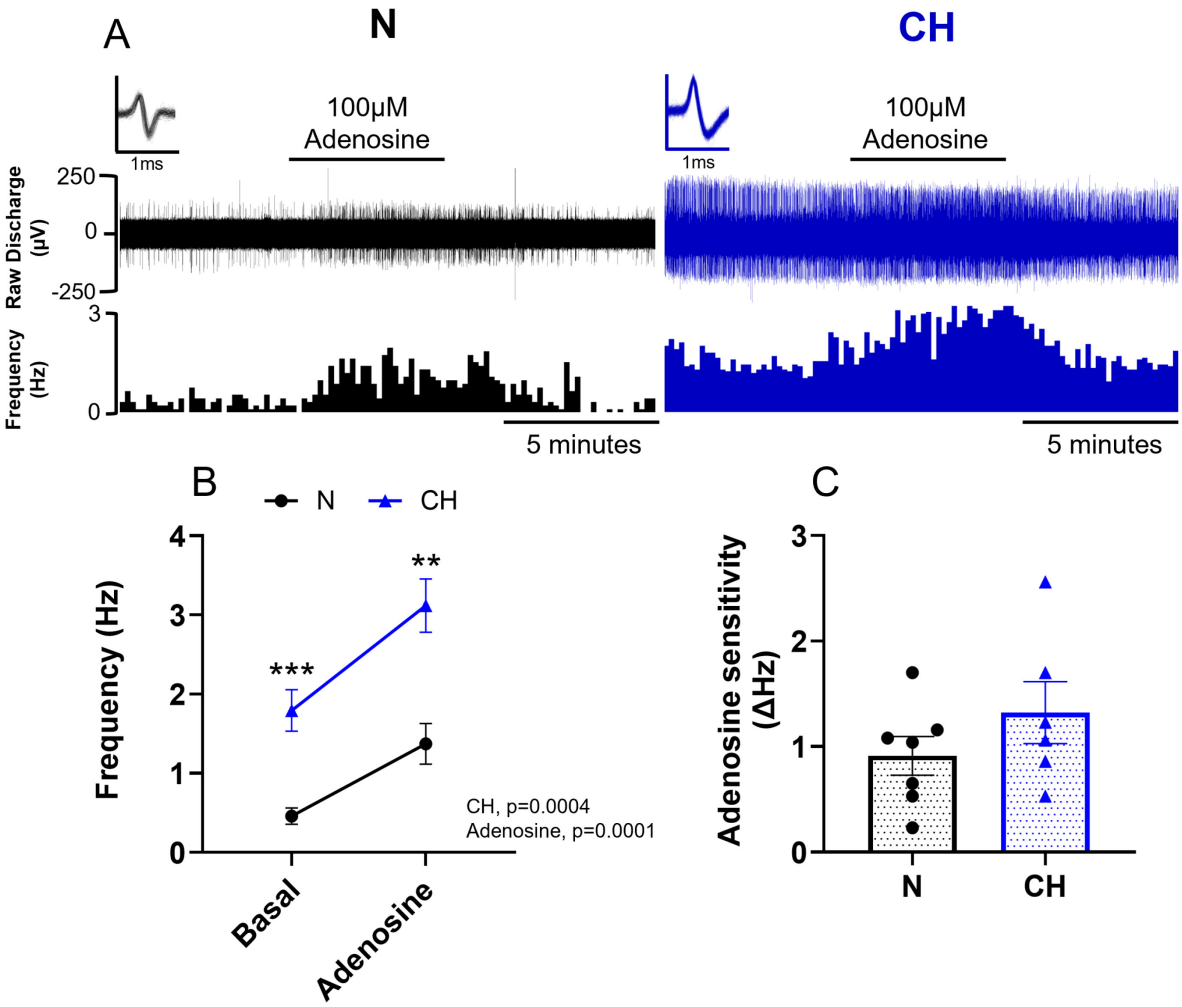

Figure 5.1 Sensitivity to exogenous adenosine is unchanged in chronic hypoxia

(A) representative raw recordings of chemoafferent activity from a normoxic (N-left) and chronically hypoxic (CH-right) carotid body ± 100μM adenosine. Raw discharge (upper) and frequency histograms (lower) shows number of action potentials binned into 10 second intervals. Inset shows overdrawn action potentials for single fibre discrimination. **(B)** comparison of mean basal frequency and in response to 100μM adenosine in N and CH groups. **(C)** the difference between basal frequency and the frequency in the presence of adenosine used to determine adenosine sensitivity. Data expressed as mean ± SEM with individual data points representing a single fibre. For N, n=7 fibres from 6 rats and for CH, n=6 fibres from 6 rats. Statistical significance was assessed using a two-way repeated measures ANOVA in B with overall p values shown. Bonferroni post-hoc analysis used for multiple comparisons, **p<0.01, ***p<0.001 compared to N group. An unpaired Student's t-test was performed in C

5.2.2 AOPCP abolished carotid body discharge in both N and CH in a concentration-dependent manner

To determine the relative potency of AOPCP in N and CH carotid bodies *ex vivo*, concentration response experiments were performed ranging from 10nM to 330μM. This range covers concentrations close to its stated IC50 from the manufacturer and previously used concentrations in the same *ex vivo* carotid body preparation (Conde et al., 2012b; Holmes et al., 2018b). Generating concentration-response curves allowed for the estimation of IC50 for AOPCP in both groups. Figure 5.2 A shows a representative raw trace of the experimental protocol. AOPCP decreased chemoafferent activity to almost zero in a concentration dependent manner in almost all fibres recorded from (Figure 5.2 B & C). Despite the elevated basal discharge in CH, high concentrations of AOPCP still managed to almost completely abolish chemoafferent frequency (Figure 5.2 D & E). As such, the absolute reduction in frequency caused by AOPCP was greater in CH (Figure 5.2 F). To compare potency and IC50 of AOPCP, the percentage reduction in basal frequency was calculated. This data shows a rightward shift in the concentration response curve in CH, and a five-fold increase in the IC50 in CH. IC50s for N and CH were 1.4μM (95% CI, 0.97μM to 1.9μM) and 7.8μM (95% CI, 4.9μM to 12.4μM) respectively. The same maximum reduction (as a percentage of basal) was achieved in both groups (>90% decrease in basal frequency), but this occurred at a higher concentration in CH compared with N, indicative of reduced potency (Figure 5.2 G).

Whether the effects observed here are simply due to a higher basal discharge in CH are unknown. Therefore, the next set of experiments aimed to investigate the effect of AOPCP in hypoxia where firing frequency is elevated. These experiments were

performed using fixed concentrations to be able to compare between groups. Using the N concentration response curve (as a percentage reduction) an approximate IC90 value was derived. This concentration was 15μM which achieves around 90% reduction of the maximal inhibitory effect. This value was chosen as it lies near the top of the curve but before it has plateaued. A second much higher concentration of 100μM was also tested, a concentration, that provides near maximal inhibition in both N and CH (Holmes et al., 2018b).

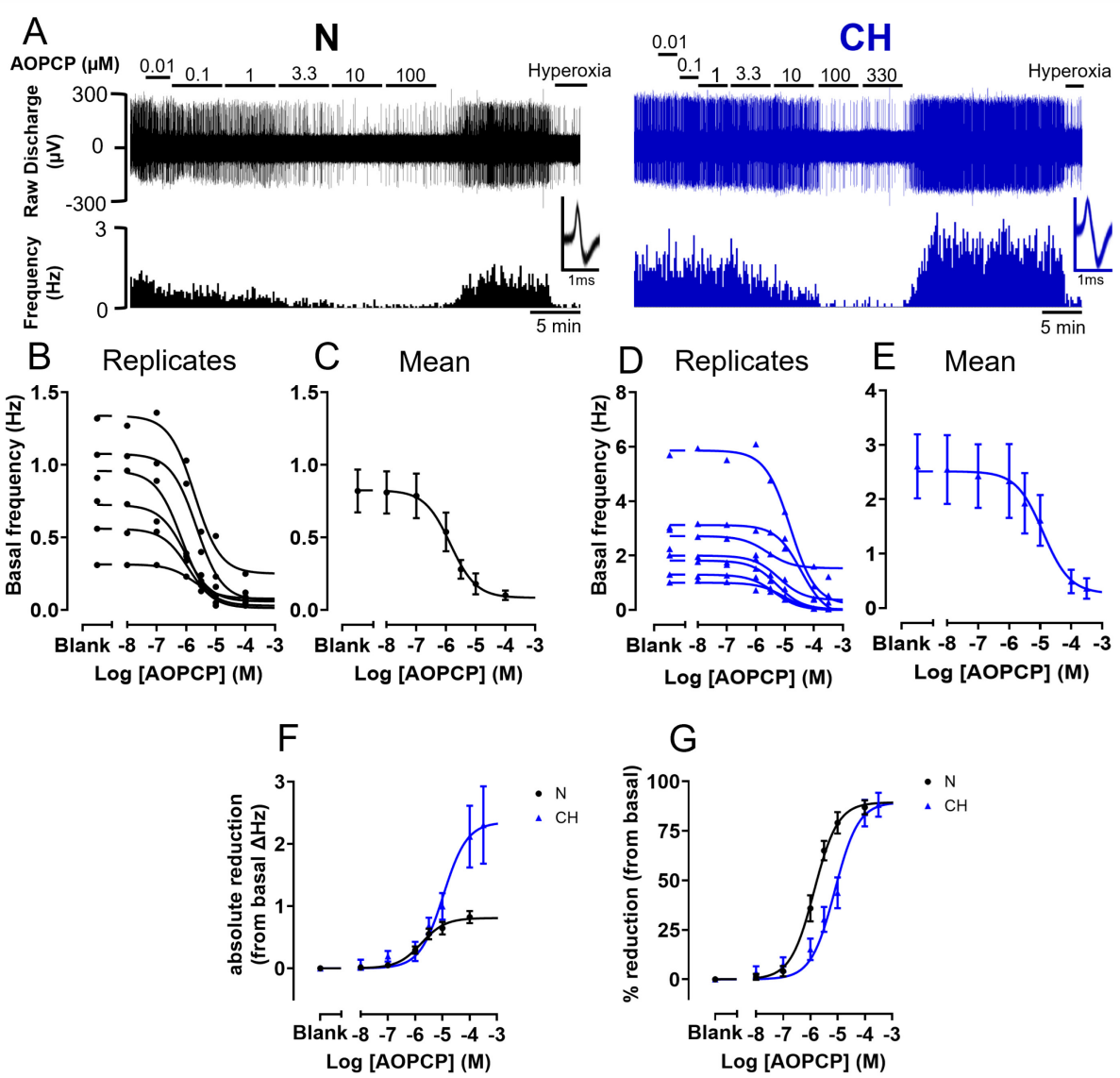

Figure 5.2 Pharmacological inhibition of CD73 with AOPCP abolished basal chemoafferent activity in a concentration-dependent manner in both normoxic and chronically hypoxic rat carotid bodies

(A) representative raw recordings of chemoafferent activity showing concentration-frequency response with AOPCP from a normoxic (N-left) and chronically hypoxic (CH-right) rat carotid body. Raw discharge (upper) and frequency (lower) shows number of action potentials binned into 10 second intervals. Inset shows overdrawn action potentials for single fibre discrimination. **(B)** individual AOPCP concentration-frequency response curve replicates for N. **(C)** mean of B. **(D)** individual AOPCP concentration-frequency response curve replicates for CH. **(E)** mean of D. **(F)** AOPCP concentration response curves for N and CH expressed as absolute reduction in basal frequency. **(G)** AOPCP concentration response curves for N and CH expressed as a percentage reduction from basal frequency. For C, E, F and G data presented as mean ± SEM. Individual data points represent a single fibre. For N, n=6 fibres from 5 rats and for CH, n=7 fibres from 5 rats.

5.2.3 CD73 inhibition with AOPCP alleviates the exaggerated hypoxic response in CH carotid bodies

This set of experiments aimed to investigate the contribution of CD73 in mediating the augmented hypoxic sensitivity of CH carotid bodies observed in Chapter 3. A steady basal discharge was established at a PO_2 of 300mmHg before being gradually lowered to approximately 40mmHg. To prevent tissue damage, the superfusate was quickly switched to a hyperoxic solution (95% O_2, 5% CO_2) before a maximum frequency had been achieved. Frequency was plotted at various PO_2 values, generating O_2-response curves fitted to an exponential decay with offset function. After returning to a normoxic solution and a steady baseline re-established, the hypoxic responses were repeated in the presence of 15μM and/or 100μM AOPCP. These pharmacological agents were given for approximately 5 minutes during normoxia and throughout the duration of graded hypoxia.

Figure 5.3 A shows an example recording of the experimental protocol taken from a CH carotid body. CH chemoafferent responses were augmented and right shifted compared to N (Figure 5.3 B & C). The addition of 15μM AOPCP to CH carotid bodies decreased, but did not abolish, chemoafferent responses to hypoxia (Figure 5.3 B). 15μM AOPCP induced a significant leftward shift in the CH PO_2 response curve quantified by a reduction in the superfusate PO_2 required to elicit a firing frequency of 5Hz (Figure 5.3 C). These effects were magnified in the presence of a higher concentration of AOPCP (100μM), such that the hypoxic response curve for a CH carotid body in the presence of 100μM was almost indistinguishable from that of an N carotid body (Figure 5.3 C & E).

To determine whether the inhibitory action of AOPCP is greater in CH vs N during graded hypoxia, the reduction in frequency caused by AOPCP was plotted over the full range of PO_2s (Figure 5.4 A & B). The reduction in frequency caused by 15μM AOPCP was unchanged in CH compared to N (Figure 5.4 A). However, 100μM AOPCP produced a greater reduction in chemoafferent frequency in CH carotid bodies compared to N throughout hypoxia (Figure 5.4 B). To compare the effect of AOPCP on hypoxic sensitivity, the size of the drug-induced leftward PO_2 shifts were compared between N and CH. Although there was a trend for a greater leftward PO_2 shift in CH at both concentrations of AOPCP, neither reached statistical significance (Figure 5.4 C) $p=0.24$ & Figure 5.4 D $p=0.09$). This indicates that AOPCP reduces chemoafferent hypoxic sensitivity to the same extent in both N and CH. The larger reduction in absolute frequency seen in CH emerges in normoxia and is sustained throughout hypoxia, rather than being amplified.

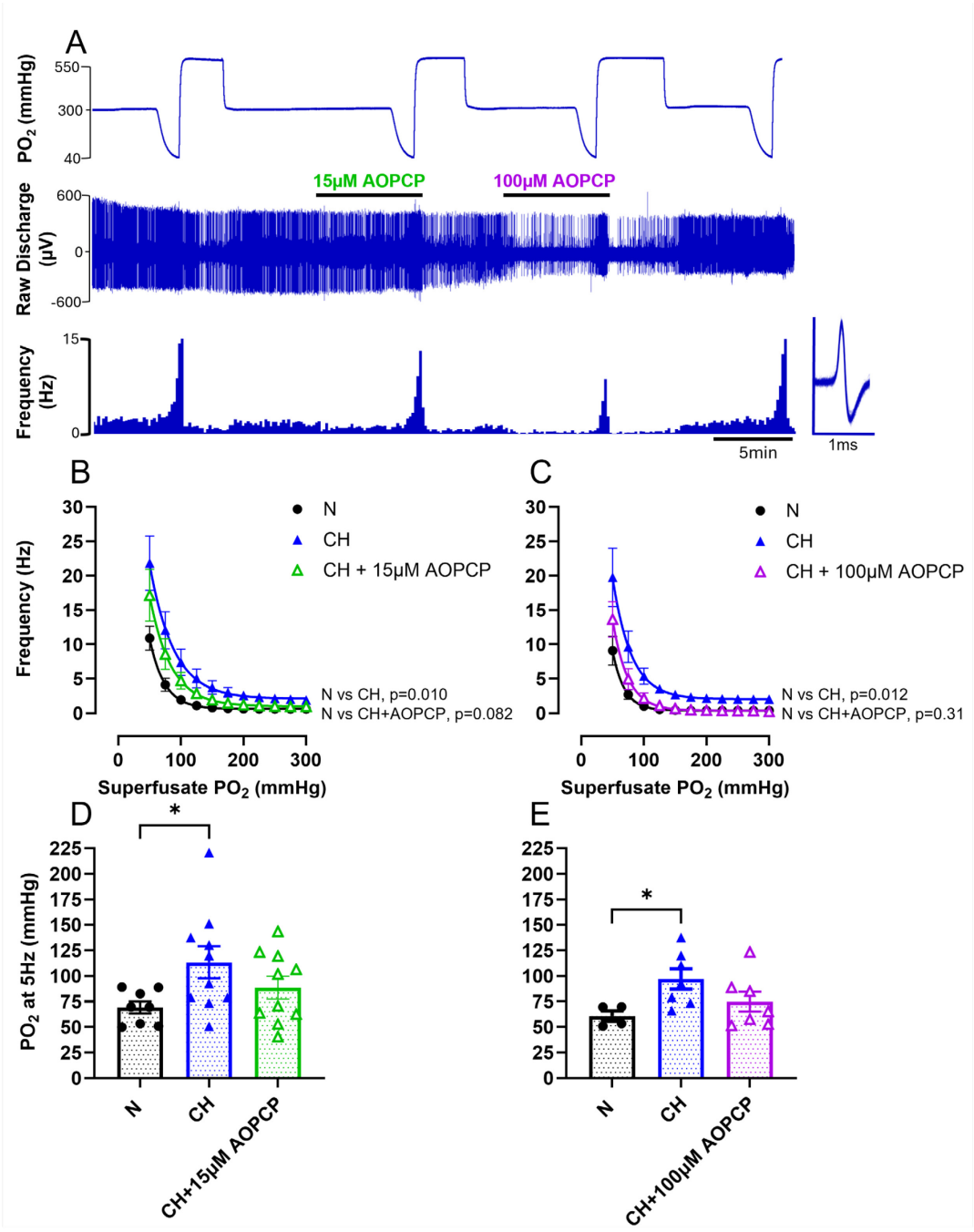

Figure 5.3 Pharmacological inhibition of CD73 normalised chronic hypoxia induced carotid body O_2 hypersensitivity *ex vivo*

(A) Raw recording of carotid body chemoafferent response to graded hypoxia from a chronically hypoxic (CH) rat in the presence and absence of varying concentrations of AOPCP (CD73 inhibitor). Raw discharge (upper) and frequency (lower) shows number of action potentials binned into 10 second intervals. Inset shows overdrawn action potentials for single fibre discrimination. **(B)** mean O_2 response curves comparing normoxic (N) carotid bodies with CH ± 15μM AOPCP or **(C)** 100μM AOPCP. **(D)** PO_2 required to elicit a discharge frequency of 5Hz with 15μM AOPCP or **(E)** 100μM AOPCP. Data expressed as mean ± SEM with individual data points representing a single fibre. For N, n=4-8 fibres from 8 rats and for CH, n=7-10 fibres from 9 rats. Statistical significance was assessed using a two-way repeated measures ANOVA for B & C with overall p values shown on the graph. A one-way ANOVA with Dunnett's post-hoc analysis was performed on D & E, *p<0.05 compared to N.

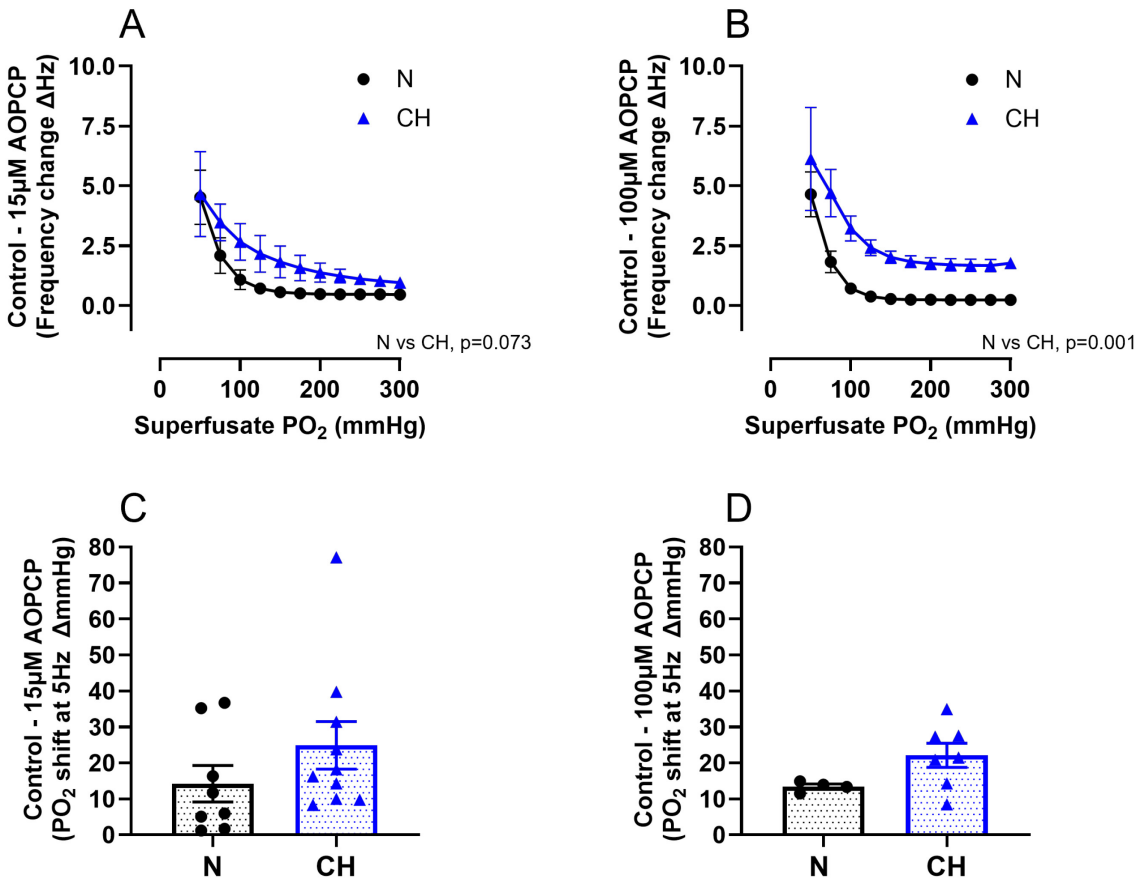

Figure 5.4 Sensitivity to AOPCP during graded hypoxia

Comparison of the reduction in frequency caused by **(A)** 15µM AOPCP and **(B)** 100µM AOPCP during graded hypoxia between normoxic (N) and chronically hypoxic (CH) rat carotid bodies from Figure 5.3 data. Comparison of the leftward PO_2 shift produced by **(C)** 15µM AOPCP and **(D)** 100µM AOPCP between N and CH. Data is presented as mean ± SEM with individual data points representing a single fibre recording. For N, n=4-8 fibres from 8 rats and for CH, n=7-10 fibres from 9 rats. Statistical significance was assessed using a two-way repeated measures ANOVA in A & B with overall p values displayed. An unpaired Student's t-test was performed on C & D.

5.2.4 CD73 inhibition using AOPCP abolished CO_2 sensitivity at a high concentration in N but was only partially blunted in CH

It is well establihsed that the carotid body acts as a polymodal receptor, being able to respond to a multitude of stimuli. Although hypoxia is considered the primary stimulus, the carotid body also responds to hypercapnia, albeit more modestly. Previous data has shown that CD73 inhibition using the same drug used throughout this thesis (AOPCP) completely abolished the response to hypercapnia at a concentration of 100μM in control carotid bodies (Holmes et al., 2015). However, it is unknown whether the slightly enhanced CO_2 sensitivtiy in CH (Chapter 3) is being driven by extracellularly derived adenosine and whether the same inhibitory effects of AOPCP can be achieved by using a lower concentration. To investigate this, carotid body chemoafferent activity was measured in normocapnia (PCO_2 = 40mmHg) until a steady baseline was reached and then the superfusate was switched to hypercapnia (PCO_2 = 80mmHg). This was repeated in the presence of AOPCP (CD73 inhibitor) at 15μM and 100μM.

Example chemoafferent responses to hypercapnia in the presence and absence of 15μM AOPCP for both N and CH are shown in Figure 5.5 A. In N, 15μM AOPCP sginificantly decreased the absolute frequency in both normocapnia and hypercapnia (Figure 5.5 B). However, the magnitude of the hypercapnic response was unaffected, signifying no change in CO_2 sensitivity (Figure 5.5 D, p=0.16). Similarly in CH, there were significant reductions in the absolute frequency during both normocapnia and hypercapnia in the presence of 15μM AOPCP but no alteration in CO_2 sensitivity (Figure 5.5 C & E). Unpaired analysis comparing CO_2 sensitivities to 15μM AOPCP in N and CH revealed no difference (unpaired student's t-test, p=0.17).

Example responses to hypercapnia, with and without 100μM AOPCP, for N and CH are presented in Figure 5.6 A. As N basal discharge in normocapnia was essentially abolished at 15μM, 100μM had no additional effect and remained near 0 Hz, but unlike 15μM AOPCP, 100μM severely attenuated the hypercapnic response (Figure 5.5 B). Calculated CO_2 sensitivity was severely depleted to approximately 80% of control (Figure 5.5 D). In CH, increasing the AOPCP concentration to 100μM diminished normocapnic discharge to almost 0 Hz, and attenuated the frequency measured in hypercapnia (Figure 5.5 C). This was accompanied by a strong trend for a blunted CO_2 sensitivity (Figure 5.5 E, p=0.05). Similar to hypoxia, the magnitude of the reduction in CO_2 sensitivity produced by AOPCP in a CH carotid body reversed its hypersensitivity back to levels consistent with that of an N carotid body. CO_2 sensitivities in ΔHz/mmHg CO_2 were N: 0.025±0.006, CH: 0.039±0.009 (p=0.29 vs N) and CH+100μM AOPCP: 0.018±0.2 (p=0.73 vs N, unpaired one-way ANOVA, Dunnett's post hoc).

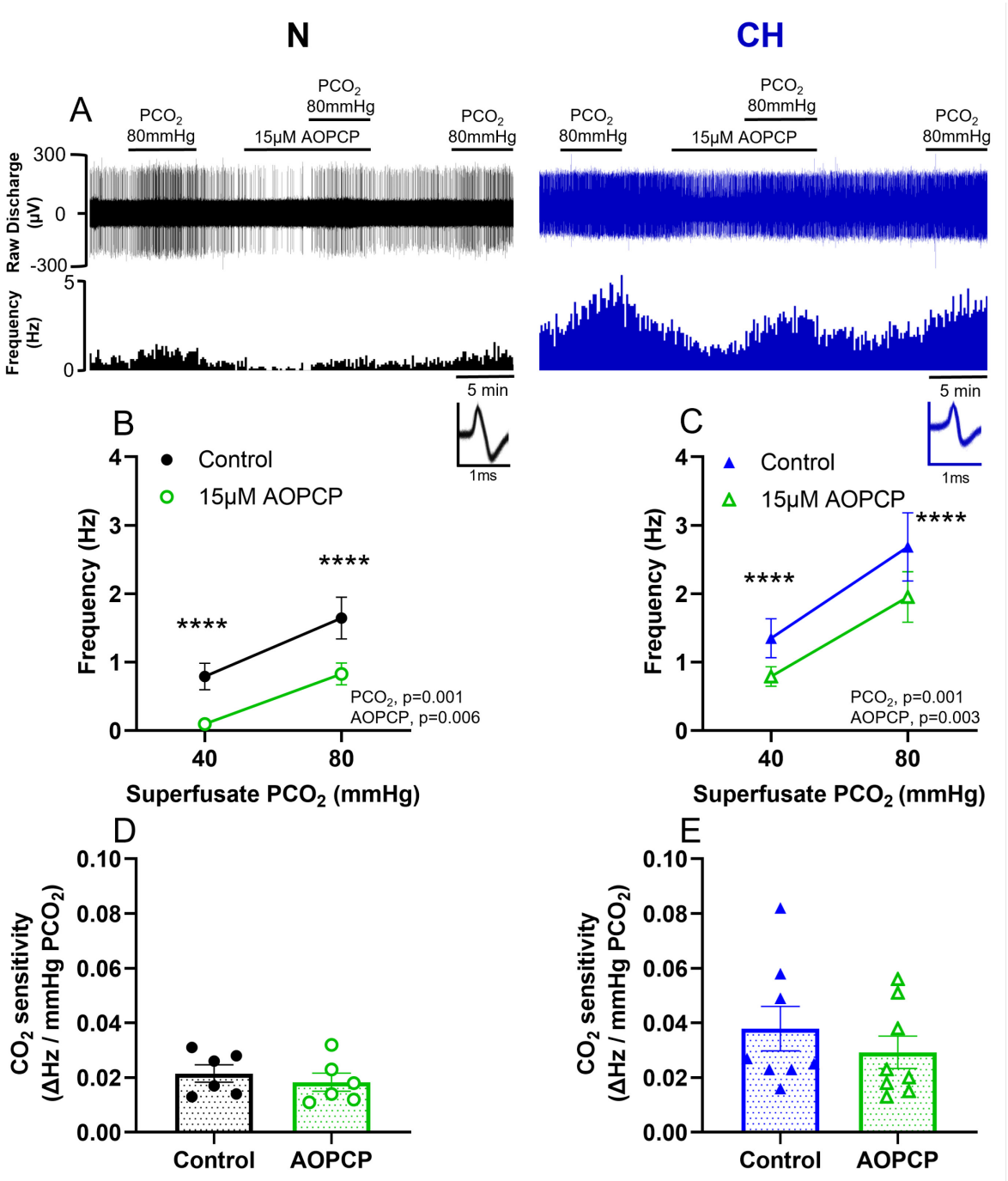

Figure 5.5 15μM AOPCP does not alter carotid body CO_2 sensitivity from normoxic or chronically hypoxic rats

(A) characteristic raw recordings showing chemoafferent response to hypercapnia ±15μM AOPCP in normoxic (N-left) and chronically hypoxic (CH-right) rat carotid bodies. Mean frequencies recorded in normocapnia (PCO_2= 40mmHg) and hypercapnia (PCO_2= 80mmHg) in control and in the presence of 15μM AOPCP in **(B)** N and **(C)** CH. CO_2 sensitivity ±15μM AOPCP in **(D)** N and **(E)** CH. CO_2 sensitivities were calculated as the frequency difference between normocapnia and hypercapnia in control and AOPCP groups per mmHg change in PCO_2. Data is presented as mean ± SEM with individual data points representing a single fibre. For N, n=6 fibres from 6 rats and for CH, n=8 fibres from 8 rats. Statistical significance was assessed using a two-way repeated measures ANOVA in B & C with overall p values displayed. Bonferroni post-hoc analysis used for multiple comparisons. ****p<0.0001 compared to control group. Paired Student's t-test performed on D & E.

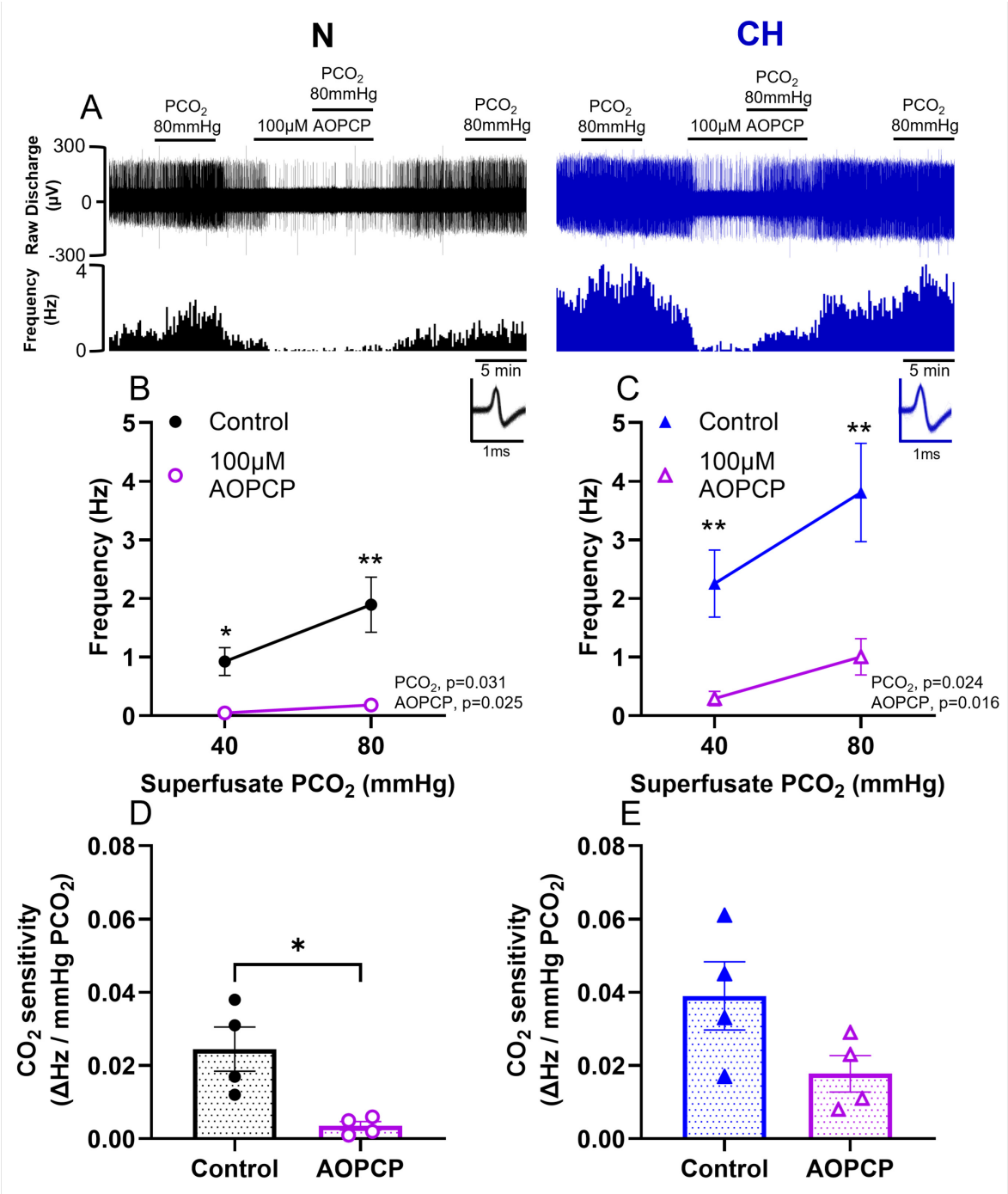

Figure 5.6 100μM AOPCP blunts carotid body CO_2 sensitivity to a larger extent in normoxic than chronically hypoxic rats

(A) characteristic raw recordings showing chemoafferent response to hypercapnia ±100μM AOPCP in normoxic (N-left) and chronically hypoxic (CH-right) rat carotid bodies. Mean frequencies recorded in normocapnia (PCO_2= 40mmHg) and hypercapnia (PCO_2= 80mmHg) in control and in the presence of 100μM AOPCP in **(B)** N and **(C)** CH. CO_2 sensitivity ±100μM AOPCP in **(D)** N and **(E)** CH. CO_2 sensitivities were calculated as the frequency difference between normocapnia and hypercapnia in control and AOPCP groups per mmHg change in PCO_2. Data is presented as mean ± SEM with individual data representing a single fibre. For N, n=4 fibres from 4 rats and for CH, n=4 fibres from 4 rats. Statistical significance was assessed using a two-way repeated measures ANOVA in B & C with overall p values displayed. Bonferroni post-hoc analysis used for multiple comparisons. *p<0.05, **p<0.01 compared to control group. Paired Student's t-test performed on D & E.

5.2.5 tmAC inhibition with SQ22536 decreased basal chemoafferent activity in a concentration-dependent manner in both N and CH

Data up until now has specifically looked at the effect of targeting CD73 in the carotid body and whether pharmacological antagonism of CD73 with AOPCP can reverse CH-induced hyperactivity. The next set of experiments aimed to determine the role of second messenger signalling molecules downstream of CD73. CD73 increases adenosine production in the carotid body and via stimulation of A_{2A} and A_{2B} receptors, tmAC is activated thus elevating cAMP. If all the effects of CD73 inhibition seen with AOPCP are due to a depletion in cAMP, then it could be hypothesised that the reversal of CH-induced hyperactivity should be replicated via pharmacological inhibition of tmAC.

Previous reports have shown that inhibition of tmAC using the same compound used in this thesis (SQ22536) caused a 60-70% reduction in basal single fibre frequency and attenuates the hypoxic response in control carotid bodies (Holmes et al., 2015; Rocher et al., 2009). However, various IC50s have been reported for this compound and so whether the lack of full inhibition is due to not reaching a high enough concentration to achieve full saturation is not known. Therefore, concentration response experiments were initially performed to characterise the potency of SQ22536 in N and CH carotid bodies. Concentrations given ranged from 100nM to 500μM and raw recordings are shown in Figure 5.7 A. In all fibres tested, in both N and CH, SQ22536 reduced, but did not abolish, basal discharge with a measurable effect being observed between 1μM and 10μM and maximal effect at around 300μM (Figure 5.7 B-E).

The absolute reduction in frequency was greater in CH (Figure 5.7 F). Due to the variation in basal activity between N and CH, raw data was normalised by calculating the reduction in basal frequency, expressed as a percentage. This data shows a rightward shift in the concentration response curve and subsequently a higher IC50 in CH (Figure 5.7 G). IC50s for N and CH were 22.1μM (95% CI; 11μM to 41μM) and 46.4μM (95% CI; 21μM to 97μM) respectively.

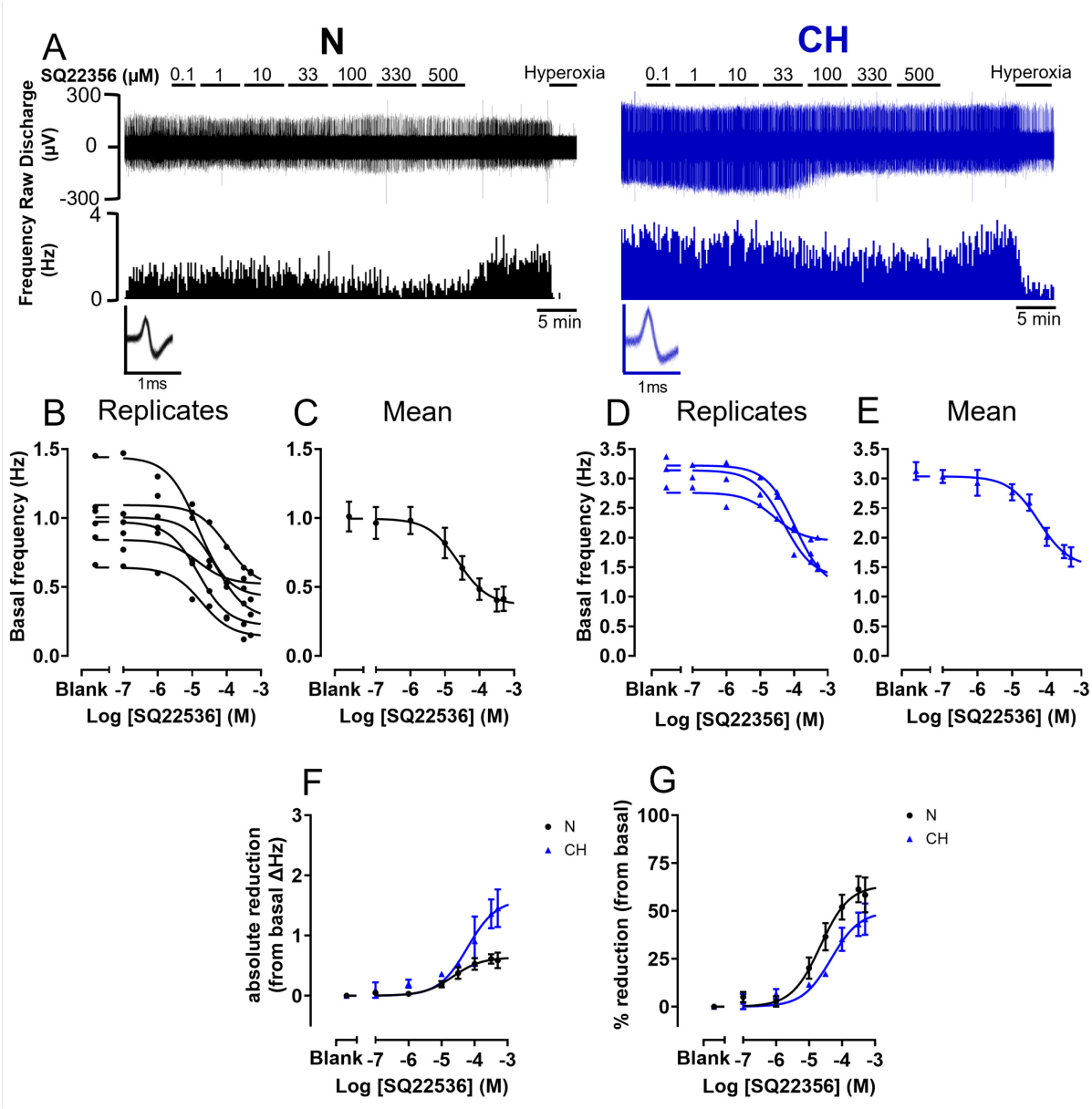

Figure 5.7 Transmembrane adenylyl cyclase inhibition with SQ22536 markedly decreased basal chemoafferent activity in a concentration-dependent manner in both normoxic and chronically hypoxic rat carotid bodies

(A) representative raw recordings of chemoafferent activity showing concentration-frequency response with SQ22536 from a normoxic (N-left) and chronically hypoxic (CH-right) rat carotid body. Raw discharge (upper) and frequency (lower) shows number of action potentials binned into 10 second intervals. Inset shows overdrawn action potentials for single fibre discrimination. **(B)** individual SQ22536 concentration-frequency response curve replicates for N. **(C)** mean of B. **(D)** individual SQ22536 concentration-frequency response curve replicates for CH. **(E)** mean of D. **(F)** SQ22536 concentration response curves comparing N and CH expressed as a reduction in absolute frequency. **(G)** SQ22536 concentration response curves comparing N and CH, expressed as a percentage reduction in basal frequency. For C, E, F and G data presented as mean ± SEM. Individual data points represent a single fibre. For N, n=6 fibres from 6 rats and for CH, n=3 fibres from 3 rats.

5.2.6 tmAC inhibition with SQ22536 normalises the exaggerated hypoxic sensitivity in CH carotid bodies

This section aimed to investigate the role of cAMP generated from tmAC in mediating the hypersensitivity to graded hypoxia observed in CH. Frequency was plotted at various PO_2 values, generating hypoxic-response curves fitted to an exponential decay with offset function. A steady baseline was established, and the superfusate PO_2 was reduced from 300mmHg to approximately 40mmHg before being rapidly switched to a hyperoxic solution to immediately silence the carotid body to prevent tissue damage. After a steady normoxic baseline was re-established, the hypoxic responses were repeated in the presence of 171μM SQ22536. This concentration gives rise to approximately 90% of the maximum inhibitory effect observed in N. SQ22536 was applied for approximately 5 minutes during normoxia and throughout the duration of graded hypoxia.

Figure 5.8 A shows an example CH recording of the experimental protocol with its respective O_2-response curves shown in Figure 5.8 B. The addition of 171μM SQ22536 to a CH carotid body decreased the frequency recorded throughout hypoxia (Figure 5.8 A-C). SQ22536 also caused a significant leftward shift in the CH O_2 response curve (Figure 5.8 D). This led to the observation that the hypoxic response curve of a CH carotid body in the presence of SQ22536 was very similar to that of an N carotid body, i.e. SQ22536 decreased the exaggerated hypoxic sensitivity of a CH carotid body back to pre-adapted levels. Interestingly, the magnitude of inhibition caused by SQ22536 on hypoxic chemoafferent frequency and O_2 sensitivity was consistent between N and CH (Figure 5.8 D & F).

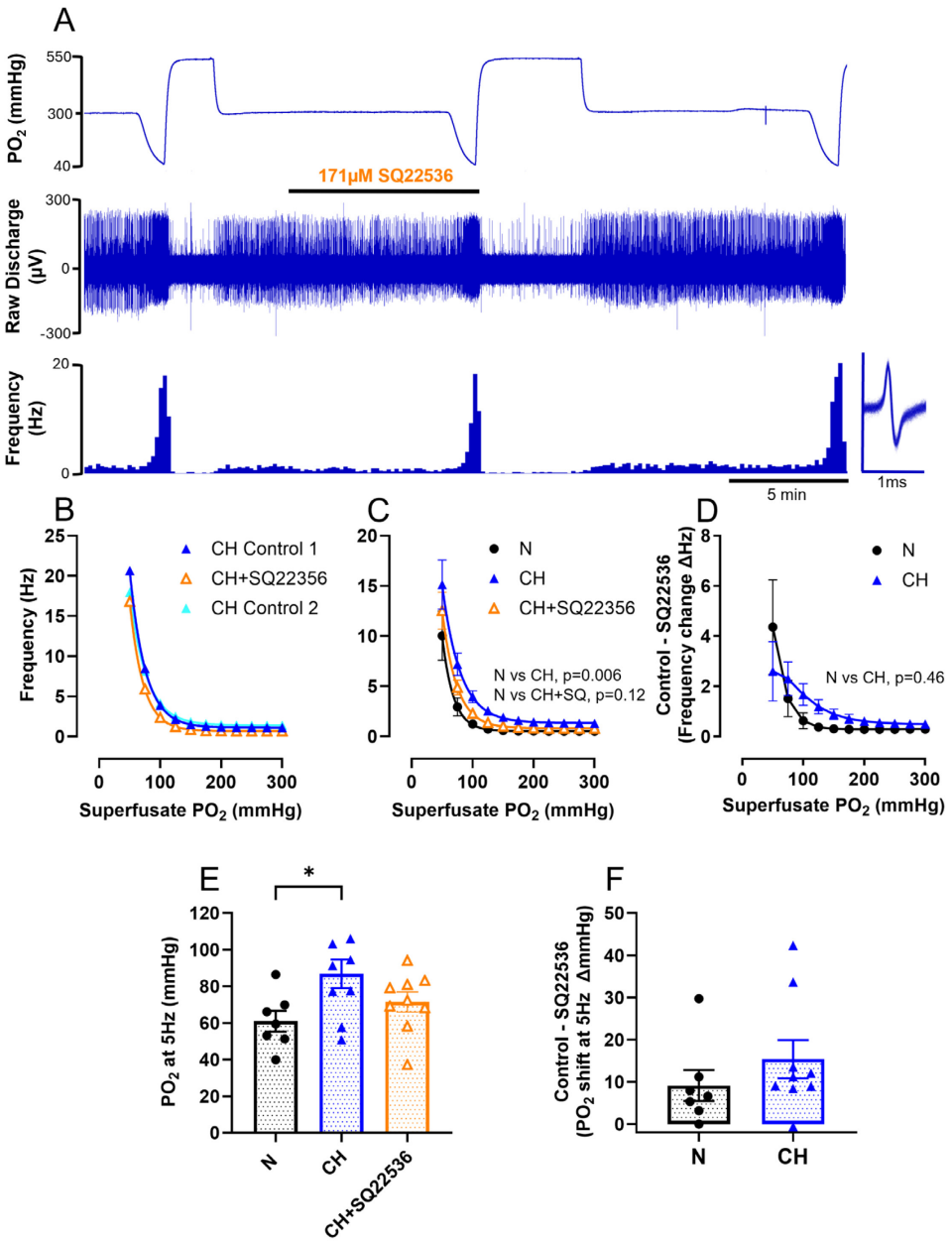

Figure 5.8 Transmembrane adenylyl cyclase inhibition normalised chronic hypoxia induced carotid body O_2 hypersensitivity *ex vivo*

(A) raw recording of chemoafferent response to graded hypoxia from a chronically hypoxic (CH) rat carotid body ±SQ22536. Raw discharge (upper) and frequency (lower) shows number of action potentials binned into 10 second intervals. Inset shows overdrawn action potentials for single fibre discrimination. **(B)** shows individual O_2 response curves derived from the raw trace in A, including SQ22536 in addition to the pre and post control. **(C)** mean O_2 response curves comparing normoxic (N) carotid bodies with CH ± 171μM SQ22536. **(D)** comparison of the reduction in frequency caused by SQ22536 between N and CH. **(E)** PO_2 required to elicit a discharge frequency of 5Hz. **(F)** comparison of the leftward PO_2 shift produced by SQ22536 at 5Hz between N and CH. Data expressed as mean ± SEM with individual data points representing a single fibre. For N, n=7 fibres from 6 rats and for CH, n=9 fibres from 8 rats. Statistical significance was assessed using a two-way repeated measures ANOVA in C & D with overall p values displayed. One-way ANOVA with Dunnett's post-hoc analysis performed on E, *p<0.05 vs N. Unpaired Student's t-test performed on F.

5.2.7 Transmembrane adenylyl cyclase antagonism with SQ22536 mildly blunted the response to hypercapnia in normoxic and chronically hypoxic carotid bodies

To determine whether cAMP plays a role in the response to hypercapnia and establishing carotid body CO_2 sensitivity in N and CH, the next set of experiments recorded carotid body discharge frequency in normocapnia (PCO_2= 40mmHg) and hypercapnia (PCO_2= 80mmHg) in the presence and absence of a tmAC inhibitor, SQ22536 (Figure 5.9 A).

The addition of 171μM SQ22536 signifcantly reduced the absolute frequency in normocapnia and hypercapnia in both N and CH (Figure 5.9 B & C). Furthermore, the magnitude of the hypercapnic response (CO_2 sensitivity) in the presence SQ22536 was significantly blunted in both groups (Figure 5.9 D & E). However, in contrast with hypoxia, the magnitude of the reduction in CO_2 sensitivity produced by SQ22536 in a CH carotid body, did not fully reverse it back to levels consistent with N. CO_2 sensitivities in ΔHz/mmHg PCO_2 were N: 0.019±0.003, CH: 0.037±0.004 (p=0.017 vs N) and CH+SQ22536: 0.031±0.005 (p=0.11 vs N, unpaired one-way ANOVA, Dunnett's post hoc).

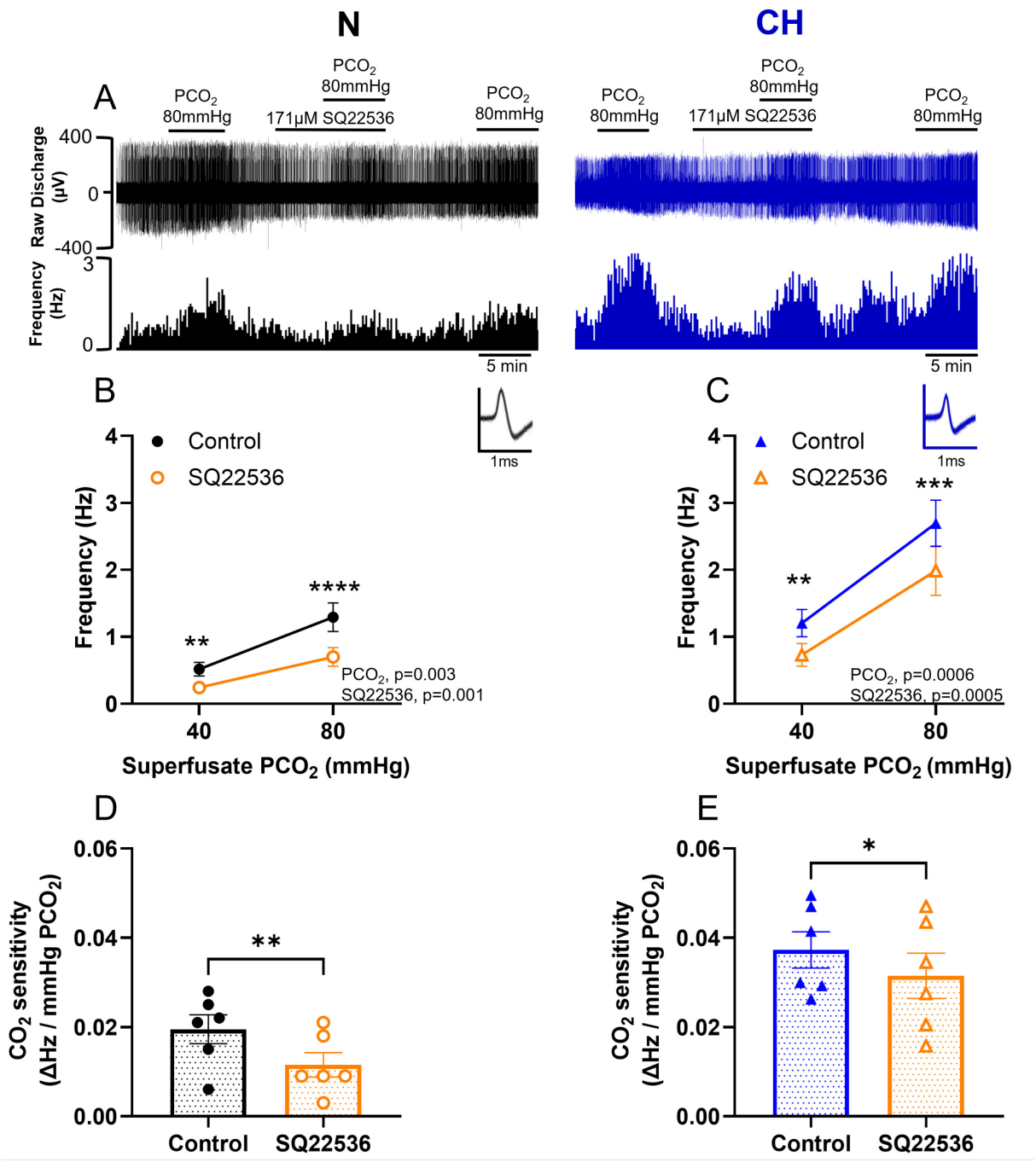

Figure 5.9 Pharmacological inhibition of transmembrane adenylyl cyclase blunted but did not fully normalise chronic hypoxia induced CO_2 hypersensitivity

(A) characteristic raw recordings showing chemoafferent response to hypercapnia ±171μM SQ22536 in normoxic (N-left) and chronically hypoxic (CH-right) rat carotid bodies. Mean frequencies recorded in normocapnia (PCO_2= 40mmHg) and hypercapnia (PCO_2= 80mmHg) in control and in the presence of 171μM SQ22536 in **(B)** N and **(C)** CH. CO_2 sensitivity ±SQ22536 in **(D)** N and **(E)** CH. CO_2 sensitivities were calculated as the frequency difference between normocapnia and hypercapnia in control and SQ22536 groups per mmHg change in PCO_2. Data is presented as mean ± SEM with individual data points representing a single fibre. For N, n=6 fibres from 4 rats and for CH, n=6 fibres from 5 rats. Statistical significance was assessed using a two-way repeated measures ANOVA in B & C with overall p values displayed. Bonferroni post-hoc analysis used for multiple comparisons. **p<0.01, ***p<0.001, ****p<0.0001 compared to control group. Paired Student's t-test performed on D and E, *p<0.05, **p<0.01.

5.3 Discussion

5.3.1 Summary of key chapter findings:

- Absolute sensitivity to exogenous adenosine was similar between groups but its relative sensitivity (% change) was blunted in CH carotid bodies

- Despite there being an elevated basal discharge in CH carotid bodies, CD73 inhibition with AOPCP was still able to diminish this by more than 90%, albeit at a slightly higher concentration compared with N

- tmAC inhibition with SQ22536 inhibited basal discharge by approximately 50-60% in both N and CH

- The augmented chemoafferent response to graded hypoxia in CH could be alleviated by antagonism of both CD73 and tmAC

- Hypercapnic sensitivity was heightened in CH and could be fully reversed to that consistent with N by inhibition of CD73 using a high concentration of AOPCP. It could only be partially reversed by inhibition of tmAC

5.3.2 A role for CD73 and cAMP in promoting CH-induced carotid body basal hyperactivity

Data presented in this chapter show that rats exposed to an F_iO_2 of 12% for 10 days develop a 2-3 fold increase in basal chemoafferent activity when measured *ex vivo*. This is consistent with other recordings of carotid sinus nerve activity showing elevated basal chemoafferent discharge following CH (Chen et al., 2002; Chen et al., 2007; Conde et al., 2012c). Among the many neurotransmitters and neuromodulators that mediate carotid body activity, adenosine has been proposed as being predominately responsible for establishing basal activity (Conde et al., 2012b; Conde et al., 2006; Holmes et al., 2018b). A key source of synaptic adenosine in the carotid body is via metabolism of AMP by CD73. However, whether CD73 and/or tmAC were causative of this elevated basal activity was unknown. These findings herein, show for the first time, that CD73 inhibition severely depresses basal activity in the CH carotid body, suggesting that increased CD73 activity is almost solely responsible for the augmented basal chemoafferent activity in CH animals. Only a proportion of this can be attributed to a concurrent increase in tmAC activity since SQ22536 could only partially mimic the chemoafferent depletion seen with AOPCP.

Pharmacology data showed that despite the elevated discharge in CH, CD73 antagonism with AOPCP can almost abolish basal activity in a concentration dependent manner but a higher concentration is needed to suppress discharge to near-zero. A right shift in the IC50, suggests that the relative sensitivity to AOPCP is blunted in CH. This finding could be potentially explained by the fact that CD73 mRNA expression is upregulated in the carotid bodies of rats exposed to chronic hypobaric hypoxia (Salman et al., 2017). Assuming that this increased transcription translates to

increased CD73 protein expression, which has been shown to occur in PC12 cells (Kobayashi et al., 2000b), then a higher concentration of drug would be needed to achieve a similar saturation and subsequent proportional effect. The interpretation of this cannot be used alone, as the absolute reduction in discharge is greater in CH, suggesting that its maximal efficacy remains uncompromised. Although no changes in the absolute nor relative density of CD73 immunostaining were observed in this model, it was observed that, in response to CH, the newly emerging TH^+ cells also co-expressed CD73 (Chapter 4). Therefore, the overall population of $CD73^+TH^+$ cells increased after CH (Chapter 4). It is logical to suggest that the expansion of TH^+ type I cells is a major contributor to the elevation in basal chemoafferent activity, and the functional activity of these 'new' TH^+ type I cells is highly sensitive to CD73 signalling. That said, precise quantification of CD73 protein and activity between N and CH carotid bodies is still warranted.

Additionally, it is important to consider that whilst adenosine generation is vital, its functional relevance is determined by activation metabotropic A_2 receptors and subsequent elevations in cAMP. Therefore, the action of adenosine and adenosine related signalling may be altered by CH. Investigations of the latter showed tmAC inhibition caused a dose-dependent reduction in carotid body discharge, with CH exhibiting a greater maximal reduction but reduced sensitivity (higher IC50) compared to N, similar to the results observed with CD73 inhibition. It must be noted that tmAC antagonism with SQ22536 could not completely abolish basal chemoafferent activity in both groups which could suggest incomplete saturation of the enzyme. Given that 6 isoforms are expressed in the carotid body, it is reasonable to suggest that pharmacological inhibition with SQ25536 may not have targeted all tmAC isoforms (Nunes et al., 2014). Perhaps future experiments could aim to use other

pharmacological inhibitors of tmAC that display broader selectivity or maybe a cocktail of antagonists to fully inhibit the complete set of enzymes. Alternatively, some of the effects of CD73 inhibition may be independent of a decrease in cAMP.

An alternative hypothesis leading into this chapter was that the rise in basal discharge in CH may simply be due to an increased sensitivity to adenosine rather than any alteration in CD73 activity and adenosine production. To address this the effect of exogenously applied adenosine on chemoafferent activity was examined in N and CH carotid bodies. Adenosine was added to the superfusate at a concentration known to increase chemoafferent activity (Vandier et al., 1999). Consistent with these findings, data in this chapter implies that adenosine can augment discharge to a greater absolute level compared to that of N, but its sensitivity with respect to an absolute change in discharge frequency is unaltered. Taking the elevated basal discharge in CH into account, proportionally compared to N, sensitivity to adenosine is in fact blunted (% change from basal). This somewhat paradoxical finding is in agreement with a previous study investigating CH on isolated rat carotid body type I cells. Increasing concentrations of exogenous adenosine led to a significantly greater catecholamine release in CH, at each concentration, and achieving approximately 6.5 fold increase in maximal secretion. However, the adenosine-response secretion curve was right shifted compared to N with an increase in the EC50 for adenosine, suggesting that in these CH type I cells, sensitivity to adenosine is also blunted, despite greater absolute catecholamine secretion rates compared to N (Livermore & Nurse, 2013). It is also worth noting that whilst dopamine secretion is commonly used as measure of type I cell function, it is an inhibitory neurotransmitter and doesn't necessarily reflect what will happen to sensory nerve activity. This is the first time that a comparison of adenosine action of chemoafferent activity has been made between N and CH. The data indicates

that exaggerated basal chemoafferent activity in CH cannot be due to enhanced adenosine sensitivity.

Detectable amounts of ATP and adenosine can be recovered in normoxia from whole N carotid body tissue, with higher amounts of adenosine being noted (Conde et al., 2012b). In other models of CH, type I cells undergo hypertrophy and increase the size and density of neurotransmitter-containing dense core vesicles (Fielding et al., 2018; Hodson et al., 2016). Electron microscopy experiments showed the ultrastructure of these dense core vesicles to be appear lighter and eccentrically distributed, suggestive of augmented vesicular neurosecretion (Fielding et al., 2018). It is therefore plausible to hypothesise that in addition to potential changes in CD73 and A_2 receptor expression, tonic vesicular secretion of ATP during normoxia is also elevated, thus contributing to enhanced ATP breakdown and the overall pool of adenosine. Clearly, measuring adenosine and ATP concentrations from CH carotid bodies would provide valuable information.

It is likely that these adaptations observed in CH are mediated by the HIF (Livermore & Nurse, 2013; Pulgar-Sepúlveda et al., 2018). TH-specific inactivation of HIF2-α completely prevents these ultrastructural changes to dense core vesicle appearance (Fielding et al., 2018). Likewise, both CD73 and A_2 receptor genes have HIF binding sites, and have been shown to increase their expressional profile in other cell types (Brown et al., 2011; Kobayashi et al., 2000a; Kong et al., 2006; Synnestvedt et al., 2002). Although not explored in this thesis, it is vital to consider the cellular/molecular targets of cAMP through adenosine A_2 receptor activation. Adenosine increases cAMP in the rat carotid body (Conde et al., 2008; Monteiro et al., 1996) and both adenosine

and cAMP have been shown to decrease the amplitude of the 4-AP-sensitive K^+ channel (Lopez-Lopez et al., 1993; Vandier et al., 1999). Adenosine also causes a rise in intracellular calcium driven by tmAC-dependent increases in cAMP (Xu et al., 2006). A classical target of cAMP is PKA, and in the same study, PKA was shown to inhibit TASK-1 channels, resulting in depolarisation and opening of voltage-gated calcium channels. Enhanced inhibition of TASK-like currents has been shown to occur in CH, but whether this is directly attributed to elevated adenosine signalling and PKA activity has not been examined (Ortiz et al., 2009). CH has also been shown to increase expression of the voltage-gated Na^+ channel, Nav1.1 (Caceres et al., 2007) and voltage-gated Ca^{2+} channel density in adult rat carotid bodies (Hempleman, 1996). Interestingly, evidence has directly implicated cAMP in altering the Na^+ channel density and long-duration Ca^{2+} components, as normoxic incubation with stable cAMP analogues mimics these changes in electrical excitability and Ca^{2+} influx observed in sister cultures exposed to CH (Stea et al., 1995).

CH and elevated adenosine therefore can effect membrane depolarisation, Ca^{2+} influx and catecholamine release, all of which could be driving heightened basal carotid body activity, ultimately through persistently elevated cAMP which has been noted in other *in vitro* CH carotid body models (Nurse et al., 1993). In addition, these downstream targets are involved in the hypoxic chemotransduction cascade and so enhancement of these mechanisms could be responsible for the increased O_2 sensitivity observed in CH carotid bodies.

5.3.3 The impact of adenosine and cAMP in mediating CH-induced carotid body O_2 hypersensitivity

In this model of CH, the chemoafferent response to graded hypoxia was exaggerated, demonstrated by a right shift in the O_2-response curve and further quantified by a higher PO_2 threshold to initiate the hypoxic response. This augmented hypoxic response is consistent with other recordings of carotid sinus nerve activity, albeit using steady state level of hypoxia instead of graded hypoxia (Chen et al., 2007; Conde et al., 2012c). Interestingly in this study, authors gave an endothelin receptor antagonist during CH induction and found that it was able to prevent any carotid body growth and proliferation of type I cells but could not fully attenuate the exaggerated hypoxic response. This suggests that CH induced carotid body hyperactivity may not solely due to an increase in the TH^+ type I cells, and that there are cell specific adaptations that sensitise the type I cells to hypoxia. This could be potentially driven by heightened CD73 signalling.

Data in this chapter showed that inhibition of CD73 and tmAC, could normalise the augmented hypoxic response in CH by causing a left shift in the O_2 response curve, suggesting that extracellular adenosine and cAMP are driving alterations in O_2 sensitivity. There was a trend for a greater leftward PO_2 shift with AOPCP in CH indicating a potentially enhanced effect of CD73 in setting the hypoxic sensitivity in this CH model. Results further indicate that the greatest effect of CD73 inhibition occurred at normoxic and mildly hypoxic levels which corroborates evidence that A_2 receptor antagonism had a greatest inhibitory effect at mild hypoxic intensities (Conde et al., 2012b). These results therefore suggest that CD73 and cAMP are important in setting the PO_2 threshold needed to initiate a hypoxic response in both N and CH carotid

bodies. This mechanism can be targeted pharmacologically in CH carotid bodies to reduce hypoxic sensitivity back to 'normal' non-adapted levels without completely abolishing it. This could be important therapeutically when aiming to reduce carotid body hyperactivity without eliminating it.

The importance of CD73 in setting the hypoxic threshold must somehow link to the currently unknown molecular sensor of oxygen and/or to multiple elements of the chemotransduction cascade. For example, measured changes in intracellular calcium are approximately 1.5 times greater in isolated CH rat type I cells in response to acute hypoxia, rising to a concentration that can be mimicked by exogenous adenosine. Both effects were mediated by A_{2B} receptor activation (Livermore & Nurse, 2013). Further studies investigating these mechanisms in the carotid body are needed. Given that hypoxia and adenosine can increase intracellular cAMP, and that both stimuli impact membrane excitability, calcium influx and catecholamine secretion potentially through direct actions of cAMP or PKA activity, then this mechanism could be altered in CH and makes future experiments investigating this plausible.

Whilst these mechanistic studies provide valuable information, they have primarily focussed on the pre-synaptic action of adenosine, yet little has been explored on the post-synaptic sensory chemoafferents. Recent experiments utilising a co-culture model of rat carotid body type I cells and sensory neurones showed that both adenosine and hypoxia increased the hyperpolarisation-activated current (I_h) through activation of the HCN4-containing cation channel. It was reported that this effect was mediated through an A_{2A} and cAMP-specific mechanism (Zhang et al., 2018). Whether

these channels are sensitised in CH through expressional changes and increased activity is subject to further investigation.

5.3.4 Is the CH-induced elevation in hypercapnic sensitivity dependent on adenosine and cAMP?

CD73 and adenosine are suggested to mediate around 50-80% of the carotid body response to hypercapnia, however whether enhanced adenosine generation and signalling is responsible for the elevation in carotid body CO_2 sensitivity in CH is unknown (Holmes et al., 2015; Sacramento et al., 2018). Indeed, this data demonstrates that the response to hypercapnia was exaggerated in CH carotid bodies. This is consistent with previous reports showing an approximate 5-fold increase in hypercapnia-induced catecholamine secretion rate in isolated type I cells previously exposed to sustained hypoxia (Livermore & Nurse, 2013). Pharmacological targeting of CD73 showed that hypercapnic sensitivity was blunted with a high concentration of AOPCP in both N and CH. Thus, CD73 is also important in setting the hypercapnic sensitivity of the carotid body in both N and CH. The data implies that targeting CD73 in the CH carotid body can be used to reverse hypercapnic sensitivity back to normal pre-adapted levels, without completely eliminating it. Interestingly, as this effect was only seen at high dose of AOPCP, it appears that almost complete blockade of CD73 is needed to impact on hypercapnic sensitivity.

An interesting hypothesis could be that only a relatively small amount of CD73 activity is required to establish the hypercapnic sensitivity in the carotid body. In contrast, basal activity and hypoxic sensitivity require larger amounts of sustained CD73 activity and are both therefore more sensitive to lower concentrations of AOPCP and relatively

lower levels of CD73 in inhibition. An even higher concentration of AOPCP may be expected to produce greater overall inhibition of CD73, preventing the enzyme from fully engaging in the hypercapnic response. Performing experiments with even higher concentrations of these or other CD73 antagonists during hypercapnia may reveal whether the response can be fully inhibited in CH or whether the residual CO_2 sensitivity demonstrates an adaptation that is adenosine independent. Radioligand binding assays could also help to determine the saturation of CD73 and tmAC at concentrations used in this study

Prevention of cAMP build up through tmAC inhibition with SQ22536 also attenuated the hypercapnic response but this was much milder compared to CD73 inhibition. The exact reasons for a milder effect with SQ22536 are unknown but could be due to the incomplete saturation of tmAC as describe previously with multiple isoforms of the enzyme present in the carotid body. Alternatively, the exaggerated actions of CD73 inhibition may be cAMP independent.

Overall, these findings strongly suggest that in CH carotid bodies, CD73 is responsible for not only setting the basal activity but also the sensitivity to other stimuli including hypoxia and hypercapnia. Pharmacological targeting of CD73 or tmAC in a CH carotid body could be used to alleviate basal carotid body hyperactivity and stimulus hypersensitivity, without completely abolishing its ability to respond to hypoxia and hypercapnia.

5.4 Conclusions

CD73 inhibition has profound effects on carotid body activity in normoxia, hypoxia and hypercapnia being able to greatly attenuate CH-induced hyperactivity. This identifies CD73 as a potential pharmacological target to dampen excess carotid body activity caused by CH, whilst at the same time not completely eliminating it. CH is a key feature of COPD, and patients display major cardiovascular complications like hypertension, which evidence has suggested is driven by heightened carotid body activity into the brainstem, causing persistent sympathetic outflow to the vasculature. In view of this, *in vivo* pharmacological antagonism of CD73 aiming to dampen carotid body hypersensitivity and reduce blood pressure in CH rats was investigated in the next chapter.

CHAPTER 6

6. The functional role of carotid body CD73 in mediating cardio-respiratory responses to normoxia and hypoxia following chronic hypoxia

6.1 Introduction and aims

Autonomic imbalance is commonly seen in COPD, a condition marked by respiratory dysfunction and cardiovascular co-morbidities (Kent et al., 2011; Rabe et al., 2018). Cardiovascular disease is the leading cause of hospitalisations and death in COPD patients (Rabe et al., 2018; WHO, 2025). Growing evidence suggests that persistent elevated sympathetic outflow to the heart and vasculature plays a major role in driving hypertension (Narkiewicz et al., 1998; Phillips et al., 2018; Schultz et al., 2015; Stickland et al., 2016). Carotid body hyperactivity has been proposed as a key factor contributing to this abnormal sympathetic outflow, and as shown in Chapter 5, CH exacerbates carotid body hyperactivity (Del Rio et al., 2016; Iturriaga et al., 2021; Schultz et al., 2015). Consequently, reducing abnormal carotid body activity is being explored as a potential treatment to alleviate cardiovascular dysfunction in CH-related conditions such as COPD.

Promising preliminary data in other diseases with carotid body hyperactivity, including heart failure and neurogenic hypertension, showed that CSNX could reduce sympathetic outflow, improve exercise tolerance (Niewinski et al., 2017) and lower blood pressure in half of the patients studied (Niewinski et al., 2017). However, safety concerns about severe oxygen desaturation during sleep and upon exposure to mild hypoxia highlight the importance of retaining some carotid body function (Niewinski et al., 2017; Niewinski et al., 2021). This has led to the idea that pharmacologically

targeting the carotid body could offer a safer alternative to surgery, through fine-tuning its activity without complete loss of sensory function. Understanding the mechanisms that drive heightened carotid body activity is essential for identifying pharmacological targets that can dampen this excess sympathetic outflow to the brain.

In the previous chapter, data suggested that CD73 could be a promising target. Antagonising its enzymatic activity with AOPCP was shown to completely abolish carotid body hyperactivity and normalise carotid body oxygen sensitivity (without abolishing it), presenting a novel strategy to reduce basal activity without compromising the ability to respond to stressors like hypoxia.

Previous studies have shown that AOPCP can mildly blunt the hypoxic ventilatory response and associated tachycardia (Holmes et al., 2018). However, it remains unclear whether AOPCP can reduce the elevated basal ventilation in CH by a selective action on the carotid body. Furthermore, it is unknown if AOPCP modifies cardiovascular parameters in CH animals including arterial blood pressure and heart rate, and if this is exaggerated when compared to N, due to augmented input from the carotid body. This chapter aimed to explore these questions to improve our understanding of AOPCP's specific targets *in vivo*.

Aims of this chapter were as follows:

1. Investigate the importance of the carotid body in mediating minute ventilation, mABP and heart rate during normoxia and hypoxia in N and CH animals

2. Assess the impact of pharmacological inhibition of CD73 with AOPCP on minute ventilation, mABP and heart rate in N and CH animals

3. Determine if any of the observed effects of AOPCP in N and CH animals are carotid body dependent

6.2 Results

6.2.1 Determination of the 'normoxic' F_iO_2 for CH adapted animals

To determine the contribution of the carotid body to minute ventilation, blood pressure and heart rate, input from the carotid body needs to be established in normoxic conditions and then silenced or greatly reduced. In humans this is achieved non-invasively by inhaling a hyperoxic gas mixture (F_iO_2 = 95-100%) (Gibbons et al., 2022; Stickland et al., 2016). Although this does decrease ventilation, indirectly suggesting carotid body activity is diminished, there are concerns with the local effects of hyperoxia around the body, particularly on the vasculature and the brain which may confound some of the results. In animal models, direct removal of carotid body sensory output can be achieved via CSNX under anaesthetic.

Initially, rats were anaesthetised with isoflurane and the right femoral vein was cannulated to perfuse an intravenous anaesthetic (Alfaxalone). This anaesthetic helps better preserve cardiorespiratory reflexes which are heavily depressed by isoflurane (Ambros et al., 2008; Holmes et al., 2018b; Karanovic et al., 2010; Muir et al., 2008; Thomas & Marshall, 1994; Walsh & Marshall, 2006). Also, to measure ventilation, the trachea must be cannulated and connected to a spirometer, therefore the use of an inhalation anaesthetic was not possible with the equipment available. Once the animal

had maintained an appropriate depth of anaesthesia, the right femoral artery was cannulated and connected to a pressure transducer to record arterial blood pressure. The carotid bifurcation was dissected bilaterally as described in Chapter 2, in preparation for CSNX later in the protocol. Once all surgical procedures were complete, a 15-20-minute adjustment period allowed cardio-respiratory measurements to stabilise before recording any responses. This initial data set aimed to determine the effect of CSNX on ventilation, blood pressure and heart rate in N and CH rats breathing room air (F_iO_2 of 21%). This was done to assess whether for CH rats breathing room air is actually 'hyperoxic' to the animal.

When breathing room air, minute ventilation was comparable between both groups although tended to be lower in CH animals. However, CSNX caused a significant reduction in minute ventilation in N rats as expected but produced no decrease in minute ventilation in CH rats (Figure 6.1 A & B). In N rats, CNSX also caused a significant drop in blood pressure (Figure 6.1 C). Interestingly, during room air breathing blood pressure was significantly elevated in CH compared to N and CSNX failed to cause any reduction (Figure 6.1 D). Heart rate was comparable between groups and did not change in either group after CSNX (Figure 6.1 E & F). The baseline hypertensive state, along with CSNX producing no effect on ventilation and blood pressure, strongly implies that room air breathing induces significant hyperoxia in CH animals, thereby almost completely silencing the carotid body. This is perhaps unsurprising given that CH animals have already adapted to F_iO_2 of 12% for 9-10 days, have a significantly increased haematocrit (Table 3.1 in Chapter 3) and an elevated O_2 capacity. In view of this, subsequent baseline (control) comparisons were made between N rats breathing room air (F_iO_2 of 21%) and CH rats breathing an F_iO_2 of 12%,

as previously described (Marshall & Davies, 1999; Thomas & Marshall, 1997; Walsh & Marshall, 2006).

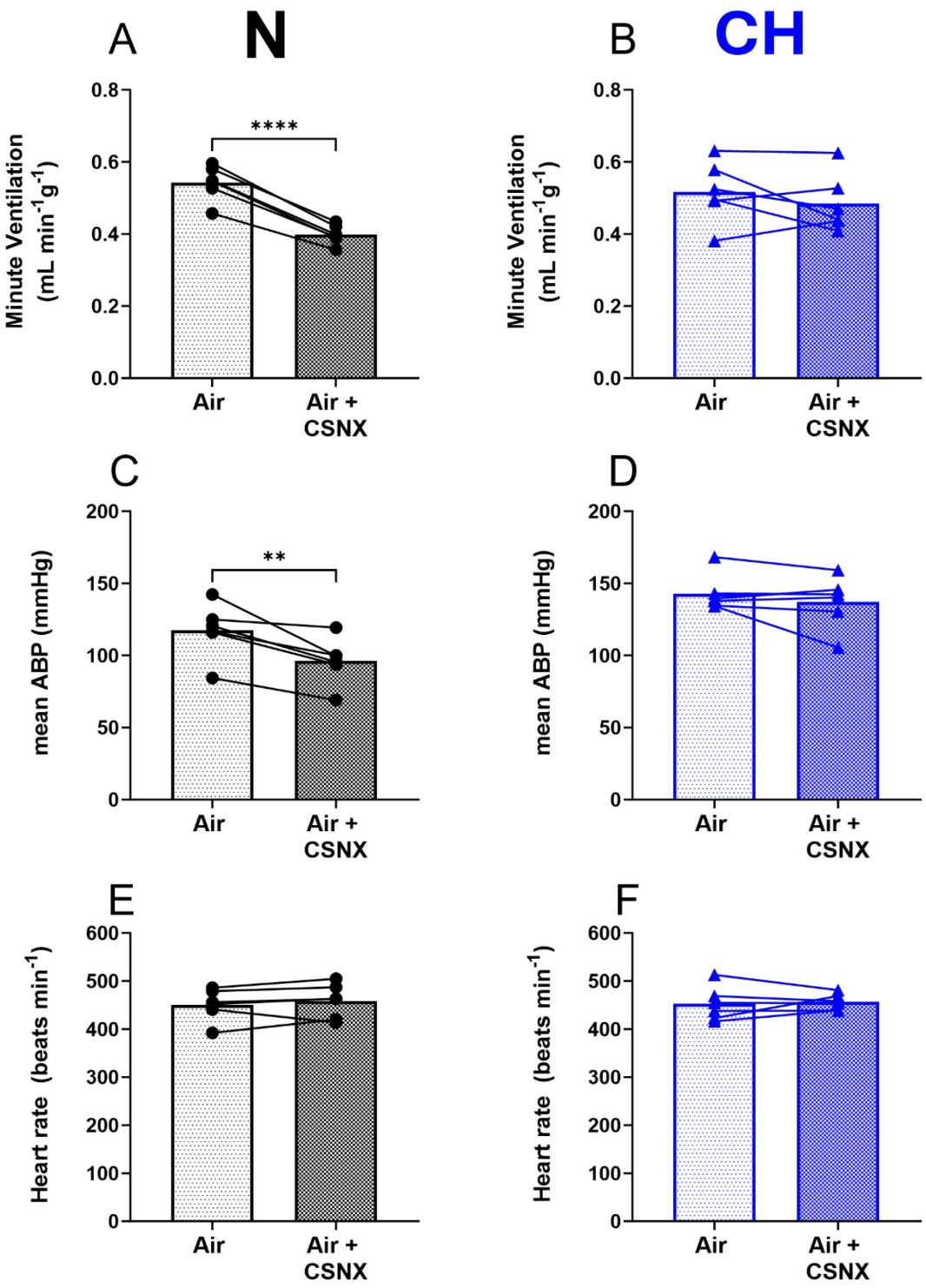

Figure 6.1 Effect of carotid sinus nerve section on cardio-respiratory measurements in normoxic and chronically hypoxic rats breathing room air

(A) minute ventilation before and after carotid sinus nerve section (CSNX) in normoxic (N, black) and chronically hypoxic (CH, blue) rats breathing room air (F_IO_2 of 21%). **(B)** mean arterial blood pressure (ABP) before and after CSNX in N and CH rats breathing room air. **(C)** heart rate before and after CSNX in N and CH rats breathing room air. Data is presented as mean ±SEM with individual data showing an individual rat. n=6 rats for both groups. Connecting lines showing before and after CSNX in each rat. Statistical significance was assessed using a paired Student's t-test, in both groups. **p<0.01, ****p<0.0001.

6.2.2 The carotid body was essential for eliciting a protective cardio-respiratory response to severe hypoxia

In many species, the ventilatory response to hypoxia is biphasic. Ventilation tends to peak and then slowly decline before reaching a steady state (Pamenter & Powell, 2016). This makes analysis challenging when comparing differences between two groups. To overcome this, time courses were plotted to visualise the dynamics of the hypoxic response (Figure 6.2 A-D). Data was plotted as a sequential 10-second average. A steady baseline was established for 2 minutes before switching to a hypoxic gas mixture (F_iO_2 = 8%) for 2 minutes followed by recovery in normoxia (Figure 6.2). The peak minute ventilation varied between rats and so to keep analysis consistent between experimental animals, fixed time points throughout the hypoxic exposure were chosen. This included the rising phase (average of time points 30 & 40 seconds) and the end of hypoxia (average of time points 110 & 120 seconds) where ventilation started to plateau. These same time points were also used to assess mABP (Figure 6.2 C) and heart rate (Figure 6.3D).

Minute ventilation during normoxia was significantly greater in CH but hypoxic responses differed between groups. N rats had a trend for greater HVR after 30-40 seconds of hypoxia compared to CH (p=0.052) but declined by the end of the exposure. Although CH rats did not show an augmented HVR compared to N, they did not show a ventilatory decline. As such minute ventilation remained higher in CH animals throughout hypoxia (Figure 6.2 & 6.3). Both N and CH displayed a reduced end-tidal CO_2 reading upon exposure to hypoxia, N (Control: 3.97±0.2%, Hx:2.87±0.2%, p=0.0006 paired t-test) and CH (Control: 2.62±0.1%, Hx:2.22±0.1%,

p=0.001 paired t-test). The degree of hyperventilation was significantly greater in N than CH (N: -Δ1.10±0.1% vs CH: -Δ0.40±0.1%, p=0.0002 unpaired t-test).

mABP tended to be lower during normoxia in CH rats (N: 121±5mmHg vs CH: 88±12mmHg, p=0.15) and a smaller change in mABP occurred at both 30-40 seconds of hypoxia (p=0.064) and the end of hypoxia. The absolute mABP, however were comparable between groups at either time point (Figure 6.3 C & D). Heart rate remained constant between groups and during normoxia and hypoxia (Figure 6.3 E & F).

After a steady baseline was established, CSNX was performed to remove any carotid body output, and the hypoxic stimulus was repeated. A striking finding was that N rats could not respond appropriately to the hypoxic stimulus after CSNX, and as such, had a period of prolonged apnoea approximately 30-50 seconds into the hypoxic exposure which caused the ventilation, mABP and heart rate to plummet. As soon as this occurred, the gas mixture was immediately switched back to normoxia. Although CH rats did not respond to hypoxia after CSNX, they were able to maintain a steady ventilation, blood pressure and heart rate, throughout the 2-minute exposure (Figure 6.2 E-G). Due to incompletion of the full hypoxic response in N rats after CSNX, comparisons could not be made to CH. Therefore, the effect of CSNX was examined specifically on normoxic breathing throughout the rest of the analysis.

6.2.3 CSNX caused a greater reduction in ventilation in CH, a comparable decrease in mABP and no change in heart rate during normoxia

CSNX caused a significant decrease in normoxic ventilation in both groups. A significantly greater reduction in minute ventilation occurred in CH animals compared to N (Figure 6.4 A-C). CSNX increased end-tidal CO_2 in both groups: N (Control: 3.97±0.2%, CSNX: 4.25±0.2%, p=0.04 paired t-test) and CH (Control: 2.75±0.1%, CSNX: 3.26±0.2%, p=0.003 paired t-test). Although there was a trend for a greater increase in end-tidal CO_2 in CH rats, this was not significant between groups (N: -Δ0.28±0.1% vs CH: -Δ0.51±0.1%, p=0.14 unpaired t-test).

CSNX caused mABP to fall by approximately 24±7mmHg in N rats (Figure 6.4 A & F). Despite a lower resting mABP, in 5 out of 6 CH rats, CSNX caused a drop in blood pressure (Figure 6.4 E, p=0.05). This reduction was the same magnitude as measured in N rats (Figure 6.4 F). Heart rate remained unchanged after CSNX in N rats and although no overall statistical differences were observed in CH rats, 4 out of 6 rats had a reduced heart rate post CSNX, however the change in heart rate in response to hypoxia was not statistically significant between N and CH (Figure 6.4 G-I).

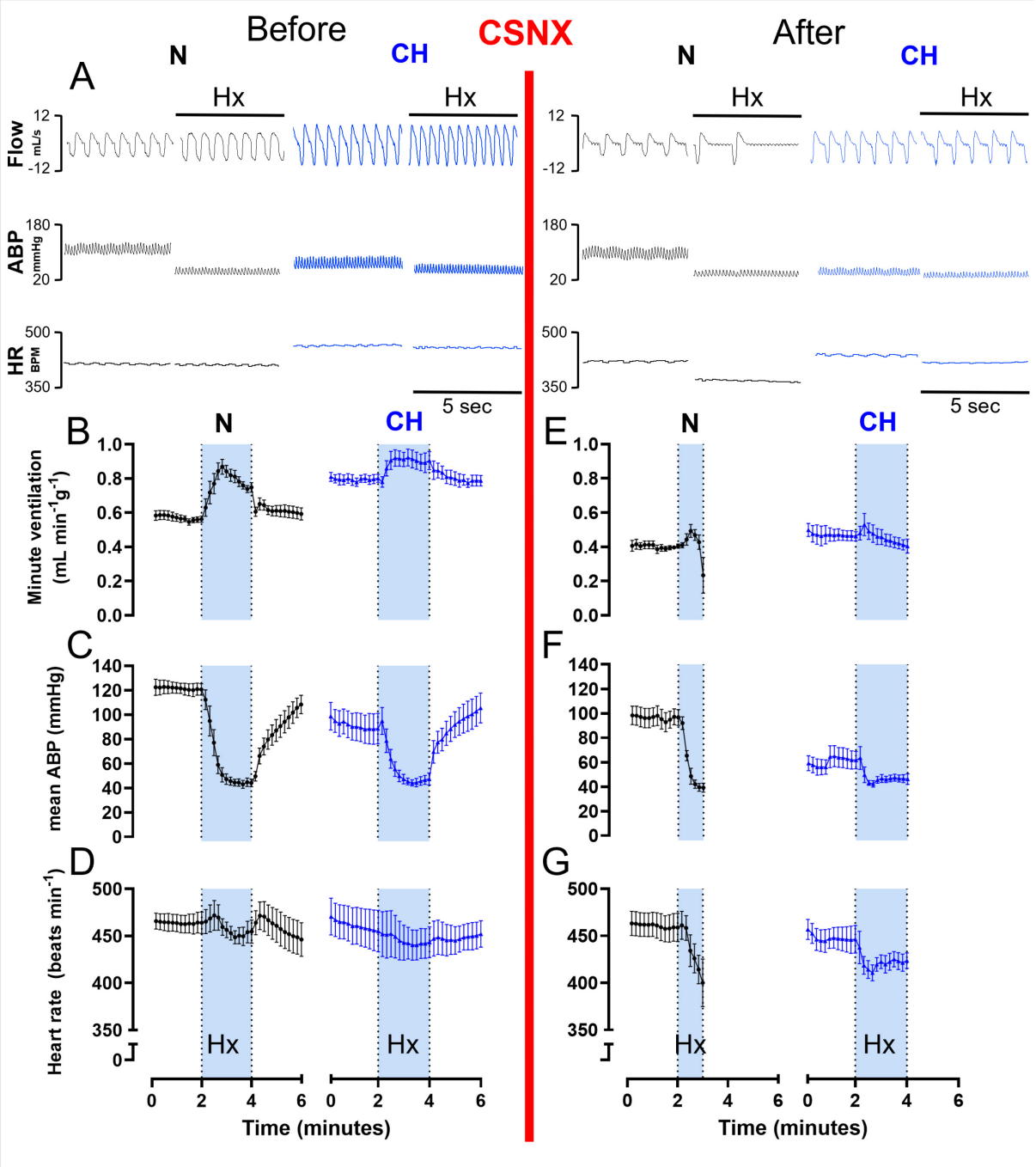

Figure 6.2 Time courses of cardio-respiratory responses to hypoxia before and after carotid sinus nerve section in normoxic and chronically hypoxic rats

(A) 5 second raw traces from normoxic (N, black) and chronically hypoxic (CH, blue) rats showing airflow (upper), mean arterial blood pressure (mABP, middle) and heart rate (lower) during control and hypoxia (Hx = F_iO_2 8%; shaded light blue) before and after CSNX (red line). **(B-D)** Time courses showing effect of hypoxia on **(B)** minute ventilation, **(C)** mABP and **(D)** heart rate in N and CH animals. **(E-G)** Time courses were repeated after CSNX showing the effect of removing carotid body output under control conditions and during hypoxic responses for **(E)** minute ventilation, **(F)** mABP and **(G)** heart rate. For B-E data presented as mean ± SEM with data points representing a single rat. n=6 rats for both groups.

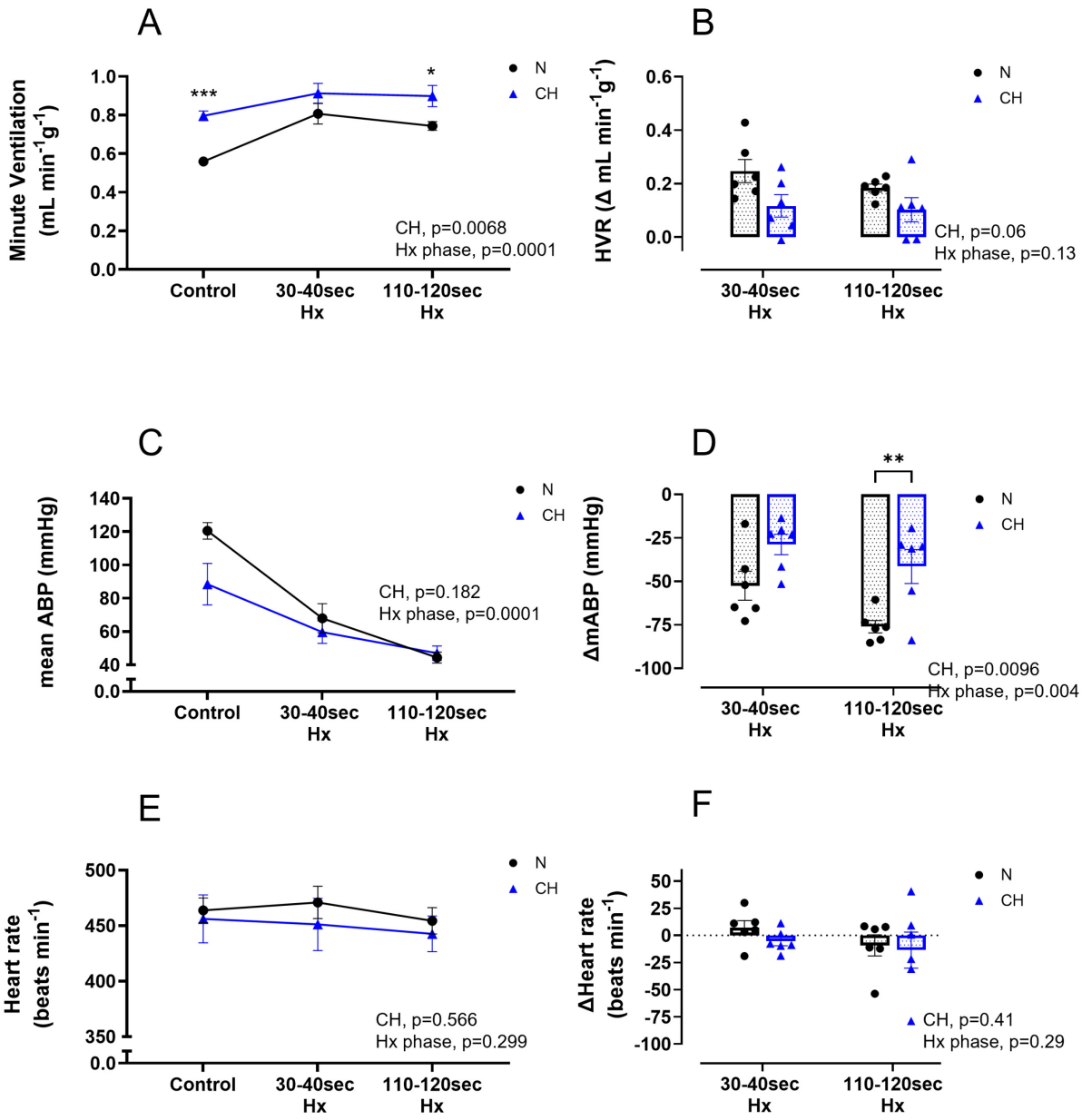

Figure 6.3 Comparison of baseline cardio-respiratory parameters and hypoxia-induced responses between normoxic and chronically hypoxic rats

(A) minute ventilation during normoxia (control) and specific time points during hypoxia (Hx = F_iO_2 8%) in normoxic (N) and chronically hypoxic (CH) rats. **(B)** hypoxic ventilatory response (HVR) at each hypoxic phase compared to control. **(C)** mean arterial blood pressure (mABP) during normoxia and specific time points during Hx. **(D)** change in mABP at each hypoxic phase compared to control. **(E)** heart rate during normoxia and specific time points during Hx. **(F)** change in heart rate at each hypoxic phase compared to control. Data presented as mean ± SEM with each point representing an individual rat. n=6 rats for both groups. Statistical significance was assessed using a two-way repeated measures ANOVA with overall p values shown. Bonferroni post-hoc analysis to compare differences within groups. *p<0.05, **p<0.01 and ***p<0.001 compared to N.

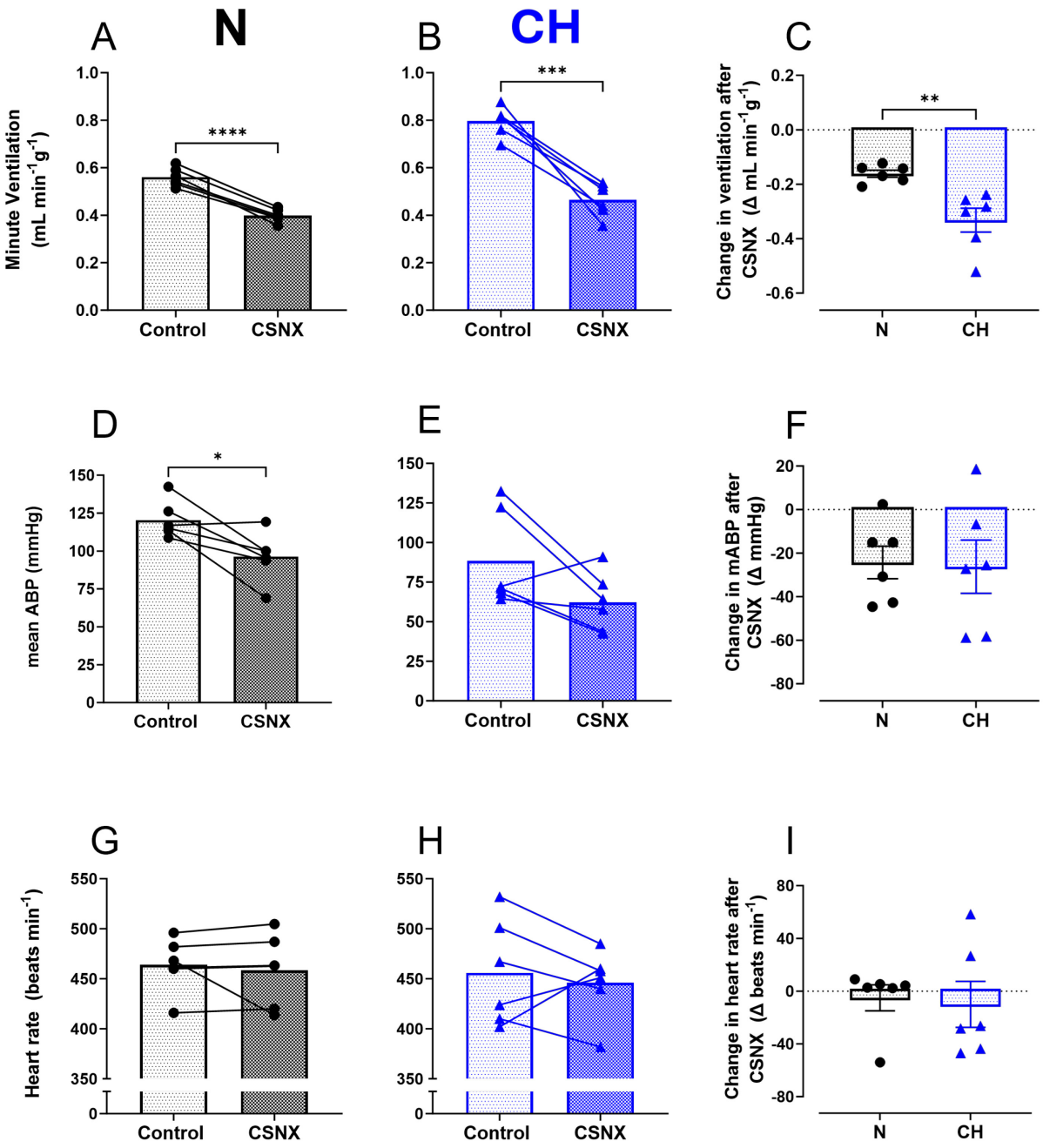

Figure 6.4 Comparison of the effect of carotid sinus nerve section on baseline ventilation, blood pressure and heart rate in normoxic and chronically hypoxic rats

The effect of CSNX on ventilation in normoxic (N, black) rats **(A)**, chronically hypoxic (CH, blue) rats **(B)** and the change in ventilation from baseline (control) in **(C)**. The effect of CSNX on mean arterial blood pressure (mABP) in N **(D)**, CH **(E)** and the change from control values **(F)**. The effect of CSNX on heart rate in N **(G)**, CH **(H)** and the change from control values **(I)**. Data presented as mean ± SEM with each point representing an individual rat and connecting line showing before and after CSNX. n=6 rats for both groups. Statistical significance was assessed using a paired Student's t-test in A, B, D, E, H & F and an unpaired Student's t-test in C, F & I. *p<0.05, **p<0.01, ***p<0.001 & ****p<0.0001.

6.2.4 Intravenous injection of AOPCP produced a dose-dependent reduction in resting minute ventilation, mABP and heart rate in CH animals

Results described above demonstrate a role for enhanced carotid body activity in driving the augmented ventilation measured in CH rats. The carotid body also was shown to contribute to tonic maintenance of mABP. The previous chapter showed that *ex vivo* CSN activity could be abolished with CD73 inhibition using AOPCP. However, whether CD73 blockade *in vivo* could blunt the augmented resting ventilation in CH rats and alter cardiovascular parameters such as mABP and heart rate was examined in these next set of experiments.

Rats were anaesthetised and prepared for cardio-respiratory measurements as previously described in section 2.8 and 6.2.1. An additional component of these experiments was the cannulation of the left femoral vein to inject AOPCP (see Figure 2.13 for schematic summary of experimental set up). Once cardio-respiratory variables had reached a steady state, 160µg kg^{-1} AOPCP was injected intravenously at a volume dose of 1mL kg^{-1}. Recordings were left to stabilise for 5 minutes and measurements made thereafter. This dose and stabilisation period has been previously used (Holmes et al., 2018b; Skinner & Marshall, 1996). As with the whole carotid body-nerve preparation, the pharmacology of AOPCP had never been characterised and so a similar approach was used in these initial *in vivo* experiments. Baseline (control) measurements were repeated in the presence of increasing doses of AOPCP including 320µg kg^{-1} and 1120µg kg^{-1} with variables allowed to return to baseline values before the next dose (see Figure 2.14 for summary of the protocol).

At baseline, minute ventilation in N rats was unchanged at any given dose of AOPCP, however in CH, a significant decrease in minute ventilation occurred at 1120μg kg^{-1} (Table 6.1). AOPCP caused a fall in mABP in both N and CH, which was dose-dependent, with the greatest reduction occurring at the highest dose of 1120μg kg^{-1} (Table 6.1). Despite the lower resting mABP in CH, the magnitude of the decrease caused by AOPCP was similar to N, and as such, AOPCP reduced mABP in CH rats to a lower absolute value. AOPCP also caused a dose-dependent decrease in heart rate in N and CH, of similar magnitude (Table 6.1).

	N				CH			
	Control	AOPCP (μg Kg^{-1})		Difference (AOPCP-Control)	Control	AOPCP (μg Kg^{-1})		Difference (AOPCP-Control)
Minute ventilation (mL min^{-1} g^{-1})	0.530 ±0.02	160	0.540 ±0.03	0.010 ±0.02	0.736 ±0.03	160	0.734 ±0.02	-0.002 ±0.02
	0.531 ± 0.01	320	0.549 ±0.02	0.018 ±0.01	0.748 ±0.03	320	0.742 ±0.03	-0.006 ±0.01
	0.525 ± 0.02	1120	0.544 ±0.02	0.019 ±0.01	0.765 ±0.03	1120	0.717** ±0.02	-0.048 ±0.01
mABP (mmHg)	128 ±5	160	113** ±4	-15 ±3	85 ±7	160	81 ±5	-4 ±7
	130 ±4	320	107*** ± 4	-23 ±4	104 ±3	320	79** ±4	-25 #### ±6
	128 ±4	1120	95*** ±5	-33 ## ±5	108 ±3	1120	69*** ±5	-39 ## ±5
Heart rate (beats min^{-1})	444 ±11	160	444 ±11	0 ±4	444 ±13	160	437 ±12	-7 ±5
	435 ±9	320	430 ±10	-5 ±6	452 ±12	320	432* ±12	-19 # ±5
	429 ±8	1120	402** ±11	-27 # ±7	454 ±9	1120	402** ±15	-52 ## ±11

Table 6.1 The effect of pharmacological inhibition of CD73 using incremental doses of AOPCP on cardio-respiratory measurements in normoxic and chronically hypoxic rats

AOPCP was given as a bolus injection at 3 incremental doses 160, 320 and 1120μg kg^{-1} to normoxic (N) and chronically hypoxic (CH) rats. AOPCP's effect on minute ventilation, mean arterial blood pressure (mABP) and heart rate were examined. Data is presented as the mean ± SEM. For N, n=8 rats and for CH, n=7 rats. Paired Student's t-test was used to compare differences between control and AOPCP in both N and CH. *p<0.05, **p<0.01, ***p<0.001, ****p<0.0001 drug vs control. One-way repeated measures ANOVA with Dunnett's post-hoc analysis was used to compare differences between the magnitude of effect caused by AOPCP (AOPCP-Control) between concentrations in N and CH. # p<0.05, ##p<0.01, ###p<0.001, ####p<0.0001 compared to 160μg kg^{-1}.

6.2.5 N and CH animals retain cardio-respiratory responses to severe hypoxia in the presence of a high dose of AOPCP

As AOPCP only reduced ventilation under baseline conditions at a dose of 1120μg kg^{-1} in CH, and the greatest effect on mABP and heart rate occurred at this same dose, to investigate if AOPCP affects the cardiorespiratory responses to acute hypoxia, a 2 minute exposure to severe hypoxia (F_iO_2=8%) was initiated before and after injection with 1120μg kg^{-1} AOPCP. Figure 6.5 shows the cardio-respiratory times courses demonstrating the hypoxic responses in the presence of AOPCP in both N and CH rats. Initial observations revealed consistent and robust responses to hypoxia (Figure 6.5 A-C). As demonstrated previously, CH rats had a depressed rather than augmented HVR and the addition of AOPCP did not blunt this further (Figure 6.6 A). In fact, due to the slight decrease in normoxic ventilation in CH caused by AOPCP, but the same robust hypoxic response, the HVR was slightly improved but still depressed with respect to N rats (Figure 6.6 B). End-tidal CO_2 readings showed a greater change in response to hypoxia in N and this was unaltered in the presence of AOPCP (overall effect: CH $p<0.0001$ and AOPCP $p=0.22$, two-way ANOVA).

A smaller fall in mABP occurred in CH rats compared to N in response to severe hypoxia and this was not exaggerated by the addition of AOPCP. Although the fall in blood pressure was reduced in both N and CH, this was attributed to the substantial fall in baseline mABP caused by AOPCP, as the same minimum blood pressure was achieved with AOPCP (Figure 6.6 C & D). There was no effect of CH or the hypoxic phase on heart rate and this remained consistent in the presence of AOPCP (Figure 6.6 E & F). Taken together, these results show that AOPCP does not prevent the ability

to respond to a single episode of severe hypoxia but does induce important changes in baseline (normoxic) cardiovascular parameters.

Following this, to examine whether the effect of AOPCP was acting in a carotid body specific manner, a proportion of animals underwent CSNX after recovery and wash out of AOPCP. This removed carotid body output that would normally integrate into the brainstem. AOPCP was administered again and hypoxic stimulus repeated (Figure 6.5 D-F). Consistent with previous experiments, these N rats were also unable to mount an appropriate hypoxic response after CSNX and so the effect of AOPCP after CSNX could only be examined during normoxia.

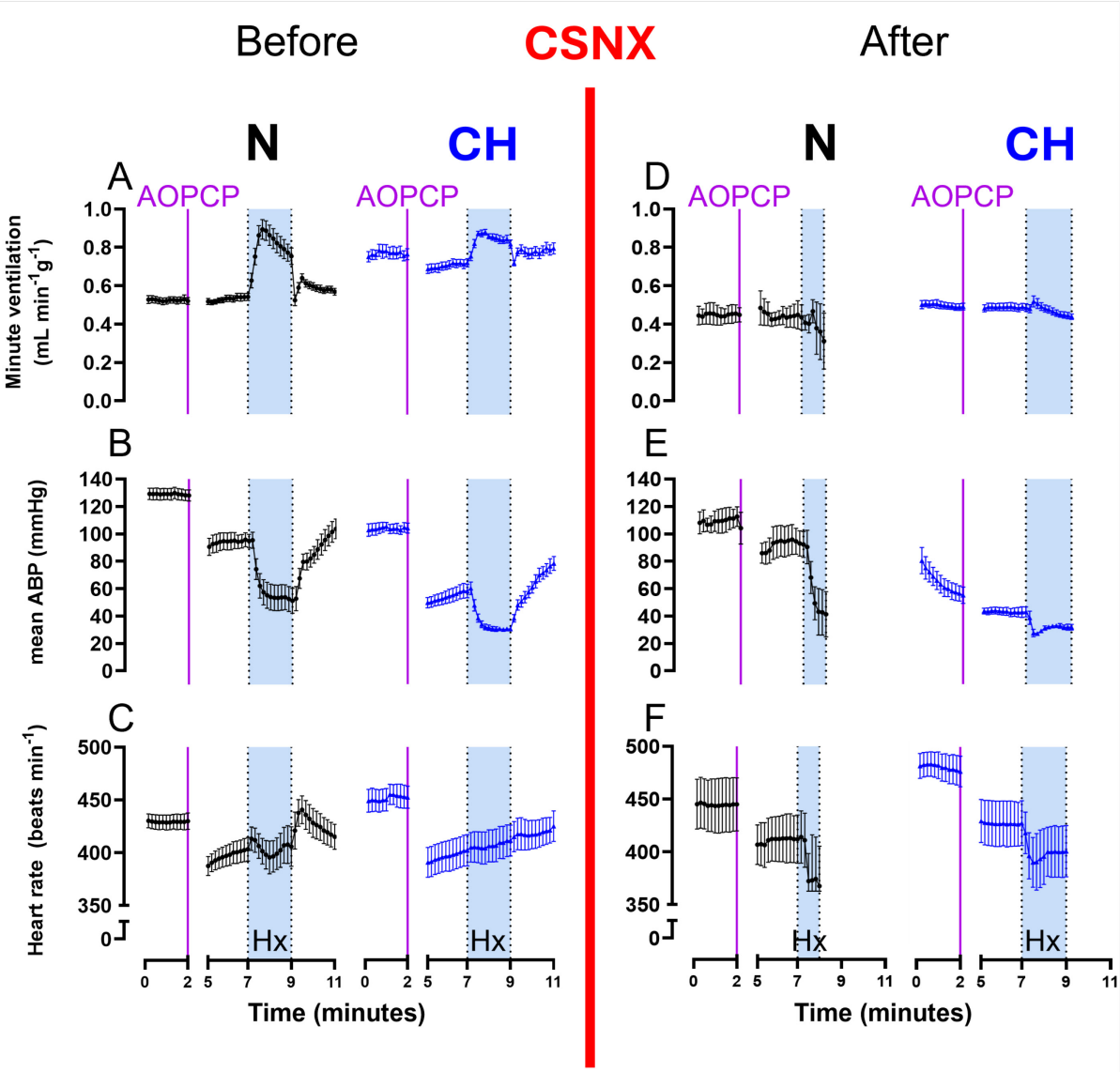

Figure 6.5 Time courses of baseline cardio-respiratory parameters and responses to severe hypoxia in the presence or absence of AOPCP before and after carotid sinus nerve section

Time course showing effect of hypoxia (Hx, F_iO_2=8%) on **(A)** minute ventilation, **(B)** mABP and **(C)** heart rate in the presence of 1120µg Kg^{-1} AOPCP i.v. in normoxic (N) and chronically hypoxic (CH) rats. For N, n=8 and for CH, n=7. In a subset of these animals, time courses were repeated after CSNX (red line) showing the effect of removing carotid body output on the hypoxic response on **(D)** minute ventilation, **(E)** mABP and **(F)** heart rate in the presence of AOPCP. For N, n=4 and for CH, n=6. Data presented as mean ± SEM.

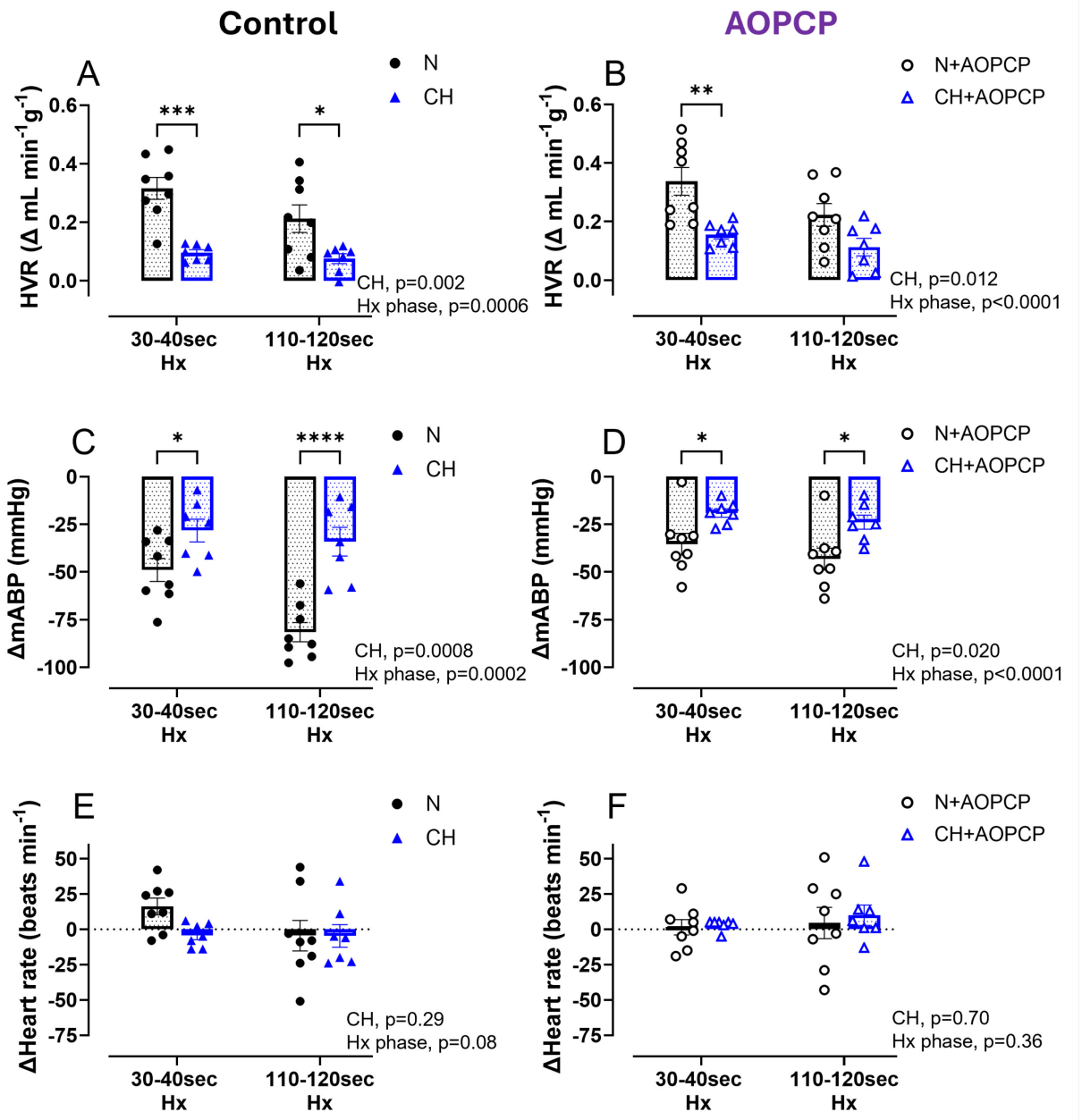

Figure 6.6 AOPCP did not prevent the cardio-respiratory responses to hypoxia in both normoxic and chronically hypoxic rats

Hypoxic ventilatory response (HVR) before **(A)** and after **(B)** AOPCP injection at different time points during hypoxia (Hx = F_iO_2 8%)in normoxic (N) and chronically hypoxic (CH) rats. Hypoxia-induced change in mean arterial blood pressure (mABP) at different time points during hypoxia before **(C)** and after **(D)** AOPCP injection. Hypoxia-induced change in heart rate at different time points during hypoxia before **(E)** and after **(F)** AOPCP injection. Data presented as mean ± SEM with each point representing an individual rat. For N, n=8 rats and for CH, n=7 rats. Significance was assessed using a two-way repeated measures ANOVA with overall p values shown. Bonferroni post-hoc analysis was used to compare differences within groups. *p<0.05, **p<0.01, ***p<0.001 and ****p<0.0001 compared to N.

6.2.6 The effect of AOPCP in the absence of carotid body sensory output

To examine whether the effects of AOPCP are acting via the carotid body, a proportion of animals underwent CSNX to remove carotid body output. Once variables achieved a steady-state, 1120μg Kg^{-1} AOPCP was administered again, and was exposed to an acute severe hypoxic stimulus for 2 minutes. Figure 6.5 shows the time-courses for minute ventilation, mABP and heart rate in the presence of AOPCP before and after CSNX.

As shown in Table 6.1, 1120 μg Kg^{-1} AOPCP caused a significant decrease in minute ventilation in CH but not N animals. However, this did not fully reverse ventilation down to levels consistent with N and remained considerably higher (Figure 6.7 A). After CSNX, ventilation significantly decreased to a comparable level between N and CH (Figure 6.7 B). The addition of AOPCP after CSNX, had no further impact on ventilation suggesting that the decrease in ventilation in CH was carotid body dependent (Figure 6.7 C). CH animals showed excessive hyperventilation compared to N at baseline as evidenced by a significantly lower end-tidal CO_2. This was still apparent after AOPCP although slightly less marked (Figure 6.8 A). This appears mainly due to AOPCP reducing end-tidal CO_2 in N whilst producing only a very small increase in CH (Figure 6.8 A & C). Following CSNX, end-tidal CO_2 remained significantly lower in CH compared to N, suggesting that a component of the baseline hyperventilation in CH is independent of the carotid body (Figure 6.8 B). Again, this difference became less marked after AOPCP due to a trend towards a decrease in end-tidal CO_2 in N but not CH (Figure 6.8 B & C).

mABP fell in response to AOPCP in both N and CH and the absolute magnitude of the fall was comparable between groups (Figure 6.9 A & C). CSNX caused resting mABP to decrease, with CH still having a significantly lower absolute mABP (Figure 6.9 B). The addition of AOPCP after CSNX, caused much smaller decrease in mABP in both N and CH indicating that approximately 50-60% of the fall in mABP observed by AOPCP is acting in a carotid body specific manner (Figure 6.9 C). AOPCP decreased heart rate in both groups. Following CSNX, AOPCP still caused a drop in heart rate by a similar magnitude indicating the changes observed with AOPCP on heart rate are acting independently of the carotid body (Figure 6.10 A-C). AOPCP produced a larger decrease in heart rate in CH irrespective of CSNX (Figure 6.10 C).

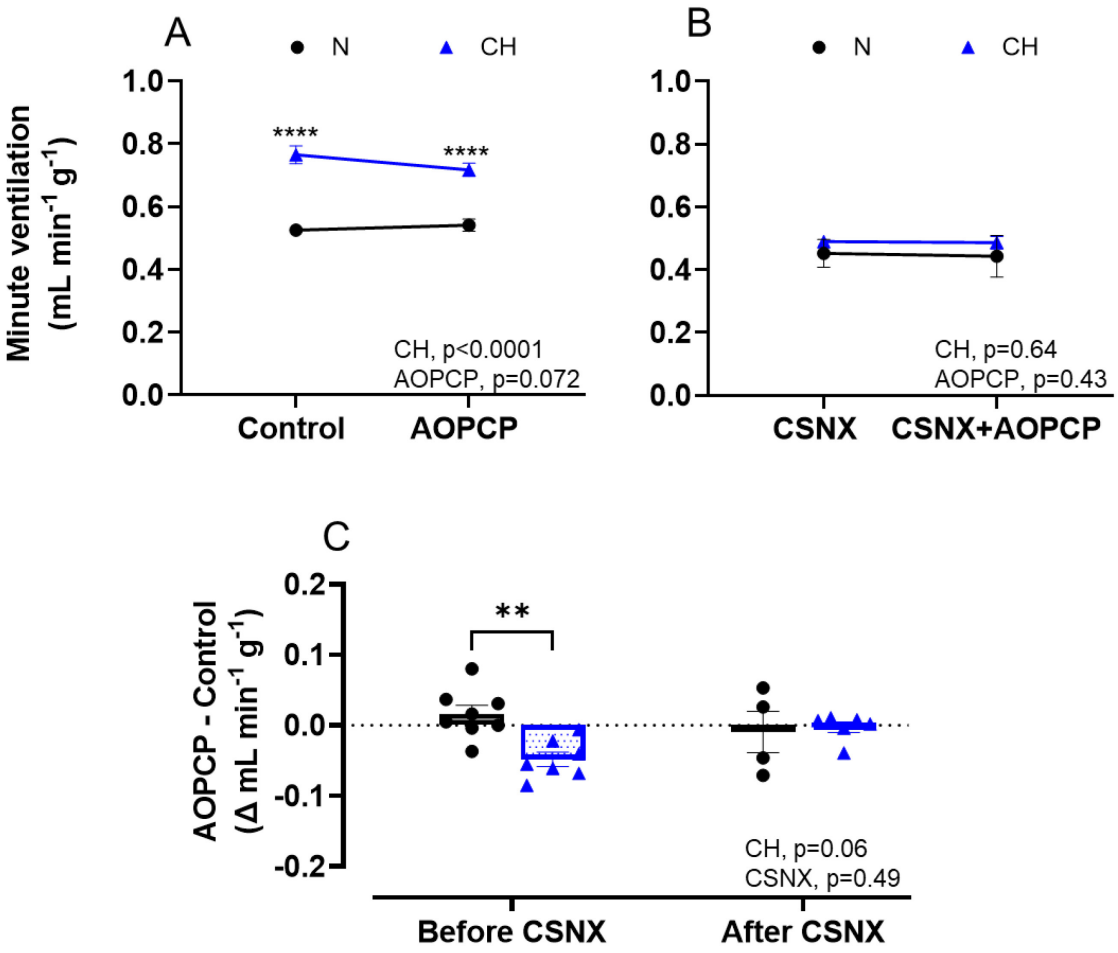

Figure 6.7 The effect of pharmacological inhibition of CD73 using AOPCP on minute ventilation before and after carotid sinus nerve section in normoxic and chronically hypoxic rats

The effect of 1120µg Kg^{-1} AOPCP (CD73 inhibitor) on minute ventilation before **(A)** and after **(B)** CSNX, in normoxic (N) and chronically hypoxic (CH) rats. **(C)** The change in minute ventilation caused by AOPCP before and after CSNX, in N and CH rats. Data presented as mean ±SEM with each data point representing an individual rat. Before CSNX, for N, n=8 rats and for CH, n=7 rats. The number of rats that underwent CSNX from this group were, for N, n=4 rats and for CH, n=6 rats. Statistical significance was assessed using a two-way repeated measures ANOVA in A & B with overall p values shown. An ordinary two-way ANOVA was performed in C, with overall p values shown. Bonferroni post-hoc analysis was used to compare within groups. **p<0.01, ****p<0.0001 compared to N.

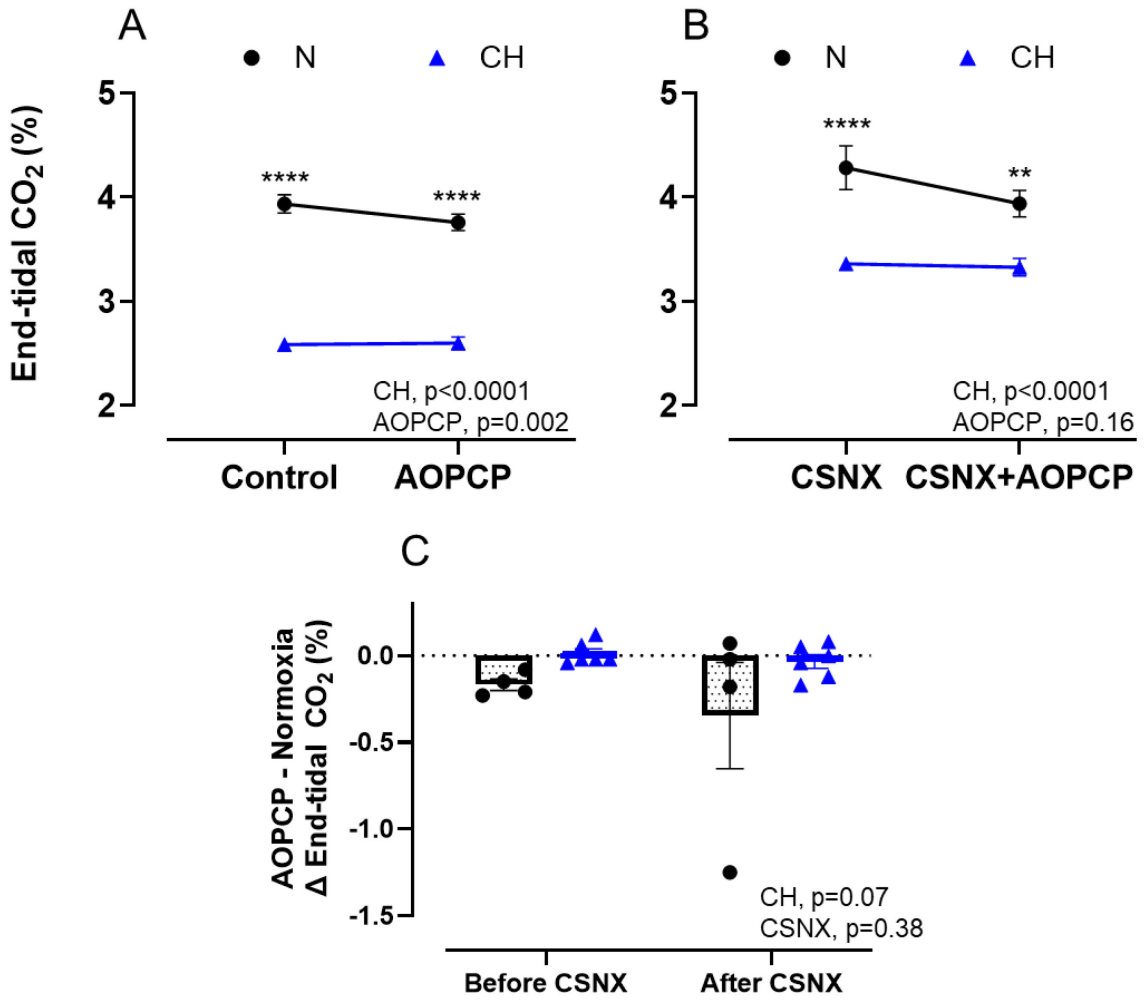

Figure 6.8 The effect of pharmacological inhibition of CD73 using AOPCP on end-tidal CO_2 before and after carotid sinus nerve section in normoxic and chronically hypoxia rats

The effect of 1120µg Kg^{-1} AOPCP on end-tidal CO_2 before **(A)** and after **(B)** CSNX in normoxic (N) and chronically hypoxic (CH) rats. **(C)** Changes in end-tidal CO_2 induced by AOPCP before and after CSNX, in N and CH rats. Data presented as mean ±SEM with each data point representing an individual rat. End-tidal readings were from N, n=4 rats and CH, n=6 rats before and after CSNX. Statistical significance was assessed using a two-way repeated measures ANOVA in A & B with overall p values shown. An ordinary two-way ANOVA was performed in C, with overall p values shown. Bonferroni post-hoc analysis was used to compare within groups. **p<0.01, ****p<0.0001 compared to N.

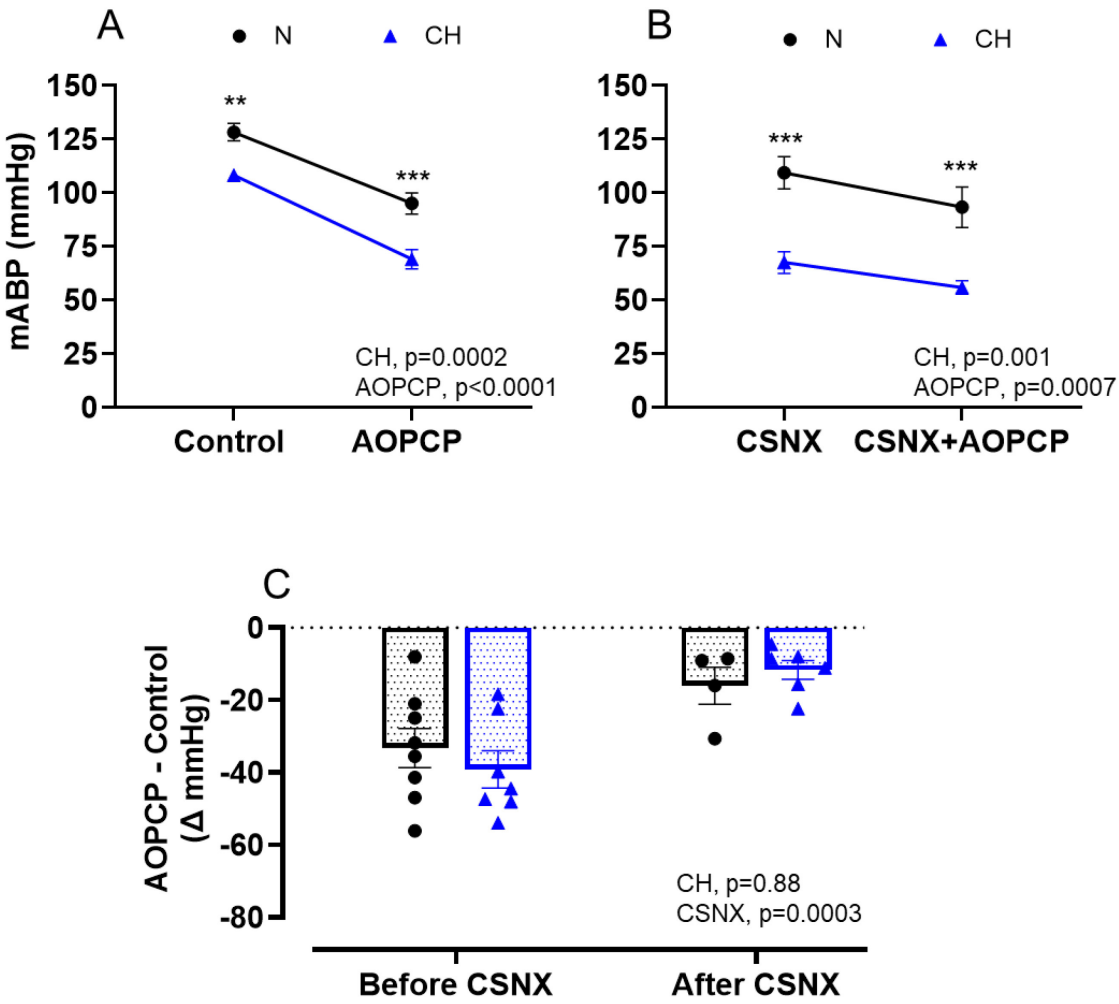

Figure 6.9 The effect of pharmacological inhibition of CD73 using AOPCP on blood pressure before and after carotid sinus nerve section in normoxic and chronically hypoxic rats

The effect of 1120µg Kg^{-1} AOPCP (CD73 inhibitor) on mean arterial blood pressure (mABP) before **(A)** and after **(B)** CSNX, in normoxic (N) and chronically hypoxic (CH) rats. **(C)** The change in mABP caused by AOPCP before and after CSNX, in N and CH rats. Data presented as mean ±SEM with each data point representing an individual rat. Before CSNX, for N, n=8 rats and for CH, n=7 rats. The number of rats that underwent CSNX from this group were, for N, n=4 rats and for CH, n=6 rats. Statistical significance was assessed using a two-way repeated measures ANOVA in A & B with overall p values shown. An ordinary two-way ANOVA was performed in C, with overall p values shown. Bonferroni post-hoc analysis was used to compare within groups**p<0.01, ***P<0.001 compared to N.

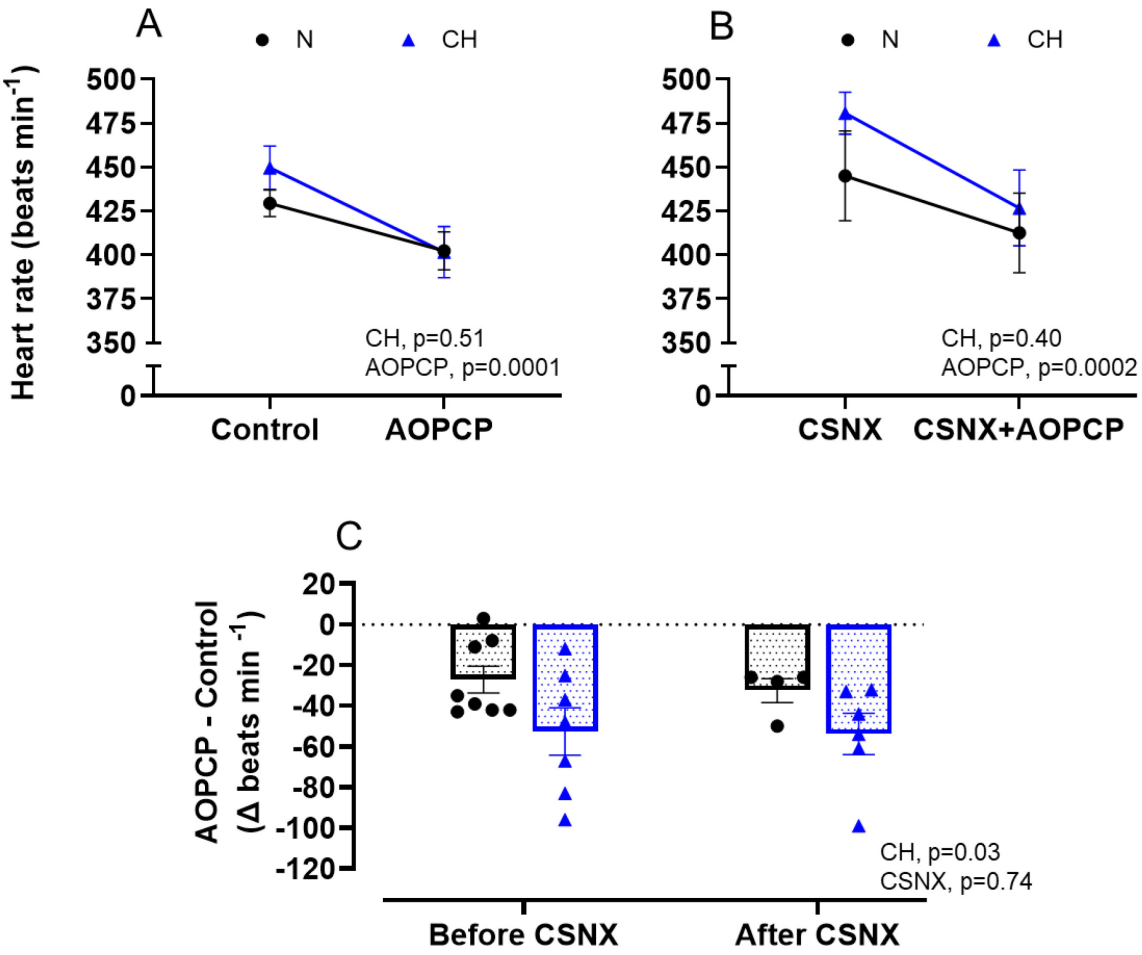

Figure 6.10 The effect of pharmacological inhibition of CD73 using AOPCP on heart rate before and after carotid sinus nerve section in normoxic and chronically hypoxic rats

The effect of 1120μg Kg^{-1} AOPCP (CD73 inhibitor) on heart rate before **(A)** and after **(B)** CSNX, in normoxic (N) and chronically hypoxic (CH) rats. **(C)** The change in heart rate caused by AOPCP before and after CSNX, in N and CH rats. Data presented as mean ±SEM with each data point representing an individual rat. Before CSNX, for N, n=8 rats and for CH, n=7 rats. The number of rats that underwent CSNX from this group were, for N, n=4 rats and for CH, n=6 rats. Statistical significance was assessed using a two-way repeated measures ANOVA in A & B with overall p values shown. An ordinary two-way ANOVA was performed in C, with overall p values shown. Bonferroni post-hoc analysis was used to compare within groups.

6.3 Discussion

6.3.1 Summary of key chapter findings

- CH caused an elevation in basal minute ventilation, a lower resting mABP and did not alter heart rate compared to N

- CSNX caused a greater fall in baseline minute ventilation in CH rats suggesting a stronger contribution of the carotid body to establishing ventilation in CH animals

- CSNX caused a comparable decrease in mABP in both N and CH suggesting that the carotid body has an important role in blood pressure regulation in N and CH animals

- Heart rate was unaffected by CSNX in N and CH

- Pharmacological antagonism of CD73 with AOPCP caused a significant drop in minute ventilation in CH but not N, an action dependent on the carotid body

- AOPCP caused a marked decrease in mABP both N and CH, an effect mainly due to its inhibition of the carotid body

- AOPCP decreased heart rate in a dose-dependent manner in N and CH, independent of the carotid body

- Cardiovascular respiratory responses to acute severe hypoxia were preserved in the presence of AOPCP in both N and CH

6.3.2 Cardio-respiratory differences between N and CH

In this CH model under general anaesthesia, CH rats showed a significantly higher basal minute ventilation, consistent with previous findings in awake, unrestrained rats in Chapter 3. Their end-tidal CO_2 readings were lower, indicating a more pronounced hyperventilation. This increased resting ventilation, known as VAH, helps maintain P_aO_2 despite lower oxygen availability, which is common in other rodent models of CH (Aaron & Powell, 1993; Thomas & Marshall, 1997; Walsh & Marshall, 2006). In previous studies, VAH also increases sensitivity to hypoxia leading to an augmented HVR (Aaron & Powell, 1993; Bishop et al., 2013; Cheng et al., 2020; Hodson et al., 2016). However, despite CH rats significantly increasing ventilation compared to N at both baseline and during hypoxia, their HVR was blunted. The exact cause is unclear, but it may depend on factors like animal strain, hypoxic intensity and hypoxic duration (Arias-Reyes et al., 2021; Pamenter & Powell, 2016). One possible explanation is the hypocapnia observed in CH, both at baseline and during hypoxia, where it decreases further. Studies suggest that an enhanced HVR in CH animals can only be observed if P_aCO_2 is elevated and maintained at a constant level during hypoxia (isocapnic hypoxia) (Aaron & Powell, 1993).

It is also worth noting here that since baseline measurements in CH were taken in 12% F_iO_2, the decrease to 8% is substantially lower than the decrease from 21% to 8% in the N animals. Normalising the rise in ventilation to the decrease in P_aO_2 or SpO_2 may be needed for a more definitive answer (Marshall & Davies, 1999; Walsh & Marshall, 2006). In addition, since the haematocrit and thus O_2 capacity is elevated in CH (Table 3.1 in Chapter 3), this is likely to increase O_2 delivery to the carotid body during the acute hypoxic episode in CH relative to N. As such the stimulus intensity may well have

been lower in the CH animal in this *in vivo* setting, masking an increase in carotid body and whole body O_2 reflex sensitivity. Although the carotid body is said to respond to P_aO_2 rather than content, the actual stimulus is accepted as the tissue/cellular PO_2. Specific measurements of carotid body tissue PO_2 during hypoxia are therefore needed for clarification.

Despite showing enhanced tonic chemoafferent activity (Chapter 5), which would usually increase vasoconstrictor reflexes, CH rats had significantly lower mABP compared to controls. Carotid body activation typically boosts sympathetic drive, and this is modulated by the brainstem, where complex neuronal interactions influence sympathetic output through the nucleus tractus solitarius (NTS) and the rostral ventrolateral medulla (RVLM) (Taylor et al., 1999; Zera et al., 2019). Heart rate did not differ between N and CH rats, which was surprising given the increased basal ventilation. Hypoxia-induced hyperventilation usually increases respiratory drive and inhibits vagal activity, suggesting a complex interaction between autonomic regulation and the direct effects of hypoxia on the heart, possibly through adenosine on the sinoatrial node (Marshall, 1998). The combination of a lower mABP and unchanged heart rate suggests reduced total peripheral resistance. This points to the dominance of local dilatory effects of hypoxia, likely mediated by adenosine, prostaglandins and nitric oxide (Ray et al., 2002). This is consistent with other studies showing comparable resting mABP in rats exposed to a similar duration of CH (Walsh & Marshall, 2006). As described in Chapter 3, increased O_2 content from haematological changes may reduce sensitivity to local dilators, possibly overcoming sympatholysis after more prolonged periods of CH.

Interestingly, 3-4 weeks of 12% F_iO_2 exposure was required to achieve comparable resting blood pressures between N and CH rats (Thomas & Marshall, 1997). Despite this longer hypoxic exposure, CH rats did not develop hypertension, however this does not necessarily mean sympathetic outflow is not elevated. Indeed, humans exposed to 4 weeks of high altitude and patients with COPD display significant increases in muscle sympathetic nerve activity (MSNA) (Hansen & Sander, 2003; Heindl et al., 2001). Future studies could therefore aim to directly measure RVLM electrical activity *in vivo* or employ microneurography to measure MSNA. Nevertheless, the fact that even longer hypoxic exposures do not display a hypertensive phenotype, suggests that the current model doesn't fully replicate the cardiovascular phenotype of COPD. Future studies are urgently needed to refine the CH model to better represent the cardiovascular changes seen in COPD patients.

6.3.3 A role for the carotid body in mediating cardio-respiratory changes caused by CH

To determine the tonic role of the carotid body in regulating ventilation, blood pressure and heart rate, carotid body chemoafferent output was removed through CSNX. Under the conditions of this study, CSNX in N rats caused a decrease in both ventilation and blood pressure but had no effect on heart rate. The reduction in normoxic ventilation after CSNX has been previously observed in multiple rat strains (Bin-Jaliah et al., 2004; Mouradian et al., 2012), supporting the idea that the carotid body plays a crucial role in normoxic breathing, similar to humans.

A striking finding was that the carotid body is essential for an appropriate hypoxic response. N rats subjected to hypoxia could not survive beyond 30-50 seconds of

exposure. This contrasts with other studies where CSNX rats, while not increasing ventilation during hypoxia, were able to survive the full exposure (Abdala et al., 2012; Angelova et al., 2015; McBryde et al., 2013; Mouradian et al., 2012). These differences may arise from methodological variations between these studies and the current one. In those studies, CSNX was performed, and recovery occurred post-surgery, with denervation confirmed in awake, unanaesthetised animals days or weeks later. Central compensatory mechanisms may have played a role in preventing a severe drop in ventilation during hypoxia. Furthermore, those studies used milder hypoxia (F_iO_2 = 10%) compared to the more severe hypoxia (F_iO_2 = 8%) in this chapter. Some also used sodium cyanide as a hypoxia proxy, which strongly stimulates carotid body activity (Abdala et al., 2012; McBryde et al., 2013), without causing the depressive effect of hypoxia on the brain, which may contribute to the observed ventilation failure in this chapter.

In addition to the lack of peripheral chemoreceptor activation and central depression during hypoxia in CSNX N rats, it is important to consider that the anaesthetic used in this study may have caused additional central respiratory depression. Interestingly, HVRs measured in this study were slightly lower than those observed in awake, unanaesthetised rats (Chapter 3), in both N and CH. However, basal minute ventilation was similar to that in their unanaesthetised counterparts, suggesting a complex interaction of the anaesthetic in the brainstem thus effecting the response to hypoxia.

The role of the carotid body in regulating resting blood pressure is less well established. Under anaesthesia, CSNX in N rats caused a 20-40 mmHg decrease in blood pressure. However, studies with the same strain of rats (Wistar) used in this thesis

found no change in blood pressure 3-4 weeks after CSNX (Abdala et al., 2012). This might reflect longer-term effects, as minute ventilation has been shown to return to baseline levels within 10 days after CSNX (Mouradian et al., 2012). Thus, it is plausible that blood pressure initially drops after CSNX but later returns to normal, possibly driven by compensatory mechanisms independent of the carotid body.

Earlier studies have shown that CSNX rats do not acclimate well to CH (Olson et al., 1988), but none had examined the effects of acute CSNX on ventilation, blood pressure and heart rate in rats exposed to CH until this thesis. The current findings show, for the first time, that in this CH model, acute CSNX caused a decrease in minute ventilation and blood pressure, with no effect on heart rate. Notably, the reduction in ventilation was more pronounced in CH rats than in N rats, suggesting that the elevated baseline ventilation in CH is driven by the carotid body. This supports the hypothesis that peripheral chemoreceptors contribute to the physiological adaptation to CH (Powell, 2007). However, the persistence of hyperventilation even after CSNX suggests that part of the increased respiratory drive is independent of the carotid body and likely results from central adaptations (Pamenter & Powell, 2016; Wilkinson et al., 2010).

6.3.4 A role for pharmacological antagonism of CD73 in mediating carotid body induced changes in cardio-respiratory function

Chapter 5 highlighted the importance of CD73 in establishing basal chemoafferent activity and sensitivity to hypoxia. The second part of this chapter investigated the potential of targeting CD73 *in vivo*, using rats exposed an F_iO_2 of 12% for 10 days. Only the highest dose of AOPCP led to a small but significant reduction in normoxic ventilation in CH rats, and this effect was dependent on the carotid body. However, the

reduction in ventilation caused by AOPCP was smaller than that achieved by CSNX alone. This could be explained by AOPCP not producing full inhibition of the basal carotid body chemoafferent activity, or alternatively that non-selective actions of AOPCP may counter the inhibition of carotid body activity.

A noteworthy finding was that AOPCP reduced blood pressure by approximately 30-50 mmHg in both N and CH rats, with about 50-60% of this effect being carotid body dependent. Thus, decreasing CD73 activity within the carotid body has a marked effect on lowering blood pressure in both N and CH animals. The exaggerated fall in arterial blood pressure compared to ventilation implies that inhibiting CD73 in the carotid body through AOPCP has a stronger impact on lowering blood pressure than on ventilation. Alternatively, since AOPCP can cross the blood-brain barrier, its effects peripherally, including the on the carotid body, could be masked or accentuated by central mechanisms. For example, adenosine inhibits respiratory centres in the medulla, so AOPCP's reduction of adenosine could increase ventilation (Eldridge & Millhorn, 1987; Herlenius et al., 1997). This has been suggested as a potential reason for the observed increase in ventilation in a previous study administering AOPCP (Holmes et al., 2018b). Indeed, in this chapter, AOPCP decreased the end-tidal PCO_2 in N but not CH animals, again pointing towards it causing a slight baseline hyperventilation in N. The absence of this effect in the CH animals suggests either a stronger inhibitory influence on the carotid body and the drive to breath (as the data suggests) and/or that carotid body independent (likely central) actions of AOPCP on breathing are blunted in CH. The difference in the drug's effects under normoxia is not fully understood, and measuring AOPCP concentrations in the blood might provide insights into the amount of drug reaching the carotid body. Potential differences in drug formulations over the years

might have also impacted its metabolism and efficacy further contributing to differences between studies.

The blood pressure reduction caused by AOPCP, independent of the carotid body, is intriguing, but the exact mechanism remains unclear. Since AOPCP crosses the blood-brain barrier, it's possible that its residual effect on blood pressure is mediated centrally. Microinjections of adenosine into the RVLM can increase blood pressure, particularly when injected rostrally, although tonic adenosine does not seem to play a role in activating the RVLM (Thomas & Spyer, 1996). However, when stimulating areas of the hypothalamus involved in defence responses, blood pressure increases can be reduced by inhibiting CD73 in the NTS or blocking adenosine receptors in the RVLM (Dale et al., 2002; Thomas & Spyer, 1996). Interestingly, N control animals in this study showed higher resting blood pressure than unanaesthetised rats, suggesting that the anaesthetic used may have increased tonic activity in the NTS or RVLM. This could have made anaesthetised rats more sensitive to CD73 inhibition due to increased ATP release and its breakdown into adenosine.

6.4 Conclusion

The carotid body plays a crucial role in regulating both resting minute ventilation and blood pressure. Removing carotid body sensory output reverses the CH-induced increase in resting minute ventilation and lowers blood pressure. This highlights the carotid body as a potential target for treating CH-related conditions like COPD. However, the carotid body is also essential for an appropriate response to hypoxia, suggesting that pharmacologically targeting it could help fine-tune its activity. The data points to CD73 as a promising candidate for this purpose. Blockade of CD73 *in vivo*

using AOPCP reduced blood pressure in CH, mainly through the carotid body, and caused a small decrease in ventilation, without abolishing the ability to respond to hypoxia. These exciting findings support the idea that targeting CD73 in the carotid body to alleviate hyperactivity could be an effective therapeutic approach to decreasing blood pressure, though more research is needed on hypertensive and COPD animal models and patients.

CHAPTER 7

7. Overall discussion

7.1 Summary of main findings

Chapter 3 characterised a CH model in Wistar rats exposed to an F_iO_2 of 12% for 10 days, validating sufficient carotid body and systemic adaptations to investigate CD73-mediated hyperactivity. CH rats exhibited increased haematocrit and right ventricular hypertrophy, reflecting an appropriate physiological response to prolonged hypoxia. They also developed carotid body-specific adaptations, including elevated basal chemoafferent discharge and an enhanced hypoxic response *ex vivo*, but maintained a comparable HVR *in vivo*. However, CH rats had higher resting minute ventilation when breathing both 21% and 12% F_iO_2. Despite increased carotid body activity in electrophysiological recordings, no changes were observed in the morphology of the carotid body including section area, volume or vascularity. A trend toward a greater number of TH^+ cells suggested a higher TH^+ cell density in CH carotid bodies.

Chapter 4 examined the distribution of CD73 protein expression in carotid body sections from N and CH rats. A novel machine-learning approach to remove RBC AF was developed and validated. Initial experiments optimised staining conditions to improve signal to noise ratios. Detection of the $CD73^+$ signal in TH^+ type I cells was enhanced using heat-mediated antigen retrieval. Most TH^+ cells co-expressed CD73 ($CD73^+TH^+$), while some $CD73^+$ cells lacked TH ($CD73^+TH^-$). CH increased the proportion of $CD73^+TH^+$ cells. CD73 protein expression was also detected in some blood vessels ($CD31^+$) but not nerve endings (NF^+) and this was consistent in both N and CH carotid bodies.

Chapter 5 aimed to determine the functional importance of CD73 in driving heightened basal chemoafferent activity and increased hypoxic sensitivity induced by CH. Using an intact carotid body-nerve preparation, chemoafferent activity was measured in normoxia and in response to graded hypoxia in the presence and absence of a commonly used CD73 inhibitor (AOPCP). AOPCP alleviated basal chemoafferent hyperactivity in CH and reversed the augmented hypoxic sensitivity, i.e. AOPCP normalised the PO_2 required to elicit a hypoxic response. A tmAC inhibitor (SQ22536) produced similar effects, indicating cAMP as a key mediator of CH-induced chemoafferent hyperactivity. Both agents also decreased carotid body chemoafferent hypercapnic sensitivity, by a similar degree in N and CH. This presents CD73 and tmAC as potential therapeutic targets for reversing carotid body hyperactivity in CH. Whether antagonism of CD73 with AOPCP *in vivo* could reverse the augmented ventilation and reduce blood pressure in CH animals was examined in the final results chapter.

Chapter 6 explored the carotid body's role in mediating cardio-respiratory differences between N and CH. Ventilation, blood pressure and heart rate were measured in anesthetised rats before and after CSNX. CSNX reduced ventilation and blood pressure but had no effect on heart rate. CD73 antagonism with AOPCP lowered blood pressure and heart rate in both N and CH, but only decreased ventilation in CH. The impact of AOPCP on lowering blood pressure and ventilation in CH animals was carotid body dependent. *In vivo* hypoxic responses were preserved in the presence of AOPCP, making it a promising strategy for lowering baseline cardiorespiratory parameters without abolishing the ability to respond to hypoxia- an important goal in developing carotid body-targeted treatments for CH-related conditions like COPD. A schematic illustration of the main findings are shown in Figure 7.1

7.2 Carotid body plasticity in CH: a role for CD73, adenosine and cAMP

The ability of an organ or system to adapt to prolonged stress is a crucial characteristic of plasticity. The carotid body functions as a polymodal receptor, responding to stressors like hypoxia (Kumar & Bin-Jaliah, 2007). During CH, molecular and cellular changes enhance its basal activity and sensitivity to acute hypoxia, facilitating cardio-respiratory adaptations that improve arterial oxygen delivery to vital tissues. This thesis highlights the critical role of CD73 in driving basal carotid body hyperactivity and increasing its hypoxic sensitivity *ex vivo*. Notably, inhibiting CD73 *ex vivo* significantly reduced baseline chemoafferent activity and normalised O_2 sensitivity in CH, strongly suggesting that CD73 is a key regulator of carotid body hyperactivity.

Many adaptive responses to CH are mediated by the transcription factor HIF. Under hypoxia, HIF-α subunits evade degradation, dimerize with HIF-1β, and activate gene transcription to enhance hypoxic adaptation (Bishop & Ratcliffe, 2015). One such adaptation is carotid body hypertrophy, resulting from cellular and vascular expansion. In this CH model, no gross morphological changes were observed, but an increased density of TH^+ cells was detected. This expansion of TH^+ cells led to a trend toward an increased pool of $CD73^+TH^+$ cells (Chapter 4). Functionally, this could contribute to greater adenosine production via CD73 which, in turn, may promote greater excitability and render type I cells more sensitive to CD73 inhibition. Evidence suggests that HIF-2α mediates type I cell expansion via endothelin-1, and vascularisation through VEGF release from type I cells (Bishop & Ratcliffe, 2025; Chen et al., 2007; Fielding et al., 2018; Hodson et al., 2016). However, even when carotid body growth and type I cell proliferation are inhibited, chemoafferent discharge remains elevated in CH, indicating the involvement of additional mechanisms (Chen et al., 2007).

Proteins along the adenosine signalling pathway, including CD73 and A_2 receptors, are transcriptionally regulated by HIF in carotid body-like cells and other tissues (Brown et al., 2011; Kobayashi et al., 2000a; Kong et al., 2006; Synnestvedt et al., 2002). While direct protein level measurements in the carotid body after CH are needed, mRNA data suggests CD73 upregulation (Salman et al., 2017). A key question remains: how does CD73 activity and adenosine signalling induce plastic changes that enhance carotid body excitability? As discussed in Chapter 5, adenosine activates A_2 receptors either post-synaptically on afferent terminals or pre-synaptically on oxygen-sensitive type I cells. The latter suggests a positive-feedback mechanism, where adenosine enhances type I cell excitability. Interestingly, the data presented in this thesis demonstrates that chemoafferent response to adenosine *per se* remains unaffected by CH, despite the basal activity being highly sensitive to CD73 inhibition. Thus, it is proposed that there is a higher basal level of adenosine derived from CD73 accounting for the rise in chemoafferent activity in CH rather than an increase in adenosine sensitivity.

Adenosine receptor stimulation activates tmACs, generating cAMP, which in turn activates effector proteins like PKA or EPAC (Nunes et al., 2014). These proteins influence membrane depolarisation, calcium influx and neurotransmitter release, thereby modulating type I cell excitability and hypoxic responses (Pulgar-Sepúlveda et al., 2018). Recently, it has been reported that cAMP can elevate carotid body hypoxic sensitivity via activation of CNG ion channels (Peng et al., 2023). A rise in cAMP leading to more persistent stimulation of these CNG ion channels is proposed to be causative of carotid body hyperactivity in response to chronic intermittent hypoxia (Peng et al., 2025). Whether CD73 signalling also converges on these channels (and is enhanced in CH) needs to be explored further. Interestingly, although tmAC did reduce chemoafferent activity in the CH carotid body, its actions appear to be less

marked than that of AOPCP. Thus, it is possible that some signalling related to CD73 is unrelated to cAMP- the identify of which warrants future investigation. A summary of the key adaptations to this CH model and the link to potential downstream targets of enhanced CD73 activity and adenosine receptor activation are shown in Figure 7.1.

These cellular and molecular adaptations drive increased carotid body output, integrating into the brainstem to enhance cardio-respiratory reflexes and compensate for low oxygen availability. A progressive rise in baseline ventilation, known as VAH, is crucial for adjusting to high-altitude environments and preventing acute mountain sickness and pulmonary oedema (Kumar & Prabhakar, 2012). Rodent models show that carotid body hypertrophy and vascularisation are reversible after eight weeks of normoxia, demonstrating its plasticity (Kusakabe et al., 2004). Investigating whether cellular adaptations and chemoafferent activity also revert to pre-CH levels remains an interesting future direction. Clinically, patients with chronic respiratory diseases like COPD often experience persistent hypoxemia, sustaining carotid body activation and increasing sympathetic vasoconstriction, which can worsen hypertension. Understanding CD73-driven mechanisms of CH-induced hyperactivity may provide new therapeutic targets, with CD73/tmACs emerging as promising candidates.

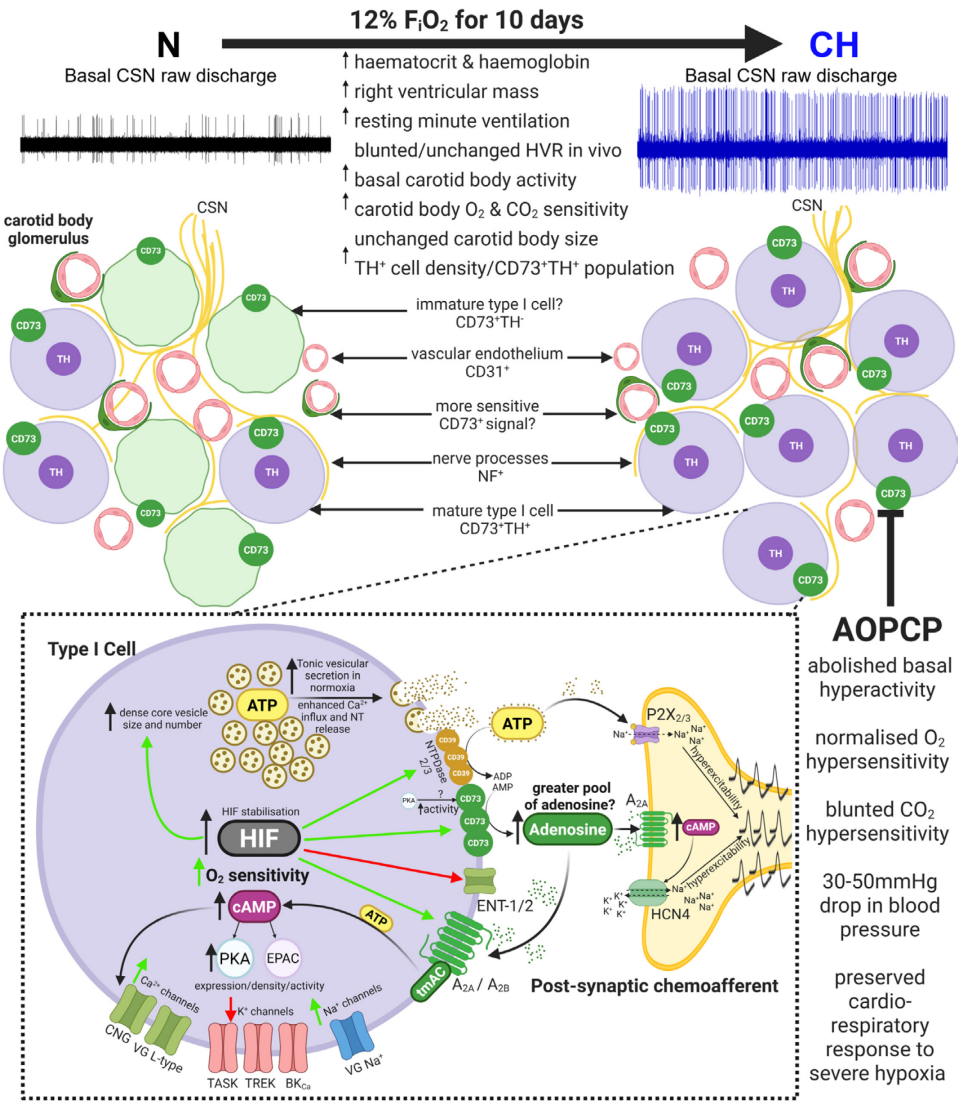

Figure 7.1 Summary of carotid body adaptations to chronic hypoxia highlighting key findings and potential downstream mechanisms of enhanced adenosine production

Schematic illustrating carotid body adaptations and cellular mechanisms following chronic hypoxia (CH; 12% F_iO_2 for 10 days). Key physiological adaptations are indicated, with representative carotid sinus nerve (CSN) activity recordings from normoxic (N, top left) and CH conditions (top right). The enlarged inset (dashed box) details type I cell signalling pathways, highlighting hypoxia-inducible factor (HIF) stabilisation and enhanced CD73 activity as central mediators of carotid body hyperactivity. Green arrows indicate positive regulation (e.g. increased expression), while red arrows indicate negative regulation. Mechanisms include enhanced tonic and hypoxia-induced ATP release, increased CD39 (NTPDase) expression and elevated CD73 expression/activity shifting to enhanced adenosine production. This greater pool of adenosine activates A_{2A}/A_{2B} receptors thus induces an elevation in cAMP which can activate protein kinase A (PKA) and/or exchange proteins activated by cAMP (EPAC), resulting in downstream modifications of ion channels through HIF-dependent transcriptional changes, post-translational modifications by PKA or direct cAMP actions. The key effects of CD73 inhibition with AOPCP are shown in the bottom right panel. Abbreviations: large-conductance calcium-activated K^+ channel (BK_{Ca}), cyclic nucleotide-gated (CNG), hyperpolarisation-activated cyclic nucleotide-gated (HCN4), hypoxic ventilatory response (HVR), TWIK-related acid-sensitive K^+ channel (TASK), TWIK-related K^+ channel (TREK) & voltage-gated (VG). Figure created using BioRender.com.

7.3 CD73 as a novel pharmacological target for the treatment of CH-related illnesses such as COPD

COPD is a progressive respiratory disorder caused by alveolar damage in the lungs. In addition to respiratory complications, COPD patients frequently develop cardiovascular abnormalities, including hypertension and arrhythmias, which are the leading causes of hospitalisations and mortality in this population (Donaldson et al., 2010; Morgan et al., 2018; Rabe et al., 2018). As the disease progresses over many years, declining arterial oxygen levels lead to a state of CH. While CH-induced carotid body activation helps sustain breathing and increase arterial oxygen (particularly in the early stages of the disease), persistent activation also elevates sympathetic drive to the vasculature (and possibly the heart), contributing to hypertension- an important risk factor for cardiovascular disease progression (Iturriaga et al., 2021).

In this CH model, rats exhibit resting hyperventilation, similar to mild-to-moderate COPD patients (Phillips et al., 2018; Stickland et al., 2016). However, it is important to note that this model represents only one aspect of COPD. COPD is a multifactorial disease influenced by systemic inflammation, often triggered by prolonged exposure to noxious chemicals from smoking and, more recently, poor air quality. Additionally, many COPD patients have co-morbidities such as obesity, which further exacerbate metabolic and respiratory dysfunction (Agusti & Soriano, 2008; Mannino & Buist, 2007). More severe COPD cases often exhibit lung hyperinflation and increased respiratory effort, leading to respiratory muscle fatigue and hypercapnia (Gagnon et al., 2014; O'Donnell & Laveneziana, 2006). Furthermore, HIF stabilisation in COPD may not solely be due to hypoxia but could be caused (or exacerbated) by iron deficiency, which has been shown to be highly prevalent in COPD patients and is

correlated with more frequent exacerbations and poorer exercise tolerance. Chronic inflammation in COPD patients has been suggested to drive hepcidin expression that leads to sequestering of iron (Nickol et al., 2015). Iron is an essential co-factor for PHD activity, thus a reduction in iron could further inhibit PHDs and cause a greater concurrent elevation of HIF. Interestingly, in a small pre-clinical human study, a single bolus injection of ferric carboxymaltose did not improve oxygenation but did improve exercise tolerance and dyspnoea scores (Santer et al., 2020). Future models should aim to replicate the full spectrum of COPD severity, from mild to advanced stages.

Oxygen supplementation is a common treatment for COPD patients that display poor respiratory function, P_aO_2<60mmHg, S_aO lower than 92% and are not majorly hypercapnic at rest (NICE, 2025). Whilst long-term oxygen therapy has been shown to improve survival rates in more advanced stages of COPD cohorts (Flenley, 1981; Kvale et al., 1980) the mechanisms behind this are debated. Acute oxygen administration has been shown to reduce breathlessness, lower MSNA and decrease arterial stiffness, suggesting that excessive carotid body activity plays a major role in these symptoms even in non-hypoxaemic COPD patients (Heindl et al., 2001; Phillips et al., 2018; Stickland et al., 2016). However, long-term supraphysiological oxygen administration carries risks, such as blunted ventilatory drive, worsening hypercapnia, and increased oxidative stress, potentially accelerating disease progression.

Current alternative treatments for carotid body-mediated diseases such as heart failure include invasive surgery to ablate the carotid body (Niewinski et al., 2013; Niewinski et al., 2017; Niewinski et al., 2021). However, bilateral removal poses tremendous risks due to complete loss of HVR. Data from this thesis showed that N rats could not survive

a 2-minute hypoxic episode after CSNX, and while CH rats endured the exposure, they failed to mount any ventilatory response. This is particularly concerning given the severe O_2 desaturations that occur during sleep, placing compromised patients at high risk. Pharmacologically targeting the carotid body offers a potential alternative to surgery, allowing for the fine-tuning of its activity without complete loss of function. This thesis highlights that pharmacological inhibition of CD73 can reduce carotid body hyperactivity and reduce resting blood pressure while preserving robust ventilatory response to hypoxia, making it a safer treatment option.

Taken together, this thesis demonstrates that inhibiting CD73 with AOPCP *in vivo* lowers resting blood pressure, partially via carotid body-specific mechanisms and without significantly affecting ventilation or hypoxic responses. While further research in hypertensive and COPD models is needed, these findings establish a foundation for exploring CD73 and its downstream signalling as potential therapeutic targets for reducing cardiovascular risk in CH-associated conditions like COPD.

7.4 Limitations

7.4.1 Carotid body isolation and *ex vivo* carotid sinus nerve recording

Experiments in this thesis predominately utilised an intact whole carotid body superfused preparation *ex vivo*. The start of this procedure involves dissecting the carotid bifurcations *in vivo* under anaesthetic and clamping the common carotid artery to halt blood flow whilst the bifurcation is being extracted. This would cause a few seconds of ischemia thus subjecting the carotid body to severe hypoxia potentially causing powerful excitation, neurotransmitter depletion and potential tissue damage. Whilst this is not ideal, it is preferable to removing the carotid bodies after confirmation

of death, which would expose the carotid bodies to significantly longer ischaemic periods. Efforts to minimise metabolic deterioration were made by immediately placing the carotid body tissue in ice-cold buffered physiological salt solution equilibrated with high oxygen (95% O_2, 5% CO_2) and using the freshly isolated tissue within hours of isolation. Furthermore, the use of the intact organ preserves important cell-cell interactions and the functional glomerular architecture. Nevertheless, it is impossible to rule out that the responses measured *ex vivo* would not be fully equivalent to the response measured *in vivo*. In this thesis, basal carotid body discharge was measured to be within range of single fibre measurements made in arterial normoxia in the rat, so confidence in tissue viability exists (Vidruk et al., 2001).

Another limitation is that superfusion results in potential barriers to diffusion of gases and pharmacological agents to reach the type I cell that the afferent nerve fibre is innervating. As a result, the actual PO_2, PCO_2 and drug concentrations at the desired target may be lower than what is recorded in the superfusate. Depending on how much connective tissue still surrounds the carotid body may also limit diffusion.

7.4.2 Immunohistochemistry

Immunohistochemistry is a widely used technique that allows the detection of proteins with preserved tissue morphology. This allows specific localisation of a protein of interest. Although antibodies are highly specific to their target, they do have the potential to bind non-specifically depending on the type of antibody and its concentration. Also, batch to batch variation exists from the manufacturers which may further impact consistency.

Typically, monoclonal antibodies result in less non-specific binding due to its ability to only bind to one epitope as monoclonal antibodies have been cloned from the same parent cell *in vitro*. Polyclonal antibodies on the other hand are usually raised in the whole animal and the serum is pooled which results in antibodies that can bind to various epitopes. Even though this may result in higher non-specific staining it does allow for the detection of lowly expressed proteins. In this thesis, a combination of monoclonal and polyclonal antibodies was used. Appropriate negative controls were performed to confirm the specificity of the secondary antibody to the primary antibody. These experiments could have been improved by utilising a positive control to determine the specificity of the primary antibody. The liver, previously shown to abundantly express CD73 when using this specific antibody, could serve effectively as a positive control (Fausther et al., 2012). Additionally, a true negative control would have further validated antibody specificity. In this thesis, samples incubated with pre-immune serum (serum collected from the same animal before it had been immunised with the CD73 antigen) showed negative reactivity.

Furthermore, as described in results Chapter 4, RBCs remained present in the carotid body which are highly autofluorescent in a range of wavelengths. This makes analysis difficult as it creates a false positive signal. Although successful efforts were made to remove RBC AF using a machine learning approach in Chapter 4 (Berg et al., 2019), to avoid time consuming processing post-acquisition, appropriate tissue processing should be applied. A simple method would be to perfuse the fixative *in vivo* therefore flushing out the blood until the solution runs clear (Nanduri & Prabhakar, 2018). Nevertheless, this required appropriate Home Office license approval.

Other methods involve quenching the autofluorescent signal during the staining protocol using a range of chemicals such Sudan Black or True Black. Although this is commonly used, issues arise over the harshness of chemicals that can damage epitope-antibody specificity and despite removing AF in one wavelength it could create AF in another wavelength (Whittington & Wray, 2017). Given the broad emission wavelengths of RBC AF, another approach would be to utilise a spare channel during the acquisition. This channel could then be used to create a binary mask which can then be subtracted from the rest of the channels. Unfortunately, this was not possible for this thesis as all channels were used at the maximum capacity of the microscope.

7.4.3 Estimation of carotid body volume

In this thesis, carotid body volume was determined from the assumption that the carotid body is an ellipsoid and therefore volume was calculated as described in section 2.6.5. However, the carotid body is likely to be irregular which also depends on the orientation during cryosectioning and the natural position at the carotid bifurcation varying between animals. Another method to determine carotid body volume is to utilise Cavalieri's principle which states that the volume of an irregular shape can be determined by summing the area of each section multiplied by the distance between them. This approach relies on stereological measurements being made such that the same slice or 'time point' is taken at regular intervals in both the N and CH groups. In these experiments however, due to the complexity of staining protocols this was not possible. Instead, to estimate the volume of an ellipsoid the largest cross-sectional area (which is usually the middle section) is required, and in these experiments, there was greater confidence that the middle section was obtained, in addition to the total number of carotid body sections.

7.4.4 *In vivo* cardio-respiratory measurements

The *in vivo* experiments performed in this thesis utilised Alfaxalone as the maintenance intravenous anaesthetic. It must be acknowledged that some central depression may have occurred. Of note, the HVRs measured in both groups appear to be slightly smaller than those measured in awake unanaesthetised animals and so the absolute effects that occur during hypoxia may not reflect exactly what would occur in a freely moving animal. However, the basal minute ventilation was comparable between anaesthetised and unanaesthetised rats. An interesting observation was that CH tended to need a lower infusion rate of the anaesthetic suggesting they were more sensitive to its effects. In Chapter 3, using awake unanaesthetised rats, CH rats had a comparable HVR compared to N despite having an augmented hypoxic chemoafferent discharge, which suggests that CH may have caused some central adaptations to blunt an augmented HVR. The anaesthetic used therefore may have accentuated this effect causing a greater central depression during hypoxia. Nevertheless, to observe an augmented HVR, maintaining P_aCO_2 during hypoxia (isocapnic hypoxia) is vital which was not performed in these experiments and so the blunted HVR may not solely be due to the anaesthetic (Aaron & Powell, 1993).

Furthermore, N rats had a high normoxic mean arterial blood pressure compared to what has been reported using tail cuff or telemetry in awake Wistar rats (Del Rio et al., 2016; McBryde et al., 2013; Nanduri et al., 2012; Nanduri et al., 2017; Nanduri et al., 2018; Peng et al., 2025; Peng et al., 2014; Rezende et al., 2022). This indicates the anaesthetic may have caused an increased sympathetic tone to the heart and vasculature. In cats and dogs, Alfaxalone was shown to decrease heart rate, cardiac output and blood pressure (Ambros et al., 2008; Muir et al., 2008), and so the unusually high blood pressure in rats is currently unexplained, although the values measured are

comparable to other studies using Alfaxalone based anaesthetics in rats (Marshall, 1998; Marshall & Metcalfe, 1988; Skinner & Marshall, 1996; Thomas & Marshall, 1994; Walsh & Marshall, 2006). Future experiments could aim to measure blood pressure in a freely moving and unanaesthetised animals using a telemetry-based approach.

7.5 Future directions

7.5.1 Confirming CD73 as the key mediator in establishing basal and hypoxic sensitivity

Most studies investigating the role of CD73 and adenosine have relied on pharmacological approaches. However, despite using similar compounds, some inconsistencies in results suggest potential non-specific drug effects or differences in carotid body preparations (e.g., isolated single cells vs. whole tissue), which may impact drug diffusion and target accessibility. A pharmacological approach was used here as it has more translational potential.

A more precise method for inhibiting CD73 would be through *in vivo* genetic knockout technology. However, global homozygous or heterozygous knockouts can lead to embryonic lethality, abnormal postnatal development or compensatory mechanisms that complicate result interpretation. Reported global homozygous CD73 knockout mice are fertile and grow normally but do display increased vascular permeability at rest which is exacerbated by hypoxia (Thompson et al., 2004). Furthermore, they develop greater myocardial infarcts and impaired renal function after ischaemic injury (Eckle et al., 2007; Grenz et al., 2007). However, other cardio-respiratory phenotypes such as ventilation, blood pressure and heart rate are unknown. Therefore, carotid body specific characterisation of these mice would be valuable. A more refined

approach would be generating a conditional CD73 knockout, where the *NT5* gene (which encodes CD73) is selectively deleted in type I cells, with controlled timing of deletion. This could be achieved using a Cre-loxP system under a TH promoter, further regulated by an oestrogen receptor- a strategy previously used in carotid body research (Arias-Mayenco et al., 2018; Fielding et al., 2018). In this model, *NT5* deletion in TH^+ type I cells would occur after administering Tamoxifen (an oestrogen receptor agonist).

Tamoxifen could be administered in the final days of CH exposure, allowing assessment of chemoafferent activity and cardio-respiratory responses to determine if the knockout replicates pharmacological CD73 inhibition. Another valuable experiment would be knocking out CD73 before CH exposure, providing mechanistic insight into whether CD73 is necessary for carotid body adaptations to CH or if other pathways contribute to its hyperactivity and enhanced hypoxic sensitivity. Genetic inactivation of downstream targets like tmACs could also be performed using a similar approach. Specifically, TH-Cre/*Adcy3*$^{fl/fl}$ (tmAC-3 tamoxifen inducible knockout) have been reported to have a normal phenotype but show impaired chemoafferent activity and type I cell calcium influx in response to hypoxia. In addition, the adaptations that occur in response to chronic intermittent hypoxia are abolished (Peng et al., 2025). Therefore, whether similar carotid body adaptions to CH are prevented in these knockout mice could be explored.

7.5.2 Characterisation of $CD73^+$ cell types in the whole carotid body and the impact of CH

A key finding from Chapter 4 was the identification of a $CD73^+TH^-$ cell population in normoxic carotid bodies, which appeared to gain TH expression ($CD73^+TH^+$) after CH exposure. This supports the hypothesis of an immature type I cell niche, where cells initially express low levels of TH but, in response to hypoxia, rapidly adjust their expression profile to become mature type I cells. Future experiments could further characterise this $CD73^+$ immature population by staining for markers such as HNK-1, previously proposed as an indicator of immature type I cells (Sobrino et al., 2018). A more sensitive approach, such as single-cell RNA sequencing, could also be employed to analyse the genetic profile of individual type I cells.

In two out of three carotid bodies analysed a slight increase in total cell number was observed, suggesting that mitotic activity may contribute to cell expansion (Chapter 4). To investigate this further, proliferation markers could be used. One method involves administering BrdU through the rats' drinking water, allowing its incorporation into newly synthesised DNA (Fielding et al., 2018; Hodson et al., 2016; Sobrino et al., 2018). Fluorescent labelling of BrdU using antibodies, along with TH and CD73 staining, would then help identify proliferating cell populations. Utilising lineage labelling genetic technology, the specific cell types that are undergoing proliferation to give rise to new cell populations could be determined.

Another notable finding was the detection of a persistent CD73 signal at low antibody concentrations. Despite efforts to identify the source of this signal that was partially co-

localised with the vascular endothelium, the specific cell type remained undetermined. The signal appeared to surround blood vessels, suggesting a resemblance to pericytes. To confirm this, staining for pericyte markers such as PDGF-β, NG2, or vimentin that have been previously shown to co-localise with CD73 in liver tissue could be performed (Fausther et al., 2012). Understanding how CH influences the number and expression profile of these cells could provide further insights into carotid body plasticity and hyperactivity, given pericytes' role in regulating blood flow and potential hypoperfusion-induced local hypoxia.

7.5.3 Investigating the molecular mechanisms of CH induced carotid body hyperactivity

A crucial step in understanding carotid body hyperactivity and identifying new therapeutic targets is determining how enhanced CD73 activity and increased synaptic adenosine levels lead to heightened carotid body excitability. As illustrated in Figure 7.1, multiple downstream targets of cAMP play a role in this process. Previous studies have shown that adenosine and cAMP reduce the amplitude of 4-AP-sensitive K^+ channels (Lopez-Lopez et al., 1993; Vandier et al., 1999). However, a direct link between CH and 4-AP K^+ channels has not been established. Additionally, investigating CNG ion channels may be worthwhile, given their activation by cAMP and their key role in promoting carotid body hyperactivity in chronic intermittent hypoxia models (Peng et al., 2025). If CH-induced changes are more sensitive to CD73/tmAC blockade, it would suggest a role for extracellularly derived adenosine and its downstream target in driving hyperactivity.

Other key K^+ channels, such as TASK-1, are inhibited by PKA activity, and CH has been shown to enhance TASK-like current inhibition (Ortiz et al., 2009). However, whether this effect is driven by increased CD73 and PKA activity remains unclear. To address this, phosphorylation-specific antibodies could be used in Western blot analyses to assess the phosphorylation status of various K^+ channels. Additionally, functional studies using electrophysiological recordings with CD73 or PKA antagonists could clarify their roles in modulating K^+ channel activity. Investigating whether CD73 itself undergoes PKA-dependent phosphorylation could provide further insight into a potential mechanism driving its enhanced enzymatic activity in CH without changes in expression or relative density.

7.6 Final conclusions

Carotid body hyperactivity is increasingly being recognised as a key mediator in the development of cardiovascular disease in numerous pathologies such as COPD, chronic heart failure, obstructive sleep apnoea, essential hypertension, metabolic syndrome and diabetes. The main focus of this thesis was to investigate how CH leads to augmented carotid body output. CH is a characteristic hallmark of COPD, and although a multifactorial disease, looking at CH in isolation allowed to understand the mechanisms of carotid body hyperactivity more clearly. This thesis had demonstrated the vital importance of CD73 activity in driving heightened basal carotid body activity and increased O_2 sensitivity in response to CH. Data showed, for the first time, that antagonism of CD73 severely depressed carotid body basal discharge but did not abolish its ability to respond to hypoxia *ex vivo*. Inhibition of CD73 *in vivo*, reduced blood pressure in CH rats, but did not alter cardio-respiratory responses to hypoxia- an ideal asset for carotid body targeted treatment that allows for fine tuning its activity

without destroying its ability to respond to stressful stimuli. Characterising the downstream molecular targets of adenosine mediated signalling may offer further insight into mechanisms of CH-induced hyperactivity, thus revealing a host of druggable targets. Currently, this thesis has shed light on the fact that CD73 could be a promising upstream candidate.

Appendix: Supplementary data

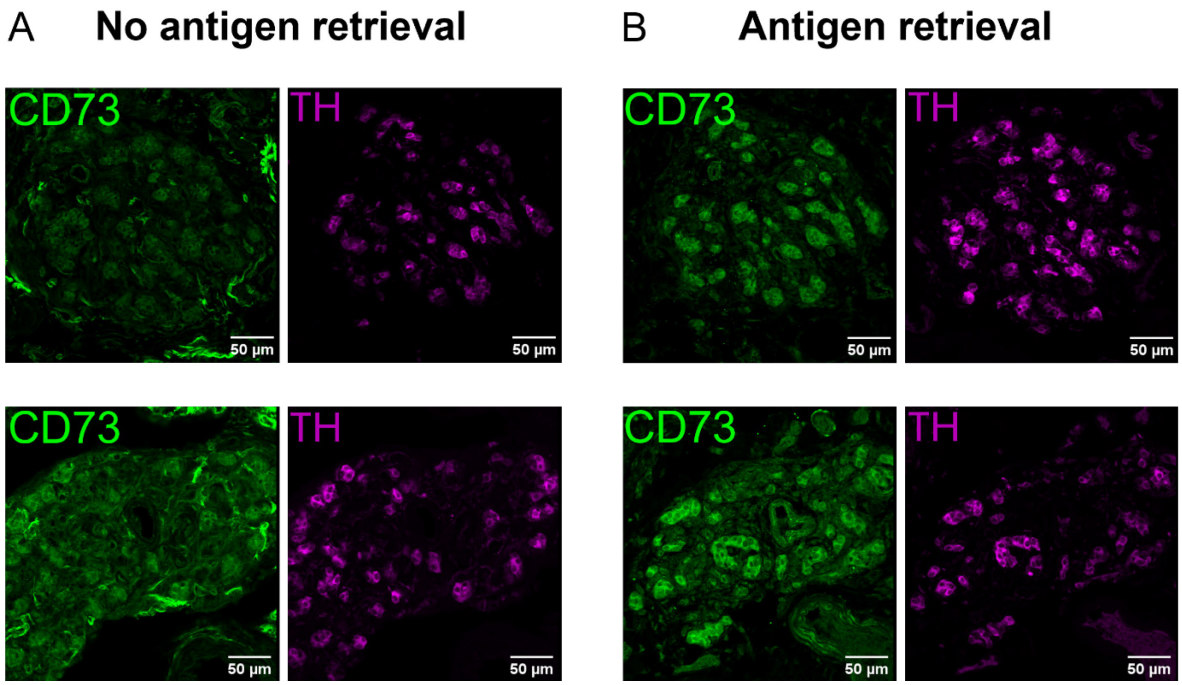

Figure S.1 CD73 antibody optimisation: antigen retrieval replicates

Replicate immunofluorescence images of carotid body sections stained with CD73 antibody (1:100) before **(A)**, or after **(B)** antigen retrieval. Tyrosine hydroxylase (TH, 1:500) was used to identify type I cells. Upper and lower panels represent individual replicates from different rat carotid bodies. Antigen retrieval involved incubating sections in citrate buffer (pH 6.0) at 60°C overnight prior to commencing the normal staining protocol.

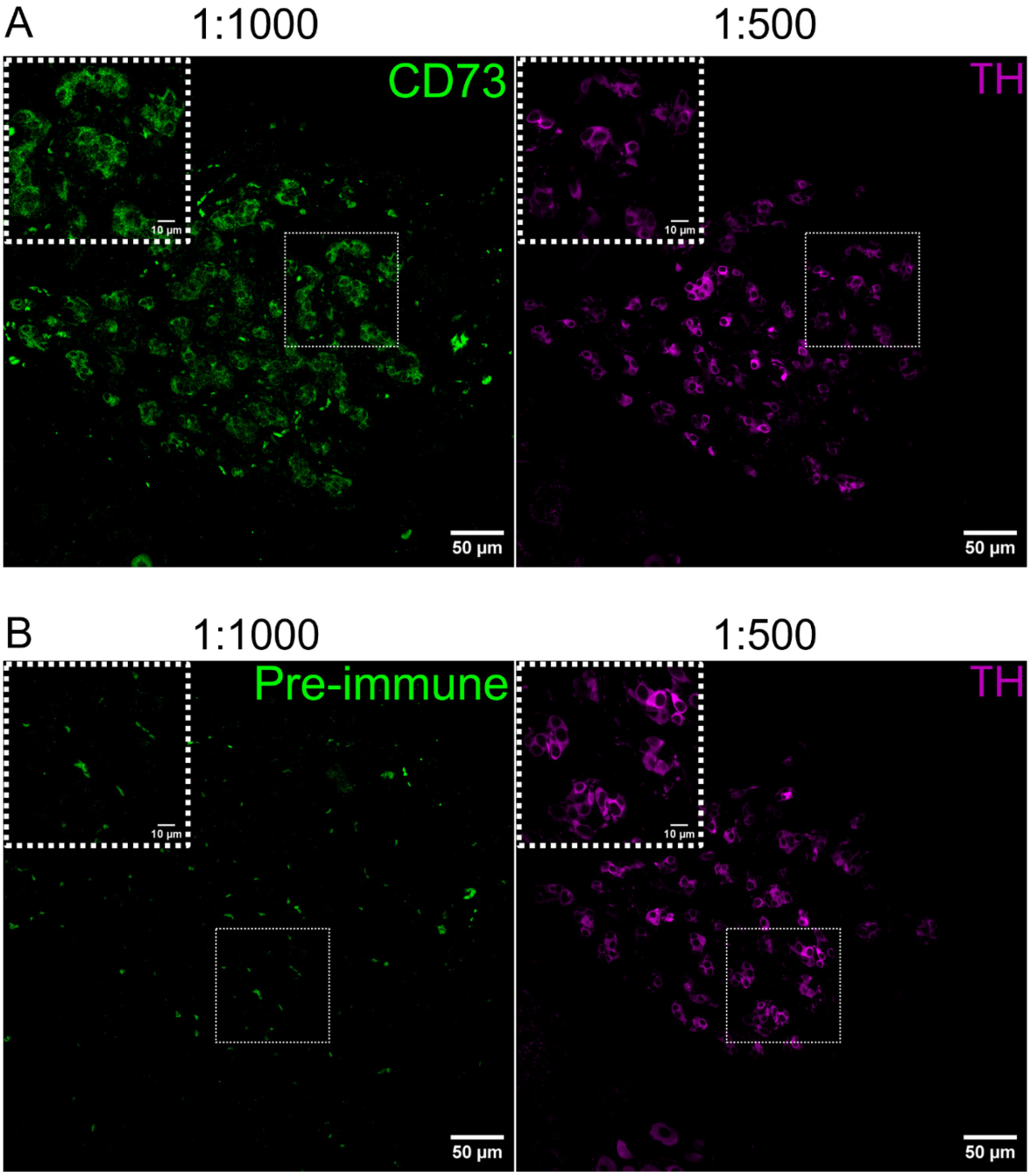

Figure S.2 CD73 detection at a dilution of 1:1000 with antigen retrieval

(A) Immunofluorescence images of carotid body (CB) sections stained with **(A)** CD73 antibody (1:1000) or **(B)** pre-immune serum (1:1000) both following antigen retrieval. Tyrosine hydroxylase (TH, 1:500) was used to identify type I cells. Positive detection with CD73 antibody and absence of signal in pre-immune control. Antigen retrieval consisted of incubating sections in citrate buffer (pH 6.0) at 60°C overnight prior to commencing normal staining protocol. Signal present in B is red blood cell autofluorescence. Insets (dotted boxes) provide a closer view of the boxed regions.

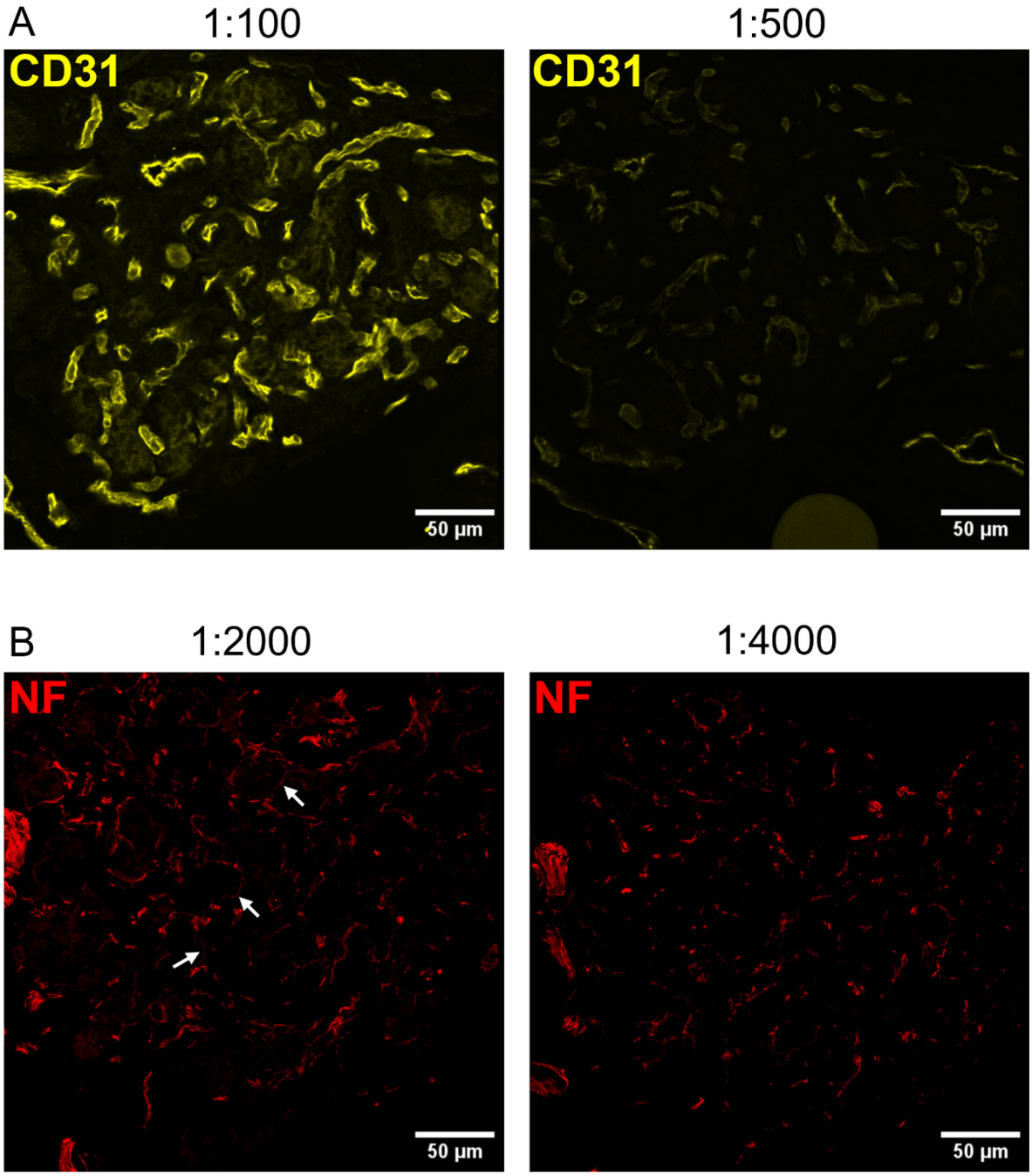

Figure S.3 Vascular endothelial (CD31) and neurofilament (NF) antibody optimisation

(A) Immunofluorescence images of carotid body (CB) sections stained with a CD31 antibody at dilutions of 1:100 (left) or 1:1500 (right). The 1:100 gives a good signal but does have background. 1:500 shows improved background staining. The signal is weaker but still detectable and laser settings can be optimised. **(B)** CB sections stained with NF at 1:2000 (left) and 1:4000 (right). Both show low background staining and strong positive staining. The 1:2000 does detect NF in more structures as indicated by the white arrows compared to the 1:4000. All confocal acquisition settings were kept the same for direct comparison.

Evaluating the role of new small molecule CD73 inhibitors on carotid body activity

Demitris Nathanael, Andrew M. Coney, Clare J Ray, Prem Kumar, Andrew P. Holmes.

School of Biomedical Sciences, Institute of Clinical Sciences, University of Birmingham, United Kingdom.

Carotid body (CB) hyperactivity is considered an important driver of cardiovascular dysfunction in patients with respiratory disorders, with limited treatment options (Kumar and Prabhakar, 2012). Whilst CB resection has been considered a potential strategy; pharmacological targeting of CB hyperactivity could offer a safer and more viable treatment alternative. Adenosine derived from CD73 acting via A_2 receptors on CB type I cells has emerged as a potential mechanistic target. We have shown that pharmacological inhibition of CD73 via AOPCP at relatively high doses, reduced basal discharge frequency by approximately 76% which was mimicked by antagonism of A_2 receptors using 8-SPT (Holmes *et al*., 2017) Recently, more potent CD73 inhibitors including PSB-12379, have become available which could decrease CB activity at lower therapeutic doses.

Using an immunocytochemical approach we identified and visualised the expression of CD73 and A_{2A} receptors in PC12 cells. Preliminary data suggests that these two may be co-localised. Recordings from chemoafferents in vitro, we investigated the dose dependency of PSB-12379 at low doses (1nM-1μM, n=3) and higher doses (1μM-100μM, n=2). PSB-12379 had no effect on basal discharge, even at the higher doses.

Our preliminary data suggests that CD73 and A_{2A} may be co-localised in PC12 cells. However, further experiments are needed to establish this and identify if a similar finding occurs in CB type I cells. It also suggests that PSB-12379 does not appear to be more effective than AOPCP at equivalent doses. Our data set does not, presently, allow us to state that PSB-12379 could be a suitable drug treatment for CB hyperactivity.

CD73 inhibition reverses chronic hypoxia induced carotid body hyperactivity

Demitris Nathanael[1], Andrew M Coney[1,2], Prem Kumar[1] & Andrew P Holmes[1,2]

[1]School of Biomedical Sciences, Institute of Clinical Sciences, University of Birmingham, Birmingham, United Kingdom.

[2]Institute of Cardiovascular Sciences, University of Birmingham, Birmingham, United Kingdom.

Carotid body (CB) hyperactivity in patients with chronic obstructive pulmonary disease (COPD) is associated with autonomic imbalance and cardiovascular disease (Phillips et al., 2018). A key feature of COPD is chronic hypoxia (CH). Mechanisms of CB hyperactivity in response to CH are unknown but could be dependent on increased CD73 activity (an enzyme that generates adenosine) (Holmes et al., 2015; Holmes et al., 2018b; Salman et al., 2017). Here, we investigated if pharmacological blockade of CD73 attenuated CH mediated CB hyperactivity.

Chemoafferent activity was measured *ex vivo* from CBs dissected from adult male Wistar rats (150-250g) exposed to either 10 days of normoxia (N, n=13 animals) or CH (F_iO_2=12%, n=14 animals). Concentration-response experiments with AOPCP (CD73 inhibitor) ranged between 10nM-330μM in normoxia. Activity was measured continuously as the superfusate PO_2 was decreased in the absence or the presence of either 15μM or 100μM AOPCP. Results are expressed as mean ±SEM and significance ($P<0.05$) was established by unpaired t-test or one-way ANOVA.

CH increased basal CB discharge (0.55±0.06 Hz vs 1.50±0.17 Hz, $P<0.001$) and increased hypoxic sensitivity. The IC50 for AOPCP in N and CH were 1.4±0.3μM and 7.8±4μM respectively. At a concentration of 15μM, AOPCP reduced basal discharge by 89±2% in N and 53±3% in CH. However, 100μM AOPCP had no additional effect on basal discharge in N but reduced it in CH to 91±1%. 100μM AOPCP caused a leftward shift in the hypoxic response curves in N and CH. Sensitivity of the hypoxic response to AOPCP was enhanced in CH ($P<0.01$) reversing the exaggerated hypoxic responses back to those seen in N animals.

This data suggests that CH leads to elevated CB sensory discharge at baseline and during hypoxia, which can be reversed by *ex vivo* pharmacological inhibition of CD73. Whether *in vivo* CD73 inhibition can dampen augmented autonomic reflexes caused by CH to prevent cardiovascular disease warrants future investigation.

References

Aaron, E. A., & Powell, F. L. (1993). EFFECT OF CHRONIC HYPOXIA ON HYPOXIC VENTILATORY RESPONSE IN AWAKE RATS [Article]. *Journal of Applied Physiology*, *74*(4), 1635-1640. https://doi.org/10.1152/jappl.1993.74.4.1635

Abdala, A. P., McBryde, F. D., Marina, N., Hendy, E. B., Engelman, Z. J., Fudim, M., Sobotka, P. A., Gourine, A. V., & Paton, J. F. R. (2012). Hypertension is critically dependent on the carotid body input in the spontaneously hypertensive rat [Article]. *Journal of Physiology-London*, *590*(17), 4269-4277. https://doi.org/10.1113/jphysiol.2012.237800

Agusti, A., & Soriano, J. B. (2008). COPD as a Systemic Disease [Review]. *Copd-Journal of Chronic Obstructive Pulmonary Disease*, *5*(2), 133-138. https://doi.org/10.1080/15412550801941349

Alcedo, K. P., Bowser, J. L., & Snider, N. T. (2021). The elegant complexity of mammalian ecto-5'-nucleotidase (CD73) [Review]. *Trends in Cell Biology*, *31*(10), 829-842. https://doi.org/10.1016/j.tcb.2021.05.008

Ambros, B., Duke-Novakovski, T., & Pasloske, K. S. (2008). Comparison of the anesthetic efficacy and cardiopulmonary effects of continuous rate infusions of alfaxalone-2-hydroxypropyl-β-cyclodextrin and propofol in dogs [Article]. *American Journal of Veterinary Research*, *69*(11), 1391-1398. https://doi.org/10.2460/ajvr.69.11.1391

Angelova, P. R., Kasymov, V., Christie, I., Sheikhbahaei, S., Turovsky, E., Marina, N., Korsak, A., Zwicker, J., Teschemacher, A. G., Ackland, G. L., Funk, G. D., Kasparov, S., Abramov, A. Y., & Gourine, A. V. (2015). Functional Oxygen Sensitivity of Astrocytes [Article]. *Journal of Neuroscience*, *35*(29), 10460-10473. https://doi.org/10.1523/jneurosci.0045-15.2015

Antuni, J. D., & Barnes, P. J. (2016). Evaluation of Individuals at Risk for COPD: Beyond the Scope of the Global Initiative for Chronic Obstructive Lung Disease [Review]. *Chronic Obstructive Pulmonary Diseases-Journal of the Copd Foundation*, *3*(3), 653-667. https://doi.org/10.15326/jcopdf.3.3.2016.0129

Arias-Mayenco, I., González-Rodríguez, P., Torres-Torrelo, H., Gao, L., Fernández-Agüera, M. C., Bonilla-Henao, V., Ortega-Sáenz, P., & López-Barneo, J. P. (2018). Acute O_2 Sensing: Role of Coenzyme QH_2/Q Ratio and Mitochondrial ROS Compartmentalization [Article]. *Cell Metabolism*, *28*(1), 145-154. https://doi.org/10.1016/j.cmet.2018.05.009

Arias-Reyes, C., Soliz, J., & Joseph, V. (2021). Mice and Rats Display Different Ventilatory, Hematological, and Metabolic Features of Acclimatization to Hypoxia [Article]. *Frontiers in Physiology*, *12*, Article 647822. https://doi.org/10.3389/fphys.2021.647822

Armulik, A., Genové, G., Mäe, M., Nisancioglu, M. H., Wallgard, E., Niaudet, C., He, L. Q., Norlin, J., Lindblom, P., Strittmatter, K., Johansson, B. R., & Betsholtz, C. (2010). Pericytes regulate the blood-brain barrier [Article]. *Nature*, *468*(7323), 557-561. https://doi.org/10.1038/nature09522

Attwell, D., Buchan, A. M., Charpak, S., Lauritzen, M., MacVicar, B. A., & Newman, E. A. (2010). Glial and neuronal control of brain blood flow [Review]. *Nature*, *468*(7321), 232-243. https://doi.org/10.1038/nature09613

Attwell, D., Mishra, A., Hall, C. N., O'Farrell, F. M., & Dalkara, T. (2016). What is a pericyte? [Editorial Material]. *Journal of Cerebral Blood Flow and Metabolism*, *36*(2), 451-455. https://doi.org/10.1177/0271678x15610340

Bachmann, S., Lehir, M., & Eckardt, K. U. (1993). COLOCALIZATION OF ERYTHROPOIETIN MESSENGER-RNA AND ECTO-5'-NUCLEOTIDASE IMMUNOREACTIVITY IN PERITUBULAR CELLS OF RAT RENAL-CORTEX INDICATES THAT FIBROBLASTS PRODUCE ERYTHROPOIETIN [Note]. *Journal of Histochemistry & Cytochemistry*, *41*(3), 335-341. https://doi.org/10.1177/41.3.8429197

Ball, M. K., Waypa, G. B., Mungai, P. T., Nielsen, J. M., Czech, L., Dudley, V. J., Beussink, L., Dettman, R. W., Berkelhamer, S. K., Steinhorn, R. H., Shah, S. J., & Schumacker, P. T. (2014). Regulation of Hypoxia-induced Pulmonary Hypertension by Vascular Smooth

Muscle Hypoxia-Inducible Factor-1α [Article]. *American Journal of Respiratory and Critical Care Medicine*, *189*(3), 314-324. https://doi.org/10.1164/rccm.201302-0302OC

Barnard, P., Andronikou, S., Pokorski, M., Smatresk, N., Mokashi, A., & Lahiri, S. (1987). TIME-DEPENDENT EFFECT OF HYPOXIA ON CAROTID-BODY CHEMOSENSORY FUNCTION [Article]. *Journal of Applied Physiology*, *63*(2), 685-691. https://doi.org/10.1152/jappl.1987.63.2.685

Barnes, P. J., Shapiro, S. D., & Pauwels, R. A. (2003). Chronic obstructive pulmonary disease: molecular and cellular mechanisms [Review]. *European Respiratory Journal*, *22*(4), 672-688. https://doi.org/10.1183/09031936.03.00040703

Barnett, S., Mulligan, E., Wagerle, L. C., & Lahiri, S. (1988). MEASUREMENT OF CAROTID-BODY BLOOD-FLOW IN CATS BY USE OF RADIOACTIVE MICROSPHERES [Article]. *Journal of Applied Physiology*, *65*(6), 2484-2489. https://doi.org/10.1152/jappl.1988.65.6.2484

Berg, S., Kutra, D., Kroeger, T., Straehle, C. N., Kausler, B. X., Haubold, C., Schiegg, M., Ales, J., Beier, T., Rudy, M., Eren, K., Cervantes, J. I., Xu, B. T., Beuttenmueller, F., Wolny, A., Zhang, C., Koethe, U., Hamprecht, F. A., & Kreshuk, A. (2019). ilastik: interactive machine learning for (bio) image analysis [Article]. *Nature Methods*, *16*(12), 1226-1232. https://doi.org/10.1038/s41592-019-0582-9

Bernardini, A., Wolf, A., Brockmeier, U., Riffkin, H., Metzen, E., Acker-Palmer, A., Fandrey, J., & Acker, H. (2020). Carotid body type I cells engage flavoprotein and Pin1 for oxygen sensing [Article]. *American Journal of Physiology-Cell Physiology*, *318*(4), C719-C731. https://doi.org/10.1152/ajpcell.00320.2019

Bianchi, V., & Spychala, J. (2003). Mammalian 5 '-nucleotidases [Review]. *Journal of Biological Chemistry*, *278*(47), 46195-46198. https://doi.org/10.1074/jbc.R300032200

Bin-Jaliah, I., Maskell, P. D., & Kumar, P. (2004). Indirect sensing of insulin-induced hypoglycaemia by the carotid body in the rat [Article]. *Journal of Physiology-London*, *556*(1), 255-266. https://doi.org/10.1113/jphysiol.2003.058321

Bishop, T., & Ratcliffe, P. J. (2014). Signaling hypoxia by hypoxia-inducible factor protein hydroxylases: a historical overview and future perspectives [Review]. *Hypoxia*, *2*, 197-213. https://doi.org/10.2147/hp.S47598

Bishop, T., & Ratcliffe, P. J. (2015). HIF Hydroxylase Pathways in Cardiovascular Physiology and Medicine [Review]. *Circulation Research*, *117*(1), 65-79. https://doi.org/10.1161/circresaha.117.305109

Bishop, T., & Ratcliffe, P. J. (2020). Genetic basis of oxygen sensing in the carotid body: HIF2α and an isoform switch in cytochrome c oxidase subunit 4 [Editorial Material]. *Science Signaling*, *13*(615), 2, Article eaba1302. https://doi.org/10.1126/scisignal.aba1302

Bishop, T., & Ratcliffe, P. J. (2025). HIF2alpha: the interface between oxygen-sensing systems in physiology and pathology [Invited Article]. *American Physiological Society*. https://doi.org/10.1152/physiol.00043.2024

Bishop, T., Talbot, N. P., Turner, P. J., Nicholls, L. G., Pascual, A., Hodson, E. J., Douglas, G., Fielding, J. W., Smith, T. G., Demetriades, M., Schofield, C. J., Robbins, P. A., Pugh, C. W., Buckler, K. J., & Ratcliffe, P. J. (2013). Carotid body hyperplasia and enhanced ventilatory responses to hypoxia in mice with heterozygous deficiency of PHD2 [Article]. *Journal of Physiology-London*, *591*(14), 3565-3577. https://doi.org/10.1113/jphysiol.2012.247254

Blain, G. M., Smith, C. A., Henderson, K. S., & Dempsey, J. A. (2009). Contribution of the carotid body chemoreceptors to eupneic ventilation in the intact, unanesthetized dog [Article]. *Journal of Applied Physiology*, *106*(5), 1564-1573. https://doi.org/10.1152/japplphysiol.91590.2008

Böck, P. (1980). Histochemical demonstration of adenine nucleotides in carotid body type I cells. *Adv Biochem Psychopharmacol*, *25*, 235-239.

Bouverot, P., Candas, V., & Libert, J. P. (1973). ROLE OF ARTERIAL CHEMORECEPTORS IN VENTILATORY ADAPTATION TO HYPOXIA OF AWAKE DOGS AND RABBITS [Article]. *Respiration Physiology*, *17*(2), 209-219. https://doi.org/10.1016/0034-5687(73)90062-5

Broch, O. J., & Ueland, P. M. (1980). REGIONAL AND SUBCELLULAR-DISTRIBUTION OF S-ADENOSYLHOMOCYSTEINE HYDROLASE IN THE ADULT-RAT BRAIN [Article]. *Journal of Neurochemistry*, *35*(2), 484-488. https://doi.org/10.1111/j.1471-4159.1980.tb06291.x

Brown, L. S., Foster, C. G., Courtney, J. M., King, N. E., Howells, D. W., & Sutherland, B. A. (2019). Pericytes and Neurovascular Function in the Healthy and Diseased Brain [Review]. *Frontiers in Cellular Neuroscience*, *13*, 9, Article 282. https://doi.org/10.3389/fncel.2019.00282

Brown, S. T., Reyes, E. P., & Nurse, C. A. (2011). Chronic hypoxia upregulates adenosine 2a receptor expression in chromaffin cells via hypoxia inducible factor-2α: Role in modulating secretion [Article]. *Biochemical and Biophysical Research Communications*, *412*(3), 466-472. https://doi.org/10.1016/j.bbrc.2011.07.122

Buckler, K. J. (2012). Effects of exogenous hydrogen sulphide on calcium signalling, background (TASK) K channel activity and mitochondrial function in chemoreceptor cells [Article]. *Pflugers Archiv-European Journal of Physiology*, *463*(5), 743-754. https://doi.org/10.1007/s00424-012-1089-8

Buckler, K. J., & Turner, P. J. (2013). Oxygen sensitivity of mitochondrial function in rat arterial chemoreceptor cells [Article]. *Journal of Physiology-London*, *591*(14), 3549-3563. https://doi.org/10.1113/jphysiol.2013.257741

Buckler, K. J., & Vaughanjones, R. D. (1994). EFFECTS OF HYPOXIA ON MEMBRANE-POTENTIAL AND INTRACELLULAR CALCIUM IN RAT NEONATAL CAROTID-BODY TYPE-I CELLS [Article]. *Journal of Physiology-London*, *476*(3), 423-428. https://doi.org/10.1113/jphysiol.1994.sp020143

Buckler, K. J., Williams, B. A., & Honore, E. (2000). An oxygen-, acid- and anaesthetic-sensitive TASK-like background potassium channel in rat arterial chemoreceptor cells [Article]. *Journal of Physiology-London*, *525*(1), 135-142. https://doi.org/10.1111/j.1469-7793.2000.00135.x

Burnstock, G. (1972). PURINERGIC NERVES [Review]. *Pharmacological Reviews*, *24*(3), 509-581.

Cabello-Rivera, D., Ortega-Sáenz, P., Gao, L., Muñoz-Cabello, A. M., Bonilla-Henao, V., Schumacker, P. T., & López-Barneo, J. (2022). Oxygen regulation of breathing is abolished in mitochondrial complex III-deficient arterial chemoreceptors [Article]. *Proceedings of the National Academy of Sciences of the United States of America*, *119*(39), 8, Article e2202178119. https://doi.org/10.1073/pnas.2202178119

Caceres, A. I., Obeso, A., Gonzalez, C., & Rocher, A. (2007). Molecular identification and functional role of voltage-gated sodium channels in rat carotid body chemoreceptor cells.: Regulation of expression by chronic hypoxia *in vivo* [Article]. *Journal of Neurochemistry*, *102*(1), 231-245. https://doi.org/10.1111/j.1471-4159.2007.04465.x

Caraftino, M. D., & Montalbetti, N. (2020). Acid-sensing ion channels in sensory signaling [Review]. *American Journal of Physiology-Renal Physiology*, *318*(3), F531-F543. https://doi.org/10.1152/ajprenal.00546.2019

Chang, A. J., Ortega, F. E., Riegler, J., Adison, D. V. M., & Krasnow, M. A. (2015). Oxygen regulation of breathing through an olfactory receptor activated by lactate [Article]. *Nature*, *527*(7577), 240-+. https://doi.org/10.1038/nature15721

Chen, J., He, L., Dinger, B., Stensaas, L., & Fidone, S. (2002). Role of endothelin and endothelin A-type receptor in adaptation of the carotid body to chronic hypoxia [Article]. *American Journal of Physiology-Lung Cellular and Molecular Physiology*, *282*(6), L1314-L1323. https://doi.org/10.1152/ajplung.00454.2001

Chen, J., He, L., Liu, X. M., Dinger, B., Stensaas, L., & Fidone, S. (2007). Effect of the endothelin receptor antagonist bosentan on chronic hypoxia-induced morphological and physiological changes in rat carotid body [Article]. *American Journal of Physiology-Lung Cellular and Molecular Physiology*, *292*(5), L1257-L1262. https://doi.org/10.1152/ajplung.00419.2006

Cheng, X. T., Prange-Barczynska, M., Fielding, J. W., Zhang, M. H., Burrell, A. L., Lima, J. D., Eckardt, L., La Argles, I., Pugh, C. W., Buckler, K. J., Robbins, P. A., Hodson, E. J., Bruick,

R. K., Collinson, L. M., Rastinejad, F., Bishop, T., & Ratcliffe, P. J. (2020). Marked and rapid effects of pharmacological HIF-2α antagonism on hypoxic ventilatory control [Article]. *Journal of Clinical Investigation*, *130*(5), 2237-2251. https://doi.org/10.1172/jci133194

Clarke, J. A., Daly, M. D., Marshall, J. M., Ead, H. W., & Hennessy, E. M. (2000). Quantitative studies of the vasculature of the carotid body in the chronically hypoxic rat [Article]. *Brazilian Journal of Medical and Biological Research*, *33*(3), 331-340. https://doi.org/10.1590/s0100-879x2000000300012

Colgan, S. P., Eltzschig, H. K., Eckle, T., & Thompson, L. F. (2006). Physiological roles for ecto-5'-nucleotidase (CD73) [Review]. *Purinergic Signalling*, *2*(2), 351-360. https://doi.org/10.1007/s11302-005-5302-5

Conde, S. V., da Silva, T. N., Gonzalez, C., Carmo, M. M., Monteiro, E. C., & Guarino, M. P. (2012a). Chronic caffeine intake decreases circulating catecholamines and prevents diet-induced insulin resistance and hypertension in rats [Article]. *British Journal of Nutrition*, *107*(1), 86-95. https://doi.org/10.1017/s0007114511002406

Conde, S. V., Gonzalez, C., Batuca, J. R., Monteiro, E. C., & Obeso, A. (2008). An antagonistic interaction between A_{2B} adenosine and D_2 dopamine receptors modulates the function of rat carotid body chemoreceptor cells [Article]. *Journal of Neurochemistry*, *107*(5), 1369-1381. https://doi.org/10.1111/j.1471-4159.2008.05704.x

Conde, S. V., & Monteiro, E. C. (2004). Hypoxia induces adenosine release from the rat carotid body [Article]. *Journal of Neurochemistry*, *89*(5), 1148-1156. https://doi.org/10.1111/j.1471-4159.2004.02380.x

Conde, S. V., Monteiro, E. C., Obeso, A., & Gonzalez, C. (2009). Adenosine in Peripheral Chemoreception: New Insights into a Historically Overlooked Molecule - Invited Article. In C. Gonzalez, C. A. Nurse, & C. Peers (Eds.), *Arterial Chemoreceptors* (Vol. 648, pp. 145-159). Springer-Verlag Berlin. https://doi.org/10.1007/978-90-481-2259-2_17

Conde, S. V., Monteiro, E. C., Rigual, R., Obeso, A., & Gonzalez, C. (2012b). Hypoxic intensity: a determinant for the contribution of ATP and adenosine to the genesis of carotid body chemosensory activity [Article]. *Journal of Applied Physiology*, *112*(12), 2002-2010. https://doi.org/10.1152/japplphysiol.01617.2011

Conde, S. V., Monteiro, E. C., & Sacramento, J. F. (2017). Purines and Carotid Body: New Roles in Pathological Conditions [Article]. *Frontiers in Pharmacology*, *8*, 15, Article 913. https://doi.org/10.3389/fphar.2017.00913

Conde, S. V., Obeso, A., Vicario, I., Rigual, R., Rocher, A., & Gonzalez, C. (2006). Caffeine inhibition of rat carotid body chemoreceptors is mediated by A(2A) and A(2B) adenosine receptors [Article]. *Journal of Neurochemistry*, *98*(2), 616-628. https://doi.org/10.1111/j.1471-4159.2006.03912.x

Conde, S. V., Ribeiro, M. J., Obeso, A., Rigual, R., Monteiro, E. C., & Gonzalez, C. (2012c). Chronic Caffeine Intake in Adult Rat Inhibits Carotid Body Sensitization Produced by Chronic Sustained Hypoxia but Maintains Intact Chemoreflex Output [Article]. *Molecular Pharmacology*, *82*(6), 1056-1065. https://doi.org/10.1124/mol.112.081216

D'Amico, F., Skarmoutsou, E., & Stivala, F. (2009). State of the art in antigen retrieval for immunohistochemistry [Review]. *Journal of Immunological Methods*, *341*(1-2), 1-18. https://doi.org/10.1016/j.jim.2008.11.007

Dale, N., Gourine, A. V., Llaudet, E., Bulmer, D., Thomas, T., & Spyer, K. M. (2002). Rapid adenosine release in the nucleus tractus solitarii during defence response in rats:: real-time measurement in vivo [Article]. *Journal of Physiology-London*, *544*(1), 149-160. https://doi.org/10.1113/jphysiol.2002.024158

Daly, M. D., Lambertsen, C. J., & Schweitzer, A. (1954). OBSERVATIONS ON THE VOLUME OF BLOOD FLOW AND OXYGEN UTILIZATION OF THE CAROTID BODY IN THE CAT [Article]. *Journal of Physiology-London*, *125*(1), 67-89. https://doi.org/10.1113/jphysiol.1954.sp005143

Decramer, M., Rennard, S., Troosters, T., Mapel, D. W., Giardino, N., Mannino, D., Wouters, E., Sethi, S., & Cooper, C. B. (2008). COPD as a Lung Disease with Systemic Consequences

- Clinical Impact, Mechanisms, and Potential for Early Intervention [Review]. *Copd-Journal of Chronic Obstructive Pulmonary Disease*, *5*(4), 235-256. https://doi.org/10.1080/15412550802237531

Del Rio, R., Andrade, D. C., Lucero, C., Arias, P., & Iturriaga, R. (2016). Carotid Body Ablation Abrogates Hypertension and Autonomic Alterations Induced by Intermittent Hypoxia in Rats [Article]. *Hypertension*, *68*(2), 436-445. https://doi.org/10.1161/hypertensionaha.116.07255

Delclaux, B., Orcel, B., Housset, B., Whitelaw, W. A., & Derenne, J. P. (1994). ARTERIAL BLOOD-GASES IN ELDERLY PERSONS WITH CHRONIC OBSTRUCTIVE PULMONARY-DISEASE (COPD) [Article]. *European Respiratory Journal*, *7*(5), 856-861.

Detweiler, N. D., Vigil, K. G., Resta, T. C., Walker, B. R., & Jernigan, N. L. (2018). Role of acid-sensing ion channels in hypoxia-and hypercapnia-induced ventilatory responses [Article]. *Plos One*, *13*(2), Article e0192724. https://doi.org/10.1371/journal.pone.0192724

Donaldson, G. C., Hurst, J. R., Smith, C. J., Hubbard, R. B., & Wedzicha, J. A. (2010). Increased Risk of Myocardial Infarction and Stroke Following Exacerbation of COPD [Article]. *Chest*, *137*(5), 1091-1097. https://doi.org/10.1378/chest.09-2029

Donnelly, D. F., Kim, I., Mulligan, E. M., & Carroll, J. L. (2014). Non-additive interactions between mitochondrial complex IV blockers and hypoxia in rat carotid body responses [Article]. *Respiratory Physiology & Neurobiology*, *190*(1), 62-69. https://doi.org/10.1016/j.resp.2013.09.009

Duchen, M. R., & Biscoe, T. J. (1992a). MITOCHONDRIAL-FUNCTION IN TYPE-I CELLS ISOLATED FROM RABBIT ARTERIAL CHEMORECEPTORS [Article]. *Journal of Physiology-London*, *450*, 13-31. https://doi.org/10.1113/jphysiol.1992.sp019114

Duchen, M. R., & Biscoe, T. J. (1992b). RELATIVE MITOCHONDRIAL-MEMBRANE POTENTIAL AND CA2+ I IN TYPE-I CELLS ISOLATED FROM THE RABBIT CAROTID-BODY [Article]. *Journal of Physiology-London*, *450*, 33-61. https://doi.org/10.1113/jphysiol.1992.sp019115

Dunn, K. W., Kamocka, M. M., & McDonald, J. H. (2011). A practical guide to evaluating colocalization in biological microscopy [Review]. *American Journal of Physiology-Cell Physiology*, *300*(4), C723-C742. https://doi.org/10.1152/ajpcell.00462.2010

Dwinell, M. R., & Powell, F. L. (1999). Chronic hypoxia enhances the phrenic nerve response to arterial chemoreceptor stimulation in anesthetized rats [Article]. *Journal of Applied Physiology*, *87*(2), 817-823. https://doi.org/10.1152/jappl.1999.87.2.817

Eckle, T., Krahn, T., Grenz, A., Köhler, D., Mittelbronn, M., Ledent, C., Jacobson, M. A., Osswald, H., Thompson, L. F., Unertl, K., & Eltzschig, H. K. (2007). Cardioprotection by ecto-5'-nucleotidase (CD73) and A2B adenosine receptors. *Circulation*, *115*(12), 1581-1590. https://doi.org/10.1161/circulationaha.106.669697

Eldridge, F. L., & Millhorn, D. E. (1987). Role of Adenosine in the Regulation of Breathing. In E. Gerlach & B. F. Becker, *Topics and Perspectives in Adenosine Research* Berlin, Heidelberg.

Enyeart, J. J., Xu, L., Danthi, S., & Enyeart, J. A. (2002). An ACTH- and ATP-regulated background K+ channel in adrenocortical cells is TREK-1 [Article]. *Journal of Biological Chemistry*, *277*(51), 49186-49199. https://doi.org/10.1074/jbc.M207233200

Evans, A. M., Hardie, D. G., Peers, C., Wyatt, C. N., Viollet, B., Kumar, P., Dallas, M. L., Ross, F., Ikematsu, N., Jordan, H. L., Barr, B. L., Rafferty, J. N., & Ogunbayo, O. (2009). Ion Channel Regulation by AMPK The Route of Hypoxia-Response Coupling in the Carotid Body and Pulmonary Artery. In C. Peers, G. G. Haddad, & N. S. Chandel (Eds.), *Hypoxia and Consequences from Molecule to Malady* (Vol. 1177, pp. 89-100). Blackwell Publishing. https://doi.org/10.1111/j.1749-6632.2009.05041.x

Fausther, M., Lecka, J., Soliman, E., Kauffenstein, G., Pelletier, J., Sheung, N., Dranoff, J. A., & Sévigny, J. (2012). Coexpression of ecto-5'-nucleotidase/CD73 with specific NTPDases differentially regulates adenosine formation in the rat liver [Article]. *American Journal of*

Physiology-Gastrointestinal and Liver Physiology, *302*(4), G447-G459. https://doi.org/10.1152/ajpgi.00165.2011

Fernández-Agüera, M. C., Gao, L., González-Rodríguez, P., Pintado, C. O., Arias-Mayenco, I., García-Flores, P., García-Pergañeda, A., Pascual, A., Ortega-Sáenz, P., & López-Barneo, J. (2015). Oxygen Sensing by Arterial Chemoreceptors Depends on Mitochondrial Complex I Signaling [Article]. *Cell Metabolism*, *22*(5), 825-837. https://doi.org/10.1016/j.cmet.2015.09.004

Fielding, J. W., Hodson, E. J., Cheng, X. T., Ferguson, D. J. P., Eckardt, L., Adam, J., Lip, P., Maton-Howarth, M., Ratnayaka, I., Pugh, C. W., Buckler, K. J., Ratcliffe, P. J., & Bishop, T. (2018). PHD2 inactivation in Type I cells drives HIF-2α-dependent multilineage hyperplasia and the formation of paraganglioma-like carotid bodies [Article]. *Journal of Physiology-London*, *596*(18), 4393-4412. https://doi.org/10.1113/jp275996

Finley, J. C. W., & Katz, D. M. (1992). THE CENTRAL ORGANIZATION OF CAROTID-BODY AFFERENT-PROJECTIONS TO THE BRAIN-STEM OF THE RAT [Article]. *Brain Research*, *572*(1-2), 108-116. https://doi.org/10.1016/0006-8993(92)90458-l

Flenley, D. C. (1981). LONG-TERM DOMICILIARY OXYGEN-THERAPY IN CHRONIC HYPOXIC COR-PULMONALE COMPLICATING CHRONIC-BRONCHITIS AND EMPHYSEMA [Article]. *Lancet*, *1*(8222), 681-686.

Forster, H. V., Bisgard, G. E., & Klein, J. P. (1981). EFFECT OF PERIPHERAL CHEMORECEPTOR DENERVATION ON ACCLIMATIZATION OF GOATS DURING HYPOXIA [Article]. *Journal of Applied Physiology*, *50*(2), 392-398. https://doi.org/10.1152/jappl.1981.50.2.392

Gagnon, P., Guenette, J. A., Langer, D., Laviolette, L., Mainguy, V., Maltais, F., Ribeiro, F., & Saey, D. (2014). Pathogenesis of hyperinflation in chronic obstructive pulmonary disease [Review]. *International Journal of Chronic Obstructive Pulmonary Disease*, *9*, 187-201. https://doi.org/10.2147/copd.S38934

Gao, L., Bonilla-Henao, V., García-Flores, P., Arias-Mayenco, I., Ortega-Sáenz, P., & López-Barneo, J. (2017). Gene expression analyses reveal metabolic specifications in acute O₂-sensing chemoreceptor cells [Review]. *Journal of Physiology-London*, *595*(18), 6091-6120. https://doi.org/10.1113/jp274684

Gauda, E. B., Northington, F. J., Linden, J., & Rosin, D. L. (2000). Differential expression of A(2a), A(1)-adenosine and D-2-dopamine receptor genes in rat peripheral arterial chemoreceptors during postnatal development [Article]. *Brain Research*, *872*(1-2), 1-10. https://doi.org/10.1016/s0006-8993(00)02314-3

Gerhardt, H., & Betsholtz, C. (2003). Endothelial-pericyte interactions in angiogenesis [Review]. *Cell and Tissue Research*, *314*(1), 15-23. https://doi.org/10.1007/s00441-003-0745-x

Gibbons, T. D., Dempsey, J. A., Thomas, K. N., Campbell, H. A., Stothers, T. A. M., Wilson, L. C., Ainslie, P. N., & Cotter, J. D. (2022). Contribution of the carotid body to thermally mediated hyperventilation in humans [Article]. *Journal of Physiology-London*, *600*(15), 3603-3624. https://doi.org/10.1113/jp282918

Gökçinar-Yagci, B., Uçkan-Çetinkaya, D., & Çelebi-Saltik, B. (2015). Pericytes: Properties, Functions and Applications in Tissue Engineering [Article]. *Stem Cell Reviews and Reports*, *11*(4), 549-559. https://doi.org/10.1007/s12015-015-9590-z

Gout, E., Rébeillé, F., Douce, R., & Bligny, R. (2014). Interplay of Mg2+, ADP, and ATP in the cytosol and mitochondria: Unravelling the role of Mg2+ in cell respiration [Article]. *Proceedings of the National Academy of Sciences of the United States of America*, *111*(43), E4560-E4567. https://doi.org/10.1073/pnas.1406251111

Grenz, A., Zhang, H., Eckle, T., Mittelbronn, M., Wehrmann, M., Köhle, C., Kloor, D., Thompson, L. F., Osswald, H., & Eltzschig, H. K. (2007). Protective role of ecto-5'-nucleotidase (CD73) in renal ischemia. *J Am Soc Nephrol*, *18*(3), 833-845. https://doi.org/10.1681/asn.2006101141

Gruber, M., Hu, C. J., Johnson, R. S., Brown, E. J., Keith, B., & Simon, M. C. (2007). Acute postnatal ablation of Hif-2α results in anemia [Article]. *Proceedings of the National*

Academy of Sciences of the United States of America, *104*(7), 2301-2306. https://doi.org/10.1073/pnas.0608382104

Guo, Y. Z., Mao, S. C., & Zhou, Z. L. (2024). Effects of intramuscular alfaxalone and dexmedetomidine alone and combined on ocular, electroretinographic, and cardiorespiratory parameters in normal cats [Article]. *Frontiers in Veterinary Science*, *11*, 9, Article 1407928. https://doi.org/10.3389/fvets.2024.1407928

Haase, V. H. (2010). Hypoxic regulation of erythropoiesis and iron metabolism [Review]. *American Journal of Physiology-Renal Physiology*, *299*(1), F1-F13. https://doi.org/10.1152/ajprenal.00174.2010

Haidl, P., Clement, C., Wiese, C., Dellweg, D., & Köhler, D. (2004). Long-term oxygen therapy stops the natural decline of endurance in COPD patients with reversible hypercapnia [Article]. *Respiration*, *71*(4), 342-347. https://doi.org/10.1159/000079637

Hall, C. N., Reynell, C., Gesslein, B., Hamilton, N. B., Mishra, A., Sutherland, B. A., O'Farrell, F. M., Buchan, A. M., Lauritzen, M., & Attwell, D. (2014). Capillary pericytes regulate cerebral blood flow in health and disease [Article]. *Nature*, *508*(7494), 55-60. https://doi.org/10.1038/nature13165

Han, M. K., Postma, D., Mannino, D. M., Giardino, N. D., Buist, S., Curtis, J. L., & Martinez, F. J. (2007). Gender and chronic obstructive pulmonary disease - Why it matters [Editorial Material]. *American Journal of Respiratory and Critical Care Medicine*, *176*(12), 1179-1184. https://doi.org/10.1164/rccm.200704-553CC

Hansen, J., & Sander, M. (2003). Sympathetic neural overactivity in healthy humans after prolonged exposure to hypobaric hypoxia [Article]. *Journal of Physiology-London*, *546*(3), 921-929. https://doi.org/10.1113/jphysiol.2002.031765

He, L., Chen, J., Dinger, B., Stensaas, L., & Fidone, S. (2006). Effect of chronic hypoxia on purinergic synaptic transmission in rat carotid body [Article]. *Journal of Applied Physiology*, *100*(1), 157-162. https://doi.org/10.1152/japplphysiol.00859.2005

Heath, D., Edwards, C., & Harris, P. (1970). POST-MORTEM SIZE AND STRUCTURE OF HUMAN CAROTID BODY - ITS RELATION TO PULMONARY DISEASE AND CARDIAC HYPERTROPHY [Article]. *Thorax*, *25*(2), 129-&. https://doi.org/10.1136/thx.25.2.129

Heeringa, J., Berkenbosch, A., Degoede, J., & Olievier, C. N. (1979). RELATIVE CONTRIBUTION OF CENTRAL AND PERIPHERAL CHEMORECEPTORS TO THE VENTILATORY RESPONSE TO CO2 DURING HYPEROXIA [Article]. *Respiration Physiology*, *37*(3), 365-379. https://doi.org/10.1016/0034-5687(79)90082-3

Heindl, S., Lehnert, M., Criée, C. P., Hasenfuss, G., & Andreas, S. (2001). Marked sympathetic activation in patients with chronic respiratory failure [Article]. *American Journal of Respiratory and Critical Care Medicine*, *164*(4), 597-601. https://doi.org/10.1164/ajrccm.164.4.2007085

Hempleman, S. C. (1995). SODIUM AND POTASSIUM CURRENT IN NEONATAL RAT CAROTID-BODY CELLS FOLLOWING CHRONIC IN-VIVO HYPOXIA [Article]. *Brain Research*, *699*(1), 42-50. https://doi.org/10.1016/0006-8993(95)00850-p

Hempleman, S. C. (1996). Increased calcium current in carotid body glomus cells following in vivo acclimatization to chronic hypoxia [Article]. *Journal of Neurophysiology*, *76*(3), 1880-1886. https://doi.org/10.1152/jn.1996.76.3.1880

Herlenius, E., Lagercrantz, H., & Yamamoto, Y. (1997). Adenosine modulates inspiratory neurons and the respiratory pattern in the brainstem of neonatal rats [Article]. *Pediatric Research*, *42*(1), 46-53. https://doi.org/10.1203/00006450-199707000-00008

Hess, A. (1975). *THE SIGNIFICANCE OF THE ULTRASTRUCTURE OF THE RAT CAROTID BODY IN STRUCTURE AND FUNCTION OF CHEMO RECEPTORS*.

Hodson, E. J., Nicholls, L. G., Turner, P. J., Llyr, R., Fielding, J. W., Douglas, G., Ratnayaka, I., Robbins, P. A., Pugh, C. W., Buckler, K. J., Ratcliffe, P. J., & Bishop, T. (2016). Regulation of ventilatory sensitivity and carotid body proliferation in hypoxia by the PHD2/HIF-2 pathway [Article]. *Journal of Physiology-London*, *594*(5), 1179-1195. https://doi.org/10.1113/jp271050

Holmes, A. P., Nunes, A. R., Cann, M. J., & Kumar, P. (2015). Ecto-5 '-Nucleotidase, Adenosine and Transmembrane Adenylyl Cyclase Signalling Regulate Basal Carotid Body Chemoafferent Outflow and Establish the Sensitivity to Hypercapnia. In C. Peers, P. Kumar, C. N. Wyatt, E. Gauda, C. A. Nurse, & N. Prabhakar (Eds.), *Arterial Chemoreceptors in Physiology and Pathophysiology* (Vol. 860, pp. 279-289). Springer-Verlag Berlin. https://doi.org/10.1007/978-3-319-18440-1_32

Holmes, A. P., Ray, C. J., Coney, A. M., & Kumar, P. (2018a). Is Carotid Body Physiological O-2 Sensitivity Determined by a Unique Mitochondrial Phenotype? [Review]. *Frontiers in Physiology*, *9*, 8, Article 562. https://doi.org/10.3389/fphys.2018.00562

Holmes, A. P., Ray, C. J., Pearson, S. A., Coney, A. M., & Kumar, P. (2018b). Ecto-5'-nucleotidase (CD73) regulates peripheral chemoreceptor activity and cardiorespiratory responses to hypoxia [Article]. *Journal of Physiology-London*, *596*(15), 3137-3148. https://doi.org/10.1113/jp274498

Holmes, A. P., Turner, P. J., Buckler, K. J., & Kumar, P. (2016). Moderate inhibition of mitochondrial function augments carotid body hypoxic sensitivity [Article]. *Pflugers Archiv-European Journal of Physiology*, *468*(1), 143-155. https://doi.org/10.1007/s00424-015-1745-x

Holmes, A. P., Turner, P. J., Carter, P., Leadbeater, W., Ray, C. J., Hauton, D., Buckler, K. J., & Kumar, P. (2014). Glycogen metabolism protects against metabolic insult to preserve carotid body function during glucose deprivation [Article]. *Journal of Physiology-London*, *592*(20), 4493-4506. https://doi.org/10.1113/jphysiol.2014.276105

Horscroft, J. A., Burgess, S. L., Hu, Y. Q., & Murray, A. J. (2015). Altered Oxygen Utilisation in Rat Left Ventricle and Soleus after 14 Days, but Not 2 Days, of Environmental Hypoxia [Article]. *Plos One*, *10*(9), 16, Article e0138564. https://doi.org/10.1371/journal.pone.0138564

Horscroft, J. A., O'Brien, K. A., Clark, A. D., Lindsay, R. T., Steel, A. S., Procter, N. E. K., Devaux, J., Frenneaux, M., Harridge, S. D. R., & Murray, A. J. (2019). Inorganic nitrate, hypoxia, and the regulation of cardiac mitochondrial respiration-probing the role of PPARα [Article]. *Faseb Journal*, *33*(6), 7563-7577. https://doi.org/10.1096/fj.201900067R

Ingebrigtsen, T., Thomsen, S. F., Vestbo, J., van der Sluis, S., Kyvik, K. O., Silverman, E. K., Svartengren, M., & Backer, V. (2010). Genetic influences on chronic obstructive pulmonary disease - A twin study [Article]. *Respiratory Medicine*, *104*(12), 1890-1895. https://doi.org/10.1016/j.rmed.2010.05.004

Iturriaga, R. (2018). Translating carotid body function into clinical medicine [Article; Proceedings Paper]. *Journal of Physiology-London*, *596*(15), 3067-3077. https://doi.org/10.1113/jp275335

Iturriaga, R., Alcayaga, J., Chapleau, M. W., & Somers, V. K. (2021). CAROTID BODY CHEMORECEPTORS: PHYSIOLOGY, PATHOLOGY, AND IMPLICATIONS FOR HEALTH AND DISEASE [Review]. *Physiological Reviews*, *101*(3), 1177-1235. https://doi.org/10.1152/physrev.00039.2019

Iturriaga, R., Lahiri, S., & Mokashi, A. (1991). CARBONIC-ANHYDRASE AND CHEMORECEPTION IN THE CAT CAROTID-BODY [Article]. *American Journal of Physiology*, *261*(4), C565-C573. https://doi.org/10.1152/ajpcell.1991.261.4.C565

Kaissling, B., & Le Hir, M. (2008). The renal cortical interstitium: morphological and functional aspects [Review]. *Histochemistry and Cell Biology*, *130*(2), 247-262. https://doi.org/10.1007/s00418-008-0452-5

Karanovic, N., Pecotic, R., Valic, M., Jeroncic, A., Carev, M., Karanovic, S., Ujevic, A., & Dogas, Z. (2010). The acute hypoxic ventilatory response under halothane, isoflurane, and sevoflurane anaesthesia in rats [Article]. *Anaesthesia*, *65*(3), 227-234. https://doi.org/10.1111/j.1365-2044.2009.06194.x

Kent, B. D., Mitchell, P. D., & McNicholas, W. T. (2011). Hypoxemia in patients with COPD: cause, effects, and disease progression [Review]. *International Journal of Chronic Obstructive Pulmonary Disease*, *6*, 199-208. https://doi.org/10.2147/copd.S10611

Kim, D., Cavanaugh, E. J., Kim, I., & Carroll, J. L. (2009). Heteromeric TASK-1/TASK-3 is the major oxygen-sensitive background K+ channel in rat carotid body glomus cells [Article]. *Journal of Physiology-London*, *587*(12), 2963-2975. https://doi.org/10.1113/jphysiol.2009.171181

Kim, D., Kang, D., Martin, E. A., Kim, I., & Carroll, J. L. (2014). Effects of modulators of AMP-activated protein kinase on TASK-1/3 and intracellular Ca2+ concentration in rat carotid body glomus cells [Article]. *Respiratory Physiology & Neurobiology*, *195*, 19-26. https://doi.org/10.1016/j.resp.2014.01.020

Kline, D. D., Peng, Y. J., Manalo, D. J., Semenza, G. L., & Prabhakar, N. R. (2002). Defective carotid body function and impaired ventilatory responses to chronic hypoxia in mice partially deficient for hypoxia-inducible factor 1α [Article]. *Proceedings of the National Academy of Sciences of the United States of America*, *99*(2), 821-826. https://doi.org/10.1073/pnas.022634199

Knowles, A. F. (2011). The GDA1_CD39 superfamily: NTPDases with diverse functions [Review]. *Purinergic Signalling*, *7*(1), 21-45. https://doi.org/10.1007/s11302-010-9214-7

Kobayashi, S., Conforti, L., & Millhorn, D. E. (2000a). Gene expression and function of adenosine A(2A) receptor in the rat carotid body [Article]. *American Journal of Physiology-Lung Cellular and Molecular Physiology*, *279*(2), L273-L282. https://doi.org/10.1152/ajplung.2000.279.2.L273

Kobayashi, S., Zimmermann, H., & Millhorn, D. E. (2000b). Chronic hypoxia enhances adenosine release in rat PC12 cells by altering adenosine metabolism and membrane transport [Article]. *Journal of Neurochemistry*, *74*(2), 621-632. https://doi.org/10.1046/j.1471-4159.2000.740621.x

Kong, T. Q., Westerman, K. A., Faigle, M., Eltzschig, H. K., & Colgan, S. P. (2006). HIF-dependent induction of adenosine A2B receptor in hypoxia [Article]. *Faseb Journal*, *20*(13), 2242-2250. https://doi.org/10.1096/fj.06-6419com

Krock, B. L., Skuli, N., & Simon, M. C. (2011). Hypoxia-induced angiogenesis: good and evil. *Genes & cancer*, *2*(12), 1117-1133. https://doi.org/10.1177/1947601911423654

Kumar, P. (2009). Systemic Effects Resulting from Carotid Body Stimulation - Invited Article. In C. Gonzalez, C. A. Nurse, & C. Peers (Eds.), *Arterial Chemoreceptors* (Vol. 648, pp. 223-233). Springer-Verlag Berlin. https://doi.org/10.1007/978-90-481-2259-2_26

Kumar, P., & Bin-Jaliah, I. (2007). Adequate stimuli of the carotid body: More than an oxygen sensor? [Review]. *Respiratory Physiology & Neurobiology*, *157*(1), 12-21. https://doi.org/10.1016/j.resp.2007.01.007

Kumar, P., & Prabhakar, N. R. (2012). Peripheral Chemoreceptors: Function and Plasticity of the Carotid Body [Article]. *Comprehensive Physiology*, *2*(1), 141-219. https://doi.org/10.1002/cphy.c100069

Kusakabe, T., Hirakawa, H., Oikawa, S., Matsuda, H., Kawakami, T., Takenaka, T., & Hayashida, Y. (2004). Morphological changes in the rat carotid body 1, 2, 4, and 8 weeks after the termination of chronically hypocapnic hypoxia [Article]. *Histology and Histopathology*, *19*(4), 1133-1140.

Kvale, P., Conway, W., & Coates, E. (1980). CONTINUOUS OR NOCTURNAL OXYGEN-THERAPY IN HYPOXEMIC CHRONIC OBSTRUCTIVE LUNG-DISEASE - A CLINICAL-TRIAL [Article]. *Annals of Internal Medicine*, *93*(3), 391-398.

Lahiri, S., Delaney, R. G., Brody, J. S., Simpser, M., Velasquez, T., Motoyama, E. K., & Polgar, C. (1976). RELATIVE ROLE OF ENVIRONMENTAL AND GENETIC FACTORS IN RESPIRATORY ADAPTATION TO HIGH-ALTITUDE [Article]. *Nature*, *261*(5556), 133-135. https://doi.org/10.1038/261133a0

Lando, D., Peet, D. J., Whelan, D. A., Gorman, J. J., & Whitelaw, M. L. (2002). Asparagine hydroxylation of the HIF transactivation domain: A hypoxic switch [Article]. *Science*, *295*(5556), 858-861. https://doi.org/10.1126/science.1068592

Leonard, E. M., & Nurse, C. A. (2022, Jun 27-30). The Carotid Body "Tripartite Synapse": Role of Gliotransmission.*Advances in Experimental Medicine and Biology* [Arterial

chemoreceptors]. 21st International-Society-of-Arterial-Chemoreception (ISAC) Meeting, Univ Nova Lisboa, Nova Med Sch, Lisbon, PORTUGAL.

Linz, D., Linz, B., Hohl, M., & Böhm, M. (2016). Atrial arrhythmogenesis in obstructive sleep apnea: Therapeutic implications [Review]. *Sleep Medicine Reviews*, *26*, 87-94. https://doi.org/10.1016/j.smrv.2015.03.003

Livermore, S., & Nurse, C. A. (2013). Enhanced adenosine A(2b) receptor signaling facilitates stimulus-induced catecholamine secretion in chronically hypoxic carotid body type I cells [Article]. *American Journal of Physiology-Cell Physiology*, *305*(7), C739-C750. https://doi.org/10.1152/ajpcell.00137.2013

Lopez-Barneo, J., Gonzalez-Rodriguez, P., Gao, L., Fernandez-Aguera, M. C., Pardal, R., & Ortega-Saenz, P. (2016). Oxygen sensing by the carotid body: mechanisms and role in adaptation to hypoxia [Article]. *American Journal of Physiology-Cell Physiology*, *310*(8), C629-C642. https://doi.org/10.1152/ajpcell.00265.2015

Lopez-Barneo, J., Lopez-Lopez, J. R., Urena, J., & Gonzalez, C. (1988). CHEMOTRANSDUCTION IN THE CAROTID-BODY - K+ CURRENT MODULATED BY PO2 IN TYPE-I CHEMORECEPTOR CELLS [Article]. *Science*, *241*(4865), 580-582. https://doi.org/10.1126/science.2456613

Lopez-Lopez, J. R., Deluis, D. A., & Gonzalez, C. (1993). PROPERTIES OF A TRANSIENT K+ CURRENT IN CHEMORECEPTOR CELLS OF RABBIT CAROTID-BODY [Article]. *Journal of Physiology-London*, *460*, 15-32. https://doi.org/10.1113/jphysiol.1993.sp019456

Loring, S. H., Garcia-Jacques, M., & Malhotra, A. (2009). Pulmonary characteristics in COPD and mechanisms of increased work of breathing [Review]. *Journal of Applied Physiology*, *107*(1), 309-314. https://doi.org/10.1152/japplphysiol.00008.2009

Lu, Y. J., Whiteis, C. A., Sluka, K. A., Chapleau, M. W., & Abboud, F. M. (2013). Responses of glomus cells to hypoxia and acidosis are uncoupled, reciprocal and linked to ASIC3 expression: selectivity of chemosensory transduction [Article]. *Journal of Physiology-London*, *591*(4), 919-932. https://doi.org/10.1113/jphysiol.2012.247189

Macias, D., Cowburn, A. S., Torres-Torrelo, H., Ortega-Sáenz, P., López-Barneo, J., & Johnson, R. S. (2018). HIF-2α is essential for carotid body development and function [Article]. *Elife*, *7*, 26, Article e34681. https://doi.org/10.7554/elife.34681

Mahmoud, A. D., Lewis, S., Juricic, L., Udoh, U. A., Hartmann, S., Jansen, M. A., Ogunbayo, O. A., Puggioni, P., Holmes, A. P., Kumar, P., Navarro-Dorado, J., Foretz, M., Viollet, B., Dutia, M. B., Marshall, I., & Evans, A. M. (2016). AMP-activated Protein Kinase Deficiency Blocks the Hypoxic Ventilatory Response and Thus Precipitates Hypoventilation and Apnea [Article]. *American Journal of Respiratory and Critical Care Medicine*, *193*(9), 1032-1043. https://doi.org/10.1164/rccm.201508-1667OC

Mannino, D. M., & Buist, A. S. (2007). Global burden of COPD: risk factors, prevalence, and future trends [Review]. *Lancet*, *370*(9589), 765-773. https://doi.org/10.1016/s0140-6736(07)61380-4

Marshall, J. M. (1998). Chemoreceptors and cardiovascular control in acute and chronic systemic hypoxia [Review]. *Brazilian Journal of Medical and Biological Research*, *31*(7), 863-888. https://doi.org/10.1590/s0100-879x1998000700002

Marshall, J. M. (2015). Interactions between local dilator and sympathetic vasoconstrictor influences in skeletal muscle in acute and chronic hypoxia [Review]. *Experimental Physiology*, *100*(12), 1400-1411. https://doi.org/10.1113/ep085139

Marshall, J. M., & Davies, W. R. (1999). The effects of acute and chronic systemic hypoxia on muscle oxygen supply and oxygen consumption in the rat [Article]. *Experimental Physiology*, *84*(1), 57-68. https://doi.org/10.1111/j.1469-445X.1999.tb00072.x

Marshall, J. M., & Metcalfe, J. D. (1988). ANALYSIS OF THE CARDIOVASCULAR CHANGES INDUCED IN THE RAT BY GRADED-LEVELS OF SYSTEMIC HYPOXIA [Article]. *Journal of Physiology-London*, *407*, 385-403. https://doi.org/10.1113/jphysiol.1988.sp017422

Maxwell, D. L., Fuller, R. W., Nolop, K. B., Dixon, C. M. S., & Hughes, J. M. B. (1986). EFFECTS OF ADENOSINE ON VENTILATORY RESPONSES TO HYPOXIA AND HYPERCAPNIA IN

HUMANS [Article]. *Journal of Applied Physiology*, *61*(5), 1762-1766. https://doi.org/10.1152/jappl.1986.61.5.1762

Maxwell, P. H., Osmond, M. K., Pugh, C. W., Heryet, A., Nicholls, L. G., Tan, C. C., Doe, B. G., Ferguson, D. J., Johnson, M. H., & Ratcliffe, P. J. (1993). Identification of the renal erythropoietin-producing cells using transgenic mice. *Kidney International*, *44*(5), 1149-1162.

McBryde, F. D., Abdala, A. P., Hendy, E. B., Pijacka, W., Marvar, P., Moraes, D. J. A., Sobotka, P. A., & Paton, J. F. R. (2013). The carotid body as a putative therapeutic target for the treatment of neurogenic hypertension [Article]. *Nature Communications*, *4*, 11, Article 2395. https://doi.org/10.1038/ncomms3395

McDonald, D. M. (1981). Peripheral chemoreceptors: structure-function relationships of the carotid body. *Regulation of breathing*, *17*(pt 1), 105-319.

McDonald, D. M. (1983). A MORPHOMETRIC ANALYSIS OF BLOOD-VESSELS AND PERIVASCULAR NERVES IN THE RAT CAROTID-BODY [Article]. *Journal of Neurocytology*, *12*(1), 155-199. https://doi.org/10.1007/bf01148091

McDonald, D. M., & Blewett, R. W. (1981). LOCATION AND SIZE OF CAROTID BODY-LIKE ORGANS (PARAGANGLIA) REVEALED IN RATS BY THE PERMEABILITY OF BLOOD-VESSELS TO EVANS BLUE-DYE [Article]. *Journal of Neurocytology*, *10*(4), 607-+. https://doi.org/10.1007/bf01262593

McDonald, D. M., & Larue, D. T. (1983). The ultrastructure and connections of blood vessels supplying the rat carotid body and carotid sinus. *Journal of Neurocytology*, *12*, 117-153.

McQueen, D. S., & Ribeiro, J. A. (1981). EFFECT OF ADENOSINE ON CAROTID CHEMORECEPTOR ACTIVITY IN THE CAT [Article]. *British Journal of Pharmacology*, *74*(1), 129-136. https://doi.org/10.1111/j.1476-5381.1981.tb09964.x

McQueen, D. S., & Ribeiro, J. A. (1983). ON THE SPECIFICITY AND TYPE OF RECEPTOR INVOLVED IN CAROTID-BODY CHEMORECEPTOR ACTIVATION BY ADENOSINE IN THE CAT [Article]. *British Journal of Pharmacology*, *80*(2), 347-354. https://doi.org/10.1111/j.1476-5381.1983.tb10040.x

McQueen, D. S., & Ribeiro, J. A. (1986). PHARMACOLOGICAL CHARACTERIZATION OF THE RECEPTOR INVOLVED IN CHEMOEXCITATION INDUCED BY ADENOSINE [Article]. *British Journal of Pharmacology*, *88*(3), 615-620. https://doi.org/10.1111/j.1476-5381.1986.tb10242.x

Millhorn, D. E., Raymond, R., Conforti, L., Zhu, W., Beitner-Johnson, D., Filisko, T., Genter, M. B., Kobayashi, S., & Peng, M. (1997). Regulation of gene expression for tyrosine hydroxylase in oxygen sensitive cells by hypoxia. *Kidney Int*, *51*(2), 527-535. https://doi.org/10.1038/ki.1997.73

Minor, M., Alcedo, K. P., Battaglia, R. A., & Snider, N. T. (2019). Cell type- and tissue-specific functions of ecto-5'-nucleotidase (CD73) [Review]. *American Journal of Physiology-Cell Physiology*, *317*(6), C1079-C1092. https://doi.org/10.1152/ajpcell.00285.2019

Monteiro, E. C., & Ribeiro, J. A. (1987). VENTILATORY EFFECTS OF ADENOSINE MEDIATED BY CAROTID-BODY CHEMORECEPTORS IN THE RAT [Article]. *Naunyn-Schmiedebergs Archives of Pharmacology*, *335*(2), 143-148.

Monteiro, E. C., VeraCruz, P., Monteiro, T. C., & Sousa, M. (1996, Mar 25-29). Adenosine increases the cAMP content of the rat carotid body in vitro.*Advances in Experimental Medicine and Biology* [Frontiers in arterial chemoreception]. XIIIth International Symposium on Arterial Chemoreceptors, Catholic Univ Chile, Exptl Ctr, Santiago, Chile.

Montero, D., & Lundby, C. (2019). Arterial oxygen content regulates plasma erythropoietin independent of arterial oxygen tension: a blinded crossover study [Article]. *Kidney International*, *95*(1), 173-177. https://doi.org/10.1016/j.kint.2018.09.015

Moreno-Domínguez, A., Ortega-Sáenz, P., Gao, L., Colinas, O., Garcia-Flores, P., Bonilla-Henao, V., Aragonés, J., Hüttemann, M., Grossman, L. I., Weissmann, N., Sommer, N., & López-Barneo, J. (2020). Acute O2 sensing through HIF2α-dependent expression of atypical

cytochrome oxidase subunits in arterial chemoreceptors [Article]. *Science Signaling*, *13*(615), 13, Article eaay9452. https://doi.org/10.1126/scisignal.aay9452

Morgan, A. D., Zakeri, R., & Quint, J. K. (2018). Defining the relationship between COPD and CVD: what are the implications for clinical practice? [Review]. *Therapeutic Advances in Respiratory Disease*, *12*, 16, Article 1753465817750524. https://doi.org/10.1177/1753465817750524

Mouradian, G. C., Forster, H. V., & Hodges, M. R. (2012). Acute and chronic effects of carotid body denervation on ventilation and chemoreflexes in three rat strains [Article]. *Journal of Physiology-London*, *590*(14), 3335-3347. https://doi.org/10.1113/jphysiol.2012.234658

Moya, E. A., Go, A., Kim, C. B., Fu, Z. X., Simonson, T. S., & Powell, F. L. (2020). Neuronal HIF-1α in the nucleus tractus solitarius contributes to ventilatory acclimatization to hypoxia [Article]. *Journal of Physiology-London*, *598*(10), 2021-2034. https://doi.org/10.1113/jp279331

Muir, W., Lerche, P., Wiese, A., Nelson, L., Pasloske, K., & Whittem, T. (2008). Cardiorespiratory and anesthetic effects of clinical and supraclinical doses of alfaxalone in dogs [Article]. *Veterinary Anaesthesia and Analgesia*, *35*(6), 451-462. https://doi.org/10.1111/j.1467-2995.2008.00406.x

Murphy, M. P. (2009). How mitochondria produce reactive oxygen species [Review]. *Biochemical Journal*, *417*, 1-13. https://doi.org/10.1042/bj20081386

Nanduri, J., Makarenko, V., Reddy, V. D., Yuan, G. X., Pawar, A., Wang, N., Khan, S. A., Zhang, X., Kinsman, B., Peng, Y. J., Kumar, G. K., Fox, A. P., Godley, L. A., Semenza, G. L., & Prabhakar, N. R. (2012). Epigenetic regulation of hypoxic sensing disrupts cardiorespiratory homeostasis [Article]. *Proceedings of the National Academy of Sciences of the United States of America*, *109*(7), 2515-2520. https://doi.org/10.1073/pnas.1120600109

Nanduri, J., Peng, Y. J., Wang, N., Khan, S. A., Semenza, G. L., Kumar, G. K., & Prabhakar, N. R. (2017). Epigenetic regulation of redox state mediates persistent cardiorespiratory abnormalities after long-term intermittent hypoxia [Article]. *Journal of Physiology-London*, *595*(1), 63-77. https://doi.org/10.1113/jp272346

Nanduri, J., Peng, Y. J., Wang, N., Khan, S. A., Semenza, G. L., & Prabhakar, N. R. (2018). DNA methylation in the central and efferent limbs of the chemoreflex requires carotid body neural activity [Article]. *Journal of Physiology-London*, *596*(15), 3087-3100. https://doi.org/10.1113/jp274833

Nanduri, J., & Prabhakar, N. R. (2018). Immunohistochemistry of the Carotid Body. In L. E. Huang (Ed.), *Hypoxia: Methods and Protocols* (Vol. 1742, pp. 155-166). Humana Press Inc. https://doi.org/10.1007/978-1-4939-7665-2_14

Narkiewicz, K., Ratcliffe, L. E., Hart, E. C., Briant, L. J., Chrostowska, M., Wolf, J., Szyndler, A., Hering, D., Abdala, A. P., & Manghat, N. (2016). Unilateral carotid body resection in resistant hypertension: a safety and feasibility trial. *JACC: Basic to Translational Science*, *1*(5), 313-324.

Narkiewicz, K., van de Borne, P. J. H., Montano, N., Dyken, M. E., Phillips, B. G., & Somers, V. K. (1998). Contribution of tonic chemoreflex activation to sympathetic activity and blood pressure in patients with obstructive sleep apnea [Article]. *Circulation*, *97*(10), 943-945.

Nathan, S. D., Barbera, J. A., Gaine, S. P., Harari, S., Martinez, F. J., Olschewski, H., Olsson, K. M., Peacock, A. J., Pepke-Zaba, J., Provencher, S., Weissmann, N., & Seeger, W. (2019). Pulmonary hypertension in chronic lung disease and hypoxia [Article; Proceedings Paper]. *European Respiratory Journal*, *53*(1), 15, Article 1801914. https://doi.org/10.1183/13993003.01914-2018

NICE. (2025). *Oxygen* National Institute for Health and Care Excellence (NICE). British National Formulary (BNF). Retrieved March 2025 from https://bnf.nice.org.uk/treatment-summaries/oxygen/

Nickol, A. H., Frise, M. C., Cheng, H. Y., McGahey, A., McFadyen, B. M., Harris-Wright, T., Bart, N. K., Curtis, M. K., Khandwala, S., O'Neill, D. P., Pollard, K. A., Hardinge, F. M., Rahman, N. M., Armitage, A. E., Dorrington, K. L., Drakesmith, H., Ratcliffe, P. J., & Robbins, P. A. (2015). A cross-sectional study of the prevalence and associations of iron deficiency in a cohort of patients with chronic obstructive pulmonary disease. *BMJ Open*, *5*(7), e007911. https://doi.org/10.1136/bmjopen-2015-007911

Niewinski, P., Janczak, D., Rucinski, A., Jazwiec, P., Sobotka, P. A., Engelman, Z. J., Fudim, M., Tubek, S., Jankowska, E. A., Banasiak, W., Hart, E. C. J., Paton, J. F. R., & Ponikowski, P. (2013). Carotid body removal for treatment of chronic systolic heart failure [Article]. *International Journal of Cardiology*, *168*(3), 2506-2509. https://doi.org/10.1016/j.ijcard.2013.03.011

Niewinski, P., Janczak, D., Rucinski, A., Tubek, S., Engelman, Z. J., Piesiak, P., Jazwiec, P., Banasiak, W., Fudim, M., Sobotka, P. A., Javaheri, S., Hart, E. C. J., Paton, J. F. R., & Ponikowski, P. (2017). Carotid body resection for sympathetic modulation in systolic heart failure: results from first-in-man study [Article]. *European Journal of Heart Failure*, *19*(3), 391-400. https://doi.org/10.1002/ejhf.641

Niewinski, P., Tubek, S., Paton, J. F. R., Banasiak, W., & Ponikowski, P. (2021). Oxygenation pattern and compensatory responses to hypoxia and hypercapnia following bilateral carotid body resection in humans [Article]. *Journal of Physiology-London*, *599*(8), 2323-2340. https://doi.org/10.1113/jp281319

Nunes, A. R., Holmes, A. P., Conde, S. V., Gauda, E. B., & Monteiro, E. C. (2014). Revisiting cAMP signaling in the carotid body [Review]. *Frontiers in Physiology*, *5*, 16, Article 409. https://doi.org/10.3389/fphys.2014.00406

Nunes, A. R., Holmes, A. P. S., Sample, V., Kumar, P., Cann, M. J., Monteiro, E. C., Zhang, J., & Gauda, E. B. (2013). Bicarbonate-sensitive soluble and transmembrane adenylyl cyclases in peripheral chemoreceptors [Article]. *Respiratory Physiology & Neurobiology*, *188*(2), 83-93. https://doi.org/10.1016/j.resp.2013.05.013

Nunes, A. R., Monteiro, E. C., Johnson, S. M., & Ganda, E. B. (2009). Bicarbonate-Regulated Soluble Adenylyl Cyclase (sAC) mRNA Expression and Activity in Peripheral Chemoreceptors. In C. Gonzalez, C. A. Nurse, & C. Peers (Eds.), *Arterial Chemoreceptors* (Vol. 648, pp. 235-241). Springer-Verlag Berlin. https://doi.org/10.1007/978-90-481-2259-2_27

Nurse, C. A. (2010). Neurotransmitter and neuromodulatory mechanisms at peripheral arterial chemoreceptors [Article]. *Experimental Physiology*, *95*(6), 657-667. https://doi.org/10.1113/expphysiol.2009.049312

Nurse, C. A. (2014). Synaptic and paracrine mechanisms at carotid body arterial chemoreceptors [Review]. *Journal of Physiology-London*, *592*(16), 3419-3426. https://doi.org/10.1113/jphysiol.2013.269829

Nurse, C. A., Jackson, A., & Stea, A. (1993, Aug 09-13). PLASTICITY IN CULTURED ARTERIAL CHEMORECEPTORS - EFFECTS OF CHRONIC HYPOXIA AND CYCLIC AMP ANALOGS.*Advances in Experimental Medicine and Biology* [Arterial chemoreceptors: Cell to system]. 12th International Meeting of the International-Society-of-Arterial-Chemoreception on Chemoreceptors and Chemoreflexes in Health and Disease, Dublin, Ireland.

O'Brien, K. A., Simonson, T. S., & Murray, A. J. (2020). Metabolic adaptation to high altitude. *Current Opinion in Endocrine and Metabolic Research*, *11*, 33-41.

O'Donnell, D. E., & Laveneziana, P. (2006). Physiology and consequences of lung hyperinflation in COPD [Article]. *European Respiratory Review*, *15*(100), 61-67. https://doi.org/10.1183/09059180.00010002

Obeso, A., Almaraz, L., & Gonzalez, C. (1989). EFFECTS OF CYANIDE AND UNCOUPLERS ON CHEMORECEPTOR ACTIVITY AND ATP CONTENT OF THE CAT CAROTID-BODY [Article]. *Brain Research*, *481*(2), 250-257. https://doi.org/10.1016/0006-8993(89)90801-9

Ohta, M., Toyama, K., Gutterman, D. D., Campbell, W. B., Lemaître, V., Teraoka, R., & Miura, H. (2013). Ecto-5'-Nucleotidase, CD73, Is an Endothelium-Derived Hyperpolarizing Factor Synthase [Article]. *Arteriosclerosis Thrombosis and Vascular Biology*, *33*(3), 629-+. https://doi.org/10.1161/atvbaha.112.300600

Olson, E. B., Vidruk, E. H., & Dempsey, J. A. (1988). CAROTID-BODY EXCISION SIGNIFICANTLY CHANGES VENTILATORY CONTROL IN AWAKE RATS [Article]. *Journal of Applied Physiology*, *64*(2), 666-671. https://doi.org/10.1152/jappl.1988.64.2.666

Ortega-Sáenz, P., Levitsky, K. L., Marcos-Almaraz, M. T., Bonilla-Henao, V., Pascual, A., & López-Barneo, J. (2010). Carotid body chemosensory responses in mice deficient of TASK channels [Article]. *Journal of General Physiology*, *135*(4), 379-392. https://doi.org/10.1085/jgp.200910302

Ortiz-Barahona, A., Villar, D., Pescador, N., Amigo, J., & del Peso, L. (2010). Genome-wide identification of hypoxia-inducible factor binding sites and target genes by a probabilistic model integrating transcription-profiling data and in silico binding site prediction [Article]. *Nucleic Acids Research*, *38*(7), 2332-2345. https://doi.org/10.1093/nar/gkp1205

Ortiz, F., Iturriaga, R., & Varas, R. (2009). Sustained Hypoxia Enhances TASK-like Current Inhibition by Acute Hypoxia in Rat Carotid Body Type-I Cells. In C. Gonzalez, C. A. Nurse, & C. Peers (Eds.), *Arterial Chemoreceptors* (Vol. 648, pp. 83-88). Springer-Verlag Berlin. https://doi.org/10.1007/978-90-481-2259-2_9

Paciga, M., Vollmer, C., & Nurse, C. (1999). Role of ET-1 in hypoxia-induced mitosis of cultured rat carotid body chemoreceptors [Article]. *Neuroreport*, *10*(18), 3739-3744. https://doi.org/10.1097/00001756-199912160-00003

Pamenter, M. E., Carr, J. A., Go, A., Fu, Z. X., Reid, S. G., & Powell, F. L. (2014). Glutamate receptors in the nucleus tractus solitarius contribute to ventilatory acclimatization to hypoxia in rat [Article]. *Journal of Physiology-London*, *592*(8), 1839-1856. https://doi.org/10.1113/jphysiol.2013.268706

Pamenter, M. E., & Powell, F. L. (2016). Time Domains of the Hypoxic Ventilatory Response and Their Molecular Basis [Article]. *Comprehensive Physiology*, *6*(3), 1345-1385. https://doi.org/10.1002/cphy.c150026

Pan, X., Suzuki, N., Hirano, I., Yamazaki, S., Minegishi, N., & Yamamoto, M. (2011). Isolation and characterization of renal erythropoietin-producing cells from genetically produced anemia mice. *Plos One*, *6*(10), e25839. https://doi.org/10.1371/journal.pone.0025839

Panneton, W. M., & Loewy, A. D. (1980). PROJECTIONS OF THE CAROTID-SINUS NERVE TO THE NUCLEUS OF THE SOLITARY TRACT IN THE CAT [Note]. *Brain Research*, *191*(1), 239-244. https://doi.org/10.1016/0006-8993(80)90326-1

Pardal, R., Ortega-Sáenz, P., Durán, R., & López-Barneo, J. (2007). Glia-like stem cells sustain physiologic neurogenesis in the adult mammalian carotid body [Article]. *Cell*, *131*(2), 364-377. https://doi.org/10.1016/j.cell.2007.07.043

Park, T. I. H., Feisst, V., Brooks, A. E. S., Rustenhoven, J., Monzo, H. J., Feng, S. X., Mee, E. W., Bergin, P. S., Oldfield, R., Graham, E. S., Curtis, M. A., Faull, R. L. M., Dunbar, P. R., & Dragunow, M. (2016). Cultured pericytes from human brain show phenotypic and functional differences associated with differential CD90 expression [Article]. *Scientific Reports*, *6*, 17, Article 26587. https://doi.org/10.1038/srep26587

Paton, J. F. R., Sobotka, P. A., Fudim, M., Engleman, Z. J., Hart, E. C. J., McBryde, F. D., Abdala, A. P., Marina, N., Gourine, A. V., Lobo, M., Patel, N., Burchell, A., Ratcliffe, L., & Nightingale, A. (2013). The Carotid Body as a Therapeutic Target for the Treatment of Sympathetically Mediated Diseases [Review]. *Hypertension*, *61*(1), 5-13. https://doi.org/10.1161/hypertensionaha.111.00064

Peacock, A. J. (1998). ABC of oxygen - Oxygen at high altitude [Article]. *British Medical Journal*, *317*(7165), 1063-1066.

Peers, C. (1990). EFFECT OF LOWERED EXTRACELLULAR PH ON CA-2+-DEPENDENT K+ CURRENTS IN TYPE-I CELLS FROM THE NEONATAL RAT CAROTID-BODY [Article]. *Journal of Physiology-London*, *422*, 381-395. https://doi.org/10.1113/jphysiol.1990.sp017990

Peng, H. X., Zhang, L. L., Jiang, D., Jian, N., Zhang, T. M., Luo, J. G., & Yin, H. Y. (2024). CD73 polymorphisms are associated with schizophrenia. *Purinergic Signal*. https://doi.org/10.1007/s11302-024-10004-3

Peng, Y.-J., Nanduri, J., Raghuraman, G., Souvannakitti, D., Gadalla, M. M., Kumar, G. K., Snyder, S. H., & Prabhakar, N. R. (2010). H2S mediates O2 sensing in the carotid body. *Proceedings of the National Academy of Sciences*, *107*(23), 10719-10724.

Peng, Y. J., Gridina, A., Wang, B., Nanduri, J., Fox, A. P., & Prabhakar, N. R. (2020). Olfactory receptor 78 participates in carotid body response to a wide range of low O₂ levels but not severe hypoxia [Article]. *Journal of Neurophysiology*, *123*(5), 1886-1895. https://doi.org/10.1152/jn.00075.2020

Peng, Y. J., Nanduri, J., Wang, N., Kumar, G. K., Bindokas, V., Paul, B. D., Chen, X. M., Fox, A. P., Vignane, T., Filipovic, M. R., & Prabhakar, N. R. (2023). Hypoxia sensing requires H2S-dependent persulfidation of olfactory receptor 78 [Article]. *Science Advances*, *9*(27), 13, Article eadf3026. https://doi.org/10.1126/sciadv.adf3026

Peng, Y. J., Nanduri, J., Wang, N., Su, X. Y., Hildreth, M., & Prabhakar, N. R. (2025). Signal Transduction Pathway Mediating Carotid Body Dependent Sympathetic Activation and Hypertension by Chronic Intermittent Hypoxia [Article]. *Function*, *6*(1), 11, Article zqaf003. https://doi.org/10.1093/function/zqaf003

Peng, Y. J., Yuan, G. X., Khan, S., Nanduri, J., Makarenko, V. V., Reddy, V. D., Vasavda, C., Kumar, G. K., Semenza, G. L., & Prabhakar, N. R. (2014). Regulation of hypoxia-inducible factor-α isoforms and redox state by carotid body neural activity in rats [Article]. *Journal of Physiology-London*, *592*(17), 3841-3858. https://doi.org/10.1113/jphysiol.2014.273789

Pepper, D. R., Landauer, R. C., & Kumar, P. (1995). POSTNATAL-DEVELOPMENT OF CO2-O-2 INTERACTION IN THE RAT CAROTID-BODY IN-VITRO [Article]. *Journal of Physiology-London*, *485*(2), 531-541. https://doi.org/10.1113/jphysiol.1995.sp020749

Perezgarcia, M. T., Almaraz, L., & Gonzalez, C. (1990). EFFECTS OF DIFFERENT TYPES OF STIMULATION ON CYCLIC-AMP CONTENT IN THE RABBIT CAROTID-BODY - FUNCTIONAL-SIGNIFICANCE [Article]. *Journal of Neurochemistry*, *55*(4), 1287-1293. https://doi.org/10.1111/j.1471-4159.1990.tb03137.x

Phillips, D. B., Steinback, C. D., Collins, S. E., Fuhr, D. P., Bryan, T. L., Wong, E. Y. L., Tedjasaputra, V., Bhutani, M., & Stickland, M. K. (2018). The carotid chemoreceptor contributes to the elevated arterial stiffness and vasoconstrictor outflow in chronic obstructive pulmonary disease [Article]. *Journal of Physiology-London*, *596*(15), 3233-3244. https://doi.org/10.1113/jp275762

Pijacka, W., Moraes, D. J. A., Ratcliffe, L. E. K., Nightingale, A. K., Hart, E. C., da Silva, M. P., Machado, B. H., McBryde, F. D., Abdala, A. P., Ford, A. P., & Paton, J. F. R. (2016). Purinergic receptors in the carotid body as a new drug target for controlling hypertension [Article]. *Nature Medicine*, *22*(10), 1151-1159. https://doi.org/10.1038/nm.4173

Piskuric, N. A., & Nurse, C. A. (2013). Expanding role of ATP as a versatile messenger at carotid and aortic body chemoreceptors [Review]. *Journal of Physiology-London*, *591*(2), 415-422. https://doi.org/10.1113/jphysiol.2012.234377

Platero-Luengo, A., González-Granero, S., Durán, R., Díaz-Castro, B., Piruat, J. I., Garcia-Verdugo, J. M., Pardal, R., & López-Barneo, J. (2014). An O₂-Sensitive Glomus Cell-Stem Cell Synapse Induces Carotid Body Growth in Chronic Hypoxia [Article]. *Cell*, *156*(1-2), 291-303. https://doi.org/10.1016/j.cell.2013.12.013

Powell, F. L. (2007). The influence of chronic hypoxia upon chemoreception [Article]. *Respiratory Physiology & Neurobiology*, *157*(1), 154-161. https://doi.org/10.1016/j.resp.2007.01.009

Powell, F. L., Dwinell, M. R., & Aaron, E. A. (2000a). Measuring ventilatory acclimatization to hypoxia, comparative aspects [Article]. *Respiration Physiology*, *122*(2-3), 271-284. https://doi.org/10.1016/s0034-5687(00)00165-1

Powell, F. L., Huey, K. A., & Dwinell, M. R. (2000b). Central nervous system mechanisms of ventilatory acclimatization to hypoxia [Article]. *Respiration Physiology*, *121*(2-3), 223-236. https://doi.org/10.1016/s0034-5687(00)00130-4

Powell, F. L., Milsom, W. K., & Mitchell, G. S. (1998). Time domains of the hypoxic ventilatory response [Review]. *Respiration Physiology*, *112*(2), 123-134. https://doi.org/10.1016/s0034-5687(98)00026-7

Prabhakar, N. R., Peng, Y. J., & Nanduri, J. (2023). Carotid body hypersensitivity in intermittent hypoxia and obtructive sleep apnoea [Review]. *Journal of Physiology-London*, *601*(24), 5481-5494. https://doi.org/10.1113/jp284111

Prabhakar, N. R., & Semenza, G. L. (2015). Oxygen Sensing and Homeostasis [Review]. *Physiology*, *30*(5), 340-348. https://doi.org/10.1152/physiol.00022.2015

Prasad, M., Fearon, I. A., Zhang, M., Laing, M., Vollmer, C., & Nurse, C. A. (2001). Expression of P2X2 and P2X3 receptor subunits in rat carotid body afferent neurones: role in chemosensory signalling [Article]. *Journal of Physiology-London*, *537*(3), 667-677.

Pulgar-Sepúlveda, R., Varas, R., Iturriaga, R., Del Rio, R., & Ortiz, F. C. (2018). Carotid Body Type-I Cells Under Chronic Sustained Hypoxia: Focus on Metabolism and Membrane Excitability [Review]. *Frontiers in Physiology*, *9*, 8, Article 1282. https://doi.org/10.3389/fphys.2018.01282

Rabe, K. F., Hurst, J. R., & Suissa, S. (2018). Cardiovascular disease and COPD: dangerous liaisons? [Review]. *European Respiratory Review*, *27*(149), 32. https://doi.org/10.1183/16000617.0057-2018

Ray, C. J., Abbas, M. R., Coney, A. M., & Marshall, J. M. (2002). Interactions of adenosine, prostaglandins and nitric oxide in hypoxia-induced vasodilatation:: in vivo and in vitro studies [Article]. *Journal of Physiology-London*, *544*(1), 195-209. https://doi.org/10.1113/jphysiol.2002.023440

Reyes, E., Fernández, R., Larraín, C., & Zapata, P. (2007). Effects of combined cholinergic–purinergic block upon cat carotid body chemosensory activity and ventilatory chemoreflexes. *Respir. Physiol. Neurobiol*, *156*, 23-32.

Rezende, L. M. T. d., Soares, L. L., Drummond, F. R., Suarez, P. Z., Leite, L., Rodrigues, J. A., Leal, T., Favarato, L., Reis, E. C. C., Favarato, E., Carneiro Júnior, M., Natali, A. J., Coimbra, C., & Gomes, T. P. (2022). Is the Wistar Rat a more Suitable Normotensive Control for SHR to Test Blood Pressure and Cardiac Structure and Function? [research-article]. *International Journal of Cardiovascular Sciences*, *35*(2), 161-171. https://doi.org/10.36660/ijcs.20200367

Ribeiro, J. A., & Monteiro, E. C. (1991). ON THE ADENOSINE RECEPTOR INVOLVED IN THE EXCITATORY ACTION OF ADENOSINE ON RESPIRATION - ANTAGONIST PROFILE [Article; Proceedings Paper]. *Nucleosides & Nucleotides*, *10*(5), 945-953. https://doi.org/10.1080/07328319108047232

Ribeiro, M. J., Sacramento, J. F., Gonzalez, C., Guarino, M. P., Monteiro, E. C., & Conde, S. V. (2013). Carotid Body Denervation Prevents the Development of Insulin Resistance and Hypertension Induced by Hypercaloric Diets [Article]. *Diabetes*, *62*(8), 2905-2916. https://doi.org/10.2337/db12-1463

Riesco-Fagundo, A. M., Pérez-García, M. T., González, C., & López-López, J. R. (2001). O₂ modulates large-conductance Ca2+-dependent K+channels of rat chemoreceptor cells by a membrane-restricted and CO-sensitive mechanism [Article]. *Circulation Research*, *89*(5), 430-436. https://doi.org/10.1161/hh1701.095632

Rigual, R., Lopezlopez, J. R., & Gonzalez, C. (1991). RELEASE OF DOPAMINE AND CHEMORECEPTOR DISCHARGE INDUCED BY LOW PH AND HIGH PCO2 STIMULATION OF THE CAT CAROTID-BODY [Article]. *Journal of Physiology-London*, *433*, 519-531. https://doi.org/10.1113/jphysiol.1991.sp018441

Rocher, A., Caceres, A. I., Almaraz, L., & Gonzalez, C. (2009). EPAC signalling pathways are involved in low P-O2 chemoreception in carotid body chemoreceptor cells [Article]. *Journal of Physiology-London*, *587*(16), 4015-4027. https://doi.org/10.1113/jphysiol.2009.172072

Rodman, J. R., Curran, A. K., Henderson, K. S., Dempsey, J. A., & Smith, C. A. (2001). Carotid body denervation in dogs: eupnea and the ventilatory response to hyperoxic hypercapnia

[Article]. *Journal of Applied Physiology*, *91*(1), 328-335. https://doi.org/10.1152/jappl.2001.91.1.328

Roeggla, G., Roeggla, M., Wagner, A., & Laggner, A. N. (1995). POOR VENTILATORY RESPONSE TO MILD HYPOXIA MAY INHIBIT ACCLIMATIZATION AT MODERATE ALTITUDE IN ELDERLY PATIENTS AFTER CAROTID SURGERY [Article]. *British Journal of Sports Medicine*, *29*(2), 110-112. https://doi.org/10.1136/bjsm.29.2.110

Rong, W. F., Gourine, A. V., Cockayne, D. A., Xiang, Z. H., Ford, A., Spyer, K. M., & Burnstock, G. (2003). Pivotal role of nucleotide P2X(2) receptor subunit of the ATP-gated ion channel mediating ventilatory responses to hypoxia [Article]. *Journal of Neuroscience*, *23*(36), 11315-11321. <Go to ISI>://WOS:000187232800005

Runold, M., Cherniack, N. S., & Prabhakar, N. R. (1990). EFFECT OF ADENOSINE ON ISOLATED AND SUPERFUSED CAT CAROTID-BODY ACTIVITY [Article]. *Neuroscience Letters*, *113*(1), 111-114. https://doi.org/10.1016/0304-3940(90)90504-3

Sacramento, J. F., Melo, B. F., & Conde, S. V. (2018). Adenosine Mediates Hypercapnic Response in the Rat Carotid Body via A2A and A2B Receptors. In E. B. Gauda, N. Prabhakar, H. D. Schultz, M. E. Monteiro, & C. Wyatt (Eds.), *Arterial Chemoreceptors: New Directions and Translational Perspectives* (Vol. 1071, pp. 89-93). Springer International Publishing Ag. https://doi.org/10.1007/978-3-319-91137-3_11

Sacramento, J. F., Olea, E., Ribeiro, M. J., Prieto-Lloret, J., Melo, B. F., Gonzalez, C., Martins, F. O., Monteiro, E. C., & Conde, S. V. (2019). Contribution of adenosine and ATP to the carotid body chemosensory activity in ageing [Article]. *Journal of Physiology-London*, *597*(19), 4991-5008. https://doi.org/10.1113/jp274179

Sacramento, J. F., Ribeiro, M. J., Rodrigues, T., Olea, E., Melo, B. F., Guarino, M. P., Fonseca-Pinto, R., Ferreira, C. R., Coelho, J., Obeso, A., Seiça, R., Matafome, P., & Conde, S. V. (2017). Functional abolition of carotid body activity restores insulin action and glucose homeostasis in rats: key roles for visceral adipose tissue and the liver [Article]. *Diabetologia*, *60*(1), 158-168. https://doi.org/10.1007/s00125-016-4133-y

Salman, S., & Nurse, C. A. (2018). Molecular Characterization of Equilibrative Nucleoside Transporters in the Rat Carotid Body and Their Regulation by Chronic Hypoxia. In E. B. Gauda, N. Prabhakar, H. D. Schultz, M. E. Monteiro, & C. Wyatt (Eds.), *Arterial Chemoreceptors: New Directions and Translational Perspectives* (Vol. 1071, pp. 43-50). Springer International Publishing Ag. https://doi.org/10.1007/978-3-319-91137-3_5

Salman, S., Vollmer, C., McClelland, G. B., & Nurse, C. A. (2017). Characterization of ectonucleotidase expression in the rat carotid body: regulation by chronic hypoxia [Article]. *American Journal of Physiology-Cell Physiology*, *313*(3), C274-C284. https://doi.org/10.1152/ajpcell.00328.2016

Santer, P., McGahey, A., Frise, M. C., Petousi, N., Talbot, N. P., Baskerville, R., Bafadhel, M., Nickol, A. H., & Robbins, P. A. (2020). Intravenous iron and chronic obstructive pulmonary disease: a randomised controlled trial. *BMJ Open Respir Res*, *7*(1). https://doi.org/10.1136/bmjresp-2020-000577

Scalia, C. R., Boi, G., Bolognesi, M. M., Riva, L., Manzoni, M., DeSmedt, L., Bosisio, F. M., Ronchi, S., Leone, B. E., & Cattoretti, G. (2017). Antigen Masking During Fixation and Embedding, Dissected [Article]. *Journal of Histochemistry & Cytochemistry*, *65*(1), 5-20. https://doi.org/10.1369/0022155416673995

Schnell, P. O., Ignacak, M. L., Bauer, A. L., Striet, J. B., Paulding, W. R., & Czyzyk-Krzeska, M. F. (2003). Regulation of tyrosine hydroxylase promoter activity by the von Hippel-Lindau tumor suppressor protein and hypoxia-inducible transcription factors. *J Neurochem*, *85*(2), 483-491. https://doi.org/10.1046/j.1471-4159.2003.01696.x

Schultz, H. D., Marcus, N. J., & Del Rio, R. (2015). Mechanisms of carotid body chemoreflex dysfunction during heart failure [Article]. *Experimental Physiology*, *100*(2), 124-129. https://doi.org/10.1113/expphysiol.2014.079517

Semenza, G. L. (2012). Hypoxia-Inducible Factors in Physiology and Medicine [Review]. *Cell*, *148*(3), 399-408. https://doi.org/10.1016/j.cell.2012.01.021

Semenza, G. L., Roth, P. H., Fang, H. M., & Wang, G. L. (1994). TRANSCRIPTIONAL REGULATION OF GENES ENCODING GLYCOLYTIC-ENZYMES BY HYPOXIA-INDUCIBLE FACTOR-1 [Article]. *Journal of Biological Chemistry*, *269*(38), 23757-23763.

Semenza, G. L., & Wang, G. L. (1992). A NUCLEAR FACTOR INDUCED BY HYPOXIA VIA DENOVO PROTEIN-SYNTHESIS BINDS TO THE HUMAN ERYTHROPOIETIN GENE ENHANCER AT A SITE REQUIRED FOR TRANSCRIPTIONAL ACTIVATION [Article]. *Molecular and Cellular Biology*, *12*(12), 5447-5454. https://doi.org/10.1128/mcb.12.12.5447

Sheth, S., Brito, R., Mukherjea, D., Rybak, L. P., & Ramkumar, V. (2014). Adenosine Receptors: Expression, Function and Regulation [Review]. *International Journal of Molecular Sciences*, *15*(2), 2024-2052. https://doi.org/10.3390/ijms15022024

Shi, N. R., Wang, Q., Liu, J., Zhang, J. Z., Deng, B. L., Hu, X. M., Yang, J., Wang, X., Chen, X., Zuo, Y. Q., Liu, T. T., Zheng, J. L., Yang, X., Illes, P., & Tang, Y. (2023). Association of the ADORA2A receptor and CD73 polymorphisms with epilepsy. *Front Pharmacol*, *14*, 1152667. https://doi.org/10.3389/fphar.2023.1152667

Skinner, M. R., & Marshall, J. M. (1996). Studies on the roles of ATP, adenosine and nitric oxide in mediating muscle vasodilatation induced in the rat by acute systemic hypoxia [Article]. *Journal of Physiology-London*, *495*(2), 553-560. https://doi.org/10.1113/jphysiol.1996.sp021615

Sliwinski, P., Lagosz, M., Gorecka, D., & Zielinski, J. (1994). THE ADEQUACY OF OXYGENATION IN COPD PATIENTS UNDERGOING LONG-TERM OXYGEN-THERAPY ASSESSED BY PULSE OXIMETRY AT HOME [Article]. *European Respiratory Journal*, *7*(2), 274-278. https://doi.org/10.1183/09031936.94.07020274

Smith, C. A., Rodman, J. R., Chenuel, B. J. A., Henderson, K. S., & Dempsey, J. A. (2006). Response time and sensitivity of the ventilatory response to CO₂ in unanesthetized intact dogs:: central vs. peripheral chemoreceptors [Article]. *Journal of Applied Physiology*, *100*(1), 13-19. https://doi.org/10.1152/japplphysiol.00926.2005

Smith, K., & Marshall, J. M. (1999). Physiological adjustments and arteriolar remodelling within skeletal muscle during acclimation to chronic hypoxia in the rat [Article]. *Journal of Physiology-London*, *521*(1), 261-272. https://doi.org/10.1111/j.1469-7793.1999.00261.x

Smith, K. A., Waypa, G. B., Dudley, V. J., Budinger, G. R. S., Abdala-Valencia, H., Bartom, E., & Schumacker, P. T. (2020). Role of Hypoxia-Inducible Factors in Regulating Right Ventricular Function and Remodeling during Chronic Hypoxia-induced Pulmonary Hypertension [Article]. *American Journal of Respiratory Cell and Molecular Biology*, *63*(5), 652-664. https://doi.org/10.1165/rcmb.2020-0023OC

Sobrino, V., González-Rodríguez, P., Annese, V., López-Barneo, J., & Pardal, R. (2018). Fast neurogenesis from carotid body quiescent neuroblasts accelerates adaptation to hypoxia [Article]. *Embo Reports*, *19*(3), 17, Article e44598. https://doi.org/10.15252/embr.201744598

Sommer, N., Strielkov, I., Pak, O., & Weissmann, N. (2016). Oxygen sensing and signal transduction in hypoxic pulmonary vasoconstriction [Article]. *European Respiratory Journal*, *47*(1), 288-303. https://doi.org/10.1183/13993003.00945-2015

Stea, A., Jackson, A., Macintyre, L., & Nurse, C. A. (1995). LONG-TERM MODULATION OF INWARD CURRENTS IN O-2 CHEMORECEPTORS BY CHRONIC HYPOXIA AND CYCLIC-AMP IN-VITRO [Article]. *Journal of Neuroscience*, *15*(3), 2192-2202. https://doi.org/10.1523/jneurosci.15-03-02192.1995

Stephenson, R., & Gucciardi, E. J. (2002). Theoretical and practical considerations in the application of whole body plethysmography to sleep research [Article]. *European Journal of Applied Physiology*, *87*(3), 207-219. https://doi.org/10.1007/s00421-002-0610-8

Stickland, M. K., Fuhr, D. P., Edgell, H., Byers, B. W., Bhutani, M., Wong, E. Y. L., & Steinback, C. D. (2016). Chemosensitivity, Cardiovascular Risk, and the Ventilatory Response to Exercise in COPD [Article]. *Plos One*, *11*(6), 15, Article e0158341. https://doi.org/10.1371/journal.pone.0158341

Stoller, J. K., Panos, R. J., Krachman, S., Doherty, D. E., Make, B., & Long-term Oxygen Treatment, T. (2010). Oxygen Therapy for Patients With COPD Current Evidence and the Long-Term Oxygen Treatment Trial [Article]. *Chest*, *138*(1), 179-187. https://doi.org/10.1378/chest.09-2555

Summers, B. A., Overholt, J. L., & Prabhakar, N. R. (2002). CO2 and pH independently modulate L-type Ca2+ current in rabbit carotid body glomus cells [Article]. *Journal of Neurophysiology*, *88*(2), 604-612. https://doi.org/10.1152/jn.2002.88.2.604

Swiderska, A., Coney, A. M., Alzahrani, A. A., Aldossary, H. S., Batis, N., Ray, C. J., Kumar, P., & Holmes, A. P. (2021). Mitochondrial Succinate Metabolism and Reactive Oxygen Species Are Important but Not Essential for Eliciting Carotid Body and Ventilatory Responses to Hypoxia in the Rat [Article]. *Antioxidants*, *10*(6), 19, Article 840. https://doi.org/10.3390/antiox10060840

Synnestvedt, K., Furuta, G. T., Comerford, K. M., Louis, N., Karhausen, J., Eltzschig, H. K., Hansen, K. R., Thompson, L. F., & Colgan, S. P. (2002). Ecto-5'-nucleotidase (CD73) regulation by hypoxia-inducible factor-1 mediates permeability changes in intestinal epithelia [Article]. *Journal of Clinical Investigation*, *110*(7), 993-1002. https://doi.org/10.1172/jci200215337

Tan, Z. Y., Lu, Y., Whiteis, C. A., Benson, C. J., Chapleau, M. W., & Abboud, F. M. (2007). Acid-sensing ion channels contribute to transduction of extracellular acidosis in rat carotid body glomus cells [Article]. *Circulation Research*, *101*(10), 1009-1019. https://doi.org/10.1161/circresaha.107.154377

Taylor, E. W., Jordan, D., & Coote, J. H. (1999). Central control of the cardiovascular and respiratory systems and their interactions in vertebrates [Review]. *Physiological Reviews*, *79*(3), 855-916. https://doi.org/10.1152/physrev.1999.79.3.855

Thakkar, P., Pauza, A. G., Murphy, D., & Paton, J. F. R. (2023). Carotid body: an emerging target for cardiometabolic co-morbidities [Review]. *Experimental Physiology*, *108*(5), 661-671. https://doi.org/10.1113/ep090090

Thomas, T., & Marshall, J. M. (1994). INTERDEPENDENCE OF RESPIRATORY AND CARDIOVASCULAR CHANGES INDUCED BY SYSTEMIC HYPOXIA IN THE RAT - THE ROLES OF ADENOSINE [Article]. *Journal of Physiology-London*, *480*, 627-636. https://doi.org/10.1113/jphysiol.1994.sp020389

Thomas, T., & Marshall, J. M. (1997). The roles of adenosine in regulating the respiratory and cardiovascular systems in chronically hypoxic, adult rats [Article]. *Journal of Physiology-London*, *501*(2), 439-447. https://doi.org/10.1111/j.1469-7793.1997.439bn.x

Thomas, T., Ralevic, V., Gadd, C. A., & Spyer, K. M. (1999). Central CO2 chemoreception:: a mechanism involving P2 purinoceptors localized in the ventrolateral medulla of the anaesthetized rat [Article]. *Journal of Physiology-London*, *517*(3), 899-905. https://doi.org/10.1111/j.1469-7793.1999.00899.x

Thomas, T., & Spyer, K. M. (1996). The role of adenosine receptors in the rostral ventrolateral medulla in the cardiovascular response to defence area stimulation in the rat [Article]. *Experimental Physiology*, *81*(1), 67-77. https://doi.org/10.1113/expphysiol.1996.sp003919

Thompson, C. M., & Wyatt, C. N. (2011). Inhibition of adenylate cyclase attenuates muscarinic Ca2+ signaling by a PKA-independent mechanism in rat carotid body Type I cells [Article]. *Respiratory Physiology & Neurobiology*, *175*(1), 90-96. https://doi.org/10.1016/j.resp.2010.09.013

Thompson, E. L., Ray, C. J., Holmes, A. P., Pye, R. L., Wyatt, C. N., Coney, A. M., & Kumar, P. (2016). Adrenaline release evokes hyperpnoea and an increase in ventilatory CO2 sensitivity during hypoglycaemia: a role for the carotid body [Article]. *Journal of Physiology-London*, *594*(15), 4439-4452. https://doi.org/10.1113/jp272191

Thompson, L. F., Eltzschig, H. K., Ibla, J. C., Van De Wiele, C. J., Resta, R., Morote-Garcila, J. C., & Colgan, S. P. (2004). Crucial role for ecto-5-' nucleotidase (CD73) in vascular leakage

during hypoxia [Article]. *Journal of Experimental Medicine*, *200*(11), 1395-1405. https://doi.org/10.1084/Jem.20040915

Timón-Gómez, A., Scharr, A. L., Wong, N. Y., Ni, E., Roy, A., Liu, M., Chau, J., Lampert, J. L., Hireed, H., Kim, N. S., Jan, M., Gupta, A. R., Day, R. W., Gardner, J. M., Wilson, R. J. A., Barrientos, A., & Chang, A. J. (2022). Tissue-specific mitochondrial HIGD1C promotes oxygen sensitivity in carotid body chemoreceptors [Article]. *Elife*, *11*, 27, Article e78915. https://doi.org/10.7554/eLife.78915

Tolstykh, G., Belugin, S., & Mifflin, S. (2004). Responses to $GABA_A$ receptor activation are altered in NTS neurons isolated from chronic hypoxic rats [Article]. *Brain Research*, *1006*(1), 107-113. https://doi.org/10.1016/j.brainres.2004.01.060

Torres-López, M., González-Rodríguez, P., Colinas, O., Rho, H. S., Torres-Torrelo, H., Castellano, A., Gao, L., Ortega-Sáenz, P., & López-Barneo, J. (2025). Intracellular signalling in arterial chemoreceptors during acute hypoxia and glucose deprivation: role of ATP [Article; Early Access]. *Journal of Physiology-London*, 17. https://doi.org/10.1113/jp287130

Torres-Torrelo, H., Ortega-Sáenz, P., Gao, L., & López-Barneo, J. (2021). Lactate sensing mechanisms in arterial chemoreceptor cells [Article]. *Nature Communications*, *12*(1), 13, Article 4166. https://doi.org/10.1038/s41467-021-24444-7

Torres-Torrelo, H., Ortega-Sáenz, P., Macías, D., Omura, M., Zhou, T., Matsunami, H., Johnson, R. S., Mombaerts, P., & López-Barneo, J. (2018). The role of Olfr78 in the breathing circuit of mice [Letter]. *Nature*, *561*(7724), E33-E40. https://doi.org/10.1038/s41586-018-0545-9

Tubek, S., Niewinski, P., Reczuch, K., Janczak, D., Rucinski, A., Paleczny, B., Engelman, Z. J., Banasiak, W., Paton, J. F. R., & Ponikowski, P. (2016). Effects of selective carotid body stimulation with adenosine in conscious humans [Article]. *Journal of Physiology-London*, *594*(21), 6225-6240. https://doi.org/10.1113/jp272109

Turner, P. J., & Buckler, K. J. (2013). Oxygen and mitochondrial inhibitors modulate both monomeric and heteromeric TASK-1 and TASK-3 channels in mouse carotid body type-1 cells [Article]. *Journal of Physiology-London*, *591*(23), 5977-5998. https://doi.org/10.1113/jphysiol.2013.262022

Uhlen, M., Fagerberg, L., Hallström, B. M., Lindskog, C., Oksvold, P., Mardinoglu, A., Sivertsson, A., Kampf, C., Sjöstedt, E., Asplund, A., Olsson, I., Edlund, K., Lundberg, E., Navani, S., Szigyarto, C. A., Odeberg, J., Djureinovic, D., Takanen, J. O., Hober, S., . . . Pontén, F. (2015). Tissue-based map of the human proteome [Article]. *Science*, *347*(6220), 10, Article 1260419. https://doi.org/10.1126/science.1260419

Urena, J., Fernandezchacon, R., Benot, A. R., Detoledo, G. A., & Lopezbarneo, J. (1994). HYPOXIA INDUCES VOLTAGE-DEPENDENT CA2+ ENTRY AND QUANTAL DOPAMINE SECRETION IN CAROTID-BODY GLOMUS CELLS [Article]. *Proceedings of the National Academy of Sciences of the United States of America*, *91*(21), 10208-10211. https://doi.org/10.1073/pnas.91.21.10208

Vandier, C., Conway, A. F., Landauer, R. C., & Kumar, P. (1999). Presynaptic action of adenosine on a 4-aminopyridine-sensitive current in the rat carotid body [Article]. *Journal of Physiology-London*, *515*(2), 419-429. https://doi.org/10.1111/j.1469-7793.1999.419ac.x

Vanlandewijck, M., He, L. Q., Mäe, M. A. A., Andrae, J., Ando, K., Del Gaudio, F., Nahar, K., Lebouvier, T., Laviña, B., Gouveia, L., Sun, Y., Raschperger, E., Räsänen, M., Zarb, Y., Mochizuki, N., Keller, A., Lendahl, U., & Betsholtz, C. (2018). A molecular atlas of cell types and zonation in the brain vasculature [Article]. *Nature*, *554*(7693), 475-480. https://doi.org/10.1038/nature25739

Varas, R., Wyatt, C. N., & Buckler, K. J. (2007). Modulation of TASK-like background potassium channels in rat arterial chemoreceptor cells by intracellular ATP and other nucleotides [Article]. *Journal of Physiology-London*, *583*(2), 521-536. https://doi.org/10.1113/jphysiol.2007.135657

Vidruk, E. H., Olson, E. B., Ling, L. M., & Mitchell, G. S. (2001). Responses of single-unit carotid body chemoreceptors in adult rats [Article]. *Journal of Physiology-London*, *531*(1), 165-170. https://doi.org/10.1111/j.1469-7793.2001.0165j.x

Wain, L. V., Shrine, N., Artigas, M. S., Erzurumluoglu, A. M., Noyvert, B., Bossini-Castillo, L., Obeidat, M., Henry, A. P., Portelli, M. A., Hall, R. J., Billington, C. K., Rimington, T. L., Fenech, A. G., John, C., Blake, T., Jackson, V. E., Allen, R. J., Prins, B. P., Campbell, A., . . . Tobin, M. D. (2017). Genome-wide association analyses for lung function and chronic obstructive pulmonary disease identify new loci and potential druggable targets. *Nat Genet*, *49*(3), 416-425. https://doi.org/10.1038/ng.3787

Walsh, M. P., & Marshall, J. M. (2006). The early effects of chronic hypoxia on the cardiovascular system in the rat: role of nitric oxide [Article]. *Journal of Physiology-London*, *575*(1), 263-275. https://doi.org/10.1113/jphysiol.2006.108753

Warne, L. N., Beths, T., Whittem, T., Carter, J. E., & Bauquier, S. H. (2015). A review of the pharmacology and clinical application of alfaxalone in cats [Review]. *Veterinary Journal*, *203*(2), 141-148. https://doi.org/10.1016/j.tvjl.2014.12.011

Watt, A. H., Reid, P. G., Stephens, M. R., & Routledge, P. A. (1987). ADENOSINE-INDUCED RESPIRATORY STIMULATION IN MAN DEPENDS ON SITE OF INFUSION - EVIDENCE FOR AN ACTION ON THE CAROTID-BODY [Article]. *British Journal of Clinical Pharmacology*, *23*(4), 486-490. https://doi.org/10.1111/j.1365-2125.1987.tb03081.x

Whittington, N. C., & Wray, S. (2017). Suppression of Red Blood Cell Autofluorescence for Immunocytochemistry on Fixed Embryonic Mouse Tissue. *Current protocols in neuroscience*, *81*, 2.28.21-22.28.12. https://doi.org/10.1002/cpns.35

WHO. (2025). *Chronic obstructive pulmonary disease (COPD)*. Retrieved March 2025 from https://www.who.int/news-room/fact-sheets/detail/chronic-obstructive-pulmonary-disease-(copd)

Wilkinson, K. A., Huey, K., Dinger, B., He, L. A., Fidone, S., & Powell, F. L. (2010). Chronic hypoxia increases the gain of the hypoxic ventilatory response by a mechanism in the central nervous system [Article]. *Journal of Applied Physiology*, *109*(2), 424-430. https://doi.org/10.1152/japplphysiol.01311.2009

Williams, B. A., & Buckler, K. J. (2004). Biophysical properties and metabolic regulation of a TASK-like potassium channel in rat carotid body type 1 cells [Article]. *American Journal of Physiology-Lung Cellular and Molecular Physiology*, *286*(1), L221-L230. https://doi.org/10.1152/ajplung.00010.2003

Williams, S. E. J., Wootton, P., Mason, H. S., Bould, J., Iles, D. E., Riccardi, D., Peers, C., & Kemp, P. J. (2004). Hemoxygenase-2 is an oxygen sensor for a calcium-sensitive potassium channel [Article]. *Science*, *306*(5704), 2093-2097. https://doi.org/10.1126/science.1105010

Wyatt, C. N., & Buckler, K. J. (2004). The effect of mitochondrial inhibitors on membrane currents in isolated neonatal rat carotid body type I cells [Article]. *Journal of Physiology-London*, *556*(1), 175-191. https://doi.org/10.1113/jphysiol.2003.058131

Wyatt, C. N., Mustard, K. J., Pearson, S. A., Dallas, M. L., Atkinson, L., Kumar, P., Peers, C., Hardie, D. G., & Evans, A. M. (2007). AMP-activated protein kinase mediates carotid body excitation by hypoxia [Article]. *Journal of Biological Chemistry*, *282*(11), 8092-8098. https://doi.org/10.1074/jbc.M608742200

Wyatt, C. N., & Peers, C. (1995). CA2+-ACTIVATED K+ CHANNELS IN ISOLATED TYPE-I CELLS OF THE NEONATAL RAT CAROTID-BODY [Article]. *Journal of Physiology-London*, *483*(3), 559-565. https://doi.org/10.1113/jphysiol.1995.sp020606

Xu, F. L., Xu, J. H., Tse, F. W., & Tse, A. (2006). Adenosine stimulates depolarization and rise in cytoplasmic Ca2+ in type I cells of rat carotid bodies [Article]. *American Journal of Physiology-Cell Physiology*, *290*(6), C1592-C1598. https://doi.org/10.1152/ajpcell.00546.2005

Xu, J. H., Tse, F. W., & Tse, A. (2003). ATP triggers intracellular Ca2+ release in type II cells of the rat carotid body [Article]. *Journal of Physiology-London*, *549*(3), 739-747. https://doi.org/10.1113/jphysiol.2003.039735

Yamamoto, Y., Fujimura, M., Nishita, T., Nishijima, K., Atoji, Y., & Suzuki, Y. (2003). Immunohistochemical localization of carbonic anhydrase isozymes in the rat carotid

body [Article]. *Journal of Anatomy*, *202*(6), 573-577. https://doi.org/10.1046/j.1469-7580.2003.00191.x

Zera, T., Moraes, D. J. A., da Silva, M. P., Fisher, J. P., & Paton, J. F. R. (2019). The Logic of Carotid Body Connectivity to the Brain [Review]. *Physiology*, *34*(4), 264-282. https://doi.org/10.1152/physiol.00057.2018

Zhang, M., & Nurse, C. A. (2004). CO2 pH chemosensory signaling in co-cultures of rat carotid body receptors and petrosal neurons:: Role of ATP and ACh [Article]. *Journal of Neurophysiology*, *92*(6), 3433-3445. https://doi.org/10.1152/jn.01099.2003

Zhang, M., Piskuric, N. A., Vollmer, C., & Nurse, C. A. (2012). P2Y2 receptor activation opens pannexin-1 channels in rat carotid body type II cells: potential role in amplifying the neurotransmitter ATP [Article]. *Journal of Physiology-London*, *590*(17), 4335-4350. https://doi.org/10.1113/jphysiol.2012.236265

Zhang, M., Vollmer, C., & Nurse, C. A. (2018). Adenosine and dopamine oppositely modulate a hyperpolarization-activated current I_h in chemosensory neurons of the rat carotid body in co-culture [Article]. *Journal of Physiology-London*, *596*(15), 3101-3117. https://doi.org/10.1113/jp274743

Zhang, M., Zhong, H. J., Vollmer, C., & Nurse, C. A. (2000). Co-release of ATP and ACh mediates hypoxic signalling at rat carotid body chemoreceptors [Article]. *Journal of Physiology-London*, *525*(1), 143-158. https://doi.org/10.1111/j.1469-7793.2000.t01-1-00143.x

Zhou, T., Chien, M. S., Kaleem, S., & Matsunami, H. (2016). Single cell transcriptome analysis of mouse carotid body glomus cells [Article]. *Journal of Physiology-London*, *594*(15), 4225-4251. https://doi.org/10.1113/jp271936

Zimmermann, H., Mishra, S. K., Shukla, V., Langer, D., Gampe, K., Grimm, I., Delic, J., & Braun, N. (2007). Ecto-nucleotidases, molecular properties and functional impact [Review]. *Anales De La Real Academia Nacional De Farmacia*, *73*(2), 537-566.